
High Order Boundary Element Methods

Dissertation

zur Erlangung des Grades des
Doktors der Naturwissenschaften
der Naturwissenschaftlich-Technischen Fakultäten
der Universität des Saarlandes

von
Lucy Weggler

Saarbrücken
August 2011

Tag des Kolloquiums: 19. Dezember 2011

Mitglieder des Prüfungsausschusses:

Vorsitzender:	Prof. Dr. A. K. Louis, Universität des Saarlandes
Protokollführer:	Dr. R. Grzibovskis, Universität des Saarlandes
1. Berichterstatter:	Prof. Dr. S. Rjasanow, Universität des Saarlandes
2. Berichterstatter:	Prof. Dr. S. Kurz, Tampere University of Technology
3. Berichterstatter:	Prof. Dr. U. Langer, Johannes Kepler Universität Linz (nicht anwesend)

Eidesstattliche Erklärung

Hiermit versichere ich an Eides statt, dass ich die vorliegende Arbeit selbstständig und ohne Benutzung anderer als der angegebenen Hilfsmittel angefertigt habe. Die aus anderen Quellen oder indirekt übernommenen Daten und Konzepte sind unter Angabe der Quelle gekennzeichnet. Die Arbeit wurde bisher weder im In- noch im Ausland in gleicher oder ähnlicher Form in einem Verfahren zur Erlangung eines akademischen Grades vorgelegt.

Saarbrücken, 18. August 2011

(Lucy Weggler)

Abstract

This thesis is a major contribution to the state of research in the field of boundary element methods in general and to the electromagnetic engineering sciences in particular. The first contribution is the development and implementation of high order boundary element methods. It is explained how to set up a high order boundary element implementation which provides solvers for elliptic, Maxwell and mixed problems. The second contribution is a complete mathematical theory for a stabilized boundary variational formulation describing scattering problems. The stabilized formulation presented in this thesis is equivalent to the classical formulations, however, it does not suffer from the low-frequency break-down. The high order methods have been applied to the classical and stabilized formulations describing electromagnetic scattering and the theoretical results on asymptotic convergence and stability have been verified by the numerical computations.

Kurze Zusammenfassung

Die vorliegende Arbeit befaßt sich mit der Entwicklung von Randelementmethoden höherer Ordnung. Die Implementierung, die im Zuge dieser Arbeit entstand, unterscheidet sich von herkömmlicher Software dadurch, dass sie zur numerischen Lösung von elliptischen Problemen, von Maxwell Problemen und insbesondere zur numerischen Lösung von gemischten Formulierungen benutzt werden kann. In der Arbeit werden die theoretisch bewiesenen Konvergenzraten für all diese Problemklassen verifiziert. Um die Leistungsfähigkeit der Software zu demonstrieren, wird insbesondere eine gemischte Formulierung zur Lösung eines elektromagnetischen Streuproblems entwickelt. Diese sogenannte stabilisierte Formulierung ist gleichsam das zweite Forschungsergebnis dieser Arbeit. Im Unterschied zu der klassischen Formulierung gewährleistet die stabilisierte Formulierung numerische Stabilität im Grenzfall quasi-elektrostatistischer Prozesse. Die theoretischen und numerischen Resultate, die diese Aussage rechtfertigen, werden in der Arbeit geliefert.

Zusammenfassung

Der Begriff Randelementmethoden bezeichnet eine Klasse numerischer Verfahren zur Lösung von Randwertproblemen. Eine der grundlegenden Voraussetzungen zur Anwendung der Randelementmethode ist, dass der im Randwertproblem auftauchende Differentialoperator eine Fundamentallösung besitzt. Ist dies der Fall, dann unterscheidet man weiterhin elliptische Probleme, Maxwell Probleme und gemischte Formulierungen. Diese Art von Einteilung ermöglicht eine Klassifizierung der Randintegralgleichungen und insbesondere die Klassifizierung der abgeleiteten Galerkin Variationsformulierungen. Die Diskretisierung dieser Variationsformulierungen in geeigneten endlich-dimensionalen Ansatz- und Testräumen wird als Randelementmethode bezeichnet und der Zusatz 'höhere Ordnung' bezieht sich auf die polynomiale Ordnung der Ansatz- und Testfunktionen. Theoretischen Ergebnissen zufolge, führen die Randelementmethoden höherer Ordnung zu hohen asymptotischen Konvergenzraten. Aus diesem Grund ist das Interesse von Seiten der Industrie an der Realisierung von Randelementmethoden höherer Ordnung groß, zumal in kommerziellen Softwarepaketen oft nur lineare Ansatz- und Testfunktionen zur Verfügung stehen. Die vorliegende Arbeit beschäftigt sich mit der Definition und der Anwendung von geeigneten Ansatz- und Testräumen, die Funktionen von polynomialem Grad $p \geq 1$ bereitstellen. Die grundlegende Idee hierbei ist, dass ein und dieselbe Implementierung neben elliptischen Problemen auch Maxwell Probleme und gemischte Formulierungen behandeln soll. Das ist eine nicht-triviale Aufgabe, da die Ansatz- und Testräume sich je nach Typ des Problems unterscheiden. Die Räume sind allerdings auf kontinuierlicher Ebene durch exakte Sequenzen verknüpft und die zielführende Strategie, um zu einer numerisch stabilen und praktikablen Implementierung zu gelangen, ist, diese Eigenschaft auf diskretem Level zu erhalten und auszunutzen. Ein in sich geschlossenes Konzept hierfür wird in dieser Arbeit entwickelt. Das wiederkehrende Leitmotiv dieses Konzeptes ist das sogenannte Bidualitätprinzip. Das Bidualitätsprinzip ist Ausdruck eines fundamentalen Zusammenhangs zwischen dem metrik-freien differentialgeometrischen Apparat und den metrik-behafteten Funktionalen, die zur Anwendung der Hilbert Raum Theorie benötigt werden. Dieses Erkenntnis ist das bemerkenswerteste theoretische Ergebnis, das im Zuge dieser Arbeit entstand.

Um die Leistungsfähigkeit der höheren Elemente zu demonstrieren, wird die Streuung einer elektromagnetischen Welle an einem perfekt leitenden Körper betrachtet. Dieses Modellproblem kann mit Hilfe der Randelementmethoden gelöst werden und die Galerkin Lösung besitzt theoretisch quasi-optimales Konvergenzverhalten. Das bedeutet, dass die Konvergenzrate p erreicht wird bei Verwendung von Randelementen der Ordnung p . Um ein solches Konvergenzverhalten nachzuweisen, wird die Streuung an der perfekt leitenden Kugel untersucht. In diesem Fall ist eine analytische Lösung durch die Mie Reihe gegeben und die Konvergenzrate p wird bei Verwendung von isoparametrischen Randelementen der Ordnung p verifiziert. Darüber hinaus wird gezeigt, dass die Randelemente höherer Ordnung zur Lösung von hochfrequenten Streuproblemen geeignet sind. Hierzu wird ein realistisches Streuproblem an einer komplizierten Geometrie gelöst. Die Aufgabenstellung und eine numerische Referenzlösung wurden von EM Software & Systems bereitgestellt.

Die Struktur der Implementierung ermöglicht einen flexiblen Einsatz der Software, weil neben Maxwell Problemen auch elliptische Probleme gelöst werden können. Um dies zu demonstrieren, wird eine gemischte Formulierung zur Lösung des elektromagnetischen Streuproblems entwickelt. Diese sogenannte stabilisierte Formulierung ist das zweite Forschungsergebnis dieser Arbeit. Die eindeutige Lösbarkeit der stabilisierten Formulierung läßt sich aus der eindeutigen Lösbarkeit der klassischen Formulierung auf Grund der Äquivalenz der Formulierungen folgern. Die stabilisierende Eigenschaft im elektrostatischen Grenzfall kann theoretisch begründet werden, da die stabilisierte Formulierung in eine Sattelpunktformulierung für ein elektrostatisches Potentialproblem übergeht. Das hat zur Folge, dass die stabilisierte Formulierung, im Unterschied zu der klassischen Formulierung, numerische Stabilität im Grenzfall quasi-elektrostatischer Prozesse gewährleistet. Diese Aussage wird mit der notwendigen mathematischen Theorie und den entsprechenden numerischen

Resultaten unterlegt.

Nach dem Kenntnisstand der Autorin, ist diese Arbeit die erste, die den Stand der Wissenschaft im Bereich der Randelementmethoden höherer Ordnung in dieser Vollständigkeit zusammenfaßt und mit numerischen Experimenten verifiziert. Im Hinblick auf die Lösung elektromagnetischer Streuprobleme, kann man zusammenfassend sagen, dass erstmalig gezeigt worden ist, wie mit ein und derselben numerischen Methode Streuprobleme im gesamten Frequenzspektrum numerisch stabil und effizient gelöst werden können.

Thank-You

To enter building E.1.1 on Saturdays and Sundays, you need this little plastic card. You press it onto the electronic reader, it makes 'piep' and the door opens. Time enough to read the yellow slogan on the card saying 'Die Lösung ist immer nur so gut wie das Team!' which means 'The solution is only as good as the team!'. I am getting aware of how true this is because, in what concerns my thesis, the thesis that I actually call my work or my solution, there are so many marvelous people involved without whom this thesis would not have become what it is. Now it is time to express my deepest gratitude to them.

I would like to thank my doctoral advisor Professor Sergej Rjasanow for his advising and motivating words and especially his realistic statements during the last four years. Further, I would like to thank my secret advisor Professor Leszek Demkowicz for the cooperation that started in 2008 during my stay at the University of Texas at Austin and that will hopefully revive every now and then at conferences all over the world. Third, I would like to thank Professor Stefan Kurz for his interest in my work and especially for the great discussions leading to the insights that still give rise to joy and curiosity when I read my thesis. The input of these three distinguished personalities was necessary to initiate deeper thinking or, more often maybe, a more critical questioning of my deeper thinking. I am thankful for having the opportunity to work with and to learn from these three persons.

Moreover, I would like to thank Sabine Zaglmayr. During my stay in Graz, Summer 2010, she was always free to answer my questions concerning her work and, which is as important, she was an awesome companion to hang out with after work. I enjoyed it so much - thank you, Sabine! Among the people in the working group of Professor Steinbach, there are also Markus Windisch and Sarah Engleder to name explicitly. Somehow I feel that we went through the PhD time together even if we were not at the same place, not even in the same country. I hope so much to see you back in academy and for that reason I hope that industry bores you soon.

Johann van Tonder and Martin Jochum answered all my questions about how to relate my numerical data to real world engineering sciences and I am very thankful for their advice and patience.

During the passed four years the whole Rjasanow-group was standing behind me facing every time and weather. A great thank to them because they seem to come along well with my joyful, my nervous and occasionally hysteric faces. Special thanks goes to Richards Grzibovskis and Marvin Fleck for immediate help in what concerns computer break-downs (or what I felt a computer break-down but was a ventilator problem), compiler problems, plotting shell scrips and, as important as that, general philosophic questions.

The last group of people that I would like to thank is the Lucy's-friends-and-family group. If I named everybody explicitly, you would never read my thesis. However, here are at least three representatives, namely, my mother Gabriele Weggler-Morgott, my father Klaus Weggler and my twin sister and best friend Sophie. There is no need to become pathetic although I really tend to become pathetic sometimes. I make it short: Thank you all so much for staying by my side!

Writing the following pages was fun for me and I hope you enjoy reading them!

Contents

1. Overview	1
2. Mathematical Framework	7
2.1. Manifolds	7
2.2. Distributions	15
2.3. Hilbert Spaces	15
2.4. Energy spaces	18
2.5. Trace Spaces	22
3. Perfect Electric Conductor Problem	29
3.1. Introduction	29
3.2. The Classical Formulation	30
3.2.1. Second order equation	34
3.2.2. Boundary Element Formulation	39
3.3. The Stabilized Formulation	40
3.3.1. Second order equation	41
3.3.2. Boundary Element Formulation	45
3.4. The Electrostatic Case	45
3.5. Conclusion	48
4. High Order Boundary Elements	51
4.1. Introduction	51
4.2. Hierarchical High Order Boundary Elements	52
4.2.1. The Master Element	52
4.2.2. The Parametric Element	57
4.2.3. The Parametric Spaces	59
4.2.4. Projection Based Interpolation	62
4.2.5. The Bidual Spaces	67
4.3. Conclusion	69
5. High Order BEM for PEC	71
5.1. Introduction	71
5.2. The Classical Formulation	71
5.3. The Stabilized Formulation	74
5.4. The Electrostatic Case	76
5.5. The Linear Operators	76
5.6. Conclusion	79
6. Numerical Results	81
6.1. Introduction	81
6.2. The Classical Formulation	83
6.2.1. Icosaeder	83
6.2.2. Isoparametric Sphere	85

6.2.3. Ship	89
6.3. The Stabilized Formulation	90
6.4. Conclusion	96
7. Summary	99
A. Code Verification	101
B. Mie Series	105
C. Elliptic Problems	109
D. Polynomial Exact Sequences	115

OVERVIEW

Research on high order finite element methods started in the late 1980s with results on the adaptive *hp*-version [33]. Babuška and Gui considered an elliptic problem in two dimensions and they showed that the discretization error decreases exponentially with the number of degrees of freedom when geometrically graded meshes are used. During the last thirty years, research on optimal mesh generation lead to the so-called adaptive *hp*-methods delivering exponential convergence [27]. Here, h refers to the mesh size and p denotes the polynomial degree of the trial and test functions on the master element. The idea is to adaptively optimize the mesh with respect to those two parameters. A local error estimator decides whether to refine an element or to increase its order p . There are finite element implementations for automatic *hp*-refinement available solving two-dimensional or three-dimensional elliptic and Maxwell problems. The existing expertise is mainly due to Demkowicz and his coworkers. A self-contained documentation of the current state of research in this field can be found in [27] and [28].

In what concerns the boundary element method, one barely finds any publication on numerics of high order discretization. This is because the boundary element method itself has been developed much later [20]. The origin of the first numerical implementation for boundary integral equations can be traced back to the late 1960s. However, the full emergence of the boundary element method occurred in the 1980s when its theoretical foundation has been given [23, 24]. We refer to the monographs [44, 52, 54] for a detailed derivation and discussion. Since elliptic problems have been understood, the attention turned towards Maxwell problems. For pioneering work on the analysis of integral equations connected to scattering problems, we refer to the monographs written by Colton and Kress [21, 22], and to the book by Nédélec [48]. During the last few years, different mathematicians revisited the topic Maxwell equations in order to complete and generalize the numerical analysis. The latest contributions of Costabel, Buffa, Hiptmair and their collaborators, cover the solution theory for Lipschitz polyhedra [14, 18].

The Galerkin discretization of boundary integral equations yields fully populated matrices. This peculiarity has long been a major disadvantage of the numerical scheme. However, the latest research shows how to generate the system matrices efficiently. The method mentioned explicitly is called the adaptive cross approximation and it is developed by Rjasanow and Bebendorf [51]. The idea is to exploit the behavior of the kernel function in order to compute low rank approximations of the matrix whenever it is possible. The adaptive cross approximation makes the boundary element method competitive for industrial applications.

Coming back to the question whether there are *hp*-adaptive high order implementations for solving boundary integral equations, the answer is no. The solvers which were developed use mainly linear shape functions and work with linear meshes only [8, 51]. However, latest publications confirm an increasing interest in high order discretization. In what concerns elliptic problems, theoretical and numerical results are found in [43, 52]. In what concerns the Maxwell equations, Bespalov, Heuer and Bespalov, Heuer and Hiptmair proved that the high order boundary element method solving the Maxwell equations converges with quasi optimal rates [5, 6] and corresponding numerical results are reported in a paper written by Maischak, Stephan and Leydecker [55]. Inspired by this, we came

up with a simple question: Is there a feasible way of implementing a boundary element method which has the following features:

1. High order discretization of the geometry (optimal manifold representation).
2. Simultaneous discretization of all trace spaces that appear in boundary element formulations (mixed methods).
3. Fast assembling of the system matrices and optimal memory requirements (fast methods).
4. Uniform h -refinement and uniform p -refinements (better convergence rates).
5. Administration of locally varying orders of approximation (projection-based interpolation).
6. Administration of irregular meshes (projection-based interpolation).

A new boundary element code which fulfills these requirements has been developed. The implementation builds up on a finite element implementation for two-dimensional problems. The source code for the latter is published in [27]. The success of the research presented in this thesis is due to a fundamental knowledge of theory and numerics of boundary element methods and thus, the development of the high order boundary elements is a consolidation of current research in two different fields of applied mathematics. It is the goal of this thesis to explain the different steps which are necessary to realize this.

In order to demonstrate the features of this high order boundary element implementation, an electromagnetic scattering problem is solved. The boundary value problem which characterizes the scattering of an electromagnetic field from a perfectly conducting body is derived from the Maxwell equations. The Maxwell equations are four partial differential equations which describe electromagnetic phenomena. Table 1.1 contains a list of all physical quantities which appear in the Maxwell equations. The Gauß law relates the electric flux density \mathbf{D} with the electric charge distribution ρ . For $\mathbf{x} \in \mathbb{R}^3$ and $t > 0$, it reads

$$\operatorname{div} \mathbf{D}(\mathbf{x}, t) = \rho(\mathbf{x}, t).$$

The Gauß law for magnetism states that the divergence of the magnetic flux density \mathbf{B} vanishes for $\mathbf{x} \in \mathbb{R}^3$ and $t > 0$

$$\operatorname{div} \mathbf{B}(\mathbf{x}, t) = 0.$$

Due to the Ampère law, the magnetic field \mathbf{H} is generated either by an electrical current \mathbf{J} or by changing the electric flux density \mathbf{D} . For $\mathbf{x} \in \mathbb{R}^3$ and $t > 0$, it holds

$$\operatorname{curl} \mathbf{H}(\mathbf{x}, t) = \frac{\partial}{\partial t} \mathbf{D}(\mathbf{x}, t) + \mathbf{J}(\mathbf{x}, t).$$

The Faraday law describes how a change of the magnetic flux density \mathbf{B} creates an electric field \mathbf{E} . For $\mathbf{x} \in \mathbb{R}^3$ and $t > 0$, it holds

$$\operatorname{curl} \mathbf{E}(\mathbf{x}, t) = -\frac{\partial}{\partial t} \mathbf{B}(\mathbf{x}, t).$$

Under the assumption that the constitutive relations are linear, there exist linear operators ε and μ such that [41]

$$\begin{aligned} \mathbf{D} &= \varepsilon(\mathbf{E}), \\ \mathbf{B} &= \mu(\mathbf{H}). \end{aligned}$$

Physical quantity	Symbol	SI Unit
Electric flux density	\mathbf{D}	N/Vm
Magnetic flux density	\mathbf{B}	Vs/m ²
Electric field	\mathbf{E}	V/m
Magnetic field	\mathbf{H}	A/m
Electric current	\mathbf{J}	A/m ²
Electric surface current	\mathbf{j}	A/m
Volume charge	ρ	C/m ³
Surface charge	ρ_Γ	C/m ²
Permittivity	ε	As/Vm
Permeability	μ	Vs/Am

Table 1.1.: The physical quantities

We further consider a local, isotropic and homogeneous material which leads to the simple relations

$$\begin{aligned}\mathbf{D}(\mathbf{x}, t) &= \varepsilon \mathbf{E}(\mathbf{x}, t), \\ \mathbf{B}(\mathbf{x}, t) &= \mu \mathbf{H}(\mathbf{x}, t),\end{aligned}$$

where $\varepsilon > 0$ and $\mu > 0$ are constant for all $\mathbf{x} \in \mathbb{R}^3$ and $t > 0$ [39]. Thus, the original Maxwell equations turn into the so-called linear Maxwell equations. By the validity of linear material laws, the number of unknown fields in the Maxwell equations reduces to the electrical field \mathbf{E} and the magnetic field \mathbf{H} . The pair (\mathbf{E}, \mathbf{H}) is called the electromagnetic field.

The harmonic Maxwell equations describe fields which propagate harmonically in time, i.e.,

$$\mathbf{F}(\mathbf{x}, t) = e^{-i\omega t} \tilde{\mathbf{F}}(\mathbf{x}),$$

where \mathbf{F} stands for \mathbf{E} or \mathbf{H} . The oscillatory term $e^{-i\omega t}$ factors out and the harmonic Maxwell equations are usually written in terms of the vector-valued amplitudes depending only on $\mathbf{x} \in \mathbb{R}^3$

$$\begin{aligned}\operatorname{div}(\varepsilon \tilde{\mathbf{E}}(\mathbf{x})) &= \tilde{\rho}(\mathbf{x}), \\ \operatorname{div}(\mu \tilde{\mathbf{H}}(\mathbf{x})) &= 0, \\ \operatorname{curl} \tilde{\mathbf{H}}(\mathbf{x}) &= -i\omega \varepsilon \tilde{\mathbf{E}}(\mathbf{x}) + \tilde{\mathbf{J}}(\mathbf{x}), \\ \operatorname{curl} \tilde{\mathbf{E}}(\mathbf{x}) &= i\omega \mu \tilde{\mathbf{H}}(\mathbf{x}).\end{aligned}$$

As we consider only the harmonic Maxwell equations, we omit the tilde and keep in mind that the time variation is harmonic. Moreover, we assume that there are no volume sources, i.e.,

$$\rho(\mathbf{x}) = 0 \quad \text{and} \quad \mathbf{J}(\mathbf{x}) = \mathbf{0}.$$

Let $(\mathbf{E}^i, \mathbf{H}^i)$ be the incoming electromagnetic field which impinges on a perfectly conducting body $\Omega \subset \mathbb{R}^3$. The incoming field leaves a surface current \mathbf{j} on the boundary $\Gamma = \partial\Omega$ [39]. The surface current \mathbf{j} is the unknown source of a new electromagnetic field, the so-called scattered electromagnetic field (\mathbf{E}, \mathbf{H}) . The superposition of the incoming and the scattered field is the total electromagnetic field $(\mathbf{E}^t, \mathbf{H}^t)$, i.e.,

$$\mathbf{E}^t = \mathbf{E}^i + \mathbf{E} \quad \text{and} \quad \mathbf{H}^t = \mathbf{H}^i + \mathbf{H}.$$

As the total electromagnetic field vanishes inside the conductor, i.e.,

$$\mathbf{E}^t|_{\Omega} = \mathbf{0} \quad \text{and} \quad \mathbf{H}^t|_{\Omega} = \mathbf{0},$$

the scattered field (\mathbf{E}, \mathbf{H}) is unknown only in the exterior domain $\Omega^c = \mathbb{R}^3 \setminus \bar{\Omega}$. The mathematical model describing it are the linear, harmonic Maxwell equations in Ω^c . Let $\mathbf{x} \in \Omega^c$, it holds

$$\begin{aligned} \operatorname{div}(\varepsilon \mathbf{E}(\mathbf{x})) &= 0, \\ \operatorname{div}(\mu \mathbf{H}(\mathbf{x})) &= 0, \\ \operatorname{curl} \mathbf{H}(\mathbf{x}) &= -i\omega \varepsilon \mathbf{E}(\mathbf{x}), \\ \operatorname{curl} \mathbf{E}(\mathbf{x}) &= i\omega \mu \mathbf{H}(\mathbf{x}). \end{aligned}$$

The values of the scattered field on Γ are prescribed by the incoming signal $(\mathbf{E}^i, \mathbf{H}^i)$. If the boundary Γ is a Lipschitz surface, the outer normal vector field \mathbf{n} exists at almost every $\mathbf{x} \in \Gamma$ and for those \mathbf{x} , the Dirichlet boundary conditions read

$$\begin{aligned} \mathbf{n}(\mathbf{x}) \times \mathbf{E}(\mathbf{x}) &= -\mathbf{n}(\mathbf{x}) \times \mathbf{E}^i(\mathbf{x}), \\ \mathbf{n}(\mathbf{x}) \cdot (\mu \mathbf{H})(\mathbf{x}) &= -\mathbf{n}(\mathbf{x}) \cdot (\mu \mathbf{H}^i)(\mathbf{x}). \end{aligned}$$

Moreover, the decrease of the electromagnetic field for $|\mathbf{x}| \rightarrow \infty$ is given by the radiation condition of Silver-Müller, i.e.,

$$\begin{aligned} \left| (\operatorname{curl} \mathbf{E}(\mathbf{x})) \times \frac{\mathbf{x}}{|\mathbf{x}|} - i\omega \varepsilon \mathbf{E}(\mathbf{x}) \right| &= \mathcal{O}\left(\frac{1}{|\mathbf{x}|^2}\right), \\ \left| (\operatorname{curl} \mathbf{H}(\mathbf{x})) \times \frac{\mathbf{x}}{|\mathbf{x}|} - i\omega \mu \mathbf{H}(\mathbf{x}) \right| &= \mathcal{O}\left(\frac{1}{|\mathbf{x}|^2}\right). \end{aligned}$$

In the subsequent chapters, it is explained how to solve this boundary value problem by the use of high order boundary element methods.

Chapter 2 contains an introduction to the functional analytic background of boundary element methods. Most fundamental for this is the definition of manifolds given in Section 2.1. Test function spaces and the space of distributions are defined in Section 2.2. Variational formulations are studied in Hilbert spaces. Basic properties of Hilbert spaces are stated in Section 2.3. The energy spaces,

$$H^1(\Omega), \quad \mathbf{H}(\operatorname{curl}, \Omega), \quad \mathbf{H}(\operatorname{div}, \Omega),$$

are Hilbert spaces which provide the functional analytic tools to analyze integral equations. They are introduced in Section 2.4. In the context of boundary element methods, we need the so-called generalized formulae of partial integration. The trace spaces

$$H^{\frac{1}{2}}(\Gamma), \quad H^{-\frac{1}{2}}(\operatorname{curl}_{\Gamma}, \Gamma), \quad H^{-\frac{1}{2}}(\operatorname{div}_{\Gamma}, \Gamma), \quad H^{-\frac{1}{2}}(\Gamma),$$

from Section 2.5 are necessary to derive them.

As mentioned above, the scattering of an incoming electromagnetic field at a perfectly conducting body $\Omega \subset \mathbb{R}^3$ is our model problem. The goal of Chapter 3 is to provide the Galerkin variational formulations which are later solved by high order boundary element methods. Also, the basic theorems on solvability of the Galerkin formulations in the infinite-dimensional setting are stated. In Section 3.1 a short overview on the contents of the chapter is given. The original Maxwell equations are considered in Section 3.2. The Stratton-Chu representation formula leads to the

classical Galerkin formulations with respect to the duality of the trace spaces $H^{-\frac{1}{2}}(\text{curl}_\Gamma, \Gamma)$ and $H^{-\frac{1}{2}}(\text{div}_\Gamma, \Gamma)$. Besides this well known approach, the so-called stabilized representation formula is derived in Section 3.3. The starting point for the stabilized formulation is the so-called Picard system. It leads to a mixed Galerkin formulation where, also, the duality between the trace spaces $H^{\frac{1}{2}}(\Gamma)$ and $H^{-\frac{1}{2}}(\Gamma)$ appears. For the classical and the stabilized formulations it is assumed that the frequency of the incoming electromagnetic wave is greater than zero, namely $\omega > 0$. This assumption is dropped in Section 3.4 and the electrostatic case, $\omega = 0$, is considered. The contents of Chapter 3 is shortly summarized in Section 3.5.

Chapter 4 is about the definition of finite-dimensional high order function spaces which are appropriate to approximate the infinite-dimensional trace spaces. By an introductory section, Section 4.1, an overview is given on the contents of the five subsections of Section 4.2. In Subsection 4.2.1, the master element is defined as a structure which comprises a parametrization of the reference triangle and a polynomial exact sequence of arbitrary order. In Subsection 4.2.2, the parametric element is defined as a conforming lift of the reference triangle onto a physical triangle. The parametric element is also a structure equipped with the parametrization of the triangle and an exact sequence. The introduction of parametric spaces is done in Subsection 4.2.3. The parametric spaces contain the actual basis functions attributed to global degrees of freedom. An important class of operators for high order discretization are the projection-based interpolation operators Π^1 , Π^c and Π^0 . They are defined in Subsection 4.2.4 and basic properties are discussed. To complete the set of parametric spaces involved in variational formulations for boundary integral equations the bidual spaces are introduced in Subsection 4.2.5. A short conclusion and an outlook for ongoing work is given in Section 4.3.

The numerical analysis of the high order boundary element methods is addressed in Chapter 5. Our special interest concerns the algebraic properties of the system matrices. After the short introduction given in Section 5.1, the classical method is treated in Section 5.2. The stabilized method is considered in Section 5.3 and the electrostatic case is, finally, considered in Section 5.4. Section 5.5 is most fundamental for the implementation of the high order boundary element methods because explicit formulae for the entries of the system matrices and the right hand side are presented. Chapter 5 is thematically closed by a short outlook given in Section 5.6.

The verification of the theoretical results is the subject of Chapter 6. Section 6.1 serves to recall the basic mathematical task. Results for the high order boundary element methods applied to the scattering problem in its classical and its stabilized formulation are presented in the Sections 6.2 and 6.3, respectively. A conclusion concerning the principal results of convergence and stability of the high order methods is drawn in Section 6.4.

A short summary and an outlook concerning this work are given in Chapter 7.

The appendix comprises four chapters. They contain supplementary material on the numerics of high order methods. They are closely connected to the contents of the chapters of this work and we refer to them at the actual position in the text.

MATHEMATICAL FRAMEWORK

The goal of this chapter is to introduce the basic vocabulary and to state theoretical results needed in the Chapters 3-6. This vocabulary and the fundamental tools for a solution theory concerning partial differential equations stem mainly from functional analysis.

The discussion on functionals starts in Section 2.1 with the case of the differentiable functions defined on manifolds M^n embedded in the Euclidean space \mathbb{R}^3 . The outcome of the first section is the definition of differentiable manifolds and the introduction of differential operators for the so-called smooth case. The closing example of Section 2.1 clarifies, however, that these regularity assumptions are too restrictive. Lipschitz manifolds which appear most often in applications do not belong to the class of differentiable manifolds. To develop an analogous vocabulary for this situation, we need two more concepts from functional analysis. The first are the distributions introduced in Section 2.2 and the second are the Hilbert spaces explained in Section 2.3. A special class of Hilbert spaces is defined in Section 2.4. The so-called energy spaces contain square integrable functions with square integrable derivatives. Due to this last property, the energy spaces are appropriate within the context of partial differential equations. For boundary element methods, we further need the so-called trace spaces introduced in Section 2.5.

The results of the Sections 2.1-2.5 are used at many places in this work and it might help to get an idea of their central role before we go into detail. To apply theorems from functional analysis one needs a functional setting, i.e., a topological vector space and its dual space, the space of all functionals defined on the vector space. A realization of the dual space is explained when a representation of any functional is known. In general vector spaces, we call such a representation a duality. In a Hilbert space, a possible duality is given by the inner product. There is a crucial difference between finite and infinite-dimensional vector spaces. A vector space of finite dimension n identifies naturally with \mathbb{R}^n and, therefore, its topology is simple. Infinite-dimensional vector spaces do not identify with \mathbb{R}^n and their topology is more difficult. It turns out that the smooth setting discussed in Section 2.1 leads to a finite-dimensional setting with Euclidean structures whereas the energy and trace spaces are infinite-dimensional and, thus, their topology is much more complicated. However, on an abstract level, the smooth setting from Section 2.1 and the setting induced by square integrable functions from Section 2.4 and Section 2.5 are very similar. Of particular importance here is the characterization of differential operators as functionals on tangent spaces. Finally, it is not the vocabulary which changes but the duality pairing.

2.1. Manifolds

The boundary element methods are numerical schemes to solve boundary value problems. This means that we seek a solution of a partial differential equation in a three-dimensional domain $\Omega \subset \mathbb{R}^3$ under specific boundary conditions on the boundary Γ of Ω . As $\Omega \cup \Gamma$ is the domain of definition of our solution, it is clear that the mathematical theory leading to the boundary element method relies on the topology, the metric structure and the regularity of Ω and Γ . In what concerns the topology, we consider the simplest possible case, i.e., Ω is an open, connected and

simply-connected domain and, therefore, Γ is closed, connected and simply-connected.

In order to describe the metric structure of Ω and Γ , respectively, the metric structure of the background manifold \mathbb{R}^3 must be stated first. We assume \mathbb{R}^3 to be Euclidean space spanned by the standard basis $\{\mathbf{e}_l\}_{l=1}^3$. A point $P \in \mathbb{R}^3$ possesses a vector representation which is typically denoted \mathbf{x} with Cartesian coordinates x_l , $l = 1, 2, 3$, i.e.,

$$\mathbf{x} = \sum_{l=1}^3 x_l \mathbf{e}_l. \quad (2.1)$$

In the following, the boldface letters \mathbf{x} and \mathbf{y} are used to denote the vector representations in Cartesian coordinates of points in \mathbb{R}^3 . The inner product of any two vectors $\mathbf{x}, \mathbf{y} \in \mathbb{R}^3$ is defined by

$$\mathbf{x} \cdot \mathbf{y} = \sum_{l,k=1}^3 x_l y_k \mathbf{e}_l \cdot \mathbf{e}_k = \sum_{l=1}^3 x_l y_l, \quad (2.2)$$

and the norm of \mathbf{x} is $|\mathbf{x}| = \sqrt{\mathbf{x} \cdot \mathbf{x}}$.

A convenient tool to assess the analytical properties of Ω and Γ is to classify them as manifolds [40].

Definition 1 A set of points $M^n \subset \mathbb{R}^3$ is called a manifold of dimension $n \leq 3$, if there exists a cover of M^n ,

$$M^n = \bigcup_{i=1}^N U_i, \quad (2.3)$$

with mappings $\mathbf{X}_i: U_i \rightarrow \mathbb{R}^n$ such that the domains $U_i \subset M^n$ are open and homeomorphic to their images $\mathbf{X}_i(U_i)$. The mappings \mathbf{X}_i are called charts. Given the Cartesian coordinates \mathbf{x} of a point $P \in U_i$, then \mathbf{X}_i returns the representation of P in terms of parameter coordinates.

For a three-dimensional manifold, the parameter coordinates coincide with the Cartesian coordinates and both are denoted \mathbf{x} . For a two-dimensional manifold, the parameter coordinates are typically denoted $\boldsymbol{\xi}$ and in case $n = 1$ the parameter coordinate ξ is used.

A collection of charts with (2.3) is called an atlas $\mathcal{A} = \{\mathbf{X}_i\}_{i=1}^N$ for M^n . Let $\mathbf{X}_i: U_i \rightarrow \mathbb{R}^n$ and $\mathbf{X}_j: U_j \rightarrow \mathbb{R}^n$, $i, j \in \{1, \dots, N\}$ be two charts with overlapping domains. The continuous injection

$$\mathbf{X}_j \circ \mathbf{X}_i^{-1}: \mathbf{X}_i(U_i \cap U_j) \rightarrow \mathbb{R}^n$$

is called a transition function. Each transition function maps \mathbb{R}^n to \mathbb{R}^n and, thus, we can ask whether it is continuously differentiable. The manifold M^n is said to be of class C^r if all transition functions can be r times continuously differentiable. We call a manifold smooth if the transition functions are infinitely often differentiable. Due to homeomorphy of $\mathbf{X}_i(U_i)$ and $U_i \subset M^n$ the inverse \mathbf{X}_i^{-1} is a parametrization of $U_i \subset M^n$

$$\mathbf{X}_i^{-1}: \mathbf{X}_i(U_i) \rightarrow U_i.$$

When the local parametrizations are given explicitly, the preimages are denoted $V_i = \mathbf{X}_i(U_i)$ and, instead of \mathbf{X}_i^{-1} , we write $\hat{\mathbf{X}}_i$, i.e.,

$$\hat{\mathbf{X}}_i: V_i \rightarrow U_i \subset M^n.$$

An atlas \mathcal{A} for M^n allows us to define differentiable mappings to and from M^n . A function $\varphi: M^n \rightarrow \mathbb{R}$ is said to be of class $C^k(M^n)$ if all functions

$$\hat{\varphi}_i = \varphi \circ \hat{\mathbf{X}}_i: V_i \rightarrow \mathbb{R} \quad \text{with } V_i = \mathbf{X}_i(U_i) \subset \mathbb{R}^n, \quad i = 1, \dots, N, \quad (2.4)$$

are k times continuously differentiable. A function $\varphi \in C^\infty(M^n)$ is called smooth.

The tangent space $T_{\mathbf{x}}M^n$ at $\mathbf{x} \in M^n$ is the subspace of \mathbb{R}^3 consisting of all vectors $\boldsymbol{\tau}$ such that

$$\boldsymbol{\tau} = \frac{d\boldsymbol{\gamma}}{dt}(0) \text{ for some } C^1 \text{ curve } \boldsymbol{\gamma}: (-1, 1) \rightarrow M^n \text{ with } \boldsymbol{\gamma}(0) = \mathbf{x}. \quad (2.5)$$

Thus, $T_{\mathbf{x}}M^n$ is a linear approximation of the manifold at $\mathbf{x} \in M^n$.

We have a closer look now at the types of manifolds which are relevant for this work starting with a smooth, three-dimensional manifold Ω . Obviously, Ω is canonically embedded in \mathbb{R}^3 and all charts are identity mappings. The tangent space $T_{\mathbf{x}}\Omega$ at arbitrary $\mathbf{x} \in \Omega$ coincides with Euclidean space \mathbb{R}^3 and we choose the standard basis $\{\mathbf{e}_l\}_{l=1}^3$ to span $T_{\mathbf{x}}\Omega$. The standard unit vectors are especially orthonormal with respect to the Euclidean metric, meaning that

$$\mathbf{e}_l \cdot \mathbf{e}_k = \delta_{lk} = \begin{cases} 1, & l = k, \\ 0, & l \neq k, \end{cases} \quad l, k = 1, 2, 3. \quad (2.6)$$

We consider smooth functions and vector fields with smooth coefficient functions given in parameter coordinates as follows

$$\begin{aligned} \varphi(\mathbf{x}) &= \hat{\varphi}(\mathbf{x}), \quad \hat{\varphi} \in C^\infty(\Omega), \\ \boldsymbol{\varphi}(\mathbf{x}) &= \sum_{l=1}^3 \hat{\varphi}_l(\mathbf{x}) \mathbf{e}_l, \quad \hat{\varphi}_l \in C^\infty(\Omega). \end{aligned}$$

Although trivial in this case, we indicate the switch from Cartesian to parameter coordinates by the hat. The differential operators ∇ , **curl** and **div** are well defined and yield the well-known formulae

$$\begin{aligned} \nabla \varphi(\mathbf{x}) &= \frac{\partial \hat{\varphi}(\mathbf{x})}{\partial x_1} \mathbf{e}_1 + \frac{\partial \hat{\varphi}(\mathbf{x})}{\partial x_2} \mathbf{e}_2 + \frac{\partial \hat{\varphi}(\mathbf{x})}{\partial x_3} \mathbf{e}_3, \\ \mathbf{curl} \boldsymbol{\varphi}(\mathbf{x}) &= \left(\frac{\partial \hat{\varphi}_3(\mathbf{x})}{\partial x_2} - \frac{\partial \hat{\varphi}_2(\mathbf{x})}{\partial x_3} \right) \mathbf{e}_1 + \left(\frac{\partial \hat{\varphi}_1(\mathbf{x})}{\partial x_3} - \frac{\partial \hat{\varphi}_3(\mathbf{x})}{\partial x_1} \right) \mathbf{e}_2 + \left(\frac{\partial \hat{\varphi}_2(\mathbf{x})}{\partial x_1} - \frac{\partial \hat{\varphi}_1(\mathbf{x})}{\partial x_2} \right) \mathbf{e}_3, \\ \mathbf{div} \boldsymbol{\varphi}(\mathbf{x}) &= \frac{\partial \hat{\varphi}_1(\mathbf{x})}{\partial x_1} + \frac{\partial \hat{\varphi}_2(\mathbf{x})}{\partial x_2} + \frac{\partial \hat{\varphi}_3(\mathbf{x})}{\partial x_3}. \end{aligned}$$

These differential operators are related to each other, meaning that

$$\varphi \xrightarrow{\nabla} \boldsymbol{\varphi} = \sum_{j=1}^3 \hat{\varphi}_j \mathbf{e}_j \xrightarrow{\mathbf{curl}} \boldsymbol{\varphi} = \sum_{j=1}^3 \hat{\varphi}_j \mathbf{e}_j \xrightarrow{\mathbf{div}} \varphi \quad \text{with} \quad \mathbf{curl} \nabla \varphi = \mathbf{0} \quad \text{and} \quad \mathbf{div} \mathbf{curl} \boldsymbol{\varphi} = 0. \quad (2.7)$$

An important observation is that the Riesz representation theorem applies on (2.6) in the sense that \mathbf{e}_l is the unique vector representation of a functional $e^l \in (T_{\mathbf{x}}\Omega)'$ provided the duality pairing between $(T_{\mathbf{x}}\Omega)'$ and $T_{\mathbf{x}}\Omega$ is realized by the inner product (2.2), i.e.,

$$e^l(\mathbf{e}_k) = \mathbf{e}_l \cdot \mathbf{e}_k, \quad l, k = 1, 2, 3. \quad (2.8)$$

The differential operators can, therefore, equivalently be defined in terms of the functionals e^l , $l = 1, 2, 3$. This consideration leads to the notion of the exterior derivatives known from differential geometry [40]. In what concerns the manifold Ω , there is obviously no need to distinguish between these points of view. However, this is a special feature of the canonical embedding of Ω into \mathbb{R}^3 and the orthonormality of the standard basis vectors.

The situation is different for manifolds which are not canonically embedded in \mathbb{R}^3 as it is the case for Γ . Before general Γ are considered, we look at the simpler case of an open domain T

parametrized by a smooth function

$$\hat{\mathbf{X}}: \hat{T} \rightarrow T, \quad \boldsymbol{\xi} \mapsto \mathbf{x}, \quad (2.9)$$

where \hat{T} is the parameter domain. Recall that the parametrization $\hat{\mathbf{X}}$ is a bijection relating the Cartesian coordinates \mathbf{x} and the parameter coordinates $\boldsymbol{\xi}$ of any point $P \in T$ such that $\mathbf{x} = \hat{\mathbf{X}}(\boldsymbol{\xi})$. Thus, differentiation of $\hat{\mathbf{X}}$ with respect to ξ_1 and ξ_2 , respectively, is well defined and yields a holonomic basis of the tangent space $\mathbf{T}_{\mathbf{x}}T$. The tangent vectors and the Jacobian at fixed $\mathbf{x} \in T$ are given by

$$\mathbf{a}_l = \frac{\partial \hat{\mathbf{X}}}{\partial \xi_l}, \quad l = 1, 2, \quad (2.10)$$

$$J = \sqrt{\det(D\hat{\mathbf{X}}^\top D\hat{\mathbf{X}})}, \quad D\hat{\mathbf{X}} = (\mathbf{a}_1 : \mathbf{a}_2) \in \mathbb{R}^{3 \times 2}. \quad (2.11)$$

In the following, the Jacobian also appears as scalar-valued basis function. To emphasize the difference, another notation is used in this case, namely,

$$\mathbf{a}_{12} = |\mathbf{a}_1 \times \mathbf{a}_2| = J. \quad (2.12)$$

We consider smooth functions and tangent vector fields with smooth coefficient functions given in the form

$$\varphi(\mathbf{x}) = \hat{\varphi}^{12}(\boldsymbol{\xi}) \mathbf{a}_{12}, \quad \hat{\varphi}^{12} \in C^\infty(\hat{T}), \quad (2.13)$$

$$\boldsymbol{\varphi}(\mathbf{x}) = \hat{\varphi}^1(\boldsymbol{\xi}) \mathbf{a}_1 + \hat{\varphi}^2(\boldsymbol{\xi}) \mathbf{a}_2 \in \mathbf{T}_{\mathbf{x}}T, \quad \hat{\varphi}^l \in C^\infty(\hat{T}), \quad l = 1, 2. \quad (2.14)$$

Then, applying the classical surface differential operators \mathbf{curl}_Γ and \mathbf{div}_Γ yields [45]

$$\mathbf{curl}_\Gamma \boldsymbol{\varphi} = \frac{1}{J} \left(\frac{\partial(J\hat{\varphi}^{12})}{\partial \xi_2} \mathbf{a}_1 - \frac{\partial(J\hat{\varphi}^{12})}{\partial \xi_1} \mathbf{a}_2 \right), \quad (2.15)$$

$$\mathbf{div}_\Gamma \boldsymbol{\varphi} = \frac{1}{J} \left(\frac{\partial(J\hat{\varphi}^1)}{\partial \xi_1} + \frac{\partial(J\hat{\varphi}^2)}{\partial \xi_2} \right). \quad (2.16)$$

These differential operators are related to each other, meaning that

$$\varphi = \hat{\varphi}^{12} \mathbf{a}_{12} \xrightarrow{\mathbf{curl}_\Gamma} \boldsymbol{\varphi} = \hat{\varphi}^1 \mathbf{a}_1 + \hat{\varphi}^2 \mathbf{a}_2 \xrightarrow{\mathbf{div}_\Gamma} \varphi = \hat{\varphi} \quad \text{with} \quad \mathbf{div}_\Gamma \mathbf{curl}_\Gamma \boldsymbol{\varphi} = 0. \quad (2.17)$$

The tangent vectors $\{\mathbf{a}_l\}_{l=1}^2$, are intrinsically defined and they are, in general, neither normed nor orthogonal to each other with respect to the Euclidean metric and the exterior derivatives will, therefore, not canonically identify with the classical surface differential operators (2.15) and (2.16). In order to show this, we consider a holonomic basis $\{\mathbf{a}^l\}_{l=1}^2$ of the dual space $(\mathbf{T}_{\mathbf{x}}T)'$ and, further, smooth functions and functionals on the tangent space with smooth coefficient functions given in the form

$$\varphi(\mathbf{x}) = \hat{\varphi}(\boldsymbol{\xi}), \quad \hat{\varphi} \in C^\infty(\hat{T}), \quad (2.18)$$

$$\underline{\boldsymbol{\varphi}}(\mathbf{x}) = \hat{\varphi}_1(\boldsymbol{\xi}) \mathbf{a}^1 + \hat{\varphi}_2(\boldsymbol{\xi}) \mathbf{a}^2 \in (\mathbf{T}_{\mathbf{x}}T)', \quad \hat{\varphi}_l \in C^\infty(\hat{T}), \quad l = 1, 2. \quad (2.19)$$

Then, applying the exterior derivatives d_0 and d_1 yields [40]

$$d_0\varphi = \frac{\partial\hat{\varphi}}{\partial\xi_1}a^1 + \frac{\partial\hat{\varphi}}{\partial\xi_2}a^2, \quad (2.20)$$

$$d_1\underline{\varphi} = \left(\frac{\partial\hat{\varphi}_2}{\partial\xi_1} - \frac{\partial\hat{\varphi}_1}{\partial\xi_2}\right)a^{12}, \quad a^{12} = a^1 \wedge a^2, \quad (2.21)$$

where \wedge denotes the wedge product known from differential forms. The exterior derivatives are related to each other, meaning that

$$\varphi = \hat{\varphi} \xrightarrow{d_0} \underline{\varphi} = \hat{\varphi}_1 a^1 + \hat{\varphi}_2 a^2 \xrightarrow{d_1} \underline{\varphi} = \hat{\varphi}_{12} a^{12} \quad \text{with} \quad d_1 d_0 \varphi = 0. \quad (2.22)$$

Obviously, the definition of the operators d_0 and d_1 requires nothing but a holonomic basis of $(T_{\mathbf{x}}T)'$. The path-leading idea is to pick a specific basis among the infinitely many possible bases spanning $(T_{\mathbf{x}}T)'$. We choose the basis functionals such that

$$a^l(\mathbf{a}_k) = \delta_{lk}, \quad l, k = 1, 2. \quad (2.23)$$

Thus, the functionals $a^l, l = 1, 2$, belong to the tangent vectors $\mathbf{a}_l, l = 1, 2$, and the complete set $\{a^l, \mathbf{a}_l\}_{l=1}^2$ is called a bidual basis. Once, a bidual basis is determined, a^{12} is given by $a^{12} = a^1 \wedge a^2$ and it must hold

$$a^{12}(\mathbf{a}_{12}) = 1. \quad (2.24)$$

So far, we specified properties for the functionals of the bidual basis, however, we did not specify the duality pairing in (2.23). Also there are many possible realizations. The one we choose relies on the metric structure of the background manifold \mathbb{R}^3 . To obtain the vector representation \mathbf{a}^l of the functional a^l for $l = 1, 2$, we require

$$a^l(\mathbf{a}_k) = \mathbf{a}^l \cdot \mathbf{a}_k = \delta_{lk}, \quad l, k = 1, 2. \quad (2.25)$$

Thus, our construction is extrinsic and, in order to satisfy the condition (2.25), we need the unit normal vector given by

$$\mathbf{n} = J^{-1}\mathbf{a}_1 \times \mathbf{a}_2. \quad (2.26)$$

Then, (2.25) and (2.24) is satisfied for

$$\mathbf{a}^1 = J^{-1}\mathbf{n} \times \mathbf{a}_2, \quad \mathbf{a}^2 = J^{-1}\mathbf{a}_1 \times \mathbf{n}, \quad (2.27)$$

$$\mathbf{a}^{12} = |\mathbf{a}^1 \times \mathbf{a}^2| = J^{-1}. \quad (2.28)$$

In the following, the boldface letters $\mathbf{a}^l, l = 1, 2$, and \mathbf{a}^{12} denote the vector representations (2.27) and (2.28) of the corresponding functionals. Note, that $\{\mathbf{a}^l\}_{l=1}^2$ is also a holonomic basis for $T_{\mathbf{x}}T$.

In terms of the surface differential operators, the identifying of functionals with their vector representation yields, consequently,

$$\underline{\varphi}(\mathbf{x}) \hat{=} \varphi(\mathbf{x}) = \hat{\varphi}_{12}(\boldsymbol{\xi})\mathbf{a}^{12}, \quad \hat{\varphi} \in C^\infty(\hat{T}), \quad (2.29)$$

$$\underline{\varphi}(\mathbf{x}) \hat{=} \varphi(\mathbf{x}) = \hat{\varphi}_1(\boldsymbol{\xi})\mathbf{a}^1 + \hat{\varphi}_2(\boldsymbol{\xi})\mathbf{a}^2 \in T_{\mathbf{x}}T, \quad \hat{\varphi}_l \in C^\infty(\hat{T}), \quad l = 1, 2. \quad (2.30)$$

The corresponding differential operators are denoted surface gradient ∇_Γ and scalar-valued surface

curl operator curl_Γ and it holds

$$\nabla_\Gamma \varphi = \frac{\partial \hat{\varphi}}{\partial \xi_1} \mathbf{a}^1 + \frac{\partial \hat{\varphi}}{\partial \xi_2} \mathbf{a}^2, \quad (2.31)$$

$$\text{curl}_\Gamma \varphi = \left(\frac{\partial \hat{\varphi}_2}{\partial \xi_1} - \frac{\partial \hat{\varphi}_1}{\partial \xi_2} \right) \mathbf{a}^{12}. \quad (2.32)$$

These differential operators are related to each other, meaning that

$$\varphi = \hat{\varphi} \xrightarrow{\nabla_\Gamma} \boldsymbol{\varphi} = \hat{\varphi}_1 \mathbf{a}^1 + \hat{\varphi}_2 \mathbf{a}^2 \xrightarrow{\text{curl}_\Gamma} \varphi = \hat{\varphi}_{12} \mathbf{a}^{12} \quad \text{with} \quad \text{curl}_\Gamma \nabla_\Gamma \varphi = 0, \quad (2.33)$$

The difference between (2.22) and (2.33) is that the original sequence (2.22) is based on functionals and, therefore, it is metric-free. The sequence (2.33) is not metric-free since the functionals are realized and this always requires a metric structure – in our case it is the inner product of \mathbb{R}^3 .

Finally, the sequences on the level of vector fields, (2.33) and (2.17), are related by the commuting diagram

$$\begin{array}{ccccc} \varphi = \hat{\varphi} & \xrightarrow{\nabla_\Gamma} & \boldsymbol{\varphi} = \hat{\varphi}_1 \mathbf{a}^1 + \hat{\varphi}_2 \mathbf{a}^2 & \xrightarrow{\text{curl}_\Gamma} & \varphi = \hat{\varphi}_{12} \mathbf{a}^{12} \\ \downarrow 1 & & \downarrow \mathbf{n} \times & & \downarrow 1 \\ \varphi = J^{-1} \hat{\varphi} \mathbf{a}_{12} & \xrightarrow{\text{curl}_\Gamma} & \boldsymbol{\varphi} = J^{-1} (\hat{\varphi}_2 \mathbf{a}_1 - \hat{\varphi}_1 \mathbf{a}_2) & \xrightarrow{\text{div}_\Gamma} & \varphi = J^{-1} \hat{\varphi}_{12}. \end{array} \quad (2.34)$$

Recall that Γ denotes a closed, connected and simply-connected manifold of dimension two. For now, Γ is assumed smooth and exactly described by an atlas of the form

$$\Gamma = \bigcup_{i=1}^N \overline{\Gamma}_i \quad \text{with} \quad \Gamma_i \cap \Gamma_j = \emptyset \text{ for } i \neq j, \quad \text{and} \quad \hat{\mathbf{X}}_i: \hat{T} \rightarrow \Gamma_i, \quad i = 1, \dots, N. \quad (2.35)$$

Let $\{\mathbf{a}^{i,12}, \mathbf{a}_{i,12}\}$ and $\{\mathbf{a}^{i,k}, \mathbf{a}_{i,k}\}_{k=1}^2$ denote the bidual bases induced by the parametrization $\hat{\mathbf{X}}_i$ of the element Γ_i and consider a function φ given piecewise in parameter coordinates

$$\varphi|_{\Gamma_i} = \hat{\varphi}_i, \quad \hat{\varphi}_i \in C^\infty(\hat{T}), \quad i = 1, \dots, N.$$

We define the surface gradient of the function φ piecewise by

$$(\nabla_\Gamma \varphi)|_{\Gamma_i} = \nabla_\Gamma(\varphi|_{\Gamma_i}), \quad i = 1, \dots, N. \quad (2.36)$$

To render $\nabla_\Gamma \varphi$ well defined on Γ , necessary and sufficient conditions at the intersection points of elements need to be found. Let the two elements Γ_i and Γ_j intersect at \mathbf{x} . The regularity of Γ guarantees that the tangent planes $\mathbf{T}_\mathbf{x}\Gamma_i$, $\mathbf{T}_\mathbf{x}\Gamma_j$ coincide and, without restriction of any kind, we can, therefore, assume that the parametrizations $\hat{\mathbf{X}}_i$, $\hat{\mathbf{X}}_j$ are such that the bidual basis vectors at \mathbf{x} also coincide and there is no need to keep the indices i, j , i.e., let

$$\begin{aligned} \mathbf{a}_l &= \mathbf{a}_{i,l} = \mathbf{a}_{j,l}, & \text{with} \quad \mathbf{a}^l \cdot \mathbf{a}_k &= \delta_{lk}, \quad l, k = 1, 2, \\ \mathbf{a}^l &= \mathbf{a}^{i,l} = \mathbf{a}^{j,l}, \end{aligned} \quad (2.37)$$

and

$$\begin{aligned} \mathbf{a}_{12} &= \mathbf{a}_{i,12} = \mathbf{a}_{j,12}, & \text{with} \quad \mathbf{a}^{12} \cdot \mathbf{a}_{12} &= 1. \\ \mathbf{a}^{12} &= \mathbf{a}^{i,12} = \mathbf{a}^{j,12}, \end{aligned} \quad (2.38)$$

Thus, we obtain at the intersection point \mathbf{x}

$$\nabla_{\Gamma}(\varphi|_{\Gamma_i}) = \frac{\partial \hat{\varphi}_i}{\partial \xi_1} \mathbf{a}^1 + \frac{\partial \hat{\varphi}_i}{\partial \xi_2} \mathbf{a}^2 \quad \text{and} \quad \nabla_{\Gamma}(\varphi|_{\Gamma_j}) = \frac{\partial \hat{\varphi}_j}{\partial \xi_1} \mathbf{a}^1 + \frac{\partial \hat{\varphi}_j}{\partial \xi_2} \mathbf{a}^2, \quad (2.39)$$

and from (2.39) we conclude, that the surface gradient at \mathbf{x} is well defined if

$$\frac{\partial \hat{\varphi}_i}{\partial \xi_l} = \frac{\partial \hat{\varphi}_j}{\partial \xi_l} \quad \text{for } l = 1, 2. \quad (2.40)$$

Let φ be a tangent vector field given piecewise in parameter coordinates

$$\varphi|_{\Gamma_i} = \hat{\varphi}_{i,1} \mathbf{a}^{i,1} + \hat{\varphi}_{i,2} \mathbf{a}^{i,2} \quad \hat{\varphi}_{i,l} \in C^\infty(\hat{T}), \quad l = 1, 2, \quad i = 1, \dots, N. \quad (2.41)$$

We define the scalar-valued surface curl operator piecewise by

$$(\text{curl}_{\Gamma} \varphi)|_{\Gamma_i} = \text{curl}_{\Gamma}(\varphi|_{\Gamma_i}), \quad i = 1, \dots, N, \quad (2.42)$$

and we obtain at the intersection point \mathbf{x}

$$\text{curl}_{\Gamma}(\varphi|_{\Gamma_i}) = \left(\frac{\partial \hat{\varphi}_{i,2}}{\partial \xi_1} - \frac{\partial \hat{\varphi}_{i,1}}{\partial \xi_2} \right) \mathbf{a}^{12} \quad \text{and} \quad \text{curl}_{\Gamma}(\varphi|_{\Gamma_j}) = \left(\frac{\partial \hat{\varphi}_{j,2}}{\partial \xi_1} - \frac{\partial \hat{\varphi}_{j,1}}{\partial \xi_2} \right) \mathbf{a}^{12}, \quad (2.43)$$

and from here, we conclude that the scalar-valued curl operator at \mathbf{x} is well defined if

$$\frac{\partial \hat{\varphi}_{i,2}}{\partial \xi_1} - \frac{\partial \hat{\varphi}_{i,1}}{\partial \xi_2} = \frac{\partial \hat{\varphi}_{j,2}}{\partial \xi_1} - \frac{\partial \hat{\varphi}_{j,1}}{\partial \xi_2}. \quad (2.44)$$

Analogously, the surface differential operators \mathbf{curl}_{Γ} and div_{Γ} are defined piecewise and their definition is independent of the atlas.

So far, we considered smooth manifolds and smooth functions only. Due to regularity, it is clear that differentiation was not an issue. However, whenever the manifold is not differentiable, the surface differential operators cannot be defined as in the smooth case. A more general setting must be considered. For instance, let Γ be the boundary of a Lipschitz polyhedron. This means that Γ is infinitely smooth almost everywhere and the transition functions are Lipschitz continuous. Now, the regularity of Γ does not guarantee that the tangent planes $\mathbf{T}_{\mathbf{x}}\Gamma_i$ and $\mathbf{T}_{\mathbf{x}}\Gamma_j$ at an intersection point \mathbf{x} of two elements Γ_i and Γ_j coincide. This means that the piecewise definition of the surface differential operators is not meaningful. We consider the case that the elements Γ_i and Γ_j share an edge e_{ij} . Without restriction of any kind it is assumed that e_{ij} is parametrized on both elements for $\xi_2 = 0$. Then, it holds for any $\mathbf{x} \in e_{ij}$

$$\mathbf{a}_{i,1} \parallel \mathbf{a}_{j,1}, \quad (2.45)$$

and, in general,

$$\mathbf{a}_{i,2} \not\parallel \mathbf{a}_{j,2}, \quad \mathbf{a}^{i,1} \not\parallel \mathbf{a}^{j,1}, \quad \mathbf{a}^{i,2} \not\parallel \mathbf{a}^{j,2} \quad \text{and} \quad \mathbf{a}_{i,12} \neq \mathbf{a}_{j,12} \quad \text{and} \quad \mathbf{a}^{i,12} \neq \mathbf{a}^{j,12}. \quad (2.46)$$

Thus, even if (2.40) holds, the surface gradient at any $\mathbf{x} \in e_{ij}$ is not uniquely defined by (2.36) since

$$\nabla_{\Gamma}(\varphi|_{\Gamma_i}) = \frac{\partial \hat{\varphi}_i}{\partial \xi_1} \mathbf{a}^{i,1} + \frac{\partial \hat{\varphi}_i}{\partial \xi_2} \mathbf{a}^{i,2} \neq \frac{\partial \hat{\varphi}_j}{\partial \xi_1} \mathbf{a}^{j,1} + \frac{\partial \hat{\varphi}_j}{\partial \xi_2} \mathbf{a}^{j,2} = \nabla_{\Gamma}(\varphi|_{\Gamma_j}). \quad (2.47)$$

However, we may consider the projections with respect to the tangent vectors $\mathbf{a}_{i,1}$ and $\mathbf{a}_{j,1}$, respec-

tively. Provided (2.40), we obtain by use of the biduality of the tangent vectors

$$\nabla_{\Gamma}(\varphi|_{\Gamma_i}) \cdot \mathbf{a}_{i,1} = \frac{\partial \hat{\varphi}_i}{\partial \xi_1} = \nabla_{\Gamma}(\varphi|_{\Gamma_j}) \cdot \mathbf{a}_{j,1} = \frac{\partial \hat{\varphi}_j}{\partial \xi_1}. \quad (2.48)$$

This observation suggests to define the surface gradient in weak sense, meaning that (2.48) holds. However, for points on Γ where more than two elements intersect, even this definition fails because we cannot assume (2.48) anymore. Let us call these points the critical points. A meaningful definition of the surface gradient using (2.48) requires a comprehensive functional setting where the critical points do not matter.

Also, the piecewise definition of the scalar-valued curl operator (2.42) is not unique on any intersection point because of geometrical reasons. However, the surface curl operator is given a weak sense by the piecewise multiplication with $\mathbf{a}_{i,12}$ and $\mathbf{a}_{j,12}$ respectively, because

$$\operatorname{curl}_{\Gamma}(\varphi|_{\Gamma_i}) \cdot \mathbf{a}_{i,12} = \frac{\partial \hat{\varphi}_{i,2}}{\partial \xi_1} - \frac{\partial \hat{\varphi}_{i,1}}{\partial \xi_2} = \operatorname{curl}_{\Gamma}(\varphi|_{\Gamma_j}) \cdot \mathbf{a}_{j,12} = \frac{\partial \hat{\varphi}_{j,2}}{\partial \xi_1} - \frac{\partial \hat{\varphi}_{j,1}}{\partial \xi_2}, \quad (2.49)$$

provided (2.44) holds.

Similarly, consider a function given piecewise in parameter coordinates

$$\varphi|_{\Gamma_i} = \hat{\varphi}^{i,12} \mathbf{a}_{i,12}. \quad (2.50)$$

Due to geometrical reasons, this function is in general not globally continuous, however, we can define weak continuity because

$$\mathbf{a}^{i,12} \cdot \varphi|_{\Gamma_i} = \mathbf{a}^{j,12} \cdot \varphi|_{\Gamma_j}, \quad (2.51)$$

provided

$$\hat{\varphi}^{i,12} = \hat{\varphi}^{j,12}. \quad (2.52)$$

Also, to explain the vector-valued surface curl operator at intersection points on edges a projection is used. With the same notation as above, we obtain

$$J_i \mathbf{a}^{i,2} \cdot \mathbf{curl}_{\Gamma}(\varphi|_{\Gamma_i}) = J_j \mathbf{a}^{j,2} \cdot \mathbf{curl}_{\Gamma}(\varphi|_{\Gamma_j}), \quad (2.53)$$

provided

$$\frac{\partial(J_i \hat{\varphi}_i)}{\partial \xi_l} = \frac{\partial(J_j \hat{\varphi}_j)}{\partial \xi_l} \quad \text{for } l = 1, 2. \quad (2.54)$$

There are some important observations left to state. The non-smoothness of the Lipschitz boundary requires to define the surface differential operators in weak sense. A convenient tool to end with this is to consider the tangent vectors decomposed with respect to bidual basis vectors. We have seen that vectors given in terms of $\mathbf{a}_1, \mathbf{a}_2$ are classical tangent vectors and vectors given in terms of $\mathbf{a}^1, \mathbf{a}^2$ are vector representations of functionals. The construction of the bidual basis vectors requires the well-definedness of point evaluation and relies on the metric structure of Euclidean space \mathbb{R}^3 . In order to generalize the definition of differential operators and make them robust with respect to critical intersection points, the inner product of Euclidean space is not appropriate. The Sobolev spaces introduced in Section 2.5 provide an appropriate functional setting.

Note, that the manifold Ω is always smooth and, thus, the only regularity assumption to be weakened concerns the regularity of the functions.

From now on, $\Omega \subset \mathbb{R}^3$ denotes an open domain of dimension three. Its boundary Γ is a manifold of dimension two, which is non-canonically embedded in Euclidean space \mathbb{R}^3 . Γ is given in the form (2.35) where the parametrizations are smooth and globally Lipschitz continuous or r times continuously differentiable with $r \geq 1$.

2.2. Distributions

The space of test functions and the space of distributions are defined in this section. The functional setting connecting these two spaces will be used in Chapter 3 to reformulate the boundary value problems we are interested in.

Definition 2 1. The space of infinitely smooth functions with compact support in \mathbb{R}^3 is

$$\mathcal{D}(\mathbb{R}^3) = \{ \varphi \in \mathcal{C}^\infty(\mathbb{R}^3) : \exists K \subset \mathbb{R}^3; \text{compact}, \text{supp } \varphi \subset K \} .$$

$\mathcal{D}(\mathbb{R}^3)$ is called the space of test functions. A sequence $(\varphi_j)_{j=1}^\infty$ is said to converge towards $\varphi \in \mathcal{D}(\mathbb{R}^3)$ if there exists a compact set $K \subset \mathbb{R}^3$ such that $\text{supp } \varphi_j \subset K$ for all j

$$\lim_{j \rightarrow \infty} \sup_{\mathbf{x} \in K} |D^\alpha(\varphi_j(\mathbf{x}) - \varphi(\mathbf{x}))| = 0 ,$$

for all $\alpha \in \mathbb{N}_0^3$ [58,59]. Due to [57], the topology of the test function space is defined as inductive limit with respect to the compact sets $K \subset \mathbb{R}^3$ of the subspaces

$$\text{for } K \subset \mathbb{R}^3 \text{ compact : } \mathcal{D}_K(\mathbb{R}^3) = \{ \varphi \in \mathcal{C}^\infty(\mathbb{R}^3) : \text{supp } \varphi \subset K \} .$$

We use the notation $\mathcal{D}(\mathbb{R}^3)$ for the space of three-dimensional test vector fields, i.e., each component belongs to $\mathcal{D}(\mathbb{R}^3)$.

2. A continuous, linear map $V : \mathcal{D}(\mathbb{R}^3) \rightarrow \mathbb{C}$ is called distribution. Let V be a distribution, then, for all compact sets $K \subset \mathbb{R}^3$, there are constants $c = c(K) > 0$ and $m \in \mathbb{N}_0$ with

$$\forall \varphi \in \mathcal{D}(\mathbb{R}^3), \text{supp } \varphi \subset K : |V(\varphi)| < c \max_{|\alpha| \leq m} \sup_{\mathbf{x} \in K} |D^\alpha \varphi(\mathbf{x})| ,$$

for $\alpha, |\alpha| = \sum_{i=1}^3 \alpha_i \leq m$. The angular brackets denote the evaluation of a functional on a test function

$$V \in \mathcal{D}(\mathbb{R}^3)', \varphi \in \mathcal{D}(\mathbb{R}^3) : V(\varphi) = \langle V, \varphi \rangle .$$

We use the notation $\mathcal{D}(\mathbb{R}^3)'$ for the space of distributions on $\mathcal{D}(\mathbb{R}^3)$.

Moreover, we define the support of a distribution.

Definition 3 A distribution $V \in \mathcal{D}(\mathbb{R}^3)'$ is said to vanish on an open subset $G \subset \mathbb{R}^3$ if its evaluation on every test function whose support is contained in G vanishes:

$$\forall \varphi \in \mathcal{D}(\mathbb{R}^3), \text{supp } \varphi \subset G : \langle V, \varphi \rangle = 0 .$$

The complement of this subset G is called the support of the distribution V

$$\text{supp } V \subset \mathbb{R}^3 \setminus G .$$

2.3. Hilbert Spaces

Besides the test functions and the distributions, complex Hilbert spaces are needed in this work. A Hilbert space H is a complete vector space equipped with an inner product. The inner product satisfies

$$\begin{aligned} (u, v)_H &= \overline{(v, u)_H} , \\ (\alpha u_1 + \beta u_2, v)_H &= \alpha (u_1, v)_H + \beta (u_2, v)_H , \\ (u, u)_H &\geq 0, \quad (u, u)_H = 0 \Leftrightarrow u = 0 . \end{aligned}$$

Thus, it is a sesquilinear map, which induces a norm on H by

$$\|v\|_H = \sqrt{(v, v)_H}.$$

H turns into a Banach space with respect to this norm.

Classical examples for Hilbert spaces are the Lebesgue spaces $L^2(\mathbb{R}^n)$ equipped with the inner product

$$(u, v)_{L^2(\mathbb{R}^n)} = \int_{\mathbb{R}^n} \bar{v} u \, dL^n.$$

Here, L^n denotes the Lebesgue measure of \mathbb{R}^n [59]. The associated L^2 -norm of a function $u \in L^2(\mathbb{R}^n)$ is finite, i.e.,

$$\|u\|_{L^2(\mathbb{R}^n)} = \left(\int_{\mathbb{R}^n} |u|^2 \, dL^n \right)^{\frac{1}{2}} < \infty.$$

In what concerns Hilbert spaces, one of the most important results is the representation theorem of Riesz [59]. It says that the spaces H and H' are isomorphic to each other. However, the duality pairing which characterizes the dual space H' is not specified by the Riesz isomorphism: let H denote a Hilbert space with inner product $(\cdot, \cdot)_H$. We consider H' equipped with the norm

$$\|V\|_{H'} = \sup_{\|u\|_H=1} |V(u)|.$$

Then, for any $v \in H$, $V(u) = (v, u)_H$ defines a continuous linear functional

$$V \in H' \quad \text{with} \quad \|V\|_{H'} = \|v\|_H.$$

It follows from the Riesz theorem, that for any $V \in H'$ there is a unique $v \in H$ such that

$$\forall u \in H : \quad V(u) = (v, u)_H \quad \text{with} \quad \|V\|_{H'} = \|v\|_H.$$

Evidently, there exists an isometric isomorphism J

$$v \in H : \quad J(v) = V \in H',$$

and one can define an abstract duality pairing on $H' \times H$ by

$$\langle V, u \rangle_{H' \times H} = V(u) = (J^{-1}V, u)_H, \quad \text{for } V \in H', \quad u \in H.$$

In this example, H' is an abstract dual space in the sense that we have no characterization for the elements of H' other than the assertion that they are continuous linear functionals on H . In order to have a concrete characterization for the elements in the dual space, we can choose, for instance, the inner product of H and identify the Hilbert space itself with its dual, i.e., $H' \hat{=} H$.

However, this is not the only possible choice: to realize the dual space of the Sobolev spaces on \mathbb{R}^n another duality is used, for instance. Sobolev spaces can be defined by the Fourier transform, i.e.,

$$\begin{aligned} H &= H^s(\mathbb{R}^n) = \left\{ u \in L^2(\mathbb{R}^n), (1 + |\boldsymbol{\xi}|^2)^{\frac{s}{2}} \hat{u}(\boldsymbol{\xi}) \in L^2(\mathbb{R}^n) \right\}, \quad s \geq 0, \quad n \geq 1, \\ (u, v)_s &= \int_{\mathbb{R}^n} (1 + |\boldsymbol{\xi}|^2)^s \overline{\hat{v}(\boldsymbol{\xi})} \hat{u}(\boldsymbol{\xi}) \, dL^n(\boldsymbol{\xi}), \end{aligned}$$

where \hat{u} denotes the unique extension of the Fourier transform of a square integrable function [59].

The Plancherel identity

$$\forall u, v \in L^2(\mathbb{R}^n) : \int_{\mathbb{R}^n} u(\mathbf{x}) v(\mathbf{x}) dL^n(\mathbf{x}) = \int_{\mathbb{R}^n} \hat{u}(\boldsymbol{\xi}) \hat{v}(\boldsymbol{\xi}) dL^n(\boldsymbol{\xi})$$

and the dense embedding $H \hookrightarrow L^2(\mathbb{R}^n)$ are necessary tools to show that

$$H' \cong H^{-s}(\mathbb{R}^n) = \left\{ f \in \mathcal{S}'(\mathbb{R}^n), \quad (1 + |\boldsymbol{\xi}|^2)^{-\frac{s}{2}} \hat{f}(\boldsymbol{\xi}) \in L^2(\mathbb{R}^n) \right\}$$

is a realization for the dual of H . Here, $\mathcal{S}(\mathbb{R}^n)$ denotes the Schwartz space of infinitely smooth functions [59]. It is important to note that the realization of the duality pairing is the inner product of $L^2(\mathbb{R}^n)$, extended to $H' \times H$. The first advantage of this construction is that the duality pairing results from the inner product of $L^2(\mathbb{R}^n)$ and not from the inner product of H which might be more complicated. The second is that one obtains a precise characterization for H' in terms of regularity. In this context, one often calls the L^2 -space the pivot space meaning that it occupies a position that is precisely between H and H' .

Let X be a topological, linear space and H a Hilbert space and the embedding $i : X \rightarrow H$ is continuous. By this, we mean, that $X \subset H$ and any convergent sequence $x_n \rightarrow 0$ in X implies $i(x_n) \rightarrow 0$ in H , we write $X \hookrightarrow H$. The continuity of a $V \in H'$ means, moreover, that $y_n \rightarrow 0$ in H implies $V(y_n) \rightarrow 0$ in \mathbb{R} . Then, it is evident that the continuous embedding $X \hookrightarrow H$ implies the continuous embedding $H' \hookrightarrow X'$, i.e.,

$$i' : H' \rightarrow X' \quad \text{is continuous.}$$

If $i : X \rightarrow H$ has a dense image, then $i' : H' \rightarrow X'$ is injective. To see this, suppose that $i(X)$ is dense in H , and $i'(V) = 0$. Then

$$\forall x \in X : \langle i'(V), x \rangle = 0.$$

But

$$\langle i'(V), x \rangle = \langle V, i(x) \rangle = 0$$

and since the elements $i(x)$ are dense in H and V is continuous on H , V must be zero whenever $i'(V)$ is zero. From this discussion it follows that the dual space of any Hilbert space in which the test functions $\mathcal{D}(\mathbb{R}^3)$ or $\mathcal{D}'(\mathbb{R}^3)$ are densely included can be identified with a subspace of the space of distributions $\mathcal{D}'(\mathbb{R}^n)$, or $\mathcal{D}'(\mathbb{R}^3)$.

We end this section with the definition of an important class of Hilbert spaces. Let M^n denote a Lipschitz manifold of dimension n , $1 \leq n \leq 3$ embedded in \mathbb{R}^3 . Similar to the $L^2(\mathbb{R}^n)$ case, we classify functions defined on M^n according to their square integrability on the manifold. Instead of the Lebesgue measure L^n , the Hausdorff measure must be employed in order to take into account the curvature of the manifold. When M^n is parametrized by a Lipschitz continuous function [59]

$$\hat{\mathbf{X}} : \boldsymbol{\xi} \rightarrow \mathbf{x}, \quad \boldsymbol{\xi} = (\xi_1, \dots, \xi_n)^\top, \quad \mathbf{x} = (x_1, x_2, x_3)^\top,$$

we obtain the explicit formulae for the Hausdorff measure H^n in terms of the parametrization $\hat{\mathbf{X}}$ and the usual n -dimensional Lebesgue measure L^n , namely,

$$dH^n = J dL^n, \quad J = \sqrt{\det(D\hat{\mathbf{X}}^\top D\hat{\mathbf{X}})}, \quad D\hat{\mathbf{X}} = \left(\frac{\partial \hat{\mathbf{X}}_i}{\partial \xi_j} \right)_{ij} \in \mathbb{R}^{3 \times n}, \quad i = 1, \dots, 3, \quad j = 1, \dots, n.$$

Definition 4 Let $M^n \subset \mathbb{R}^3$ be a Lipschitz manifold of dimension n .

1. The space of square integrable functions

$$L^2(M^n) = \{v: M^n \rightarrow \mathbb{C} : \|v\|_{L^2(M^n)} < \infty\}, \quad \|v\|_{L^2(M^n)}^2 = \int_{M^n} |v|^2 dH^n \quad (2.55)$$

is a Hilbert space endowed with the inner product [59],

$$\forall u, v \in L^2(M^n) : (u, v)_{M^n} = \int_{M^n} \bar{v}u dH^n. \quad (2.56)$$

2. The space of square integrable vector fields

$$\mathbf{L}^2(M^n) = \{\mathbf{v}: M^n \rightarrow \mathbb{C}^3 : \|\mathbf{v}\|_{\mathbf{L}^2(M^n)} < \infty\}, \quad \|\mathbf{v}\|_{\mathbf{L}^2(M^n)}^2 = \int_{M^n} |\mathbf{v}|^2 dH^n \quad (2.57)$$

is a Hilbert space endowed with the inner product

$$\forall \mathbf{u}, \mathbf{v} \in \mathbf{L}^2(M^n) : (\mathbf{u}, \mathbf{v})_{M^n} = \int_{M^n} \bar{\mathbf{v}} \cdot \mathbf{u} dH^n. \quad (2.58)$$

Table 2.1 contains a list of the notations we choose in the following for the representatives of manifolds M^n of specific dimension n .

Table 2.1.: Notations for manifolds of specific dimension.

Manifold M^n	Dimension n	Differential dH^n
Ω	3	dx
Γ	2	$d\sigma$
γ	1	dl

2.4. Energy spaces

Appropriate Hilbert spaces for solving problems of theoretical physics are the energy spaces [25]

$$H^1(\Omega), \quad \mathbf{H}(\mathbf{curl}, \Omega), \quad \mathbf{H}(\mathbf{div}, \Omega).$$

All of them are defined as the completion of the test function spaces with respect to graph norms. The graph norms contain differential operators. The energy spaces naturally inherit the Hilbert space structure of $L^2(\Omega)$ and $\mathbf{L}^2(\Omega)$, respectively. Different from the Lebesgue spaces, the energy spaces guarantee the existence of weak derivatives. Thus, it is natural to integrate by parts because integration and differentiation are defined in L^2 -sense. However, the extension of the integration by parts formulae on energy spaces is non-trivial and it must be postponed until we know more about trace spaces. But certainly, the embeddings

$$H^1(\Omega) \hookrightarrow \mathcal{D}(\mathbb{R}^3)', \quad \mathbf{H}(\mathbf{curl}, \Omega) \hookrightarrow \mathcal{D}(\mathbb{R}^3)', \quad \mathbf{H}(\mathbf{div}, \Omega) \hookrightarrow \mathcal{D}(\mathbb{R}^3)'$$

allow integration by parts in distributional sense. The subject of this section is to develop explicit formulae for this integration by parts.

The Hilbert spaces introduced in Definition 4 give rise to an important class of distributions.

1. For an arbitrary compact subset $K \subset \mathbb{R}^3$ and arbitrary $\varphi \in \mathcal{D}(\mathbb{R}^3)$ with $\text{supp } \varphi \subset K$ and $v \in L^2(\mathbb{R}^3)$, it holds

$$|(v, \varphi)_{\mathbb{R}^3}| \leq \|v\|_{L^2(\mathbb{R}^3)} \|\varphi\|_{L^2(\mathbb{R}^3)} \leq |K| \|v\|_{L^2(\mathbb{R}^3)} \sup_{\mathbf{x} \in K} |\varphi(\mathbf{x})|.$$

Thus, according to Definition 2, v can be identified with a distribution $V \in \mathcal{D}(\mathbb{R}^3)'$. We call V a regular distribution and we write

$$\forall \varphi \in \mathcal{D}(\mathbb{R}^3) : \quad \langle V, \varphi \rangle = (v, \varphi)_{\mathbb{R}^3}.$$

If it is clear from the context, $v \in L^2(\mathbb{R}^3)$ and $V \in \mathcal{D}(\mathbb{R}^3)'$ are not distinguished.

2. Let us consider $v \in L^2(\Omega)$. Thus, v is given only in $\Omega \subset \mathbb{R}^3$. By the operator

$$E: v \mapsto \tilde{v}, \quad \tilde{v} = \begin{cases} v & \text{in } \Omega, \\ 0 & \text{in } \Omega^c, \end{cases}$$

a continuous embedding $L^2(\Omega) \hookrightarrow L^2(\mathbb{R}^3)$ is defined because

$$\|E(v)\|_{L^2(\mathbb{R}^3)} = \|v\|_{L^2(\Omega)}.$$

According to the first example, $E(v) \in L^2(\mathbb{R}^3)$ identifies with a distribution $V \in \mathcal{D}(\mathbb{R}^3)'$ in the sense that

$$\forall \varphi \in \mathcal{D}(\mathbb{R}^3) : \quad \langle V, \varphi \rangle = (E(v), \varphi)_{\mathbb{R}^3} = (v, \varphi)_{\Omega}.$$

By the use of the weak differentiation the energy spaces are defined [44, 59].

$$H^1(\mathbb{R}^3) = \{v \in L^2(\mathbb{R}^3) : \nabla v \in \mathbf{L}^2(\mathbb{R}^3)\}, \quad (2.59)$$

$$\mathbf{H}(\mathbf{curl}, \mathbb{R}^3) = \{\mathbf{v} \in \mathbf{L}^2(\mathbb{R}^3) : \mathbf{curl} \mathbf{v} \in \mathbf{L}^2(\mathbb{R}^3)\}, \quad (2.60)$$

$$\mathbf{H}(\mathbf{div}, \mathbb{R}^3) = \{\mathbf{v} \in \mathbf{L}^2(\mathbb{R}^3) : \mathbf{div} \mathbf{v} \in L^2(\mathbb{R}^3)\}. \quad (2.61)$$

$H^1(\mathbb{R}^3)$, $\mathbf{H}(\mathbf{curl}, \mathbb{R}^3)$ and $\mathbf{H}(\mathbf{div}, \mathbb{R}^3)$ turn into Hilbert spaces equipped with the inner products

$$u, v \in H^1(\mathbb{R}^3) : \quad (u, v)_{1, \mathbb{R}^3} = (u, v)_{\mathbb{R}^3} + (\nabla u, \nabla v)_{\mathbb{R}^3}, \quad (2.62)$$

$$\mathbf{u}, \mathbf{v} \in \mathbf{H}(\mathbf{curl}, \mathbb{R}^3) : \quad (\mathbf{u}, \mathbf{v})_{\mathbf{curl}, \mathbb{R}^3} = (\mathbf{u}, \mathbf{v})_{\mathbb{R}^3} + (\mathbf{curl} \mathbf{u}, \mathbf{curl} \mathbf{v})_{\mathbb{R}^3}, \quad (2.63)$$

$$\mathbf{u}, \mathbf{v} \in \mathbf{H}(\mathbf{div}, \mathbb{R}^3) : \quad (\mathbf{u}, \mathbf{v})_{\mathbf{div}, \mathbb{R}^3} = (\mathbf{u}, \mathbf{v})_{\mathbb{R}^3} + (\mathbf{div} \mathbf{u}, \mathbf{div} \mathbf{v})_{\mathbb{R}^3}. \quad (2.64)$$

The corresponding graph norms are

$$v \in H^1(\mathbb{R}^3) : \quad \|v\|_{H^1(\mathbb{R}^3)} = ((v, v)_{\mathbb{R}^3} + (\nabla v, \nabla v)_{\mathbb{R}^3})^{\frac{1}{2}}, \quad (2.65)$$

$$\mathbf{v} \in \mathbf{H}(\mathbf{curl}, \mathbb{R}^3) : \quad \|\mathbf{v}\|_{\mathbf{H}(\mathbf{curl}, \mathbb{R}^3)} = ((\mathbf{v}, \mathbf{v})_{\mathbb{R}^3} + (\mathbf{curl} \mathbf{v}, \mathbf{curl} \mathbf{v})_{\mathbb{R}^3})^{\frac{1}{2}}, \quad (2.66)$$

$$\mathbf{v} \in \mathbf{H}(\mathbf{div}, \mathbb{R}^3) : \quad \|\mathbf{v}\|_{\mathbf{H}(\mathbf{div}, \mathbb{R}^3)} = ((\mathbf{v}, \mathbf{v})_{\mathbb{R}^3} + (\mathbf{div} \mathbf{v}, \mathbf{div} \mathbf{v})_{\mathbb{R}^3})^{\frac{1}{2}}. \quad (2.67)$$

The functions and vector fields, respectively, have square integrable derivatives and the following identities hold true for all $\varphi \in \mathcal{D}(\mathbb{R}^3)$ and $\varphi \in \mathcal{D}(\mathbb{R}^3)$

$$v \in H^1(\mathbb{R}^3) : \quad \langle \nabla v, \varphi \rangle = -\langle v, \mathbf{div} \varphi \rangle = -(v, \mathbf{div} \varphi)_{\mathbb{R}^3} = (\nabla v, \varphi)_{\mathbb{R}^3}, \quad (2.68)$$

$$\mathbf{v} \in \mathbf{H}(\mathbf{curl}, \mathbb{R}^3) : \quad \langle \mathbf{curl} \mathbf{v}, \varphi \rangle = \langle \mathbf{v}, \mathbf{curl} \varphi \rangle = (\mathbf{v}, \mathbf{curl} \varphi)_{\mathbb{R}^3} = (\mathbf{curl} \mathbf{v}, \varphi)_{\mathbb{R}^3}, \quad (2.69)$$

$$\mathbf{v} \in \mathbf{H}(\mathbf{div}, \mathbb{R}^3) : \quad \langle \mathbf{div} \mathbf{v}, \varphi \rangle = -\langle \mathbf{v}, \nabla \varphi \rangle = -(\mathbf{v}, \nabla \varphi)_{\mathbb{R}^3} = (\mathbf{div} \mathbf{v}, \varphi)_{\mathbb{R}^3}. \quad (2.70)$$

For truncated test functions

$$\varphi \in \mathcal{D}(\overline{\Omega}) = \{\varphi = \psi|_{\overline{\Omega}}, \psi \in \mathcal{D}(\mathbb{R}^3)\} \quad (2.71)$$

and truncated test vector fields

$$\boldsymbol{\varphi} \in \mathcal{D}(\overline{\Omega}) = \{\boldsymbol{\varphi} = \boldsymbol{\psi}|_{\overline{\Omega}}, \boldsymbol{\psi} \in \mathcal{D}(\mathbb{R}^3)\}, \quad (2.72)$$

we distinguish the following traces on the boundary Γ .

Definition 5 Let Ω be a bounded Lipschitz domain with a simply connected boundary Γ , the unit normal vector exists almost everywhere on Γ and is denoted by \mathbf{n} . Let $\mathbf{x} \in \Gamma$, $\mathbf{y} \in \Omega$, for $\boldsymbol{\varphi} \in \mathcal{D}(\overline{\Omega})$ and $\varphi \in \mathcal{D}(\overline{\Omega})$, we define

$$\gamma_0 \varphi(\mathbf{x}) = \lim_{\mathbf{y} \rightarrow \mathbf{x}} \varphi(\mathbf{y}), \quad (2.73)$$

$$\gamma_1 \varphi(\mathbf{x}) = \lim_{\mathbf{y} \rightarrow \mathbf{x}} \mathbf{n}(\mathbf{x}) \cdot \nabla \varphi(\mathbf{y}), \quad (2.74)$$

$$\gamma_R \boldsymbol{\varphi}(\mathbf{x}) = \lim_{\mathbf{y} \rightarrow \mathbf{x}} (\mathbf{n}(\mathbf{x}) \times \boldsymbol{\varphi}(\mathbf{y})) \times \mathbf{n}(\mathbf{x}), \quad (2.75)$$

$$\gamma_D \boldsymbol{\varphi}(\mathbf{x}) = \lim_{\mathbf{y} \rightarrow \mathbf{x}} \mathbf{n}(\mathbf{x}) \times \boldsymbol{\varphi}(\mathbf{y}), \quad (2.76)$$

$$\gamma_N \boldsymbol{\varphi}(\mathbf{x}) = \lim_{\mathbf{y} \rightarrow \mathbf{x}} \mathbf{n}(\mathbf{x}) \times \mathbf{curl} \boldsymbol{\varphi}(\mathbf{y}), \quad (2.77)$$

$$\gamma_{\mathbf{n}} \boldsymbol{\varphi}(\mathbf{x}) = \lim_{\mathbf{y} \rightarrow \mathbf{x}} \mathbf{n}(\mathbf{x}) \cdot \boldsymbol{\varphi}(\mathbf{y}). \quad (2.78)$$

For a test vector field $\boldsymbol{\varphi} \in \mathcal{D}(\overline{\Omega})$, we denote

$$\gamma_0 \boldsymbol{\varphi} = (\gamma_0 \varphi_1, \gamma_0 \varphi_2, \gamma_0 \varphi_3)^\top.$$

Thus, the trace operators are well defined when the normal vector is well defined and thus, the operators

$$\begin{aligned} \gamma_0 &: \mathcal{D}(\overline{\Omega}) \rightarrow L^2(\Gamma), \\ \gamma_1 &: \mathcal{D}(\overline{\Omega}) \rightarrow L^2(\Gamma), \\ \gamma_R &: \mathcal{D}(\overline{\Omega}) \rightarrow \mathbf{L}_t^2(\Gamma), \\ \gamma_D &: \mathcal{D}(\overline{\Omega}) \rightarrow \mathbf{L}_t^2(\Gamma), \\ \gamma_N &: \mathcal{D}(\overline{\Omega}) \rightarrow \mathbf{L}_t^2(\Gamma), \\ \gamma_{\mathbf{n}} &: \mathcal{D}(\overline{\Omega}) \rightarrow L^2(\Gamma) \end{aligned}$$

are continuous. Here, $\mathbf{L}_t^2(\Gamma) \subset \mathbf{L}^2(\Gamma)$ is the space of tangential, thus two-dimensional, vector fields which are square integrable on Γ ,

$$\mathbf{L}_t^2(\Gamma) = \{\mathbf{u} \in \mathbf{L}^2(\Gamma), \mathbf{n} \cdot \mathbf{u} = 0 \text{ a.e. on } \Gamma\}. \quad (2.79)$$

Until now, we have not yet defined function spaces that contain functions which possess weak derivatives in $\Omega \subsetneq \mathbb{R}^3$ only. By this we mean, for example, $v \in L^2(\mathbb{R}^3)$ with $\nabla v \in \mathbf{L}^2(\Omega)$. For such v , it obviously holds

$$\forall \boldsymbol{\varphi} \in \mathcal{D}(\mathbb{R}^3), \text{ supp } \boldsymbol{\varphi} \subset \Omega: \quad (v, \text{div } \boldsymbol{\varphi})_\Omega = -(\nabla v, \boldsymbol{\varphi})_\Omega.$$

Let the Hilbert spaces

$$H^1(\Omega) = \{v \in L^2(\Omega) : \nabla v \in \mathbf{L}^2(\Omega)\}, \quad (2.80)$$

$$\mathbf{H}(\mathbf{curl}, \Omega) = \{\mathbf{v} \in \mathbf{L}^2(\Omega) : \mathbf{curl} \mathbf{v} \in \mathbf{L}^2(\Omega)\}, \quad (2.81)$$

$$\mathbf{H}(\mathbf{div}, \Omega) = \{\mathbf{v} \in \mathbf{L}^2(\Omega) : \mathbf{div} \mathbf{v} \in L^2(\Omega)\}, \quad (2.82)$$

be equipped with the inner products

$$u, v \in H^1(\Omega) : \quad (u, v)_{1, \Omega} = (u, v)_{\Omega} + (\nabla u, \nabla v)_{\Omega}, \quad (2.83)$$

$$\mathbf{u}, \mathbf{v} \in \mathbf{H}(\mathbf{curl}, \Omega) : \quad (\mathbf{u}, \mathbf{v})_{\mathbf{curl}, \Omega} = (\mathbf{u}, \mathbf{v})_{\Omega} + (\mathbf{curl} \mathbf{u}, \mathbf{curl} \mathbf{v})_{\Omega}, \quad (2.84)$$

$$\mathbf{u}, \mathbf{v} \in \mathbf{H}(\mathbf{div}, \Omega) : \quad (\mathbf{u}, \mathbf{v})_{\mathbf{div}, \Omega} = (\mathbf{u}, \mathbf{v})_{\Omega} + (\mathbf{div} \mathbf{u}, \mathbf{div} \mathbf{v})_{\Omega}. \quad (2.85)$$

Recall that for $\mathbf{v} \in \mathbf{L}^2(\Omega)$, we denote by $\tilde{\mathbf{v}} \in \mathbf{L}^2(\mathbb{R}^3)$ the vector field

$$\tilde{\mathbf{v}} = \begin{cases} \mathbf{v} & \text{in } \Omega, \\ \mathbf{0} & \text{in } \Omega^c. \end{cases} \quad (2.86)$$

For $\mathbf{v} \in \mathbf{H}(\mathbf{div}, \Omega)$, it holds, by definition,

$$\forall \varphi \in \mathcal{D}(\mathbb{R}^3) : \quad \langle \mathbf{div} \tilde{\mathbf{v}}, \varphi \rangle = -\langle \tilde{\mathbf{v}}, \nabla \varphi \rangle = -(\mathbf{v}, \nabla \varphi)_{\Omega},$$

and, moreover, we introduce

$$\langle \gamma_{\mathbf{n}} \mathbf{v} \delta_{\Gamma}, \varphi \rangle = (\mathbf{div} \mathbf{v}, \varphi)_{\Omega} + (\mathbf{v}, \nabla \varphi)_{\Omega}. \quad (2.87)$$

Provided $\gamma_{\mathbf{n}} \mathbf{v} \delta_{\Gamma} \in \mathcal{D}(\mathbb{R}^3)'$ is well defined, it has support Γ as for all φ with $\text{supp} \varphi \subset \Omega$ or with $\text{supp} \varphi \subset \Omega^c$, it holds

$$(\mathbf{div} \mathbf{v}, \varphi)_{\Omega} + (\mathbf{v}, \nabla \varphi)_{\Omega} = 0.$$

Lemma 2.4.1 *For $\mathbf{v} \in \mathbf{H}(\mathbf{div}, \Omega)$, $\gamma_{\mathbf{n}} \mathbf{v} \delta_{\Gamma} \in \mathcal{D}(\mathbb{R}^3)'$ is well defined and the following characterization of $\mathbf{div} \tilde{\mathbf{v}}$ is valid*

$$\forall \varphi \in \mathcal{D}(\mathbb{R}^3) : \quad \langle \mathbf{div} \tilde{\mathbf{v}}, \varphi \rangle = (\mathbf{div} \mathbf{v}, \varphi)_{\Omega} - \langle \gamma_{\mathbf{n}} \mathbf{v} \delta_{\Gamma}, \varphi \rangle. \quad (2.88)$$

Proof: First, let $\mathbf{v} \in \mathcal{D}(\bar{\Omega})$, then for any $\varphi \in \mathcal{D}(\mathbb{R}^3)$ with $\text{supp} \varphi \subset K$, it holds

$$\begin{aligned} \left| \int_{\Gamma} \gamma_{\mathbf{n}} \mathbf{v} \gamma_0 \varphi \, d\sigma \right| &= |(\mathbf{div} \mathbf{v}, \varphi)_{\Omega} + (\mathbf{v}, \nabla \varphi)_{\Omega}| \\ &\leq 2 \|\mathbf{v}\|_{\mathbf{H}(\mathbf{div}, \Omega)} \|\varphi\|_{H^1(\Omega)} \\ &\leq c \max_{|\alpha| \leq 1} \sup_{\mathbf{x} \in K} |D^{\alpha} \varphi(\mathbf{x})|, \quad c = 2 |\Omega| \|\mathbf{v}\|_{\mathbf{H}(\mathbf{div}, \Omega)}. \end{aligned}$$

By density, there exists a unique distribution extending this functional on vector fields $\mathbf{v} \in \mathbf{H}(\mathbf{div}, \Omega)$. This distribution is $\gamma_{\mathbf{n}} \mathbf{v} \delta_{\Gamma} \in \mathcal{D}(\mathbb{R}^3)'$. The characterization (2.88) follows from (2.87). \square

Similarly, for $\mathbf{v} \in \mathbf{H}(\mathbf{curl}, \Omega)$, it holds, by definition,

$$\forall \varphi \in \mathcal{D}(\mathbb{R}^3) : \quad \langle \mathbf{curl} \tilde{\mathbf{v}}, \varphi \rangle = \langle \tilde{\mathbf{v}}, \mathbf{curl} \varphi \rangle = (\mathbf{v}, \mathbf{curl} \varphi)_{\Omega},$$

and we introduce

$$\langle \gamma_D \mathbf{v} \delta_{\Gamma}, \varphi \rangle = (\mathbf{curl} \mathbf{v}, \varphi)_{\Omega} - (\mathbf{v}, \mathbf{curl} \varphi)_{\Omega}. \quad (2.89)$$

Provided $\gamma_D \mathbf{v} \delta_\Gamma \in \mathcal{D}(\mathbb{R}^3)'$ is well defined, it has support Γ as for all φ with $\text{supp } \varphi \subset \Omega$ or with $\text{supp } \varphi \subset \Omega^c$, it holds

$$(\mathbf{curl } \mathbf{v}, \varphi)_\Omega - (\mathbf{v}, \mathbf{curl } \varphi)_\Omega = 0.$$

Lemma 2.4.2 *For $\mathbf{v} \in \mathbf{H}(\mathbf{curl}, \Omega)$, $\gamma_D \mathbf{v} \delta_\Gamma \in \mathcal{D}(\mathbb{R}^3)'$ is well defined and the following characterization of $\mathbf{curl } \tilde{\mathbf{v}}$ is valid*

$$\forall \varphi \in \mathcal{D}(\mathbb{R}^3): \quad \langle \mathbf{curl } \tilde{\mathbf{v}}, \varphi \rangle = (\mathbf{curl } \mathbf{v}, \varphi)_\Omega - \langle \gamma_D \mathbf{v} \delta_\Gamma, \varphi \rangle. \quad (2.90)$$

Proof: First, let $\mathbf{v} \in \mathbf{D}(\bar{\Omega})$ be a test vector field. Then, for $\varphi \in \mathcal{D}(\mathbb{R}^3)$ with $\text{supp } \varphi \subset K$, the integration by parts yields

$$\begin{aligned} \left| \int_\Gamma \gamma_D \mathbf{v} \cdot \gamma_0 \varphi \, d\sigma \right| &= |(\mathbf{curl } \mathbf{v}, \varphi)_\Omega - (\mathbf{v}, \mathbf{curl } \varphi)_\Omega| \\ &\leq 2 \|\mathbf{v}\|_{\mathbf{H}(\mathbf{curl}, \Omega)} \|\varphi\|_{\mathbf{H}(\mathbf{curl}, \Omega)} \\ &\leq c \max_{|\alpha| \leq 1} \sup_{\mathbf{x} \in K} |D^\alpha \varphi(\mathbf{x})|, \quad c = 2 |\Omega| \|\mathbf{v}\|_{\mathbf{H}(\mathbf{curl}, \Omega)}. \end{aligned}$$

Thus, there exists a unique distribution extending this functional on vector fields $\mathbf{v} \in \mathbf{H}(\mathbf{curl}, \Omega)$. This distribution is $\gamma_D \mathbf{v} \delta_\Gamma \in \mathcal{D}(\mathbb{R}^3)'$. The characterization (2.90) follows from (2.89). \square

So far, we considered the energy spaces apart from each other. However, provided $\Omega \subset \mathbb{R}^3$ is simply connected, it is well known that the gradient and the curl operator, along with the divergence operator, form an exact sequence relating the energy spaces in the following way

$$H^1(\Omega) \xrightarrow{\nabla} \mathbf{H}(\mathbf{curl}, \Omega) \xrightarrow{\mathbf{curl}} \mathbf{H}(\text{div}, \Omega) \xrightarrow{\text{div}} L^2(\Omega).$$

In an exact sequence of operators, the range of each operator coincides with the null-space of the operator next in the sequence. A vector field with $\mathbf{curl } \mathbf{u} = \mathbf{0}$ almost everywhere in Ω must have the following representation

$$\mathbf{u} = \nabla u \quad \text{with } u \in H^1(\Omega).$$

Similarly, if the divergence of a vector field vanishes $\text{div } \mathbf{u} = 0$ almost everywhere in Ω , \mathbf{u} must have the following representation

$$\mathbf{u} = \mathbf{curl } \mathbf{v} \quad \text{with } \mathbf{v} \in \mathbf{H}(\mathbf{curl}, \Omega).$$

2.5. Trace Spaces

In order to study solutions to boundary value problems in the energy spaces defined in Section 2.4, boundary values of the corresponding functions should be defined. The graph norms of the energy spaces do not take into account boundary values and, thus, it is not clear whether traces exist or not. It turns out that the energy spaces possess weak traces and it is the subject of this section to define the trace spaces. Moreover, their characterization will yield duality pairings which are appropriate to replace the distributional pairings from the previous section.

To obtain the most general results, we assume that Γ is the boundary of a curvilinear Lipschitz polyhedron. For this case, the results are standard for $H^1(\Omega)$ and can be found in [44]. The definition of the trace spaces of $\mathbf{H}(\mathbf{curl}, \Omega)$ builds up on the original papers [12, 13]. The characterization

developed here is, however, slightly more general and accounts also for the curvilinear case. A more abstract definition of the trace spaces is found in [15].

As usual, Γ is assumed to be the boundary of a curvilinear Lipschitz polyhedron given by an atlas of the following kind

$$\Gamma = \bigcup_{i=1}^N \overline{\Gamma_i} \quad \text{with } \Gamma_i \cap \Gamma_j = \emptyset \text{ for } i \neq j, \quad \text{and } \hat{\mathbf{X}}_i: \hat{T} \rightarrow \Gamma_i, \quad i = 1, \dots, N. \quad (2.91)$$

Recall that for any vector field $\mathbf{v} \in \mathbf{H}(\text{div}, \Omega)$ and any test function $\varphi \in \mathcal{D}(\mathbb{R}^3)$ it holds

$$\langle \gamma_{\mathbf{n}} \mathbf{v} \delta_{\Gamma}, \varphi \rangle = (\text{div } \mathbf{v}, \varphi)_{\Omega} + (\mathbf{v}, \nabla \varphi)_{\Omega}.$$

The distribution $\gamma_{\mathbf{n}} \mathbf{v} \delta_{\Gamma}$ has support Γ and its evaluation on $\varphi \in \mathcal{D}(\mathbb{R}^3)$ depends only on $\varphi|_{\Gamma}$. Further, it holds

$$|\langle \gamma_{\mathbf{n}} \mathbf{v} \delta_{\Gamma}, \varphi \rangle| = |(\text{div } \mathbf{v}, \varphi)_{\Omega} + (\mathbf{v}, \nabla \varphi)_{\Omega}| \leq 2 \|\varphi\|_{H^1(\Omega)} \|\mathbf{v}\|_{\mathbf{H}(\text{div}, \Omega)}.$$

Thus, for fixed $\mathbf{v} \in \mathbf{H}(\text{div}, \Omega)$ the distribution $\gamma_{\mathbf{n}} \mathbf{v} \delta_{\Gamma}$ possesses a unique extension to a continuous functional on $H^1(\Omega)$. This is clear because for arbitrary $w \in H^1(\Omega)$, there is a sequence of test functions $(\varphi_j)_{j=1}^{\infty}$, $\varphi_j \in \mathcal{D}(\mathbb{R}^3)$ with

$$\lim_{j \rightarrow \infty} \|w - \varphi_j\|_{H^1(\Omega)} = 0.$$

This density argument makes also clear that the Dirichlet trace $\gamma_0 w$ exists for functions in $H^1(\Omega)$. The corresponding trace space $H^{\frac{1}{2}}(\Gamma)$ is introduced in Definition 6.

Definition 6 Let Γ be the boundary of a curvilinear Lipschitz polyhedron. The Sobolev space $H^{\frac{1}{2}}(\Gamma)$ is defined as the function space which contains all scalar-valued functions $\varphi \in L^2(\Gamma)$ that fulfill the following two conditions:

1. For all elements Γ_i , $i = 1, \dots, N$, $\varphi|_{\Gamma_i} \in H^{\frac{1}{2}}(\Gamma_i)$, i.e., it holds

$$\int_{\Gamma_i} \int_{\Gamma_i} \frac{|\varphi(\mathbf{x}) - \varphi(\mathbf{y})|^2}{|\mathbf{x} - \mathbf{y}|^3} d\sigma_x d\sigma_y < \infty. \quad (2.92)$$

2. For all edges, i.e., $\partial\Gamma_i \cap \partial\Gamma_j = e_{ij}$, it holds

$$\mathcal{N}_{ij}(\varphi) = \int_{\Gamma_i} \int_{\Gamma_j} \frac{|\varphi(\mathbf{x}) - \varphi(\mathbf{y})|^2}{|\mathbf{x} - \mathbf{y}|^3} d\sigma_x d\sigma_y < \infty. \quad (2.93)$$

The second condition of the definition guarantees that functions in $H^{\frac{1}{2}}(\Gamma)$ are globally weakly continuous.

A realization for the dual space $H^{\frac{1}{2}}(\Gamma)'$ is obtained as an extension of the $L^2(\Gamma)$ inner product [44]. This realization of $H^{\frac{1}{2}}(\Gamma)'$ is denoted $H^{-\frac{1}{2}}(\Gamma)$ and for the corresponding duality pairing we write $\langle \cdot, \cdot \rangle_{\frac{1}{2}}$. Moreover, it is proved in [44] that the operators

$$\begin{aligned} \gamma_0: \quad H^1(\Omega) &\rightarrow H^{\frac{1}{2}}(\Gamma), \\ \gamma_{\mathbf{n}}: \quad \mathbf{H}(\text{div}, \Omega) &\rightarrow H^{-\frac{1}{2}}(\Gamma) \end{aligned} \quad (2.94)$$

are continuous and surjective with continuous right inverses. The generalized integration by parts

formula applies for $\mathbf{v} \in \mathbf{H}(\operatorname{div}, \Omega)$, $w \in H^1(\Omega)$ and it reads

$$(\operatorname{div} \mathbf{v}, w)_\Omega = -(\mathbf{v}, \nabla w)_\Omega + \langle \gamma_{\mathbf{n}} \mathbf{v}, \gamma_0 w \rangle_{\frac{1}{2}}. \quad (2.95)$$

Further, we need the following two subspaces of $H^{\frac{1}{2}}(\Gamma)$ and $H^{-\frac{1}{2}}(\Gamma)$, respectively,

$$\begin{aligned} H_*^{\frac{1}{2}}(\Gamma) &= \left\{ \varphi \in H^{\frac{1}{2}}(\Gamma) : \langle 1, \varphi \rangle_{\frac{1}{2}} = 0 \right\}, \\ H_*^{-\frac{1}{2}}(\Gamma) &= \left\{ \varphi \in H^{-\frac{1}{2}}(\Gamma) : \langle \varphi, 1 \rangle_{\frac{1}{2}} = 0 \right\}. \end{aligned}$$

Recall that for $\mathbf{v} \in \mathbf{H}(\operatorname{curl}, \Omega)$ and for $\varphi \in \mathcal{D}(\mathbb{R}^3)$

$$\langle \gamma_D \mathbf{v} \delta_\Gamma, \varphi \rangle = (\operatorname{curl} \mathbf{v}, \varphi)_\Omega - (\mathbf{v}, \operatorname{curl} \varphi)_\Omega.$$

The following inequality holds

$$|\langle \gamma_D \mathbf{v} \delta_\Gamma, \varphi \rangle| = |(\operatorname{curl} \mathbf{v}, \varphi)_\Omega - (\mathbf{v}, \operatorname{curl} \varphi)_\Omega| \leq 2 \|\mathbf{v}\|_{\mathbf{H}(\operatorname{curl}, \Omega)} \|\varphi\|_{\mathbf{H}(\operatorname{curl}, \Omega)}.$$

It is clear that there exists a unique extension of the left hand side to a functional on $\mathbf{H}(\operatorname{curl}, \Omega)$ because the test vector fields are dense in $\mathbf{H}(\operatorname{curl}, \Omega)$, i.e., each $\mathbf{w} \in \mathbf{H}(\operatorname{curl}, \Omega)$ can be represented as the limit of a convergent sequence of test vector fields $(\varphi_j)_{j=1}^\infty$, $\varphi_j \in \mathcal{D}(\mathbb{R}^3)$, i.e.,

$$\lim_{j \rightarrow \infty} \|\mathbf{w} - \varphi_j\|_{\mathbf{H}(\operatorname{curl}, \Omega)} = 0.$$

The same reasoning as for $H^1(\Omega)$ allows to conclude that vector fields in $\mathbf{H}(\operatorname{curl}, \Omega)$ possess weak traces. In order to define them, we first introduce the Sobolev spaces $\mathbf{H}_{\frac{1}{R}}^{\frac{1}{2}}(\Gamma)$ and $\mathbf{H}_{\frac{1}{D}}^{\frac{1}{2}}(\Gamma)$ of tangential vector fields with regularity $\frac{1}{2}$. To explicitly describe the regularity of tangent vector fields defined on triangles Γ_i and Γ_j with common edge e_{ij} , it is convenient to introduce bidual vector fields $\{\mathbf{a}_l, \mathbf{a}^l\}_{l=1}^2$. Bidual vector fields are orthogonal to each other in the sense that it holds

$$\int_{\Gamma_i \cup \Gamma_j} \mathbf{a}_l \cdot \mathbf{a}^k \, d\sigma = c \delta_{lk}, \quad l, k = 1, 2, \quad c = |\Gamma_i| + |\Gamma_j|. \quad (2.96)$$

The bidual basis vectors (2.10) and (2.27) can be defined element wise yielding bidual vector fields in $\mathbf{L}_t^2(\Gamma_i \cup \Gamma_j)$ with (2.96). Without restriction of any kind it is assumed that the parametrizations $\hat{\mathbf{X}}_i$ and $\hat{\mathbf{X}}_j$ are such that the common edge e_{ij} is parametrized for $\xi_2 = 0$. Thus, it holds

$$\mathbf{a}_1 = \begin{cases} \mathbf{a}_{i,1} & \text{on } \Gamma_i, \\ \mathbf{a}_{j,1} & \text{on } \Gamma_j, \end{cases} \quad \text{with } \mathbf{a}_{i,1} \parallel \mathbf{a}_{j,1} \quad \text{for all } \mathbf{x} \in e_{ij}, \quad (2.97)$$

$$\mathbf{a}^2 = \begin{cases} \mathbf{a}^{i,2} & \text{on } \Gamma_i, \\ \mathbf{a}^{j,2} & \text{on } \Gamma_j, \end{cases} \quad \text{with } \mathbf{a}^{i,2} \perp \mathbf{a}_1, \quad \mathbf{a}^{j,2} \perp \mathbf{a}_1 \quad \text{for all } \mathbf{x} \in e_{ij}, \quad (2.98)$$

$$\mathbf{a}_2 = \begin{cases} \mathbf{a}_{i,2} & \text{on } \Gamma_i, \\ \mathbf{a}_{j,2} & \text{on } \Gamma_j, \end{cases} \quad \text{and} \quad \mathbf{a}^1 = \begin{cases} \mathbf{a}^{i,1} & \text{on } \Gamma_i, \\ \mathbf{a}^{j,1} & \text{on } \Gamma_j. \end{cases} \quad (2.99)$$

All those vector fields are smooth on Γ_i and Γ_j but, in general, they are discontinuous across e_{ij} .

Definition 7 Let Γ be the boundary of a curvilinear Lipschitz polyhedron. The Sobolev space $\mathbf{H}_{\frac{1}{R}}^{\frac{1}{2}}(\Gamma)$ is

defined as the function space which contains all tangent vector fields $\boldsymbol{\varphi} \in \mathbf{L}_t^2(\Gamma)$ that fulfill the following two conditions:

1. For all elements $\Gamma_i, i = 1, \dots, N$, $\boldsymbol{\varphi}|_{\Gamma_i} \in \mathbf{H}^{\frac{1}{2}}(\Gamma_i)$, i.e., (2.92) holds for every scalar-valued component.
2. For all edges, i.e., $\partial\Gamma_i \cap \partial\Gamma_j = e_{ij}$, it holds

$$\mathcal{N}_{R,ij}(\boldsymbol{\varphi}) = \mathcal{N}_{ij}(\varphi_R) < \infty, \quad \text{where } \varphi_R = \boldsymbol{\varphi}|_{\Gamma_i \cup \Gamma_j} \cdot \mathbf{a}_1. \quad (2.100)$$

The Sobolev space $\mathbf{H}_D^{\frac{1}{2}}(\Gamma)$ is defined as the function space which contains all tangent vector fields $\boldsymbol{\varphi} \in \mathbf{L}_t^2(\Gamma)$ that fulfill the following two conditions:

1. For all elements $\Gamma_i, i = 1, \dots, N$, $\boldsymbol{\varphi}|_{\Gamma_i} \in \mathbf{H}^{\frac{1}{2}}(\Gamma_i)$, i.e., (2.92) holds for every scalar-valued component.
2. For all edges, i.e., $\partial\Gamma_i \cap \partial\Gamma_j = e_{ij}$, it holds

$$\mathcal{N}_{D,ij}(\boldsymbol{\varphi}) = \mathcal{N}_{ij}(\varphi_D) < \infty, \quad \text{where } \varphi_D = \boldsymbol{\alpha}^2 \cdot \boldsymbol{\varphi}|_{\Gamma_i \cup \Gamma_j}. \quad (2.101)$$

The spaces $\mathbf{H}_D^{\frac{1}{2}}(\Gamma)$ and $\mathbf{H}_R^{\frac{1}{2}}(\Gamma)$ are endowed with the norms

$$\begin{aligned} \|\mathbf{v}\|_{\mathbf{H}_R^{\frac{1}{2}}(\Gamma)} &= \left(\sum_{i=1}^N \|\mathbf{v}\|_{\mathbf{H}^{\frac{1}{2}}(\Gamma_i)}^2 + \sum_{e_{ij}} \mathcal{N}_{R,ij}(\mathbf{v}) \right)^{\frac{1}{2}}, \\ \|\mathbf{v}\|_{\mathbf{H}_D^{\frac{1}{2}}(\Gamma)} &= \left(\sum_{i=1}^N \|\mathbf{v}\|_{\mathbf{H}^{\frac{1}{2}}(\Gamma_i)}^2 + \sum_{e_{ij}} \mathcal{N}_{D,ij}(\mathbf{v}) \right)^{\frac{1}{2}}, \end{aligned}$$

where $e_{ij} \in \Gamma$ indicates that the sum runs over all edges.

It is shown in [12] that the Sobolev spaces $\mathbf{H}_R^{\frac{1}{2}}(\Gamma)$ and $\mathbf{H}_D^{\frac{1}{2}}(\Gamma)$ are complete and, moreover, they can be equipped with an inner product given by the parallelogram law. As usual, $\mathbf{H}_D^{-\frac{1}{2}}(\Gamma)$ and $\mathbf{H}_R^{-\frac{1}{2}}(\Gamma)$ denote the realizations for the dual spaces of $\mathbf{H}_D^{\frac{1}{2}}(\Gamma)$ and $\mathbf{H}_R^{\frac{1}{2}}(\Gamma)$ with $\mathbf{L}_t^2(\Gamma)$ as pivot space. $\mathbf{H}_D^{-\frac{1}{2}}(\Gamma)$ and $\mathbf{H}_R^{-\frac{1}{2}}(\Gamma)$ are Hilbert spaces endowed with their natural norms.

The Sobolev spaces defined in Definition 7 are tailored to assess the regularity of the vector-valued surface differential operators. To see this, remember that, at the end of Section 2.5, we were left with the question how to define an appropriate functional to check on the regularity of the surface differentials in the case of curvilinear Lipschitz polyhedral domains. This question is now sufficiently answered. Namely, (2.100) may be considered to testify exactly the weak continuity of the surface gradient (2.48) for $\boldsymbol{\varphi} \in \mathbf{H}^1(\Gamma)$ and (2.101) is appropriate to check if the vector-valued surface curl (2.53) of $\boldsymbol{\varphi} \in \mathbf{H}^1(\Gamma)$ is weakly continuous on Γ . More generality is, however, necessary if less regular functions are considered. It has been proved in [15] that the surface gradient can be extended such that

$$\nabla_{\Gamma}: \mathbf{H}_*^{\frac{1}{2}}(\Gamma) \rightarrow \mathbf{H}_D^{-\frac{1}{2}}(\Gamma),$$

is continuous and normally solvable. Consequently, the surface divergence div_{Γ} , the dual operator, is continuous and surjective regarding

$$\text{div}_{\Gamma}: \mathbf{H}_D^{\frac{1}{2}}(\Gamma) \rightarrow \mathbf{H}_*^{-\frac{1}{2}}(\Gamma).$$

Also, it has been proved in [15] that the vector-valued surface curl operator can be extended such that

$$\text{curl}_{\Gamma}: \mathbf{H}_*^{\frac{1}{2}}(\Gamma) \rightarrow \mathbf{H}_R^{-\frac{1}{2}}(\Gamma),$$

is continuous and normally solvable. Consequently, the scalar-valued surface curl operator curl_Γ , the dual operator, is continuous and surjective with respect to

$$\text{curl}_\Gamma: \mathbf{H}_R^{\frac{1}{2}}(\Gamma) \rightarrow H_*^{-\frac{1}{2}}(\Gamma).$$

We define

$$H^{-\frac{1}{2}}(\text{div}_\Gamma, \Gamma) = \left\{ \mathbf{v} \in \mathbf{H}_R^{-\frac{1}{2}}(\Gamma), \quad \text{div}_\Gamma(\mathbf{v}) \in H^{-\frac{1}{2}}(\Gamma) \right\}, \quad (2.102)$$

$$H^{-\frac{1}{2}}(\text{curl}_\Gamma, \Gamma) = \left\{ \mathbf{v} \in \mathbf{H}_D^{-\frac{1}{2}}(\Gamma), \quad \text{curl}_\Gamma(\mathbf{v}) \in H^{-\frac{1}{2}}(\Gamma) \right\}. \quad (2.103)$$

They are Hilbert spaces and the corresponding norms read [12]

$$\|\mathbf{v}\|_{H^{-\frac{1}{2}}(\text{div}_\Gamma, \Gamma)} = \left(\|\mathbf{v}\|_{\mathbf{H}_R^{-\frac{1}{2}}(\Gamma)}^2 + \|\text{div}_\Gamma(\mathbf{v})\|_{H^{-\frac{1}{2}}(\Gamma)}^2 \right)^{\frac{1}{2}}, \quad (2.104)$$

$$\|\mathbf{v}\|_{H^{-\frac{1}{2}}(\text{curl}_\Gamma, \Gamma)} = \left(\|\mathbf{v}\|_{\mathbf{H}_D^{-\frac{1}{2}}(\Gamma)}^2 + \|\text{curl}_\Gamma(\mathbf{v})\|_{H^{-\frac{1}{2}}(\Gamma)}^2 \right)^{\frac{1}{2}}. \quad (2.105)$$

Most important for the theory of the Maxwell equations in the context of boundary integral equations is the following theorem. The proof can be found in [15], for instance.

Theorem 2.5.1 *The operators γ_R and γ_D can be extended to linear continuous operators acting on $\mathbf{H}(\text{curl}, \Omega)$. Namely,*

$$\begin{aligned} \gamma_R: \quad \mathbf{H}(\text{curl}, \Omega) &\rightarrow H^{-\frac{1}{2}}(\text{curl}_\Gamma, \Gamma), \\ \gamma_D: \quad \mathbf{H}(\text{curl}, \Omega) &\rightarrow H^{-\frac{1}{2}}(\text{div}_\Gamma, \Gamma) \end{aligned} \quad (2.106)$$

are linear, continuous and surjective.

Further characterizations of the trace spaces $H^{-\frac{1}{2}}(\text{div}_\Gamma, \Gamma)$ and $H^{-\frac{1}{2}}(\text{curl}_\Gamma, \Gamma)$ are given in the next theorem which is proved in [15], for instance.

Theorem 2.5.2 *Let Γ be simply connected and set*

$$\mathcal{H}(\Gamma) = \left\{ \varphi \in H^1(\Gamma) : \Delta_\Gamma \varphi \in H^{-\frac{1}{2}}(\Gamma) \right\},$$

where $\Delta_\Gamma = \text{div}_\Gamma \nabla_\Gamma$ denotes the Laplace-Beltrami operator. The following decompositions are direct

$$H^{-\frac{1}{2}}(\text{div}_\Gamma, \Gamma) = \nabla_\Gamma \mathcal{H}(\Gamma) \oplus \text{curl}_\Gamma \left(H^{\frac{1}{2}}(\Gamma) \right),$$

$$H^{-\frac{1}{2}}(\text{curl}_\Gamma, \Gamma) = \text{curl}_\Gamma \mathcal{H}(\Gamma) \oplus \nabla_\Gamma \left(H^{\frac{1}{2}}(\Gamma) \right).$$

Let $\mathbf{u} \in H^{-\frac{1}{2}}(\text{div}_\Gamma, \Gamma)$ and $\mathbf{v} \in H^{-\frac{1}{2}}(\text{curl}_\Gamma, \Gamma)$ with $\mathbf{u} = \nabla_\Gamma \varphi_u + \text{curl}_\Gamma \psi_u$ and $\mathbf{v} = \nabla_\Gamma \varphi_v + \text{curl}_\Gamma \psi_v$. We define

$$\langle \mathbf{v}, \mathbf{u} \rangle_{-\frac{1}{2}} = \langle \Delta_\Gamma \varphi_v, \varphi_u \rangle_{\frac{1}{2}} - \langle \Delta_\Gamma \psi_u, \psi_v \rangle_{\frac{1}{2}}. \quad (2.107)$$

The following integration by parts formula holds true for $\mathbf{u}, \mathbf{v} \in \mathbf{H}(\text{curl}, \Omega)$

$$(\text{curl } \mathbf{u}, \mathbf{v})_\Omega = (\mathbf{u}, \text{curl } \mathbf{v})_\Omega + \langle \gamma_R \mathbf{v}, \gamma_D \mathbf{u} \rangle_{-\frac{1}{2}}. \quad (2.108)$$

The Hodge decompositions stated in Theorem 2.5.2 are the most established theoretical results on direct decompositions of the trace spaces for $\mathbf{H}(\text{curl}, \Omega)$. The direct decomposition, however, which

is fundamental for the construction of high order boundary element spaces presented in Chapter 4 builds up on yet another direct decomposition which is proved in [6].

Lemma 2.5.3 *Let \mathcal{I} denote the identity operator and let*

$$H^{-\frac{1}{2}}(\operatorname{div}_\Gamma 0, \Gamma) = \left\{ \mathbf{v} \in H^{-\frac{1}{2}}(\operatorname{div}_\Gamma, \Gamma), \operatorname{div}_\Gamma \mathbf{v} = 0 \right\}.$$

There exists a projector $\mathcal{R}: H^{-\frac{1}{2}}(\operatorname{div}_\Gamma, \Gamma) \rightarrow \mathbf{H}_D^{\frac{1}{2}}(\Gamma)$,

$$\forall \mathbf{v} \in H^{-\frac{1}{2}}(\operatorname{div}_\Gamma, \Gamma) : \quad \operatorname{div}_\Gamma(\mathcal{R}\mathbf{v}) = \operatorname{div}_\Gamma \mathbf{v} \quad \text{and} \quad \|\mathcal{R}\mathbf{u}\|_{\mathbf{H}^{\frac{1}{2}}(\Gamma)} \leq C \|\operatorname{div}_\Gamma \mathbf{u}\|_{H^{-\frac{1}{2}}(\Gamma)}.$$

We obtain a stable and direct decomposition $H^{-\frac{1}{2}}(\operatorname{div}_\Gamma, \Gamma) = V(\Gamma) \oplus W(\Gamma)$, where

$$V(\Gamma) = \mathcal{R} \left(H^{-\frac{1}{2}}(\operatorname{div}_\Gamma, \Gamma) \right), \quad W(\Gamma) = (\mathcal{I} - \mathcal{R}) \left(H^{-\frac{1}{2}}(\operatorname{div}_\Gamma, \Gamma) \right) = H^{-\frac{1}{2}}(\operatorname{div}_\Gamma, \Gamma) \cap H^{-\frac{1}{2}}(\operatorname{div}_\Gamma 0, \Gamma).$$

An explicit realization of the $H^{-\frac{1}{2}}(\operatorname{div}_\Gamma, \Gamma)$ in terms of $H^{-\frac{1}{2}}(\operatorname{curl}_\Gamma, \Gamma)$ and vice versa is possible by the help of the extrinsic structure of Euclidean space as stated in the following theorem proved in [15].

Theorem 2.5.4 *The operator $\mathbf{n} \times: \mathbf{L}_t^2(\Gamma) \rightarrow \mathbf{L}_t^2(\Gamma)$ can be extended to a linear and continuous isomorphism from $H^{-\frac{1}{2}}(\operatorname{curl}_\Gamma, \Gamma)$ to $H^{-\frac{1}{2}}(\operatorname{div}_\Gamma, \Gamma)$ such that for $\mathbf{w} \in H^{-\frac{1}{2}}(\operatorname{curl}_\Gamma, \Gamma)$ there is a unique $\mathbf{u} \in H^{-\frac{1}{2}}(\operatorname{div}_\Gamma, \Gamma)$ with*

$$\forall \mathbf{v} \in H^{-\frac{1}{2}}(\operatorname{curl}_\Gamma, \Gamma) : \quad \langle \mathbf{v}, \mathbf{u} \rangle_{-\frac{1}{2}} = \langle \mathbf{v}, \mathbf{n} \times \mathbf{w} \rangle_{-\frac{1}{2}}. \quad (2.109)$$

The operator $\times \mathbf{n}: \mathbf{L}_t^2(\Gamma) \rightarrow \mathbf{L}_t^2(\Gamma)$ can be extended to a linear and continuous isomorphism from $H^{-\frac{1}{2}}(\operatorname{div}_\Gamma, \Gamma)$ to $H^{-\frac{1}{2}}(\operatorname{curl}_\Gamma, \Gamma)$ such that for $\mathbf{w} \in H^{-\frac{1}{2}}(\operatorname{div}_\Gamma, \Gamma)$ there is a unique $\mathbf{u} \in H^{-\frac{1}{2}}(\operatorname{curl}_\Gamma, \Gamma)$ with

$$\forall \mathbf{v} \in H^{-\frac{1}{2}}(\operatorname{div}_\Gamma, \Gamma) : \quad \langle \mathbf{u}, \mathbf{v} \rangle_{-\frac{1}{2}} = \langle \mathbf{w} \times \mathbf{n}, \mathbf{v} \rangle_{-\frac{1}{2}}. \quad (2.110)$$

Now, we have all tools at hand to explain the following de Rahm diagram

$$\begin{array}{ccccccc} H_*^{\frac{1}{2}}(\Gamma) & \xrightarrow{\nabla_\Gamma} & H^{-\frac{1}{2}}(\operatorname{curl}_\Gamma, \Gamma) & \xrightarrow{\operatorname{curl}_\Gamma} & H_*^{-\frac{1}{2}}(\Gamma) & & \\ \downarrow 1 & & \downarrow \mathbf{n} \times & & \downarrow 1 & & \\ H_*^{\frac{1}{2}}(\Gamma) & \xrightarrow{\operatorname{curl}_\Gamma} & H^{-\frac{1}{2}}(\operatorname{div}_\Gamma, \Gamma) & \xrightarrow{\operatorname{div}_\Gamma} & H_*^{-\frac{1}{2}}(\Gamma). & & \end{array} \quad (2.111)$$

The de Rham diagram (2.111) is suitable to summarize the results of this section as all trace spaces and all surface differential operators appear. There are three different kinds of information contained in (2.111) and we point them out now.

1. There is a (horizontal) relation between the trace spaces established by two exact sequences. The pair of surface differential operators $(\nabla_\Gamma, \operatorname{curl}_\Gamma)$ gives rise to the upper row in (2.111) and the pair of surface differential operators $(\operatorname{curl}_\Gamma, \operatorname{div}_\Gamma)$ gives rise to the lower row in (2.111).
2. There is a (diagonal) relation between the trace spaces established by the fact that the rows are in duality to each other. This means that for each space in the upper row in (2.111), we find in the lower row its assigned dual. The duality pairing is either $\langle \cdot, \cdot \rangle_{\frac{1}{2}}$ for the scalar-valued

functions or $\langle \cdot, \cdot \rangle_{-\frac{1}{2}}$ for the vector-valued functions. The diagonality of this relation can be read off the regularity index of the Sobolev spaces.

3. There is a (vertical) relation between the trace spaces established by isomorphisms, i.e., the identity mapping 1 and the isomorphism $\mathbf{n} \times$ from Theorem 2.5.4. This vertical relation shows how to realize the functionals by the use of extrinsic structures explicitly.

When the convergence of boundary element methods is examined qualitatively, extra smoothness of the functions to be approximated is indispensable. This extra regularity is restricted to the regularity of Γ . In case Γ is the boundary of a Lipschitz domain, Sobolev spaces with index $s > 1$ cannot be defined. It is however possible to require more regularity wherever Γ is more regular, namely, on the elements Γ_i . According to [52], we define for $s \geq 0$

$$\begin{aligned} H_{pw}^s(\Gamma) &= \left\{ u \in H^{\min(s,1)}(\Gamma), u_i = u|_{\Gamma_i} \in H^s(\Gamma_i), i = 1, \dots, N \right\}, \\ \|u\|_{H_{pw}^s(\Gamma)} &= \left(\sum_{i=1}^N \|u_i\|_{H^s(\Gamma_i)}^2 \right)^{\frac{1}{2}}, \end{aligned} \quad (2.112)$$

And, we define as proposed in [17],

$$\begin{aligned} \mathbf{H}^s(\text{curl}_\Gamma, \Gamma) &= \left\{ \mathbf{u} \in \mathbf{L}_t^2(\Gamma), \mathbf{u}_i = \mathbf{u}|_{\Gamma_i} \in \mathbf{H}^s(\Gamma_i), i = 1, \dots, N, \text{curl}_\Gamma \mathbf{u} \in H_{pw}^s(\Gamma) \right\}, \\ \|\mathbf{u}\|_{\mathbf{H}^s(\text{curl}_\Gamma, \Gamma)} &= \left(\sum_{i=1}^N \|\mathbf{u}_i\|_{\mathbf{H}^s(\Gamma_i)}^2 + \|\text{curl}_\Gamma \mathbf{u}\|_{H_{pw}^s(\Gamma)}^2 \right)^{\frac{1}{2}}, \end{aligned} \quad (2.113)$$

$$\begin{aligned} \mathbf{H}^s(\text{div}_\Gamma, \Gamma) &= \left\{ \mathbf{u} \in \mathbf{L}_t^2(\Gamma), \mathbf{u}_i = \mathbf{u}|_{\Gamma_i} \in \mathbf{H}^s(\Gamma_i), i = 1, \dots, N, \text{div}_\Gamma \mathbf{u} \in H_{pw}^s(\Gamma) \right\}, \\ \|\mathbf{u}\|_{\mathbf{H}^s(\text{div}_\Gamma, \Gamma)} &= \left(\sum_{i=1}^N \|\mathbf{u}_i\|_{\mathbf{H}^s(\Gamma_i)}^2 + \|\text{div}_\Gamma \mathbf{u}\|_{H_{pw}^s(\Gamma)}^2 \right)^{\frac{1}{2}}. \end{aligned} \quad (2.114)$$

For unbounded domains, the Lebesgue spaces contain functions which are only locally square integrable, i.e., for all compact subsets $K \subset \Omega^c$ it holds

$$u, v \in L_{loc}^2(\Omega^c) : \int_K \bar{v} u \, dx \leq \infty.$$

Then, the energy spaces for unbounded Lipschitz domains

$$\mathbf{H}^1(\Omega^c), \quad \mathbf{H}(\mathbf{curl}, \Omega^c), \quad \mathbf{H}(\text{div}, \Omega^c),$$

inherit the Hilbert spaces structure of $L_{loc}^2(\Omega^c)$ and $\mathbf{L}_{loc}^2(\Omega^c)$, respectively. The formulae of integration of this section hold also in this case. The boundary value problems which we consider in the following section prescribe boundary values of the unknown function. We denote the set of functions with prescribed boundary values, as follows

$$\begin{aligned} H_m^1(\Omega^c) &= \{ v \in H^1(\Omega^c) : \gamma_0 v = m \text{ on } \Gamma \}, \\ H_m(\mathbf{curl}, \Omega^c) &= \{ \mathbf{v} \in \mathbf{H}(\mathbf{curl}, \Omega^c) : \gamma_D \mathbf{v} = \mathbf{m} \text{ on } \Gamma \}. \end{aligned}$$

PERFECT ELECTRIC CONDUCTOR PROBLEM

3.1. Introduction

In 1861, the Scottish physicist James Clerk Maxwell published a set of four partial differential equations that relate the electromagnetic field to its sources, i.e., the charge density and the current density. Since that time, the so-called Maxwell system is studied in physics, in mathematics and in the engineering sciences. Current research focuses mainly on industrial application and, thus, one is interested in fast and accurate solvers for all limiting cases such as electrostatics, magnetostatics, perfect conducting materials or dielectrics. To satisfy this request, it is necessary to study the mathematical foundation of the Maxwell system.

The problem, we look at here, is the scattering of an incoming electromagnetic field on a perfect electric conductor $\Omega \subset \mathbb{R}^3$. The scattered electromagnetic field (\mathbf{E}, \mathbf{H}) solves the following exterior Dirichlet boundary value problem

$$\begin{pmatrix} \operatorname{div} \varepsilon & 0 \\ i\omega \varepsilon & \mathbf{curl} \\ -\mathbf{curl} & i\omega \mu \\ 0 & \operatorname{div} \mu \end{pmatrix} \begin{pmatrix} \mathbf{E} \\ \mathbf{H} \end{pmatrix}(\mathbf{x}) = \begin{pmatrix} 0 \\ \mathbf{0} \\ \mathbf{0} \\ 0 \end{pmatrix}, \quad \text{in } \Omega^c, \quad (3.1)$$

$$\begin{aligned} \gamma_D \mathbf{E}(\mathbf{x}) &= \mathbf{m}(\mathbf{x}), \\ \gamma_n(\mu \mathbf{H}(\mathbf{x})) &= \theta(\mathbf{x}), \end{aligned} \quad \text{on } \Gamma, \quad (3.2)$$

$$\left| \mathbf{curl} \mathbf{E}(\mathbf{x}) \times \frac{\mathbf{x}}{|\mathbf{x}|} - i\omega \varepsilon \mathbf{E}(\mathbf{x}) \right| = O\left(\frac{1}{|\mathbf{x}|^2}\right), \quad \text{for } |\mathbf{x}| \rightarrow \infty. \quad (3.3)$$

$$\left| \mathbf{curl} \mathbf{H}(\mathbf{x}) \times \frac{\mathbf{x}}{|\mathbf{x}|} - i\omega \mu \mathbf{H}(\mathbf{x}) \right| = O\left(\frac{1}{|\mathbf{x}|^2}\right),$$

Here, i is the imaginary unit and $\omega > 0$ denotes the angular frequency of the incoming electromagnetic signal. Further, the boundary conditions (3.2) are related to each other by the following differential equation posed on Γ , namely,

$$i\omega \theta(\mathbf{x}) = \operatorname{div}_\Gamma \mathbf{m}(\mathbf{x}).$$

The equations (3.3) are called the radiation conditions of Silver-Müller [48]. In this work we consider the unbounded domain Ω^c to be connected and simply connected. We assume, further, that Ω^c is a dielectric with constant permeability μ and constant permittivity ε .

The boundary value problem (3.1)-(3.3) is overdetermined, as there are eight scalar equations for six scalar unknowns. However, a closer look at the Ampère law,

$$\mathbf{curl} \mathbf{H} + i\omega \varepsilon \mathbf{E} = \mathbf{0} \quad \text{in } \Omega^c,$$

makes clear that the electric field is automatically divergence free

$$\operatorname{div}(\varepsilon \mathbf{E}) = 0 \quad \text{in } \Omega^c.$$

This last equation is called the Gauß law for the electric field. The same argument shows that the Faraday law

$$-\operatorname{curl} \mathbf{E} + i\omega \mu \mathbf{H} = \mathbf{0} \quad \text{in } \Omega^c,$$

contains the Gauß law for the magnetic field, namely,

$$\operatorname{div}(\mu \mathbf{H}) = 0 \quad \text{in } \Omega^c,$$

is automatically fulfilled. This means that the Gauß laws are redundant provided $\omega > 0$ and skipping them turns the Maxwell system into six scalar equations for six scalar unknowns. However, it will turn out that the implicit built-in of the Gauß laws is problematic for low frequencies. The reason is that the Gauß laws become independent equations characterizing electrostatic and magnetostatic phenomena for $\omega = 0$. All further considerations focus on the electric field and this is why the Gauß law for the electric field will remain enlisted in the set of relevant Maxwell equations whereas the Gauß law for the magnetic field is neglected.

In the context of boundary integral methods, a theoretical analysis of (3.1)-(3.3) is done in [22, 48] for Ω^c with smooth boundary Γ . Recent results on trace operators and function spaces on Lipschitz domains [12, 13, 15], pave the way for a successful theory in this case [14, 18, 19]. In the context of finite element methods, we refer to the monographs [27, 28, 35] for a theoretical analysis.

The aim of this chapter is to develop boundary element formulations describing weak solutions of (3.1)-(3.3). The focus here is to use the distributional settings from Section 2.4. This allows for an explicit incorporation of the traces of the solution. Besides the classical boundary element formulation analyzed in Section 3.2, we develop a new boundary element formulation in Section 3.3. By this so-called stabilized formulation the Gauß law is explicitly recovered. In Section 3.4 we investigate the relation between the electrostatic case and the stabilized formulation. We summarize the main results in Section 3.5.

3.2. The Classical Formulation

The original transmission problem describing the total field $(\mathbf{E}^t, \mathbf{H}^t)$ is the starting point of our discussion. First, we derive the induced problem, denoted the Maxwell system, for the scattered field (\mathbf{E}, \mathbf{H}) . In Subsection 3.2.1, it is shown that the Maxwell system can be written in terms of the electric field \mathbf{E} only. The so-called second order equation in distributional sense gives rise to the classical variational formulation in the energy space $\mathbf{H}(\operatorname{curl}, \Omega^c)$. Of particular interest for this work are the boundary element formulations connected to the second order equation. The most important results, as representation formulae for \mathbf{E} , the mapping properties of the layer potentials $\mathbf{S}_E, \mathbf{S}_M$ and the boundary integral equations are further stated. In Subsection 3.2.2, the solvability of the variational formulations of these integral equations is discussed.

Let Ω be a perfect electric conductor which is externally irradiated by an electromagnetic wave $(\mathbf{E}^i, \mathbf{H}^i)$. The conductor is impenetrable for the incoming signal $(\mathbf{E}^i, \mathbf{H}^i)$ and electromagnetic energy is reflected in form of the so-called scattered field (\mathbf{E}, \mathbf{H}) . The total electromagnetic field is

$$\tilde{\mathbf{E}}^t = \begin{cases} \mathbf{E}^t = \mathbf{E}^i + \mathbf{E} & \text{in } \Omega^c, \\ \mathbf{0} & \text{in } \Omega, \end{cases} \quad \text{and} \quad \tilde{\mathbf{H}}^t = \begin{cases} \mathbf{H}^t = \mathbf{H}^i + \mathbf{H} & \text{in } \Omega^c, \\ \mathbf{0} & \text{in } \Omega. \end{cases} \quad (3.4)$$

Note, that $(\tilde{\mathbf{E}}^t, \tilde{\mathbf{H}}^t)$ belongs formally to the class of vector fields analyzed in Section 2.4. A classical

solution $(\tilde{\mathbf{E}}^t, \tilde{\mathbf{H}}^t)$ of the Maxwell equations fulfills at $\mathbf{x} \in \Omega \cup \Omega^c$

$$\begin{pmatrix} \operatorname{div} \varepsilon & 0 \\ i\omega \varepsilon & \operatorname{curl} \\ -\operatorname{curl} & i\omega \mu \end{pmatrix} \begin{pmatrix} \tilde{\mathbf{E}}^t \\ \tilde{\mathbf{H}}^t \end{pmatrix}(\mathbf{x}) = \begin{pmatrix} 0 \\ \mathbf{0} \\ \mathbf{0} \end{pmatrix} \quad \text{in } \Omega \cup \Omega^c. \quad (3.5)$$

On the boundary Γ , the transmission conditions

$$\begin{aligned} [\gamma_D \tilde{\mathbf{E}}^t](\mathbf{x}) &= \mathbf{0}, \\ [\gamma_n(\mu \tilde{\mathbf{H}}^t)](\mathbf{x}) &= 0, \end{aligned} \quad \text{on } \Gamma, \quad (3.6)$$

hold. Here, the brackets $[\cdot]$ denote the jumps of the actual trace across Γ . The scattered field (\mathbf{E}, \mathbf{H}) must decay at infinity such that the radiation condition of Silver-Müller is fulfilled,

$$\begin{aligned} \left| (\operatorname{curl} \mathbf{E}(\mathbf{x})) \times \frac{\mathbf{x}}{|\mathbf{x}|} - i\omega \varepsilon \mathbf{E}(\mathbf{x}) \right| &= \mathcal{O}\left(\frac{1}{|\mathbf{x}|^2}\right), \\ \left| (\operatorname{curl} \mathbf{H}(\mathbf{x})) \times \frac{\mathbf{x}}{|\mathbf{x}|} - i\omega \mu \mathbf{H}(\mathbf{x}) \right| &= \mathcal{O}\left(\frac{1}{|\mathbf{x}|^2}\right), \end{aligned} \quad \text{for } |\mathbf{x}| \rightarrow \infty. \quad (3.7)$$

Due to finite energy considerations for the electromagnetic field [49], it makes sense to study the existence of solutions for (3.5)-(3.7) in weak form. Thus, our modelling assumptions are

$$\begin{aligned} \mathbf{E}^t &\in \mathbf{H}(\operatorname{div}, \Omega^c) & \text{and} & & \tilde{\mathbf{E}}^t &\in \mathbf{H}(\operatorname{curl}, \mathbb{R}^3), \\ \mathbf{H}^t &\in \mathbf{H}(\operatorname{curl}, \Omega^c) & \text{and} & & \mu \tilde{\mathbf{H}}^t &\in \mathbf{H}(\operatorname{div}, \mathbb{R}^3). \end{aligned} \quad (3.8)$$

These regularity assumptions account for the decomposition of the electromagnetic field given by (3.4) and, also, the behavior of the different contributions on Γ as reported in Table 3.1 is induced. It is clear that the Maxwell equations are point-wise fulfilled inside the perfect electric conductor Ω as the total electromagnetic field identically vanishes there, i.e.,

$$\begin{aligned} \tilde{\mathbf{E}}^t &= \mathbf{0} \quad \text{in } \Omega, \\ \tilde{\mathbf{H}}^t &= \mathbf{0} \quad \text{in } \Omega. \end{aligned}$$

In Ω^c , however, the regularity assumptions require a reformulation of the Maxwell equations because point evaluations of $(\tilde{\mathbf{E}}^t, \tilde{\mathbf{H}}^t)$ in Ω^c are not allowed. Therefore, the Gauß law is imposed in $L^2(\Omega^c)$, i.e., for all $\varphi \in \mathcal{D}(\mathbb{R}^3)$ it holds

$$(\operatorname{div}(\varepsilon \mathbf{E}^t), \varphi)_{\Omega^c} = 0.$$

Similarly, the Ampère law is only defined in $L^2(\Omega^c)$, i.e., for all $\varphi \in \mathcal{D}(\mathbb{R}^3)$ it holds

$$i\omega(\varepsilon \mathbf{E}^t, \varphi)_{\Omega^c} + (\operatorname{curl} \mathbf{H}^t, \varphi)_{\Omega^c} = 0.$$

The Faraday law even holds in $L^2(\mathbb{R}^3)$ because $[\gamma_D \mathbf{E}] = \mathbf{0}$ on Γ and $\tilde{\mathbf{E}}^t \in \mathbf{H}(\operatorname{curl}, \mathbb{R}^3)$, i.e., for all $\varphi \in \mathcal{D}(\mathbb{R}^3)$ it holds

$$i\omega(\mu \mathbf{H}^t, \varphi)_{\mathbb{R}^3} - (\operatorname{curl} \mathbf{E}^t, \varphi)_{\mathbb{R}^3} = 0.$$

Except for the Faraday law, the domains Ω and Ω^c were considered separately. In order to obtain a global formulation, the differential operators must be understood in distributional sense.

Table 3.1.: The electromagnetic fields $(\mathbf{E}^i, \mathbf{H}^i)$, $(\mathbf{E}^t, \mathbf{H}^t)$ and $(\tilde{\mathbf{E}}^t, \tilde{\mathbf{H}}^t)$.

Notation	Regularity assumptions		Boundary data
\mathbf{E}^i	$\mathbf{H}(\operatorname{div}, \mathbb{R}^3)$	$\mathbf{H}(\operatorname{curl}, \mathbb{R}^3)$	$[\gamma_D \mathbf{E}^i] = \mathbf{0}$
\mathbf{E}^t	$\mathbf{H}(\operatorname{div}, \Omega^c)$	$\mathbf{H}(\operatorname{curl}, \Omega^c)$	$\gamma_D \mathbf{E}^t = -\gamma_D \mathbf{E}^i$
$\tilde{\mathbf{E}}^t$	$\mathbf{H}(\operatorname{div}, \Omega \cup \Omega^c)$	$\mathbf{H}(\operatorname{curl}, \mathbb{R}^3)$	$[\gamma_D \tilde{\mathbf{E}}^t] = \mathbf{0}$
$\mu \mathbf{H}^i$	$\mathbf{H}(\operatorname{div}, \mathbb{R}^3)$	$\mathbf{H}(\operatorname{curl}, \mathbb{R}^3)$	$[\gamma_n(\mu \mathbf{H}^i)] = 0$
$\mu \mathbf{H}^t$	$\mathbf{H}(\operatorname{div}, \Omega^c)$	$\mathbf{H}(\operatorname{curl}, \Omega^c)$	$\gamma_n(\mu \mathbf{H}^t) = -\gamma_n(\mu \mathbf{H}^i)$
$\mu \tilde{\mathbf{H}}^t$	$\mathbf{H}(\operatorname{div}, \mathbb{R}^3)$	$\mathbf{H}(\operatorname{curl}, \Omega \cup \Omega^c)$	$[\gamma_n(\mu \tilde{\mathbf{H}}^t)] = 0$

Lemma 3.2.1 *Let $(\tilde{\mathbf{E}}^t, \tilde{\mathbf{H}}^t)$ be such that for all $\varphi \in \mathcal{D}(\mathbb{R}^3)$, $\varphi \in \mathcal{D}(\mathbb{R}^3)$, it holds*

$$(\operatorname{div}(\varepsilon \mathbf{E}^t), \varphi)_{\Omega^c} = 0, \quad (3.9)$$

$$(\operatorname{curl} \mathbf{H}^t, \varphi)_{\Omega^c} = -i\omega(\varepsilon \mathbf{E}^t, \varphi)_{\Omega^c}, \quad (3.10)$$

$$-(\operatorname{curl} \mathbf{E}^t, \varphi)_{\mathbb{R}^3} = -i\omega(\mu \mathbf{H}^t, \varphi)_{\mathbb{R}^3}. \quad (3.11)$$

Then, it holds in distributional sense

$$\langle \operatorname{div}(\varepsilon \tilde{\mathbf{E}}^t), \varphi \rangle = -\langle \gamma_n(\varepsilon \mathbf{E}^t) \delta_\Gamma, \varphi \rangle, \quad (3.12)$$

$$\langle \operatorname{curl} \tilde{\mathbf{H}}^t, \varphi \rangle = -i\omega(\varepsilon \mathbf{E}^t, \varphi)_{\Omega^c} - \langle \gamma_D \mathbf{H}^t \delta_\Gamma, \varphi \rangle, \quad (3.13)$$

$$-\langle \operatorname{curl} \tilde{\mathbf{E}}^t, \varphi \rangle = -i\omega(\mu \tilde{\mathbf{H}}^t, \varphi)_{\mathbb{R}^3}. \quad (3.14)$$

Proof: Due to Lemma 2.4.1, it holds for all $\varphi \in \mathcal{D}(\mathbb{R}^3)$

$$\langle \operatorname{div}(\varepsilon \tilde{\mathbf{E}}^t), \varphi \rangle = (\operatorname{div}(\varepsilon \mathbf{E}^t), \varphi)_{\Omega^c} - \langle \gamma_n(\varepsilon \mathbf{E}^t) \delta_\Gamma, \varphi \rangle.$$

The Gauß law in distributional sense (3.12) follows from (3.9). Due to Lemma 2.4.2, it holds for all $\varphi \in \mathcal{D}(\mathbb{R}^3)$

$$\langle \operatorname{curl} \tilde{\mathbf{H}}^t, \varphi \rangle = (\operatorname{curl} \mathbf{H}^t, \varphi)_{\Omega^c} - \langle \gamma_D \mathbf{H}^t \delta_\Gamma, \varphi \rangle.$$

Thus, the Ampère law in distributional sense (3.13) follows from (3.10). For the Faraday law, note that $\operatorname{curl} \tilde{\mathbf{E}}^t \in \mathbf{L}^2(\mathbb{R}^3)$, hence a regular distribution, and due to (2.69), it holds

$$\langle \operatorname{curl} \tilde{\mathbf{E}}^t, \varphi \rangle = (\operatorname{curl} \tilde{\mathbf{E}}^t, \varphi)_{\mathbb{R}^3}.$$

□

The Gauß law in distributional sense (3.12) means that the distribution $\operatorname{div}(\varepsilon \tilde{\mathbf{E}}^t)$ vanishes almost everywhere in \mathbb{R}^3 and it exhibits a surface delta distribution with weight $\gamma_n(\varepsilon \mathbf{E}^t)$. Similarly, (3.13) means that the distribution $\operatorname{curl} \tilde{\mathbf{H}}^t$ can be identified almost everywhere in \mathbb{R}^3 with the vector field $i\omega \varepsilon \mathbf{E}^t$ and it exhibits a surface delta distribution with weight $\gamma_D \mathbf{H}^t$. The surface delta distributions, $\gamma_n(\varepsilon \mathbf{E}^t) \delta_\Gamma$ and $\gamma_n \mathbf{E}^t \delta_\Gamma$ are supplementary unknowns of the problem but they are connected by the continuity equation as the next lemma shows. The fact that the continuity equation shrinks to an identity of traces is peculiar for the perfect electric conductor problem.

Lemma 3.2.2 *Let $(\tilde{\mathbf{E}}^t, \tilde{\mathbf{H}}^t)$ be given with (3.12)-(3.14). For $\omega > 0$, the surface delta distributions $\gamma_n \mathbf{E}^t \delta_\Gamma$ and $\gamma_N \mathbf{E}^t \delta_\Gamma$ are connected by the continuity equation*

$$\forall \varphi \in \mathcal{D}(\mathbb{R}^3) : \quad \langle \gamma_N \mathbf{E}^t \delta_\Gamma, \nabla \varphi \rangle = \omega^2 \mu \langle \gamma_n (\varepsilon \mathbf{E}^t) \delta_\Gamma, \varphi \rangle. \quad (3.15)$$

Moreover, for $\omega = 0$, it holds

$$\forall \varphi \in \mathcal{D}(\mathbb{R}^3) : \quad \langle \gamma_N \mathbf{E}^t \delta_\Gamma, \varphi \rangle = 0. \quad (3.16)$$

Proof: The Faraday law says that $\mathbf{curl} \tilde{\mathbf{E}}^t$ identifies with $i\omega \mu \tilde{\mathbf{H}}^t \in \mathbf{L}^2(\mathbb{R}^3)$. Thus, for $\omega > 0$ it holds

$$\tilde{\mathbf{H}}^t = -i(\omega\mu)^{-1} \mathbf{curl} \tilde{\mathbf{E}}^t \quad \text{with} \quad \gamma_D \mathbf{H}^t = -i(\omega\mu)^{-1} \gamma_N \mathbf{E}^t.$$

Inserting these identities in the Ampère law (3.13) leads to

$$\langle \mathbf{curl} (-i(\omega\mu)^{-1} \mathbf{curl} \tilde{\mathbf{E}}^t), \varphi \rangle + i\omega \langle \varepsilon \tilde{\mathbf{E}}^t, \varphi \rangle = i(\omega\mu)^{-1} \langle \gamma_N \mathbf{E}^t \delta_\Gamma, \varphi \rangle.$$

For the special choice of test vector fields $\varphi = \nabla \varphi$, $\varphi \in \mathcal{D}(\mathbb{R}^3)$, it holds by definition

$$\langle \mathbf{curl} (-i(\omega\mu)^{-1} \mathbf{curl} \tilde{\mathbf{E}}^t), \nabla \varphi \rangle = -i(\omega\mu)^{-1} \langle \mathbf{curl} \tilde{\mathbf{E}}^t, \mathbf{curl} \nabla \varphi \rangle = 0,$$

and we obtain

$$\omega^2 \mu \langle \varepsilon \tilde{\mathbf{E}}^t, \nabla \varphi \rangle = \langle \gamma_N \mathbf{E}^t \delta_\Gamma, \nabla \varphi \rangle.$$

By virtue of (3.12), it holds

$$\langle \text{div} (\varepsilon \tilde{\mathbf{E}}^t), \varphi \rangle = -\langle \varepsilon \tilde{\mathbf{E}}^t, \nabla \varphi \rangle = -\langle \gamma_n (\varepsilon \mathbf{E}^t) \delta_\Gamma, \varphi \rangle$$

and, therefore, for all $\omega > 0$

$$\omega^2 \mu \langle \gamma_n (\varepsilon \mathbf{E}^t) \delta_\Gamma, \varphi \rangle = \langle \gamma_N \mathbf{E}^t \delta_\Gamma, \nabla \varphi \rangle.$$

In case $\omega = 0$, the Faraday law

$$\langle \mathbf{curl} \mathbf{E}^t, \varphi \rangle = 0$$

yields that $\text{supp}(\mathbf{curl} \tilde{\mathbf{E}}^t) = \emptyset$ and (3.16) must hold. \square

So far, we considered the total electromagnetic field $(\tilde{\mathbf{E}}^t, \tilde{\mathbf{H}}^t)$. However, we are interested in $(\tilde{\mathbf{E}}, \tilde{\mathbf{H}})$, namely, the scattered field restricted to Ω^c

$$\tilde{\mathbf{E}} = \begin{cases} \mathbf{E} & \text{in } \Omega^c, \\ \mathbf{0} & \text{in } \Omega, \end{cases} \quad \text{and} \quad \tilde{\mathbf{H}} = \begin{cases} \mathbf{H} & \text{in } \Omega^c, \\ \mathbf{0} & \text{in } \Omega, \end{cases} \quad (3.17)$$

where

$$\mathbf{E}, \mathbf{H} \in \mathbf{H}(\mathbf{curl}, \Omega^c) \cap \mathbf{H}(\text{div}, \Omega^c). \quad (3.18)$$

Due to the linearity of the problem, the interface conditions (3.6) turn into boundary conditions for the scattered electromagnetic field. By the use of the notations $\gamma_D \mathbf{E}^i = -\mathbf{m}$ and $\gamma_n(\mu \mathbf{H}^i) = -\theta$ for the given traces of the incoming electromagnetic field, it must hold

$$\gamma_D \mathbf{E} = \mathbf{m} \quad \text{and} \quad \gamma_n(\mu \mathbf{H}) = \theta. \quad (3.19)$$

Following the same procedure as for the total field, we obtain the harmonic Maxwell equations in

distributional sense for the scattered electromagnetic field. An overview on the regularity assumptions which underly the different field components that appear in Lemma 3.2.3 is given in Table 3.2.

Lemma 3.2.3 *Let $(\tilde{\mathbf{E}}, \tilde{\mathbf{H}})$ as in (3.17)-(3.19) with (\mathbf{E}, \mathbf{H}) such that*

$$\langle \operatorname{div}(\varepsilon \mathbf{E}), \varphi \rangle_{\Omega^c} = 0, \quad (3.20)$$

$$\langle \operatorname{curl} \mathbf{H}, \varphi \rangle_{\Omega^c} = -i\omega \langle \varepsilon \mathbf{E}, \varphi \rangle_{\Omega^c}, \quad (3.21)$$

$$-\langle \operatorname{curl} \mathbf{E}, \varphi \rangle_{\Omega^c} = -i\omega \langle \mu \mathbf{H}, \varphi \rangle_{\Omega^c}, \quad (3.22)$$

for all $\varphi \in \mathcal{D}(\mathbb{R}^3)$ and $\varphi \in \mathcal{D}(\mathbb{R}^3)$, respectively. Then, it holds in distributional sense

$$\langle \operatorname{div}(\varepsilon \tilde{\mathbf{E}}), \varphi \rangle = -\langle \gamma_n(\varepsilon \mathbf{E}) \delta_\Gamma, \varphi \rangle, \quad (3.23)$$

$$\langle \operatorname{curl} \tilde{\mathbf{H}}, \varphi \rangle = -i\omega \langle \varepsilon \mathbf{E}, \varphi \rangle_{\Omega^c} - \langle \gamma_D \mathbf{H} \delta_\Gamma, \varphi \rangle, \quad (3.24)$$

$$-\langle \operatorname{curl} \tilde{\mathbf{E}}, \varphi \rangle = -i\omega \langle \mu \mathbf{H}, \varphi \rangle_{\Omega^c} + \langle \mathbf{m} \delta_\Gamma, \varphi \rangle. \quad (3.25)$$

Table 3.2.: The electromagnetic fields (\mathbf{E}, \mathbf{H}) and $(\tilde{\mathbf{E}}, \tilde{\mathbf{H}})$.

Notation	Regularity assumptions		Boundary data
$\tilde{\mathbf{E}}$	$\mathbf{H}(\operatorname{div}, \Omega \cup \Omega^c)$	$\mathbf{H}(\operatorname{curl}, \Omega \cup \Omega^c)$	$[\gamma_D \tilde{\mathbf{E}}] = \mathbf{m}$
\mathbf{E}	$\mathbf{H}(\operatorname{div}, \Omega^c)$	$\mathbf{H}(\operatorname{curl}, \Omega^c)$	$\gamma_D \mathbf{E} = \mathbf{m}$
$\mu \tilde{\mathbf{H}}$	$\mathbf{H}(\operatorname{div}, \Omega \cup \Omega^c)$	$\mathbf{H}(\operatorname{curl}, \Omega \cup \Omega^c)$	$[\gamma_n(\mu \tilde{\mathbf{H}})] = \theta$
$\mu \mathbf{H}$	$\mathbf{H}(\operatorname{div}, \Omega^c)$	$\mathbf{H}(\operatorname{curl}, \Omega^c)$	$\gamma_n(\mu \mathbf{H}) = \theta$

3.2.1. Second order equation

Let $\mathbf{E} \in \mathbf{H}_m(\operatorname{curl}, \Omega^c) \cap \mathbf{H}(\operatorname{div}, \Omega^c)$ and $\mathbf{H} \in \mathbf{H}(\operatorname{curl}, \Omega^c) \cap \mathbf{H}(\operatorname{div}, \Omega^c)$ denote a solution of the Maxwell system in distributional sense

$$\begin{cases} \langle \operatorname{div}(\varepsilon \tilde{\mathbf{E}}), \varphi \rangle & = -\langle \gamma_n(\varepsilon \mathbf{E}) \delta_\Gamma, \varphi \rangle, \\ \langle \operatorname{curl} \tilde{\mathbf{H}}, \varphi \rangle + i\omega \langle \varepsilon \tilde{\mathbf{E}}, \varphi \rangle & = -\langle \gamma_D \mathbf{H} \delta_\Gamma, \varphi \rangle, \\ -\langle \operatorname{curl} \tilde{\mathbf{E}}, \varphi \rangle + i\omega \langle \mu \tilde{\mathbf{H}}, \varphi \rangle & = \langle \mathbf{m} \delta_\Gamma, \varphi \rangle. \end{cases}$$

Provided $\omega > 0$, it follows from the Faraday law

$$\begin{aligned} \tilde{\mathbf{H}} &= -i(\omega\mu)^{-1} \operatorname{curl} \tilde{\mathbf{E}} - i(\omega\mu)^{-1} \mathbf{m} \delta_\Gamma, \\ \gamma_D \mathbf{H} &= -i(\omega\mu)^{-1} \gamma_N \mathbf{E}. \end{aligned}$$

Thus, $\operatorname{curl} \operatorname{curl} \mathbf{E} \in L^2(\Omega^c)$ because for all $\varphi \in \mathcal{D}(\mathbb{R}^3)$ with $\operatorname{supp} \varphi \subset \Omega^c$ it holds

$$\langle \mathbf{H}, \varphi \rangle_{\Omega^c} = -i(\omega\mu)^{-1} \langle \operatorname{curl} \mathbf{E}, \varphi \rangle_{\Omega^c} \quad \text{and} \quad \mathbf{H} \in \mathbf{H}(\operatorname{curl}, \Omega^c).$$

Inserting this into the Ampère law yields

$$\langle \operatorname{curl}(-i(\omega\mu)^{-1} \operatorname{curl} \tilde{\mathbf{E}}), \varphi \rangle + \langle \operatorname{curl}(-i(\omega\mu)^{-1} \mathbf{m} \delta_\Gamma), \varphi \rangle + i\omega \langle \varepsilon \tilde{\mathbf{E}}, \varphi \rangle = i(\omega\mu)^{-1} \langle \gamma_N \mathbf{E} \delta_\Gamma, \varphi \rangle.$$

By definition, it holds

$$\begin{aligned}\langle \mathbf{curl}(\mathbf{m}\delta_\Gamma), \varphi \rangle &= \langle \mathbf{m}\delta_\Gamma, \mathbf{curl} \varphi \rangle, \\ \langle \mathbf{curl} \mathbf{curl} \tilde{\mathbf{E}}, \varphi \rangle &= \langle \mathbf{curl} \tilde{\mathbf{E}}, \mathbf{curl} \varphi \rangle.\end{aligned}$$

From this, we obtain

$$\langle \mathbf{curl} \tilde{\mathbf{E}}, \mathbf{curl} \varphi \rangle - \omega^2 \mu \langle \varepsilon \tilde{\mathbf{E}}, \varphi \rangle = -\langle \gamma_N \mathbf{E} \delta_\Gamma, \varphi \rangle - \langle \mathbf{m}\delta_\Gamma, \mathbf{curl} \varphi \rangle, \quad (3.26)$$

$$\langle \operatorname{div}(\varepsilon \tilde{\mathbf{E}}), \varphi \rangle = -\langle \gamma_n(\varepsilon \tilde{\mathbf{E}}) \delta_\Gamma, \varphi \rangle. \quad (3.27)$$

The next lemma shows that equation (3.26) contains (3.27) in L^2 -sense.

Lemma 3.2.4 *The validity of (3.26) for $\omega > 0$ yields the validity of the Gauß law (3.20) for all $\varphi \in \mathcal{D}(\mathbb{R}^3)$ with $\operatorname{supp} \varphi \subset \Omega^c$.*

Proof: For all test vector fields of the form $\varphi = \nabla \varphi$, $\varphi \in \mathcal{D}(\mathbb{R}^3)$, equation (3.26) reads

$$-\omega^2 \mu \langle \varepsilon \tilde{\mathbf{E}}, \nabla \varphi \rangle = -\langle \gamma_N \mathbf{E} \delta_\Gamma, \nabla \varphi \rangle.$$

This means that for all $\varphi \in \mathcal{D}(\mathbb{R}^3)$

$$-\omega^2 \mu \langle \varepsilon \tilde{\mathbf{E}}, \nabla \varphi \rangle = \omega^2 \mu \langle \operatorname{div}(\varepsilon \tilde{\mathbf{E}}), \varphi \rangle = \omega^2 \mu \langle \operatorname{div}(\varepsilon \mathbf{E}), \varphi \rangle_{\Omega^c} - \omega^2 \mu \langle \gamma_n(\varepsilon \mathbf{E}) \delta_\Gamma, \varphi \rangle = -\langle \gamma_N \mathbf{E} \delta_\Gamma, \nabla \varphi \rangle.$$

Therefore, it holds for the test functions with $\operatorname{supp} \varphi \subset \Omega^c$

$$\langle \operatorname{div}(\varepsilon \mathbf{E}), \varphi \rangle_{\Omega^c} = 0.$$

□

A closer look at the proof of Lemma 3.2.4 shows that a distributional solution $\tilde{\mathbf{E}}$ of (3.26) must also fulfill the continuity equation, namely it holds for all $\varphi \in \mathcal{D}(\mathbb{R}^3)$

$$\langle \gamma_N \mathbf{E} \delta_\Gamma, \nabla \varphi \rangle = \omega^2 \mu \langle \gamma_n(\varepsilon \mathbf{E}) \delta_\Gamma, \varphi \rangle. \quad (3.28)$$

The material parameters μ , $\varepsilon > 0$ and the frequency $\omega > 0$ are often united in one single constant, the wave number $\kappa^2 = \omega^2 \mu \varepsilon > 0$. With this notation, the second order Maxwell equation in distributional sense reads

$$\langle (\mathbf{curl} \mathbf{curl} - \kappa^2) \tilde{\mathbf{E}}, \varphi \rangle = -\langle \gamma_N \mathbf{E} \delta_\Gamma, \varphi \rangle - \langle \mathbf{m}\delta_\Gamma, \mathbf{curl} \varphi \rangle. \quad (3.29)$$

To prove that the second order equation has a unique solution $\mathbf{E} \in \mathbf{H}(\mathbf{curl}, \Omega^c)$, it is necessary to relax the regularity of the test vector fields and consider the energy space $\mathbf{H}(\mathbf{curl}, \Omega^c)$ instead of $\mathcal{D}(\mathbb{R}^3)$. The duality pairing on the left corresponds then to the inner product of $L^2(\Omega^c)$. Of particular importance in the context of boundary element formulations is that the pairings on the right hand side are the functional pairings in the trace spaces introduced in Section 2.5. The functional setting obtained in energy spaces corresponds to the setting which is suitable to develop a solution theory for the second order equation in the context of boundary element formulations. The principal theorems from this solution theory are stated in the following and references are given for details on the proofs.

Due to the following theorem, the original scattering problem has at most one solution. The proof can be found in [48], for instance.

Theorem 3.2.5 Let $\mathbf{E}^i \in \mathbf{H}(\mathbf{curl curl}, \Omega^c)$ with

$$\mathbf{curl curl} \mathbf{E}^i - \kappa^2 \mathbf{E}^i = \mathbf{0} \quad \text{in } \Omega^c$$

and

$$\gamma_D \mathbf{E}^i = \mathbf{m} \in H^{-\frac{1}{2}}(\text{div}_\Gamma, \Gamma).$$

The perfect electric conductor problem

$$\left\{ \begin{array}{ll} \mathbf{curl curl} \mathbf{E} - \kappa^2 \mathbf{E} = \mathbf{0}, & \text{in } \Omega^c, \\ \gamma_D \mathbf{E} = \mathbf{m}, & \text{on } \Gamma, \\ \left| \mathbf{curl} \mathbf{E}(\mathbf{x}) \times \frac{\mathbf{x}}{|\mathbf{x}|} - i\omega \varepsilon \mathbf{E}(\mathbf{x}) \right| = \mathcal{O}\left(\frac{1}{|\mathbf{x}|^2}\right), & \text{for } |\mathbf{x}| \rightarrow \infty, \end{array} \right. \quad (3.30)$$

has at most one solution $\mathbf{E} \in \mathbf{H}(\mathbf{curl curl}, \Omega^c)$. We call it the Maxwell solution.

To develop a boundary element formulation a fundamental solution characterizing the point sources of the involved differential operator is needed. For $\kappa > 0$, the second order Maxwell operator $\mathbf{curl curl} - \kappa^2$ has a fundamental solution. In the following, the Hesse matrix of a two times differentiable function $v: \mathbb{R}^3 \rightarrow \mathbb{C}$ is denoted $\mathbf{H}v$. The proof of the following lemma can be found in [48, 54].

Lemma 3.2.6 Let $\kappa > 0$ and let $I_3 \in \mathbb{R}^{3 \times 3}$ denote the identity matrix. The function $\mathbf{u}^* \in \mathbf{C}^\infty(\mathbb{R}^3 \setminus \{\mathbf{0}\})$,

$$\mathbf{u}^*(\mathbf{x}) = I_3 G_\kappa(\mathbf{x}) + \frac{1}{\kappa^2} \mathbf{H}G_\kappa(\mathbf{x}), \quad G_\kappa(\mathbf{x}) = \frac{e^{-i\kappa|\mathbf{x}|}}{4\pi|\mathbf{x}|} \quad (3.31)$$

is a fundamental solution of the second order Maxwell equation, i.e., for all $\varphi \in \mathcal{D}(\mathbb{R}^3)$ it holds

$$\langle (\mathbf{curl curl} - \kappa^2) \mathbf{u}^*, \varphi \rangle = \langle \delta_{\mathbf{0}}, \varphi \rangle = \varphi(\mathbf{x}). \quad (3.32)$$

For all $\kappa > 0$, $G_\kappa \in \mathbf{C}^\infty(\mathbb{R}^3 \setminus \{\mathbf{0}\})$ is a fundamental solution of the Helmholtz equation, i.e., for all $\varphi \in \mathcal{D}(\mathbb{R}^3)$ it holds

$$-\langle (\Delta + \kappa^2) G_\kappa, \varphi \rangle = \langle \delta_{\mathbf{0}}, \varphi \rangle = \varphi(\mathbf{x}). \quad (3.33)$$

For $\kappa = 0$, $G_0 \in \mathbf{C}^\infty(\mathbb{R}^3 \setminus \{\mathbf{0}\})$ is a fundamental solution of the Laplace equation, i.e., for all $\varphi \in \mathcal{D}(\mathbb{R}^3)$ it holds

$$-\langle \Delta G_0, \varphi \rangle = \langle \delta_{\mathbf{0}}, \varphi \rangle = \varphi(\mathbf{x}). \quad (3.34)$$

It is well known [52], that for any $v \in L^1(\Omega^c)$, $\mathbf{v} \in \mathbf{L}^1(\Omega^c)$ the single layer potentials for the Helmholtz operator, defined by

$$(S_\kappa v)(\mathbf{x}) = \int_\Gamma G_\kappa(\mathbf{x} - \mathbf{y}) v(\mathbf{y}) d\sigma_y, \quad (\mathbf{S}_\kappa \mathbf{v})(\mathbf{x}) = \int_\Gamma G_\kappa(\mathbf{x} - \mathbf{y}) \mathbf{v}(\mathbf{y}) d\sigma_y, \quad (3.35)$$

satisfy for $\kappa \geq 0$ and $\mathbf{x} \in \Omega^c$ the differential equations

$$-\Delta(S_\kappa(v))(\mathbf{x}) - \kappa^2 S_\kappa(v)(\mathbf{x}) = 0, \quad -\Delta(\mathbf{S}_\kappa(\mathbf{v}))(\mathbf{x}) - \kappa^2 \mathbf{S}_\kappa(\mathbf{v})(\mathbf{x}) = \mathbf{0}. \quad (3.36)$$

The analysis of boundary integral equations connected to the second order Maxwell operator relies very much on the properties of S_κ for $\kappa \geq 0$. Here, it is most important that functions of the form $S_\kappa(v)$, $\mathbf{S}_\kappa(\mathbf{v})$ possess traces on the boundary and, moreover, that the domain of definition of S_κ and \mathbf{S}_κ , respectively, can be extended to the trace spaces defined in Section 2.5. The functional analytic

properties of these extended operators depend on interior eigenvalues for the Laplace operator and the **curl curl** operator.

Definition 8 Let Ω denote a bounded Lipschitz domain in \mathbb{R}^3 . $\lambda \in \mathbb{R}$ is called an interior eigenvalue of the Laplace operator, if there is a non-vanishing $u \in H_0^1(\Omega)$ such that

$$(\nabla u, \nabla v)_\Omega = \lambda(u, v)_\Omega$$

for all $v \in H_0^1(\Omega)$.

Similarly, for a bounded Lipschitz domain $\Omega \subset \mathbb{R}^3$, $\lambda \in \mathbb{R}$ is called an interior eigenvalue of the **curl curl** operator, if there is a non-vanishing $\mathbf{E} \in \mathbf{H}_0(\mathbf{curl}, \Omega)$ such that

$$(\mathbf{curl} \mathbf{E}, \mathbf{curl} \mathbf{v})_\Omega = \lambda(\mathbf{E}, \mathbf{v})_\Omega$$

for all $\mathbf{v} \in \mathbf{H}_0(\mathbf{curl}, \Omega)$.

It is a peculiarity of many boundary integral equations connected to the Helmholtz or the second order Maxwell operator that they fail to have unique solutions if κ^2 is an interior eigenvalue of the corresponding operator, even if an exterior problem is considered. Now and in the following, we assume that κ^2 is neither an interior eigenvalue of the Laplace operator nor an interior eigenvalue of the **curl curl** operator.

The properties of S_κ and \mathbf{S}_κ are summarized in Theorem 3.2.7. The proof as found in [14, 36], for instance, build up on the fundamental results published in [23, 52, 54].

Theorem 3.2.7 *For all $\kappa \geq 0$, the operators*

$$S_\kappa : H^{-\frac{1}{2}}(\Gamma) \rightarrow H^1(\Omega^c), \quad (3.37)$$

$$\mathbf{S}_\kappa : \mathbf{H}_R^{-\frac{1}{2}}(\Gamma) \rightarrow \mathbf{H}^1(\Omega^c), \quad (3.38)$$

$$\mathbf{S}_\kappa : \mathbf{H}_D^{-\frac{1}{2}}(\Gamma) \rightarrow \mathbf{H}^1(\Omega^c), \quad (3.39)$$

are linear and continuous. Moreover, the boundary integral operators are continuous

$$\gamma_0 S_\kappa : H^{-\frac{1}{2}}(\Gamma) \rightarrow H^{\frac{1}{2}}(\Gamma), \quad (3.40)$$

$$\gamma_R \mathbf{S}_\kappa : H^{-\frac{1}{2}}(\text{div}_\Gamma, \Gamma) \rightarrow H^{-\frac{1}{2}}(\text{curl}_\Gamma, \Gamma). \quad (3.41)$$

The boundary integral operators for $\kappa = 0$ are selfadjoint with respect to the duality pairings $\langle \cdot, \cdot \rangle_{\frac{1}{2}}$, $\langle \cdot, \cdot \rangle_{-\frac{1}{2}}$ and satisfy

$$\forall v \in H^{-\frac{1}{2}}(\Gamma) : \langle \bar{v}, \gamma_0 S_0 v \rangle_{\frac{1}{2}} \geq c \|v\|_{H^{-\frac{1}{2}}(\Gamma)}^2, \quad (3.42)$$

$$\forall \phi \in H^{-\frac{1}{2}}(\text{div}_\Gamma, \Gamma) : \langle \gamma_R \mathbf{S}_0(\phi), \bar{\phi} \rangle_{-\frac{1}{2}} \geq c \|\phi\|_{H^{-\frac{1}{2}}(\text{div}_\Gamma, \Gamma)}^2, \quad (3.43)$$

with constants $c > 0$ depending only on Γ . Moreover, it holds that the following operators are compact for all $\kappa > 0$

$$\gamma_0 S_0 - \gamma_0 S_\kappa : H^{-\frac{1}{2}}(\Gamma) \rightarrow H^{\frac{1}{2}}(\Gamma), \quad (3.44)$$

$$\gamma_R \mathbf{S}_0 - \gamma_R \mathbf{S}_\kappa : H^{-\frac{1}{2}}(\text{div}_\Gamma, \Gamma) \rightarrow H^{-\frac{1}{2}}(\text{curl}_\Gamma, \Gamma). \quad (3.45)$$

Besides the single layer potential for the Helmholtz operator, S_κ , there is the single layer potential for the Maxwell operator, \mathbf{S}_E , and there is the double layer potential for the Maxwell operator, \mathbf{S}_M . Their definition and mapping properties are stated in Lemma 3.2.8 and more details can be

found in [19]. For notational brevity, we introduce the operator $[\gamma_R]$ which applies on functions $\mathbf{v} \in \mathbf{H}(\mathbf{curl}, \Omega)$ in the form $[\gamma_R](\mathbf{v}) = [\gamma_R(\mathbf{v})]$.

Lemma 3.2.8 *Let $\kappa > 0$ and $\mathbf{u} \in H^{-\frac{1}{2}}(\text{div}_\Gamma, \Gamma)$. The single layer potential for the Maxwell operator*

$$\mathbf{S}_E(\mathbf{u}) = \mathbf{S}_\kappa(\mathbf{u}) + \frac{1}{\kappa^2} \nabla S_\kappa(\text{div}_\Gamma(\mathbf{u})) \quad (3.46)$$

is a continuous operator

$$\mathbf{S}_E: H^{-\frac{1}{2}}(\text{div}_\Gamma, \Gamma) \rightarrow \mathbf{H}(\mathbf{curl curl}, \Omega^c).$$

For $\mathbf{u} \in H^{-\frac{1}{2}}(\text{div}_\Gamma, \Gamma)$, $\mathbf{S}_E(\mathbf{u})$ is a weak solution of the second order Maxwell equation, namely

$$(\mathbf{curl curl} - \kappa^2)\mathbf{S}_E(\mathbf{u}) = \mathbf{0}. \quad (3.47)$$

The boundary integral operator

$$\gamma_R \mathbf{S}_E: H^{-\frac{1}{2}}(\text{div}_\Gamma, \Gamma) \rightarrow H^{-\frac{1}{2}}(\mathbf{curl}_\Gamma, \Gamma) \quad (3.48)$$

is continuous, this means that for all $\phi \in H^{-\frac{1}{2}}(\text{div}_\Gamma, \Gamma)$ it holds

$$\langle [\gamma_R] \mathbf{S}_E(\mathbf{u}), \phi \rangle_{-\frac{1}{2}} = 0. \quad (3.49)$$

The double layer potential for the Maxwell operator

$$\mathbf{S}_M(\mathbf{u}) = \mathbf{curl} \mathbf{S}_\kappa(\mathbf{u}) \quad (3.50)$$

is a continuous operator

$$\mathbf{S}_M: H^{-\frac{1}{2}}(\text{div}_\Gamma, \Gamma) \rightarrow \mathbf{H}(\mathbf{curl curl}, \Omega^c).$$

For $\mathbf{u} \in H^{-\frac{1}{2}}(\text{div}_\Gamma, \Gamma)$, $\mathbf{S}_M(\mathbf{u})$ is a weak solution of the second order Maxwell equation, namely

$$(\mathbf{curl curl} - \kappa^2)\mathbf{S}_M(\mathbf{u}) = \mathbf{0}. \quad (3.51)$$

The boundary integral operator

$$\gamma_R \mathbf{S}_M: H^{-\frac{1}{2}}(\text{div}_\Gamma, \Gamma) \rightarrow H^{-\frac{1}{2}}(\mathbf{curl}_\Gamma, \Gamma) \quad (3.52)$$

is discontinuous, because it holds for all $\phi \in H^{-\frac{1}{2}}(\text{div}_\Gamma, \Gamma)$ that

$$\langle [\gamma_R] \mathbf{S}_M(\mathbf{u}), \phi \rangle_{-\frac{1}{2}} = -\langle [\gamma_R] \mathbf{u}, \phi \rangle_{-\frac{1}{2}}. \quad (3.53)$$

As shown in [19], the previous results yield the direct representation formula for \mathbf{E} .

Lemma 3.2.9 *Let $\mathbf{E} \in \mathbf{H}(\mathbf{curl curl}, \Omega^c)$ be the unique solution of (3.30) with $\mathbf{j} = \gamma_N \mathbf{E}$ and $\mathbf{m} = \gamma_D \mathbf{E}$. The scattered electric field \mathbf{E} can be formally represented for almost all $\mathbf{x} \in \Omega^c$ by*

$$\mathbf{E}(\mathbf{x}) = \mathbf{S}_M(\mathbf{m})(\mathbf{x}) + \mathbf{S}_E(\mathbf{j})(\mathbf{x}). \quad (3.54)$$

In the following, (3.54) is called the direct representation formula. An integral equation for the unknown Neumann trace \mathbf{j} is obtained when (3.54) is subjected to the trace operator γ_R , i.e.,

$$\gamma_R \mathbf{S}_E(\mathbf{j}) = \gamma_R(\mathbf{E} - \mathbf{S}_M(\mathbf{m})) = \mathbf{m} \times \mathbf{n} - \gamma_R \mathbf{S}_M(\mathbf{m}). \quad (3.55)$$

Recall that the Dirichlet trace \mathbf{m} is imposed by the boundary value problem (3.30) and, thus, the boundary integral equation (3.55) is an equation for the unknown Neumann trace \mathbf{j} .

Besides the direct representation (3.54), \mathbf{E} can formally be given by

$$\mathbf{E}(\mathbf{x}) = \mathbf{S}_E(\mathbf{j}^t)(\mathbf{x}), \quad (3.56)$$

because, by virtue of (3.47), the electric field given by (3.56) is a weak solution of the second order Maxwell equation. In order to obtain a solution of the boundary value problem (3.30), the density \mathbf{j}^t must be found such that

$$\gamma_R \mathbf{S}_E(\mathbf{j}^t) = \mathbf{m} \times \mathbf{n}. \quad (3.57)$$

The engineering community calls the boundary integral equation (3.57) the electric field integral equation, whereas the mathematicians refer to it as the boundary integral equation resulting from an indirect representation formula for \mathbf{E} . The latter formulation is, however, misleading because the density \mathbf{j}^t is physically meaningful as

$$\mathbf{j}^t = \gamma_N(\mathbf{E}^i + \mathbf{E}). \quad (3.58)$$

Instead of the boundary value problem for \mathbf{E} deduced from (3.17), we could have considered the transmission problem for scattered electric field, i.e.,

$$\tilde{\mathbf{E}} = \begin{cases} \mathbf{E} & \text{in } \Omega^c, \\ -\mathbf{E}^i & \text{in } \Omega. \end{cases}$$

This leads to the indirect representation formula (3.56) because $[\gamma_D \tilde{\mathbf{E}}] = \mathbf{0}$.

3.2.2. Boundary Element Formulation

The solvability of Galerkin formulations deduced from elliptic partial differential operators follows usually from the coercivity of the underlying bilinear form, that is, the fact that the zeroth order term is a compact perturbation of the second order term and that a general Gårding inequality holds. For the second order Maxwell equation, however, this concept does not apply as the null-space of the operator \mathbf{curl} is infinite-dimensional and, thus, the embedding $\mathbf{H}(\mathbf{curl}, \Omega^c) \hookrightarrow \mathbf{L}^2(\Omega^c)$ is not compact. This problem is theoretically solved by the splitting of the fields into two components. Similarly, $H^{-\frac{1}{2}}(\text{div}_\Gamma, \Gamma)$ -coercivity for the Galerkin variational formulations of the boundary integral equations (3.55) and (3.57) are established only when an appropriate Hodge decomposition of the trace space is assumed. In [14, 19], it is shown that the operator $\gamma_R \mathbf{S}_E$ is a Fredholm operator with index zero. The bilinear form which underlies the proof is derived from the duality between the trace spaces $H^{-\frac{1}{2}}(\text{div}_\Gamma, \Gamma)$ and $H^{-\frac{1}{2}}(\text{curl}_\Gamma, \Gamma)$. Provided $\kappa^2 > 0$ is not an interior eigenvalue of the $\mathbf{curl curl}$ operator for the domain Ω , $\gamma_R \mathbf{S}_E$ is also injective and, thus, the boundary integral equations (3.55) and (3.57) are uniquely solvable. The proof of this fundamental result can be found in [14, 19].

Theorem 3.2.10 *If $\kappa^2 > 0$ is not an interior eigenvalue of the $\mathbf{curl curl}$ operator, the boundary integral equation (3.55) admits a unique solution $\mathbf{j} \in H^{-\frac{1}{2}}(\text{div}_\Gamma, \Gamma)$ with*

$$\|\mathbf{j}\|_{H^{-\frac{1}{2}}(\text{div}_\Gamma, \Gamma)} \leq c \|\mathbf{m}\|_{H^{-\frac{1}{2}}(\text{div}_\Gamma, \Gamma)}. \quad (3.59)$$

The variational formulation reads: find $\mathbf{j} \in H^{-\frac{1}{2}}(\text{div}_\Gamma, \Gamma)$ such that for all $\phi \in H^{-\frac{1}{2}}(\text{div}_\Gamma, \Gamma)$ it holds

$$\langle \gamma_R \mathbf{S}_E(\mathbf{j}), \phi \rangle_{-\frac{1}{2}} = \langle \mathbf{m} \times \mathbf{n}, \phi \rangle_{-\frac{1}{2}} - \langle \gamma_R \mathbf{S}_M(\mathbf{m}), \phi \rangle_{-\frac{1}{2}}. \quad (3.60)$$

Under the same condition for κ , the boundary integral equation (3.57) admits a unique solution $\mathbf{j}^t \in H^{-\frac{1}{2}}(\operatorname{div}_\Gamma, \Gamma)$ with

$$\|\mathbf{j}^t\|_{H^{-\frac{1}{2}}(\operatorname{div}_\Gamma, \Gamma)} \leq c \|\mathbf{m}\|_{H^{-\frac{1}{2}}(\operatorname{div}_\Gamma, \Gamma)}. \quad (3.61)$$

The variational formulation reads: find $\mathbf{j}^t \in H^{-\frac{1}{2}}(\operatorname{div}_\Gamma, \Gamma)$ such that for all $\phi \in H^{-\frac{1}{2}}(\operatorname{div}_\Gamma, \Gamma)$ it holds

$$\langle \gamma_R \mathbf{S}_E(\mathbf{j}^t), \phi \rangle_{-\frac{1}{2}} = \langle \mathbf{m} \times \mathbf{n}, \phi \rangle_{-\frac{1}{2}}. \quad (3.62)$$

3.3. The Stabilized Formulation

It is well known that the numerical schemes which rely on the second order equation (3.29),

$$\langle (\operatorname{curl} \operatorname{curl} - \kappa^2) \tilde{\mathbf{E}}, \varphi \rangle = -\langle \gamma_N \mathbf{E} \delta_\Gamma, \varphi \rangle - \langle \mathbf{m} \delta_\Gamma, \operatorname{curl} \varphi \rangle, \quad \kappa^2 = \omega^2 \varepsilon \mu > 0,$$

are not stable when passing to the limit $\kappa \rightarrow 0$. This problem is often called the low frequency problem because it is actually the angular frequency ω of the incoming signal \mathbf{E}^i which tends to zero. Recall, that the reason why we concentrated on the second order equation (3.29) was that an electric field \mathbf{E} that satisfies (3.29) fulfills the Gauß law according to Lemma 3.2.4. Moreover, the mathematical theory presented in Subsection 3.2.2, is valid for all $\kappa > 0$ and, therefore, it is not clear why numerical instabilities occur. A closer look at the continuity equation (3.28),

$$\langle \gamma_N \mathbf{E} \delta_\Gamma, \nabla \varphi \rangle = \kappa^2 \langle \gamma_n \mathbf{E} \delta_\Gamma, \varphi \rangle, \quad \kappa \geq 0,$$

shows, however, that one loses control over $|\langle \gamma_N \mathbf{E} \delta_\Gamma, \nabla \varphi \rangle|$ as it is of order κ^2 . For $\kappa = 0$ the distribution $\gamma_N \mathbf{E} \delta_\Gamma$ vanishes and for this reason, magnetostatic vector potential problems are formulated in $H^{-\frac{1}{2}}(\operatorname{div}_\Gamma, \Gamma)$ [36]. The key point is that the distribution $\gamma_n \mathbf{E} \delta_\Gamma$ does not vanish unless $\mathbf{E} \equiv \mathbf{0}$ in \mathbb{R}^3 . This means that the smaller κ the more important gets the normal trace $\gamma_n \mathbf{E}$ and the idea of stabilization is to incorporate the Gauß law explicitly because $\gamma_n \mathbf{E}$ appears in it.

There are several publications concerned with numerical experiments for stabilizing formulations, for finite element formulations, see [29, 37] and, in the context of boundary integral methods, see [1, 42, 56] for instance. Stabilization is basically achieved by the incorporation of the Gauß law to recover the static phenomena. There are basically two different methods that come out of this. The first is an elliptization of the Maxwell equations as it is proposed in [42]. This leads to a uniquely solvable variational formulations posed in classical trace spaces. The draw-back of this idea is that the equivalence to the original Maxwell system gets lost at least for non-smooth domains and thus, the unique solution of this elliptic problem is in general not a Maxwell solution. More recent ideas published in the engineering community propose to accept the non-ellipticity of the second order equation and to add the Gauß law [56].

The stabilized formulation presented here is of this kind. Similar to [56] the idea is to consider an extended boundary value problem including the Gauß law for the electric field. Our contribution to the subject is to explain the mathematical justification and well-posedness of the idea. Further, we provide a complete and not yet published analysis showing the unique solvability of the boundary element formulation and stability of the numerical method.

The new approach of stabilizing the Maxwell system in the context of boundary element methods is presented in the following subsections. The basic question we start with in Subsection 3.3.1 is how to construct an extended boundary value problem which incorporates the Gauß law explicitly and which is equivalent to the original Maxwell system. The extended boundary value problem is called the Picard system. Following the same steps as in Section 3.2 for the Maxwell system, we derive in Subsection 3.3.1 a second order system of equations. It is further shown that the second order differential operator possesses a fundamental solution for all $\kappa \geq 0$. The representation for a

solution of the Picard system in terms of layer potentials is presented and the Galerkin variational formulations of the deduced boundary integral equations are, finally, discussed in Subsection 3.3.2.

3.3.1. Second order equation

In [50], Picard analyzes the low frequency asymptotic of the Maxwell system by means of an extended system. We adopted the idea of Picard to develop a novel boundary element formulation. The starting point is a boundary value problem with seven partial differential equations for seven unknowns $(\mathbf{E}, \mathbf{H}, \psi)$

$$\begin{pmatrix} i\omega \varepsilon \mu & \operatorname{div} \varepsilon & 0 \\ \nabla & i\omega \varepsilon & \operatorname{curl} \\ 0 & -\operatorname{curl} & i\omega \mu \end{pmatrix} \begin{pmatrix} \psi \\ \mathbf{E} \\ \mathbf{H} \end{pmatrix}(\mathbf{x}) = \begin{pmatrix} 0 \\ \mathbf{0} \\ \mathbf{0} \end{pmatrix}, \quad \text{in } \Omega^c, \quad (3.63)$$

with imposed boundary conditions

$$\begin{aligned} \gamma_0 \psi(\mathbf{x}) &= 0, \\ \gamma_D \mathbf{E}(\mathbf{x}) &= \mathbf{m}(\mathbf{x}), \quad \text{on } \Gamma, \\ \gamma_n \mathbf{H}(\mathbf{x}) &= \theta(\mathbf{x}), \end{aligned} \quad (3.64)$$

and radiation conditions

$$\begin{aligned} \left| \nabla \psi(\mathbf{x}) \cdot \frac{\mathbf{x}}{|\mathbf{x}|} - i\omega \psi(\mathbf{x}) \right| &= \mathcal{O}\left(\frac{1}{|\mathbf{x}|^2}\right), \\ \left| (\operatorname{curl} \mathbf{E}(\mathbf{x})) \times \frac{\mathbf{x}}{|\mathbf{x}|} - i\omega \varepsilon \mathbf{E}(\mathbf{x}) \right| &= \mathcal{O}\left(\frac{1}{|\mathbf{x}|^2}\right), \quad \text{for } |\mathbf{x}| \rightarrow \infty. \\ \left| (\operatorname{curl} \mathbf{H}(\mathbf{x})) \times \frac{\mathbf{x}}{|\mathbf{x}|} - i\omega \mu \mathbf{H}(\mathbf{x}) \right| &= \mathcal{O}\left(\frac{1}{|\mathbf{x}|^2}\right), \end{aligned} \quad (3.65)$$

The Picard system (3.63)-(3.65) differs from the Maxwell system only by the additional terms with the scalar function ψ .

Again, weak solutions $(\mathbf{E}, \mathbf{H}, \psi)$ with the following regularity

$$\psi \in H^1(\Omega^c), \quad \mathbf{E} \in \mathbf{H}(\operatorname{curl}, \Omega^c) \cap \mathbf{H}(\operatorname{div}, \Omega^c), \quad \mathbf{H} \in \mathbf{H}(\operatorname{curl}, \Omega^c) \cap \mathbf{H}(\operatorname{div}, \Omega^c) \quad (3.66)$$

are considered. Before the Picard system is written in distributional sense and a second order system is deduced, we prove a lemma which makes clear why the Picard system is equivalent to the Maxwell system in L^2 -sense.

Lemma 3.3.1 *Let $(\mathbf{E}, \mathbf{H}, \psi)$ be given with (3.64) and (3.65). If the triple $(\mathbf{E}, \mathbf{H}, \psi)$ fulfills*

$$\begin{cases} (\operatorname{div}(\varepsilon \mathbf{E}), \phi)_{\Omega^c} & + i\omega \varepsilon \mu (\psi, \phi)_{\Omega^c} = 0, \\ (\mathbf{H}, \operatorname{curl} \phi)_{\Omega^c} & + i\omega (\varepsilon \mathbf{E}, \phi)_{\Omega^c} + (\nabla \psi, \phi)_{\Omega^c} = 0, \\ -(\operatorname{curl} \mathbf{E}, \phi)_{\Omega^c} & + i\omega (\mu \mathbf{H}, \phi)_{\Omega^c} = 0, \end{cases} \quad (3.67)$$

for all $\phi \in H_0^1(\Omega^c)$, $\phi \in \mathbf{H}_0(\mathbf{curl}, \Omega^c)$, then, (\mathbf{E}, \mathbf{H}) satisfies

$$\begin{cases} (\operatorname{div}(\varepsilon \mathbf{E}), \phi)_{\Omega^c} & = 0, \\ (\mathbf{H}, \mathbf{curl} \phi)_{\Omega^c} + i\omega(\varepsilon \mathbf{E}, \phi)_{\Omega^c} & = 0, \\ -(\mathbf{curl} \mathbf{E}, \phi)_{\Omega^c} + i\omega(\mu \mathbf{H}, \phi)_{\Omega^c} & = 0, \end{cases} \quad (3.68)$$

for all $\phi \in H_0^1(\Omega^c)$, $\phi \in \mathbf{H}_0(\mathbf{curl}, \Omega^c)$ and

$$\psi \equiv 0 \quad \text{on } \overline{\Omega^c}.$$

The crucial idea for proving Lemma 3.3.1 is the unique solvability of an elliptic Dirichlet boundary value problem. This is the contents of Lemma 3.3.2. This result is proved in [48], for instance.

Lemma 3.3.2 *Let $\psi \in H_0^1(\Omega^c)$ with*

$$\left| \nabla \psi(\mathbf{x}) \cdot \frac{\mathbf{x}}{|\mathbf{x}|} - i\kappa \psi(\mathbf{x}) \right| = \mathcal{O}\left(\frac{1}{|\mathbf{x}|^2}\right), \quad \text{for } |\mathbf{x}| \rightarrow \infty.$$

The variational problem

$$\forall \phi \in H_0^1(\Omega^c) : \quad (\nabla \psi, \nabla \phi)_{\Omega^c} - \kappa^2(\psi, \phi)_{\Omega^c} = 0.$$

is uniquely solvable for all $\kappa \in \mathbb{R}$. The unique solution is $\psi \equiv 0$ on $\overline{\Omega^c}$.

Proof of Lemma 3.3.1: Assume that ψ vanishes on $\overline{\Omega^c}$, then the boundary value problem (3.67) shrinks obviously to the original Maxwell boundary value problem (3.68). Thus, let us prove that the potential ψ identically vanishes provided (3.67) holds. To see this, we employ test functions of the form $\phi = \nabla \phi$ with $\phi \in H_0^1(\Omega^c)$. This is allowed as $\nabla H_0^1(\Omega^c) \subset \mathbf{H}_0(\mathbf{curl}, \Omega^c)$ and it follows

$$\forall \phi \in H_0^1(\Omega^c) : \quad i\omega(\varepsilon \mathbf{E}, \nabla \phi)_{\Omega^c} + (\nabla \psi, \nabla \phi)_{\Omega^c} = 0.$$

Moreover, it holds

$$\forall \phi \in H_0^1(\Omega^c) : \quad (\operatorname{div}(\varepsilon \mathbf{E}), \phi)_{\Omega^c} = -(\varepsilon \mathbf{E}, \nabla \phi)_{\Omega^c} = -i\omega \varepsilon \mu (\psi, \phi)_{\Omega^c},$$

and, thus, we are left with the variational problem depicted in Lemma 3.3.2, namely, find $\psi \in H_0^1(\Omega^c)$ such that for all $\phi \in H_0^1(\Omega^c)$

$$(\nabla \psi, \nabla \phi)_{\Omega^c} - \kappa^2(\psi, \phi)_{\Omega^c} = 0.$$

The unique solution vanishes on $\overline{\Omega^c}$ for all κ . □

Thus, it makes sense to further investigate the Picard system because it contains the Gauß law explicitly. The regularity assumptions for $(\mathbf{E}, \mathbf{H}, \psi)$ can be used to reformulate the Picard system (3.63)-(3.65) in distributional sense. By use of the trivial extensions into Ω ,

$$\tilde{\mathbf{E}} = \begin{cases} \mathbf{E} & \text{in } \Omega^c, \\ \mathbf{0} & \text{in } \Omega, \end{cases} \quad \tilde{\mathbf{H}} = \begin{cases} \mathbf{H} & \text{in } \Omega^c, \\ \mathbf{0} & \text{in } \Omega, \end{cases} \quad \text{and} \quad \tilde{\psi} = \begin{cases} \psi & \text{in } \Omega^c, \\ 0 & \text{in } \Omega, \end{cases}$$

it holds for all $\varphi \in \mathcal{D}(\mathbb{R}^3)$, $\varphi \in \mathcal{D}(\mathbb{R}^3)$ that

$$\begin{cases} \langle \operatorname{div}(\varepsilon \tilde{\mathbf{E}}), \varphi \rangle & + i\omega \varepsilon \mu \langle \tilde{\psi}, \varphi \rangle & = -\langle \gamma_{\mathbf{n}}(\varepsilon \mathbf{E}) \delta_{\Gamma}, \varphi \rangle, \\ \langle \mathbf{curl} \tilde{\mathbf{H}}, \varphi \rangle & + i\omega \langle \varepsilon \tilde{\mathbf{E}}, \varphi \rangle & + \langle \nabla \tilde{\psi}, \varphi \rangle & = \langle (\gamma_0 \psi \mathbf{n}) \delta_{\Gamma}, \varphi \rangle - \langle \gamma_D \mathbf{H} \delta_{\Gamma}, \varphi \rangle, \\ -\langle \mathbf{curl} \tilde{\mathbf{E}}, \varphi \rangle & + i\omega \langle \mu \tilde{\mathbf{H}}, \varphi \rangle & & = \langle \mathbf{m} \delta_{\Gamma}, \varphi \rangle. \end{cases} \quad (3.69)$$

The additional surface distribution on the right hand side results from the distribution $\nabla\tilde{\psi}$ which fulfills for all $\varphi \in \mathcal{D}(\mathbb{R}^3)$

$$\langle \nabla\tilde{\psi}, \varphi \rangle = (\nabla\psi, \varphi)_{\Omega^c} + \langle (\gamma_0\psi\mathbf{n})\delta_\Gamma, \varphi \rangle.$$

Following the same reasoning as in Section 3.2, the magnetic field $\tilde{\mathbf{H}}$ can be eliminated, leading to a second order system. By the use of the abbreviation $\tilde{\Psi} = i\omega\mu\tilde{\psi}$ and by inserting the boundary condition $\gamma_0\tilde{\Psi} = 0$, this reads

$$\begin{cases} \langle \mathbf{curl\,curl}\tilde{\mathbf{E}}, \varphi \rangle - \kappa^2\langle \tilde{\mathbf{E}}, \varphi \rangle + \langle \nabla\tilde{\Psi}, \varphi \rangle &= -\langle \gamma_N\mathbf{E}\delta_\Gamma, \varphi \rangle - \langle \mathbf{m}\delta_\Gamma, \mathbf{curl}\varphi \rangle, \\ \langle \operatorname{div}\tilde{\mathbf{E}}, \varphi \rangle + \langle \tilde{\Psi}, \varphi \rangle &= -\langle \gamma_n\mathbf{E}\delta_\Gamma, \varphi \rangle. \end{cases} \quad (3.70)$$

The two equations in (3.70) are naturally separated by the test function spaces and, thus, we can, equivalently, consider their sum, namely,

$$\begin{aligned} \langle \mathbf{curl\,curl}\tilde{\mathbf{E}}, \varphi \rangle - \kappa^2\langle \tilde{\mathbf{E}}, \varphi \rangle + \langle \nabla\tilde{\Psi}, \varphi \rangle + \langle \operatorname{div}\tilde{\mathbf{E}}, \varphi \rangle + \langle \tilde{\Psi}, \varphi \rangle &= -\langle \gamma_N\mathbf{E}\delta_\Gamma, \varphi \rangle - \langle \mathbf{m}\delta_\Gamma, \mathbf{curl}\varphi \rangle \\ &\quad - \langle \gamma_n\mathbf{E}\delta_\Gamma, \varphi \rangle. \end{aligned}$$

Employing the definition of the distributional derivatives yields the following equation

$$\begin{aligned} \langle \tilde{\mathbf{E}}, \mathbf{curl\,curl}\varphi \rangle - \kappa^2\langle \tilde{\mathbf{E}}, \varphi \rangle - \langle \tilde{\Psi}, \operatorname{div}\varphi \rangle - \langle \tilde{\mathbf{E}}, \nabla\varphi \rangle + \langle \tilde{\Psi}, \varphi \rangle &= -\langle \gamma_N\mathbf{E}\delta_\Gamma, \varphi \rangle - \langle \mathbf{m}\delta_\Gamma, \mathbf{curl}\varphi \rangle \\ &\quad - \langle \gamma_n\mathbf{E}\delta_\Gamma, \varphi \rangle. \end{aligned}$$

Now, we introduce the Picard operators \mathcal{A} and \mathcal{A}' by

$$\mathcal{A} = \begin{pmatrix} \mathbf{curl\,curl} - \kappa^2 & \nabla \\ \operatorname{div} & \mathcal{I} \end{pmatrix}, \quad \mathcal{A}' = \begin{pmatrix} \mathbf{curl\,curl} - \kappa^2 & -\nabla \\ -\operatorname{div} & \mathcal{I} \end{pmatrix}. \quad (3.71)$$

By use of the Picard operators the previous relations obtain a clear structure, i.e.,

$$\begin{aligned} \left\langle \mathcal{A} \begin{pmatrix} \tilde{\mathbf{E}} \\ \tilde{\Psi} \end{pmatrix}, \begin{pmatrix} \varphi \\ \varphi \end{pmatrix} \right\rangle &= \left\langle \begin{pmatrix} \tilde{\mathbf{E}} \\ \tilde{\Psi} \end{pmatrix}, \mathcal{A}' \begin{pmatrix} \varphi \\ \varphi \end{pmatrix} \right\rangle = -\langle \gamma_N\mathbf{E}\delta_\Gamma, \varphi \rangle - \langle \mathbf{m}\delta_\Gamma, \mathbf{curl}\varphi \rangle \\ &\quad - \langle \gamma_n\mathbf{E}\delta_\Gamma, \varphi \rangle. \end{aligned} \quad (3.72)$$

The reason for a further investigation of (3.72) in the context of boundary integral equations is given in Lemma 3.3.3.

Lemma 3.3.3 *The operator \mathcal{A}' is elliptic in the sense of Douglas-Nirenberg [38] and it possesses a fundamental solution $(\mathbf{U}^*, \mathbf{u}^*)^\top \in \mathcal{C}^\infty(\mathbb{R}^3 \setminus \{\mathbf{0}\})^{3 \times 4} \times \mathcal{C}^\infty(\mathbb{R}^3 \setminus \{\mathbf{0}\})^4$ for all $\kappa \geq 0$. Namely,*

$$\begin{pmatrix} \mathbf{U}^*(\mathbf{x}) \\ \mathbf{u}^*(\mathbf{x}) \end{pmatrix} = \begin{pmatrix} \mathbf{I}_3 & \nabla \\ \nabla^\top & -\kappa^2 \end{pmatrix} G_\kappa(\mathbf{x}), \quad G_\kappa(\mathbf{x}) = \frac{e^{-i\kappa|\mathbf{x}|}}{4\pi|\mathbf{x}|}, \quad (3.73)$$

fulfills for all $(\varphi, \varphi) \in \mathcal{D}(\mathbb{R}^3) \times \mathcal{D}(\mathbb{R}^3)$ the distributional equation

$$\left\langle \mathcal{A}' \begin{pmatrix} \mathbf{U}^* \\ \mathbf{u}^* \end{pmatrix}, \begin{pmatrix} \varphi \\ \varphi \end{pmatrix} \right\rangle = \left\langle \begin{pmatrix} \delta_0 & \mathbf{0} \\ \mathbf{0} & \delta_0 \end{pmatrix}, \begin{pmatrix} \varphi \\ \varphi \end{pmatrix} \right\rangle = \begin{pmatrix} \varphi \\ \varphi \end{pmatrix}(\mathbf{x}).$$

Proof: The differential operators in \mathcal{A}' transform the fundamental solution in the following way

$$\begin{aligned} \mathcal{A}' \begin{pmatrix} \mathbf{U}^* \\ \mathbf{u}^* \end{pmatrix} &= \\ &= \begin{pmatrix} \mathbf{curl curl}(G_\kappa \mathbf{I}_3) - \kappa^2(G_\kappa \mathbf{I}_3) - \nabla(\nabla G_\kappa)^\top & \mathbf{curl curl}(\nabla G_\kappa) - \kappa^2 \nabla G_\kappa + \kappa^2 \nabla G_\kappa \\ -\operatorname{div}(\mathbf{I}_3 G_\kappa) + \nabla^\top G_\kappa & -\operatorname{div}(\nabla G_\kappa) - \kappa^2 G_\kappa \end{pmatrix} \\ &= \begin{pmatrix} \mathbf{I}_3 & \mathbf{0} \\ 0 & 1 \end{pmatrix} (-\Delta - \kappa^2) G_\kappa. \end{aligned}$$

□

When comparing the analytical properties of the fundamental solution of the Picard operator with the fundamental solution of the second order Maxwell operator, it turns out that (3.73) exhibits a singularity of order $\mathcal{O}(|\mathbf{x}|^{-2})$ whereas the Hesse matrix in (3.31) is hypersingular of order $\mathcal{O}(|\mathbf{x}|^{-3})$.

A representation for the Picard solution can be derived by means of the integral representation formulae for a solution of the scalar Helmholtz equation and the theory of distributions [48]. The key point is that the dual operator of the Newton potential induced by the distributional right hand side (3.72) extends the boundary data into Ω^c and is of the form (3.37), (3.38) and (3.50). This theory is standard and the details are found in [23, 44], for instance. A simple, non-rigorous explanation of the representation formula shall be given here. In order to obtain the representation formula for (\mathbf{E}, Ψ) in Ω^c , we must simply evaluate the right hand side of (3.72) for the special case $\varphi = \mathbf{U}^*$ and $\varphi = \mathbf{u}^*$. Provided the traces are regular enough, the surface distributions can be identified with boundary integral operators and an easy calculation yields that it must hold at almost every $\mathbf{x} \in \Omega^c$

$$\begin{pmatrix} \mathbf{E} \\ \Psi \end{pmatrix} = \begin{pmatrix} \mathbf{S}_M(\mathbf{m}) + \mathbf{S}_\kappa(\gamma_N \mathbf{E}) - \nabla S_\kappa(\gamma_n \mathbf{E}) \\ S_\kappa(\operatorname{div}_\Gamma(\gamma_N \mathbf{E}) + \kappa^2 \gamma_n \mathbf{E}) \end{pmatrix}. \quad (3.74)$$

Obviously, (3.74) comprises the Stratton-Chu representation formula for \mathbf{E} in its most classical form [22, 48]. Moreover, if $\Psi = 0$ in Ω^c , as anticipated, the second equation can be interpreted as a weak form of the continuity equation (3.28) by virtue of Lemma 3.3.1.

In order to formulate boundary integral equations for the unknown traces $(\gamma_N \mathbf{E}, \gamma_n \mathbf{E})$, we apply the trace operators (γ_R, γ_0) on (3.74) and obtain

$$\begin{pmatrix} \gamma_R & 0 \\ \mathbf{0} & \gamma_0 \end{pmatrix} \begin{pmatrix} \mathbf{E} \\ \Psi \end{pmatrix} = \begin{pmatrix} \gamma_R & 0 \\ \mathbf{0} & \gamma_0 \end{pmatrix} \begin{pmatrix} \mathbf{S}_M(\mathbf{m}) + \mathbf{S}_\kappa(\gamma_N \mathbf{E}) - \nabla S_\kappa(\gamma_n \mathbf{E}) \\ S_\kappa(\operatorname{div}_\Gamma(\gamma_N \mathbf{E}) + \kappa^2 \gamma_n \mathbf{E}) \end{pmatrix}. \quad (3.75)$$

Recall, that $\gamma_R \mathbf{E} = \mathbf{m} \times \mathbf{n}$ and $\gamma_0 \Psi = 0$ are prescribed by (3.64) and, thus, we are left with two boundary integral equations for the pair $(\gamma_N \mathbf{E}, \gamma_n \mathbf{E})$

$$\begin{pmatrix} \gamma_R \mathbf{S}_\kappa & -\nabla_\Gamma \gamma_0 S_\kappa \\ \gamma_0 S_\kappa(\operatorname{div}_\Gamma) & \kappa^2 \gamma_0 S_\kappa \end{pmatrix} \begin{pmatrix} \gamma_N \mathbf{E} \\ \gamma_n \mathbf{E} \end{pmatrix} = \begin{pmatrix} \mathbf{m} \times \mathbf{n} - \gamma_R \mathbf{S}_M(\mathbf{m}) \\ 0 \end{pmatrix}. \quad (3.76)$$

We summarize this result in the following lemma.

Lemma 3.3.4 *Let $\mathbf{m} \in H^{-\frac{1}{2}}(\operatorname{div}_\Gamma, \Gamma)$ and the pair of densities $(\mathbf{j}, \rho_\Gamma)$ with $\mathbf{j} \in H^{-\frac{1}{2}}(\operatorname{div}_\Gamma, \Gamma)$ and $\rho_\Gamma \in H^{-\frac{1}{2}}(\Gamma)$ given with*

$$\gamma_0 S_\kappa(\operatorname{div}_\Gamma \mathbf{j}) = -\kappa^2 \gamma_0 S_\kappa(\rho_\Gamma). \quad (3.77)$$

Then, the vector field

$$\mathbf{E}(\mathbf{x}) = \mathbf{S}_M(\mathbf{m})(\mathbf{x}) + \mathbf{S}_\kappa(\mathbf{j})(\mathbf{x}) - \nabla S_\kappa(\rho_\Gamma)(\mathbf{x}) \quad (3.78)$$

for $\mathbf{x} \in \Omega^c$ is a Maxwell solution in $\mathbf{H}(\mathbf{curl curl}, \Omega^c)$ with

$$\gamma_D \mathbf{E}(\mathbf{x}) = \mathbf{m}(\mathbf{x}), \quad \gamma_N \mathbf{E}(\mathbf{x}) = \mathbf{j}(\mathbf{x}), \quad \gamma_n \mathbf{E}(\mathbf{x}) = \rho_\Gamma(\mathbf{x}). \quad (3.79)$$

Different from the classical formulation, an additional condition, namely the weak form of the continuity equation (3.77), is built in. The continuity equation accounts for the Gauß law by means of the normal trace $\gamma_n \mathbf{E}$ and, thus, the quasi-electrostatic character of the electromagnetic field is recovered.

3.3.2. Boundary Element Formulation

The principal question is whether the system of boundary integral equations (3.76) is uniquely solvable. A positive answer is given by the following Lemma 3.3.5.

Lemma 3.3.5 *Assume that $\kappa^2 > 0$ is neither an interior eigenvalue of the Laplace nor of the $\mathbf{curl curl}$ operator.*

Then, the variational formulation for the direct formulation is uniquely solvable and it reads: find $\mathbf{j} \in H^{-\frac{1}{2}}(\mathbf{div}_\Gamma, \Gamma)$ and $\rho_\Gamma \in H^{-\frac{1}{2}}(\Gamma)$ such that for all $\phi \in H^{-\frac{1}{2}}(\mathbf{div}_\Gamma, \Gamma)$, for all $v \in H^{-\frac{1}{2}}(\Gamma)$ it holds

$$\begin{cases} \langle \gamma_R \mathbf{S}_\kappa(\mathbf{j}), \phi \rangle_{-\frac{1}{2}} + \langle \mathbf{div}_\Gamma \phi, \gamma_0 S_\kappa(\rho_\Gamma) \rangle_{\frac{1}{2}} = \langle \mathbf{m} \times \mathbf{n}, \phi \rangle_{-\frac{1}{2}} - \langle \gamma_R \mathbf{S}_M \mathbf{m}, \phi \rangle_{-\frac{1}{2}}, \\ \langle v, \gamma_0 S_\kappa(\mathbf{div}_\Gamma \mathbf{j}) \rangle_{\frac{1}{2}} + \kappa^2 \langle v, \gamma_0 S_\kappa(\rho_\Gamma) \rangle_{\frac{1}{2}} = 0. \end{cases} \quad (3.80)$$

Also, the variational formulation for the indirect formulation is uniquely solvable and it reads: find $\mathbf{j}^t \in H^{-\frac{1}{2}}(\mathbf{div}_\Gamma, \Gamma)$ and $\rho_\Gamma^t \in H^{-\frac{1}{2}}(\Gamma)$ such that for all $\phi \in H^{-\frac{1}{2}}(\mathbf{div}_\Gamma, \Gamma)$, for all $v \in H^{-\frac{1}{2}}(\Gamma)$ it holds

$$\begin{cases} \langle \gamma_R \mathbf{S}_\kappa(\mathbf{j}^t), \phi \rangle_{-\frac{1}{2}} + \langle \mathbf{div}_\Gamma \phi, \gamma_0 S_\kappa(\rho_\Gamma^t) \rangle_{\frac{1}{2}} = \langle \mathbf{m} \times \mathbf{n}, \phi \rangle_{-\frac{1}{2}} \\ \langle v, \gamma_0 S_\kappa(\mathbf{div}_\Gamma \mathbf{j}^t) \rangle_{\frac{1}{2}} + \kappa^2 \langle v, \gamma_0 S_\kappa(\rho_\Gamma^t) \rangle_{\frac{1}{2}} = 0. \end{cases} \quad (3.81)$$

Proof: Let $\mathbf{j} \in H^{-\frac{1}{2}}(\mathbf{div}_\Gamma, \Gamma)$ denote the unique solution of the classical formulation (3.60), which exists according to Theorem 3.2.10. Provided κ^2 is not an interior eigenvalue of the Laplace operator for the domain Ω , there exists a unique density $\rho_\Gamma \in H^{-\frac{1}{2}}(\Gamma)$ [44] with

$$\forall v \in H^{-\frac{1}{2}}(\Gamma) \quad \kappa^2 \langle v, \gamma_0 S_\kappa(\rho_\Gamma) \rangle_{\frac{1}{2}} = - \langle v, \gamma_0 S_\kappa(\mathbf{div}_\Gamma \mathbf{j}) \rangle_{\frac{1}{2}},$$

where the right hand side is uniquely defined by \mathbf{j} . Then, the pair $(\mathbf{j}, \rho_\Gamma)$ uniquely solves (3.80).

The same holds for the indirect stabilized formulation. \square

3.4. The Electrostatic Case

To understand the limiting behavior of the stabilized formulation, we first look at the electrostatic equations. We will find that the stabilized formulation corresponds to a saddle point formulation which yield for $\kappa = 0$ an indirect potential formulation for an electrostatic boundary value problem.

Considering the limiting case $\kappa \rightarrow 0$, we should have in mind that it is the frequency ω of the incoming signal which is sent to zero. The case $\kappa = 0$ equals $\omega = 0$ and, thus, the field \mathbf{E}^i is an electrostatic field and not an electromagnetic signal anymore. By definition, electrostatic fields can

be represented as potential fields

$$\mathbf{E}^i(\mathbf{x}) = -\nabla\varphi^i(\mathbf{x}).$$

Moreover, the Maxwell system shrinks to a decoupled system of partial differential equations, namely,

$$\begin{pmatrix} \operatorname{div} \varepsilon & 0 \\ 0 & \operatorname{curl} \\ -\operatorname{curl} & 0 \end{pmatrix} \begin{pmatrix} \mathbf{E} \\ \mathbf{H} \end{pmatrix}(\mathbf{x}) = \begin{pmatrix} 0 \\ \mathbf{0} \\ \mathbf{0} \end{pmatrix}, \quad \text{in } \Omega^c. \quad (3.82)$$

and, since Ω^c is simply connected, \mathbf{E} can be represented also in the form

$$\mathbf{E}(\mathbf{x}) = -\nabla\varphi(\mathbf{x}) \quad (3.83)$$

and it must hold $\operatorname{div}_\Gamma \mathbf{j}^t = 0$ in $H^{-\frac{1}{2}}(\Gamma)$. Recall that the Sobolev space that accounts for this conditions was denoted

$$H^{-\frac{1}{2}}(\operatorname{div}_\Gamma 0, \Gamma) = \left\{ \mathbf{u} \in H^{-\frac{1}{2}}(\operatorname{div}_\Gamma, \Gamma), \operatorname{div}_\Gamma \mathbf{u} = 0 \right\}. \quad (3.84)$$

Moreover, we need Sobolev spaces which account for the null-space of the vector-valued surface curl operator $\operatorname{curl}_\Gamma$, namely,

$$H_*^{\frac{1}{2}}(\Gamma) = \left\{ u \in H^{\frac{1}{2}}(\Gamma), \langle 1, u \rangle_{\frac{1}{2}} = 0 \right\}, \quad (3.85)$$

$$H_{**}^{-\frac{1}{2}}(\Gamma) = \left\{ u \in H^{-\frac{1}{2}}(\Gamma), \langle u, \gamma_0 S_0(1) \rangle_{\frac{1}{2}} = 0 \right\}. \quad (3.86)$$

The Dirichlet boundary condition is given in terms of the potential by

$$\gamma_D \nabla \varphi(\mathbf{x}) = \mathbf{m}(\mathbf{x}) = -\gamma_D \nabla \varphi^i(\mathbf{x}) \quad \text{on } \Gamma. \quad (3.87)$$

Note, that by (3.87), the solvability condition $\operatorname{curl}_\Gamma \mathbf{m} = 0$ is fulfilled because $\gamma_D \nabla = \nabla_\Gamma$. The decay condition reads

$$|\varphi(\mathbf{x})| = \mathcal{O}\left(\frac{1}{|\mathbf{x}|}\right) \quad \text{for } |\mathbf{x}| \rightarrow \infty.$$

Different from electrodynamics, the Faraday law plays a minor role as it is trivially fulfilled by (3.83). Thus, the boundary value problem describing our electrostatic field as limiting case of the scattering situation reads

$$\begin{cases} -\Delta \varphi = 0, & \text{in } \Omega^c, \\ \gamma_D(\nabla \varphi) = \mathbf{m}, & \text{on } \Gamma, \\ |\varphi(\mathbf{x})| = \mathcal{O}\left(\frac{1}{|\mathbf{x}|}\right), & \text{for } |\mathbf{x}| \rightarrow \infty. \end{cases} \quad (3.88)$$

It is shown in [54] that the solution $\varphi \in H^1(\Omega^c)$ of the boundary value problem (3.88) can be represented by the indirect representation formula

$$\varphi(\mathbf{x}) = \int_\Gamma \gamma_{1,\mathbf{y}} G_0(\mathbf{x} - \mathbf{y}) p(\mathbf{y}) d\sigma_y = W_0(p)(\mathbf{x}), \quad (3.89)$$

with a density $p \in H^{\frac{1}{2}}(\Gamma)$. Here, W_0 is the double layer potential for the Laplace equation and it holds

$$W_0: H^{\frac{1}{2}}(\Gamma) \rightarrow H^1(\Omega^c). \quad (3.90)$$

Provided Γ is connected, it holds that the hypersingular operator

$$\gamma_1 W_0: H^{\frac{1}{2}}(\Gamma) \rightarrow H^{-\frac{1}{2}}(\Gamma).$$

is elliptic on $H_*^{\frac{1}{2}}(\Gamma)$ [54]. Moreover, it holds for all $\phi \in H_*^{\frac{1}{2}}(\Gamma)$ [51]

$$\langle \gamma_1 W_0(p), \phi \rangle_{\frac{1}{2}} = \langle \mathbf{curl}_\Gamma \phi, \gamma_R \mathbf{S}_0(\mathbf{curl}_\Gamma p) \rangle_{-\frac{1}{2}}.$$

The function given by (3.89) solves (3.88) only if the boundary condition in (3.88) is fulfilled. To obtain the determining equation for p , note that the equations (3.81) must also hold for $\kappa = 0$. This yields for the special case of test vector fields $\mathbf{curl}_\Gamma \phi$ with $\phi \in H_*^{\frac{1}{2}}(\Gamma)$

$$\langle \mathbf{curl}_\Gamma \phi, \gamma_R \mathbf{S}_0(\mathbf{curl}_\Gamma p) \rangle_{-\frac{1}{2}} = \langle \mathbf{m} \times \mathbf{n}, \mathbf{curl}_\Gamma \phi \rangle_{-\frac{1}{2}},$$

and, thus, the density $p \in H_*^{\frac{1}{2}}(\Gamma)$ must be such that

$$\langle \gamma_1 W_0(p), \phi \rangle_{\frac{1}{2}} = \langle \mathbf{m} \times \mathbf{n}, \mathbf{curl}_\Gamma \phi \rangle_{-\frac{1}{2}}$$

for all $\phi \in H_*^{\frac{1}{2}}(\Gamma)$.

Lemma 3.4.1 *Let Ω^c be simply connected. There is a unique solution $p \in H_*^{\frac{1}{2}}(\Gamma)$ given by the variational equation*

$$\forall \phi \in H_*^{\frac{1}{2}}(\Gamma): \quad \langle \gamma_R \mathbf{S}_0(\mathbf{curl}_\Gamma p), \mathbf{curl}_\Gamma \phi \rangle_{-\frac{1}{2}} = \langle \mathbf{m} \times \mathbf{n}, \mathbf{curl}_\Gamma \phi \rangle_{-\frac{1}{2}}. \quad (3.91)$$

With this density p a solution φ of the boundary value problem (3.88) is given by (3.89) and, then, the Maxwell solution can be represented as follows

$$\mathbf{E}(\mathbf{x}) = -\nabla W_0(p)(\mathbf{x}). \quad (3.92)$$

Proof: The variational equation (3.91) is uniquely solvable due to the $H_*^{\frac{1}{2}}(\Gamma)$ -ellipticity of the hypersingular operator $\gamma_1 W_0$. \square

Now, we consider the stabilized variational formulation for $\kappa = 0$. It reads

$$\begin{cases} \langle \gamma_R \mathbf{S}_0(\mathbf{j}^t), \phi \rangle_{-\frac{1}{2}} + \langle \operatorname{div}_\Gamma \phi, \gamma_0 S_0(\rho_\Gamma^t) \rangle_{\frac{1}{2}} = \langle \mathbf{m} \times \mathbf{n}, \phi \rangle_{-\frac{1}{2}}, \\ \langle v, \gamma_0 S_0(\operatorname{div}_\Gamma \mathbf{j}^t) \rangle_{\frac{1}{2}} = 0. \end{cases} \quad (3.93)$$

This is obviously a saddle point formulation for (3.91) where the condition $\operatorname{div}_\Gamma \mathbf{j}^t = 0$ is built in as side constraint. To precisely formulate the conditions that guarantee the unique solvability of (3.93), we need the following lemma. The proof goes back to the work of Engleder and Buffa [10,31].

Lemma 3.4.2 *For $\kappa = 0$, there exists a constant $C > 0$ such that*

$$\sup_{\mathbf{0} \neq \phi \in H^{-\frac{1}{2}}(\operatorname{div}_\Gamma, \Gamma)} \frac{|\langle v, \gamma_0 S_0(\operatorname{div}_\Gamma \phi) \rangle_{\frac{1}{2}}|}{\|\phi\|_{H^{-\frac{1}{2}}(\operatorname{div}_\Gamma, \Gamma)}} \geq C \|v\|_{H^{-\frac{1}{2}}(\Gamma)}$$

*holds for all $v \in H_{**}^{-\frac{1}{2}}(\Gamma)$.*

Proof: Due to [10] there exists a constant $C > 0$ such that

$$\|\nabla_{\Gamma}\phi\|_{H^{-\frac{1}{2}}(\text{curl}_{\Gamma},\Gamma)} \geq C\|\phi\|_{H^{\frac{1}{2}}(\Gamma)}$$

holds for all $\phi \in H_{*}^{\frac{1}{2}}(\Gamma)$. Also, we have

$$\|\nabla_{\Gamma}\phi\|_{H^{-\frac{1}{2}}(\text{curl}_{\Gamma},\Gamma)} = \sup_{\mathbf{0} \neq \phi \in H^{-\frac{1}{2}}(\text{div}_{\Gamma},\Gamma)} \frac{|\langle \nabla_{\Gamma}\phi, \phi \rangle_{-\frac{1}{2}}|}{\|\phi\|_{H^{-\frac{1}{2}}(\text{div}_{\Gamma},\Gamma)}} = \sup_{\mathbf{0} \neq \phi \in H^{-\frac{1}{2}}(\text{div}_{\Gamma},\Gamma)} \frac{|\langle \text{div}_{\Gamma}\phi, \phi \rangle_{\frac{1}{2}}|}{\|\phi\|_{H^{-\frac{1}{2}}(\text{div}_{\Gamma},\Gamma)}}.$$

Therefore, the inf-sup condition holds

$$\sup_{\mathbf{0} \neq \phi \in H^{-\frac{1}{2}}(\text{div}_{\Gamma},\Gamma)} \frac{|\langle \text{div}_{\Gamma}\phi, \phi \rangle_{\frac{1}{2}}|}{\|\phi\|_{H^{-\frac{1}{2}}(\text{div}_{\Gamma},\Gamma)}} \geq C\|\phi\|_{H^{\frac{1}{2}}(\Gamma)}$$

for all $\phi \in H_{*}^{\frac{1}{2}}(\Gamma)$. The $H^{\frac{1}{2}}(\Gamma)$ -ellipticity and self-adjointness of $\gamma_0 S_0$ allows for the following transformation

$$\|\phi\|_{H^{\frac{1}{2}}(\Gamma)} = \|\gamma_0 S_0(v)\|_{H^{\frac{1}{2}}(\Gamma)} = \sup_{\mathbf{0} \neq \psi \in H^{-\frac{1}{2}}(\Gamma)} \frac{|\langle \psi, \gamma_0 S_0(v) \rangle_{\frac{1}{2}}|}{\|\psi\|_{H^{-\frac{1}{2}}(\Gamma)}} \geq \frac{|\langle \bar{v}, \gamma_0 S_0(v) \rangle_{\frac{1}{2}}|}{\|v\|_{H^{-\frac{1}{2}}(\Gamma)}} \geq C\|v\|_{H^{-\frac{1}{2}}(\Gamma)}$$

which finishes the proof. \square

The inf-sup condition of the previous lemma is used to prove the unique solvability of the saddle point formulation (3.93).

Theorem 3.4.3 *There exists a unique pair of densities $\mathbf{j}^t \in H^{-\frac{1}{2}}(\text{div}_{\Gamma},\Gamma)$ and $\rho_{\Gamma}^t \in H_{**}^{-\frac{1}{2}}(\Gamma)$ such that the variational formulation (3.93) holds for all $\phi \in H^{-\frac{1}{2}}(\text{div}_{\Gamma},\Gamma)$ and $v \in H_{**}^{-\frac{1}{2}}(\Gamma)$.*

Proof: The variational formulation (3.93) is a classical saddle point problem. The side constraint

$$\forall v \in H_{**}^{-\frac{1}{2}}(\Gamma) : \langle v, \gamma_0 S_0(\text{div}_{\Gamma}\mathbf{j}^t) \rangle_{\frac{1}{2}} = 0$$

yields that $\text{div}_{\Gamma}\mathbf{j}^t = 0$ in $H^{-\frac{1}{2}}(\Gamma)$ and, thus, $\mathbf{j}^t \in H^{-\frac{1}{2}}(\text{div}_{\Gamma}0,\Gamma)$. The ellipticity of the principal part, i.e.,

$$\forall \phi \in H^{-\frac{1}{2}}(\text{div}_{\Gamma}0,\Gamma) : \langle \gamma_R S_0(\phi), \bar{\phi} \rangle_{-\frac{1}{2}} \geq c\|\phi\|_{H^{-\frac{1}{2}}(\text{div}_{\Gamma},\Gamma)}$$

together with the inf-sup condition from Lemma 3.4.2 guarantees the unique solvability of (3.93) by the theorem of Brezzi [9]. \square

3.5. Conclusion

One of the most often studied problems in electromagnetics is the scattering of an electromagnetic field at a perfectly conducting body. The differential equations describing the characteristic of the scattered electromagnetic field are the linear, harmonic Maxwell equations. The mathematical solution theory which treats the boundary integral variational formulation deduced by the Maxwell equations is well-known. By means of this existing theory, the so-called stabilized formulation has been developed in this chapter. It has been shown that the stabilized formulation is related to the classical formulation for electromagnetics and the unique solvability of the stabilized formulation

in the infinite-dimensional setting has been proved. Different from the classical formulation, the stabilized formulation is suited to solve also problems from electrostatics.

In comparison to other publications on the stabilization of the classical boundary integral formulation, the starting point for our presentation are the original Maxwell equations. The use of the distributional setting is most important to understand that the stabilized formulation incorporates a weak form of the continuity equation whereas the classical formulation does not account for the continuity equation. The contribution of our work to the state of research is that it is shown that the stabilization strategy is not an abstract mathematical tool but it is naturally related by physics.

HIGH ORDER BOUNDARY ELEMENTS

4.1. Introduction

It has been known for a long time that elliptic and Maxwell boundary value problems can be reformulated into boundary integral equations [44, 48]. The essential point here is that, in order to boundary value problem posed in a three-dimensional domain Ω^c , one has to solve an equation on its boundary Γ , i.e., on a manifold of dimension two.

The principal theorems in the context of partial differential equations characterize the type of the differential equation and the type of the boundary data which guarantee the unique solvability. To solve the boundary value problem by a numerical scheme, the continuous formulation must be replaced by a discrete formulation. One obtains an approximation $\varphi_{hp} \in H_h^p$ of the exact solution $\varphi \in H$, provided the discretized formulation is also uniquely solvable. If the finite-dimensional space H_h^p is a subspace of H , we call the resulting numerical method conforming. The construction of H_h^p relies on an approximation of the domain of interest by a set of finite elements. The index h denotes the typical element size and p refers to the (polynomial) order of element shape functions. For our purposes, the space H is one of the trace spaces introduced in Section 2.5. The principal question to answer is how to construct appropriate finite-dimensional subspaces of the trace spaces.

Following the basic principles given in [27], the construction of the so-called parametric spaces as finite-dimensional counterparts of the trace spaces is presented in Section 4.2. The Subsections 4.2.1 to 4.2.4 build up on each other as follows. The construction of high order elements starts in Subsection 4.2.1 with a detailed discussion of the reference triangle \hat{T} . Based on Nédélec's polynomial exact sequence defined on the reference triangle \hat{T} , the master element (\hat{T}, \mathbf{p}) is introduced. The characteristics of the master element (\hat{T}, \mathbf{p}) are the fixed geometry \hat{T} and a specified exact sequence of variable polynomial order \mathbf{p} . The lifting procedure from the master element \hat{T} onto a physical boundary element Γ_i is the subject of Subsection 4.2.2. Provided $\Gamma_i \subset \mathbb{R}^3$ is parametrized by an infinitely smooth function $\hat{\mathbf{X}}_i$ with domain \hat{T} , element shape functions φ are defined in terms of master element shape functions $\hat{\varphi}$. This concept is basic for the definition of the parametric elements (Γ_i, \mathbf{p}) of variable order \mathbf{p} . In Subsection 4.2.3, the parametric spaces $\mathcal{H}_h^p(\Gamma)$, $\mathcal{E}_h^{p-1}(\Gamma)$ and $\mathcal{Q}_h^{p-2}(\Gamma)$ which contain basis functions defined on Γ are finally introduced. Subsection 4.2.4 is about the projection-based interpolation operators Π^1 , Π^c and Π^0 . These operators connect infinite-dimensional trace spaces with the finite-dimensional parametric spaces. The set of parametric spaces is completed with the definition of the bidual space $\mathcal{V}_h^{p-1}(\Gamma)$ and the projection-based interpolation operator Π^d . This is done in Subsection 4.2.5. Concluding remarks and further references are given in Section 4.3.

Closely connected to the access which is chosen here to introduce the high order boundary elements is the idea of considering the de Rham cohomology on the boundary as a structure. This relates to a differential geometrical point of view [2, 3] and is explicitly mentioned in [7].

4.2. Hierarchical High Order Boundary Elements

As usual, $\Omega \subset \mathbb{R}^3$ denotes a curvilinear Lipschitz polyhedron with boundary Γ . We assume that Γ is piecewise given by

$$\Gamma = \bigcup_{i=1}^N \bar{\Gamma}_i.$$

Thus, each element Γ_i is parametrized by a bijective and smooth map $\hat{\mathbf{X}}_i: \hat{T} \rightarrow \Gamma_i$ as described in Section 2.1. The intersection of any two elements $\bar{\Gamma}_i$ and $\bar{\Gamma}_j$, with $i \neq j$, is either empty, reduces to a single vertex or consists of a whole common edge. Such partition is called a regular mesh. As an

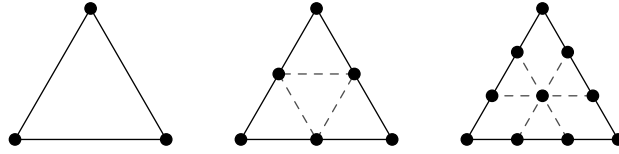


Figure 4.1.: Element degrees of freedom for \mathcal{P}^p , $p = 1$, $p = 2$ and $p = 3$.

example, let us assume $\Gamma_i \subset \Gamma$ are plane triangles and let $\mathcal{P}^3(\Gamma_i)$ denote the space of polynomials of maximal order three defined on Γ_i . It holds $\dim(\mathcal{P}^3(\Gamma_i)) = 10$ and, thus, given a basis $\{\varphi_{l_{\text{loc}}}\}_{l_{\text{loc}}=1}^{10}$, for each $q \in \mathcal{P}^3(\Gamma_i)$, there is a unique set of coefficients $\{\alpha_{l_{\text{loc}}}\}_{l_{\text{loc}}=1}^{10}$ such that

$$q \in \mathcal{P}^3(\Gamma_i) : \quad q(\mathbf{x}) = \sum_{l_{\text{loc}}=1}^{10} \alpha_{l_{\text{loc}}} \varphi_{l_{\text{loc}}}(\mathbf{x}).$$

To obtain a general rule to find the coefficients $\alpha_{l_{\text{loc}}}$ for a specific $q \in \mathcal{P}^3(\Gamma_i)$, the set of element degrees of freedom $\{\Lambda_{l_{\text{loc}}}\}_{l_{\text{loc}}=1}^{10} \subset (\mathcal{P}^3(\Gamma_i))'$ is introduced. The element degrees of freedom are chosen such that

$$q \in \mathcal{P}^3(\Gamma_i) : \quad \Lambda_{l_{\text{loc}}}(q) = \alpha_{l_{\text{loc}}}.$$

The dots in Figure 4.1 symbolize element degrees of freedom for $\mathcal{P}^1(\Gamma_i)$, $\mathcal{P}^2(\Gamma_i)$ and $\mathcal{P}^3(\Gamma_i)$.

The basis functions $\varphi_{l_{\text{loc}}}$ are called element shape functions. The lower index refers to the number of the element degree of freedom in the ordered set of element degrees of freedom. This notation is unique if the set of element shape functions and the set of element degrees of freedom are isomorphic to each other.

In order to represent a polynomial $q \in \mathcal{P}^p(\Gamma)$ on the whole surface Γ , a set of global basis functions $\{\phi_{l_{\text{glob}}}\}_{l_{\text{glob}}}$ and a set of global degrees of freedom $\{\Lambda_{l_{\text{glob}}}\}_{l_{\text{glob}}}$ are needed. Then,

$$q \in \mathcal{P}^p(\Gamma) : \quad q(\mathbf{x}) = \sum_{l_{\text{glob}}} \alpha_{l_{\text{glob}}} \phi_{l_{\text{glob}}}(\mathbf{x}), \quad \Lambda_{l_{\text{glob}}}(q) = \alpha_{l_{\text{glob}}}.$$

The global basis functions are constructed in terms of element shape functions. This means, however, that the global degrees of freedom are given by element degrees of freedom and that local coefficients $\alpha_{l_{\text{loc}}}$ coincide with the global coefficients $\alpha_{l_{\text{glob}}}$ whenever elements are connected to each other. The dots lying on the common edge of the triangles in Figure 4.2 are global degrees of freedom.

4.2.1. The Master Element

By assumption, the domain of definition of the local parametrizations $\hat{\mathbf{X}}_i$ is for all $i = 1, \dots, N$ the same, namely the reference triangle shown in Figure 4.3. It will get clear in the following subsections,

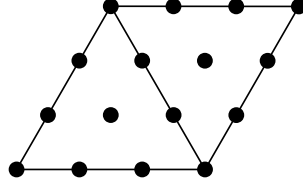


Figure 4.2.: Local degrees of freedom and global, namely shared, degrees of freedom.

that the reference triangle plays a fundamental role within the construction of the hierarchical high order boundary elements. We define

$$\bar{T} = \{\hat{\mathbf{v}}_1, \hat{\mathbf{v}}_2, \hat{\mathbf{v}}_3\} \cup \{\hat{\mathbf{e}}_1, \hat{\mathbf{e}}_2, \hat{\mathbf{e}}_3\} \cup \hat{T},$$

where the vertices $\hat{\mathbf{v}}_i$, $i = 1, 2, 3$, are

$$\hat{\mathbf{v}}_1 = (0, 0)^\top, \quad \hat{\mathbf{v}}_2 = (1, 0)^\top, \quad \hat{\mathbf{v}}_3 = (0, 1)^\top, \quad (4.1)$$

the edges $\hat{\mathbf{e}}_i$, $i = 1, 2, 3$, are parametrized as follows

$$\begin{aligned} \hat{\mathbf{e}}_1 &= \{(t, 0)^\top, t \in [0, 1]\}, & \hat{\boldsymbol{\tau}}_1 &= (1, 0)^\top, \\ \hat{\mathbf{e}}_2 &= \{(1-t, t)^\top, t \in [0, 1]\}, & \hat{\boldsymbol{\tau}}_2 &= \frac{1}{\sqrt{2}}(-1, 1)^\top, \\ \hat{\mathbf{e}}_3 &= \{(0, 1-t)^\top, t \in [0, 1]\}, & \hat{\boldsymbol{\tau}}_3 &= (0, -1)^\top, \end{aligned} \quad (4.2)$$

and the element interior is given by

$$\hat{T} = \left\{ \boldsymbol{\xi} = (\xi_1, \xi_2)^\top, 0 < \xi_1, \xi_2 < 1, \xi_1 + \xi_2 < 1 \right\}. \quad (4.3)$$

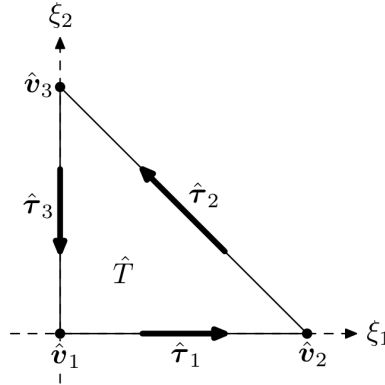


Figure 4.3.: The reference triangle.

The reference triangle is canonically embedded in \mathbb{R}^3 by simply adding the third component $\xi_3 = 0$. Thus, whenever we consider $\bar{T} \subset \mathbb{R}^3$, this canonical embedding is assumed without further comment.

In the following, functions defined on elements Γ_i are distinguished from functions defined on the reference triangle. The first are called element shape functions and the argument is typically denoted \boldsymbol{x} . The latter are called master element shape functions and they depend on master element coordinates $\boldsymbol{\xi}$. To indicate that the reference triangle is their domain of definition, the

master element shape functions are given a hat.

Let $\mathcal{P}^p(\hat{T})$ denote the space of polynomials with domain \hat{T} of order less or equal p and let, further, $\mathcal{P}^{\mathbf{p}}(\hat{T}) = \mathcal{P}^{\mathbf{p}}(\hat{T})^2$ denote the polynomial vector fields of order less or equal \mathbf{p} . Starting with $\mathcal{P}^p(\hat{T})$, we obtain for $p \geq 2$ the exact sequence

$$\mathcal{P}^p(\hat{T}) \xrightarrow{\nabla_{\Gamma}} \mathcal{P}^{p-1}(\hat{T}) \xrightarrow{\text{curl}_{\Gamma}} \mathcal{P}^{p-2}(\hat{T}).$$

For arbitrary $\hat{\varphi} \in \mathcal{P}^p(\hat{T})$ and $\hat{\boldsymbol{\varphi}} = \hat{\varphi}_1 \mathbf{e}_1 + \hat{\varphi}_2 \mathbf{e}_2 \in \mathcal{P}^{\mathbf{p}}(\hat{T})$, it holds due to (2.31) and (2.32)

$$\nabla_{\Gamma}: \hat{\varphi} \mapsto \frac{\partial \hat{\varphi}}{\partial \xi_1} \mathbf{e}_1 + \frac{\partial \hat{\varphi}}{\partial \xi_2} \mathbf{e}_2 \quad \text{and} \quad \text{curl}_{\Gamma}: \hat{\boldsymbol{\varphi}} \mapsto \frac{\partial \hat{\varphi}_2}{\partial \xi_1} - \frac{\partial \hat{\varphi}_1}{\partial \xi_2}, \quad (4.4)$$

since the bidual basis vectors coincide with the standard basis vectors

$$\mathbf{a}_l = \mathbf{a}^l = \mathbf{e}_l, \quad l = 1, 2, \quad \text{and} \quad \mathbf{a}_{12} = \mathbf{a}^{12} = 1.$$

We obtain a much finer distinction of the polynomials defined on \hat{T} when we classify the polynomials according to their polynomial degree on edges \hat{e}_i and in the interior \hat{T} . Now, let $\hat{\varphi} \in \mathcal{P}^p(\hat{T})$ and let $\hat{\varphi}|_{\hat{e}_i}$ be its restriction on the i th edge. We say that $\hat{\varphi}$ has variable order

$$\mathbf{p} = (p, p_1, p_1, p_3) \in \mathbb{N}^4, \quad 1 \leq p_i \leq p, \quad i = 1, 2, 3,$$

if $\hat{\varphi}|_{\hat{e}_i} \in \mathcal{P}^{p_i}(\hat{e}_i)$. This classification leads to the definition of the space of polynomials with variable order

$$\mathcal{P}^{\mathbf{p}}(\hat{T}) = \left\{ \hat{\varphi} \in \mathcal{P}^p(\hat{T}), \hat{\varphi}|_{\hat{e}_i} \in \mathcal{P}^{p_i}(\hat{e}_i), i = 1, 2, 3 \right\} \subset \mathcal{P}^p(\hat{T}).$$

Similarly, we define the space of vector-valued polynomials of variable order. Here, we consider the parallel projection of the restrictions on the edges \hat{e}_i , namely,

$$\hat{\boldsymbol{\varphi}}|_{\hat{e}_i} \cdot \hat{\boldsymbol{\tau}}_i, \quad i = 1, 2, 3.$$

The space of vector-valued polynomials of variable order \mathbf{p} is given by

$$\mathcal{P}^{\mathbf{p}}(\hat{T}) = \left\{ \hat{\boldsymbol{\varphi}} \in \mathcal{P}^{\mathbf{p}}(\hat{T}), \hat{\boldsymbol{\varphi}}|_{\hat{e}_i} \cdot \hat{\boldsymbol{\tau}}_i \in \mathcal{P}^{p_i}(\hat{e}_i), i = 1, 2, 3 \right\} \subset \mathcal{P}^{\mathbf{p}}(\hat{T}).$$

We adopt the notation

$$\mathbf{p} - \mathbf{1} = (p - 1, p_1 - 1, p_2 - 1, p_3 - 1).$$

Then, these polynomial spaces are related to each other by

$$\mathcal{P}^{\mathbf{p}}(\hat{T}) \xrightarrow{\nabla_{\Gamma}} \mathcal{P}^{\mathbf{p}-\mathbf{1}}(\hat{T}) \xrightarrow{\text{curl}_{\Gamma}} \mathcal{P}^{\mathbf{p}-2}(\hat{T}), \quad (4.5)$$

and this sequence is exact. When a basis for $\mathcal{P}^{\mathbf{p}}(\hat{T})$ is chosen, there is a natural access to the two subsequent spaces via differentiation. The gradient is, however, not surjective and this means that $\nabla_{\Gamma}(\mathcal{P}^{\mathbf{p}}(\hat{T}))$ is only a subspace of $\mathcal{P}^{\mathbf{p}-\mathbf{1}}(\hat{T})$. To obtain a basis for $\mathcal{P}^{\mathbf{p}-\mathbf{1}}(\hat{T})$ one has to add the missing number of linear independent polynomial vector fields. The operator curl_{Γ} in (4.5) is surjective and, thus, the last space in the sequence is given by $\mathcal{P}^{\mathbf{p}-2}(\hat{T}) = \text{curl}_{\Gamma}(\mathcal{P}^{\mathbf{p}-\mathbf{1}}(\hat{T}))$.

The definition that follows is important for understanding the complexity of the high order boundary elements and it is helpful to start with a short motivation. Consider $\mathcal{P}^{\mathbf{p}_1}(\hat{T})$ with uniform order $\mathbf{p}_1 = (1, 1, 1, 1)$ and $\mathcal{P}^{\mathbf{p}_2}(\hat{T})$ with variable order $\mathbf{p}_2 = (2, 2, 1, 1)$. These spaces are different because the latter contains quadratic polynomials and the first obviously not. However, not all quadratic

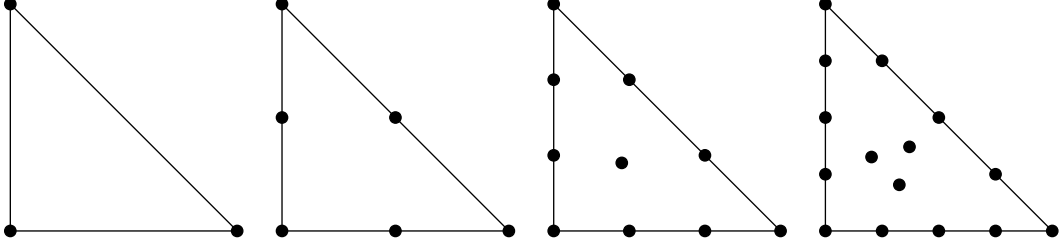

 Figure 4.4.: Number of degrees of freedom for $\mathcal{P}^p(\hat{T})$ with uniform $p = 1, p = 2, p = 3, p = 4$.

 Table 4.1.: Notations for the hierarchical master element shape functions of second kind for $p \geq 2$

	Set	Notation	Index k	Index i	Index l
$\mathcal{P}^p(\hat{T})$	\hat{a}_i	$\hat{\varphi}_k^i$	$k = 1$	$i = 1, 2, 3$	$l = 0$
	\hat{a}_{3+i}	$\hat{\varphi}_k^i$	$2 \leq k \leq p_i$	$i = 1, 2, 3$	$l = 0$
	\hat{a}_7	$\hat{\varphi}_k^{3+l}$	$3 \leq k \leq p$	$i = 0$	$1 \leq l \leq k - 2$
$\mathcal{P}^{p-1}(\hat{T})$	\hat{a}_{3+i}	$\hat{\varphi}_k^i$	$0 \leq k \leq p_i - 1$	$i = 1, 2, 3$	$l = 0$
	\hat{a}_7	$\hat{\varphi}_k^{3+l}$	$2 \leq k \leq p - 1$	$i = 0$	$1 \leq l \leq 2(k - 1) + 1$
$\mathcal{P}^{p-2}(\hat{T})$	\hat{a}_7	\hat{v}_k^l	$0 \leq k \leq p - 2$	$i = 0$	$\begin{cases} l = 1, & k = 0 \\ 1 \leq l \leq k + 1 & k > 0 \end{cases}$

polynomials are allowed in $\mathcal{P}^{p_2}(\hat{T})$ but only those with

$$\hat{\varphi}|_{\hat{e}_1} \in \mathcal{P}^2(\hat{e}_1) \quad \text{and} \quad \hat{\varphi}|_{\hat{e}_i} \in \mathcal{P}^1(\hat{e}_i), \quad i = 2, 3.$$

The dots in Figure 4.4 illustrate the number of basis functions for $\mathcal{P}^p(\hat{T})$ for uniform order of approximation $p = 1$ to $p = 4$. The distribution of points on the edges and in the element interior varies in the sense that the higher p , the more basis functions are associated with the edges and the element interior.

It is convenient to introduce for each geometrical entity an abstract notation and assign to it a polynomial order. For a vertex \hat{v}_i , $i = 1, 2, 3$, we introduce the abstract notation vertex node \hat{a}_i , $i = 1, 2, 3$, and assign to it the polynomial order one. For an edge \hat{e}_i , $i = 1, 2, 3$, we introduce the abstract notation midedge node \hat{a}_{3+i} , $i = 1, 2, 3$, and assign to it the polynomial order p_i . Finally, for the interior \hat{T} , we introduce the abstract notation middle node \hat{a}_7 and assign to it the polynomial order p .

This notation is used here to explain the hierarchical structure of the polynomial basis functions for arbitrary orders $\mathbf{p} \in \mathbb{N}^4$. In Subsection 4.2.4 it will become clear that the association of basis functions with either vertex nodes, midedge nodes or middle nodes goes along with the choice of the high order degrees of freedom.

Definition 9 The master element (\hat{T}, \mathbf{p}) of order \mathbf{p} , is a structure with the following attributes:

1. The reference triangle given by (4.1)-(4.3).
2. A set of fixed bases of $\mathcal{P}^p(\hat{T})$, $\mathcal{P}^{p-1}(\hat{T})$ and $\mathcal{P}^{p-2}(\hat{T})$. The bases for $\mathcal{P}^p(\hat{T})$ and $\mathcal{P}^{p-1}(\hat{T})$ are hierarchical.

To characterize the hierarchical bases, the notations listed in Table 4.1 are used. A set of functions

spanning $\mathcal{P}^p(\hat{T})$ is called a hierarchical basis if the functions are divided into three kinds of sets. The first set contains the linear basis functions, uniquely defined by

$$i = 1, 2, 3 : \quad \hat{\varphi}_1^i \in \mathcal{P}^1(\hat{T}) \quad \text{with} \quad \hat{\varphi}_1^i(\hat{\mathbf{v}}_j) = \delta_{ij} \quad \text{for } j = 1, 2, 3. \quad (4.6)$$

The linear basis functions are called vertex node shape functions because the only information which is necessary to specify them is related to the vertex nodes \hat{a}_i for $i = 1, 2, 3$.

The second set contains the basis functions which have polynomial order $2 \leq k \leq p_i$ and which vanish at the vertices $\hat{\mathbf{v}}_j$ such that

$$i = 1, 2, 3 : \quad 2 \leq k \leq p_i : \quad \hat{\varphi}_k^i \in \mathcal{P}^k(\hat{T}) \quad \text{with} \quad \hat{\varphi}_k^i(\hat{\mathbf{v}}_j) = 0 \quad \text{for } j = 1, 2, 3. \quad (4.7)$$

The basis functions of the second set are called midedge node shape functions because, besides (4.7), the only information which is necessary to specify them is the polynomial degree p_i associated to the midedge nodes \hat{a}_{3+i} for $i = 1, 2, 3$.

The third set contains basis functions which have polynomial order $3 \leq k \leq p$ and which vanish on the boundary of the reference triangle, i.e.,

$$3 \leq k \leq p : \quad 1 \leq l \leq k - 2 : \quad \hat{\varphi}_k^{3+l} \in \mathcal{P}^k(\hat{T}) \quad \text{with} \quad \hat{\varphi}_k^{3+l}|_{\hat{e}_j} = 0 \quad \text{for } j = 1, 2, 3. \quad (4.8)$$

The basis functions of the third set are called bubble functions because, besides (4.8), the only information which is necessary to specify them is the polynomial degree p associated to the middle node \hat{a}_7 . Note, that for polynomial degree $k \geq 2$, there are up to three functions in the set of midedge node shape functions of polynomial degree k . This is why the running index is $3 + l$.

Similarly, a set of vector fields spanning $\mathcal{P}^{p-1}(\hat{T})$ is called a hierarchical basis if the vector fields are divided into two kinds of sets. The first set contains the midedge node shape vector fields associated to the midedge nodes \hat{a}_{3+i} with associated orders p_i , i.e.,

$$i = 1, 2, 3 : \quad 0 \leq k \leq p_i - 1 : \quad \hat{\varphi}_k^i|_{\hat{e}_i} \cdot \hat{\boldsymbol{\tau}}_i \in \mathcal{P}^{p_i-1}(\hat{e}_i). \quad (4.9)$$

The second set contains the basis vector fields associated to the middle node \hat{a}_7 . They are called bubble vector fields because their parallel projection restricted to the edges vanish, i.e.,

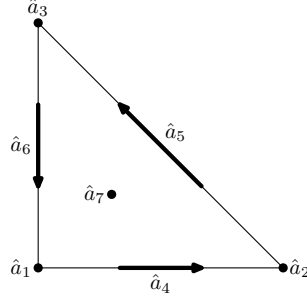
$$2 \leq k \leq p-1 : \quad 1 \leq l \leq 2(k-1)+1 : \quad \hat{\varphi}_k^{3+l} \in \mathcal{P}^k(\hat{T}) \quad \text{with} \quad \hat{\varphi}_k^{3+l}|_{\hat{e}_j} \cdot \hat{\boldsymbol{\tau}}_j = 0 \quad \text{for } j = 1, 2, 3. \quad (4.10)$$

The choice of hierarchical bases for $\mathcal{P}^p(\hat{T})$ and $\mathcal{P}^{p-1}(\hat{T})$ is not unique. The construction of the polynomial bases which underly the numerical part of this work is explained in Appendix D.

By the overview given in Table 4.1 it is easily seen that a specific master element shape function in each of the polynomial spaces is uniquely defined by the set of indices $\{i, k, l\}$. Besides this nomenclature, another notational convention is used in the following. We assume that the master element shape functions spanning the polynomial spaces are ordered and, thus, there is an isomorphism

$$\{i, k, l\} \mapsto l_{\text{loc}}, \quad (4.11)$$

which assigns to $\{i, k, l\}$ the number l_{loc} of the master element shape function in the ordered set of


 Figure 4.5.: Symbolical vertex nodes, midedge nodes and middle node of \hat{T} .

the master element shape functions spanning the specific polynomial space. Namely,

$$\begin{aligned}
 \mathcal{P}^p(\hat{T}) &= \text{span} \{ \hat{\varphi}_1^1, \hat{\varphi}_1^2, \hat{\varphi}_1^3, \hat{\varphi}_2^1, \dots, \hat{\varphi}_p^{1+p} \}, \\
 &\hat{=} \text{span} \{ \hat{\varphi}_1, \hat{\varphi}_2, \hat{\varphi}_3, \hat{\varphi}_4, \dots, \hat{\varphi}_{n_{\mathcal{H}}} \} = \{ \hat{\varphi}_{l_{\text{loc}}} \}_{l_{\text{loc}}=1}^{n_{\mathcal{H}}}, \\
 \mathcal{P}^{p-1}(\hat{T}) &= \text{span} \{ \hat{\varphi}_0^1, \hat{\varphi}_0^2, \hat{\varphi}_0^3, \hat{\varphi}_1^1, \dots, \hat{\varphi}_{p-1}^{2p} \}, \\
 &\hat{=} \text{span} \{ \hat{\varphi}_1, \hat{\varphi}_2, \hat{\varphi}_3, \hat{\varphi}_4, \dots, \hat{\varphi}_{n_{\mathcal{E}}} \} = \{ \hat{\varphi}_{l_{\text{loc}}} \}_{l_{\text{loc}}=1}^{n_{\mathcal{E}}}, \\
 \mathcal{P}^{p-2}(\hat{T}) &= \text{span} \{ \hat{v}_0^1, \hat{v}_1^1, \hat{v}_1^2, \hat{v}_2^1, \dots, \hat{v}_{p-2}^{p-1} \}, \\
 &\hat{=} \text{span} \{ \hat{v}_1, \hat{v}_2, \hat{v}_3, \hat{v}_4, \dots, \hat{v}_{n_{\mathcal{Q}}} \} = \{ \hat{v}_{l_{\text{loc}}} \}_{l_{\text{loc}}=1}^{n_{\mathcal{Q}}}.
 \end{aligned}$$

The subscript loc is used here to emphasize that l_{loc} does not coincide with the index l from Table 4.1. Whenever it is clear from the context, the subscript loc is skipped in the following.

A final remark about the master element concerns the choice of basis for $\mathcal{P}^{p-2}(\hat{T})$. The sequence (4.5) is exact and, thus, we extract from

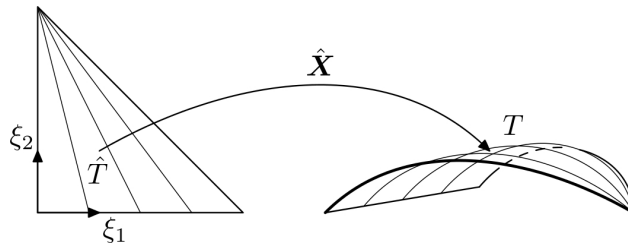
$$\{ \text{curl}_{\Gamma} \hat{\varphi}_l \}_{l=1}^{n_{\mathcal{E}}}, \quad (4.12)$$

our basis functions. In this set of basis functions $\{ \hat{v}_l \}_{l=1}^{n_{\mathcal{Q}}}$ any function has a representation of the following kind

$$\hat{v}_l = \text{curl}_{\Gamma} \hat{\varphi}_{i_l}, \quad l = 1, \dots, n_{\mathcal{Q}}, \quad i_l \in \{1, \dots, n_{\mathcal{E}}\}, \quad (4.13)$$

where i_l is the running index collecting only the linear independent functions in the set (4.12).

4.2.2. The Parametric Element


 Figure 4.6.: The parametrization $\hat{\mathbf{X}}: \hat{T} \rightarrow T$.

Let us consider a curvilinear triangle $T \subset \mathbb{R}^3$ parametrized by a smooth map $\hat{\mathbf{X}}$ as illustrated in Figure 4.6. The parametrization $\hat{\mathbf{X}}$ is, in general, non-linear and, thus, the embedding of T in \mathbb{R}^3 is not canonic. Recall that at any $\mathbf{x} = \hat{\mathbf{X}}(\boldsymbol{\xi})$ we obtain bidual basis vectors $\{\mathbf{a}^l, \mathbf{a}_l\}_{l=1}^2$ according to

(2.10),(2.27) and $\{\mathbf{a}^{12}, \mathbf{a}_{12}\}$ according to (2.12),(2.28). The bidual basis vectors are used to define the element shape functions in terms of parameter coordinates.

Definition 10 1. Let $\{\hat{\varphi}_l\}_{l=1}^{n_{\mathcal{H}}}$ denote a fixed hierarchical basis of $\mathcal{P}^{\mathcal{P}}(\hat{T})$. At $\mathbf{x} = \hat{\mathbf{X}}(\boldsymbol{\xi})$, we define

$$\begin{aligned} \mathcal{H}^{\mathcal{P}}(T) = \text{span} \{ \varphi_l \}_{l=1}^{n_{\mathcal{H}}} : \quad \varphi_l(\mathbf{x}) &= \hat{\varphi}_l(\boldsymbol{\xi}), \quad l = 1, \dots, n_{\mathcal{H}}, \\ \text{with } \nabla_{\Gamma} \varphi_l(\mathbf{x}) &= \frac{\partial \hat{\varphi}_l(\boldsymbol{\xi})}{\partial \xi_1} \mathbf{a}^1 + \frac{\partial \hat{\varphi}_l(\boldsymbol{\xi})}{\partial \xi_2} \mathbf{a}^2. \end{aligned} \quad (4.14)$$

2. Let $\{\hat{\varphi}_l\}_{l=1}^{n_{\mathcal{E}}}$ denote a fixed hierarchical basis for $\mathcal{P}^{\mathcal{P}-1}(\hat{T})$. At $\mathbf{x} = \hat{\mathbf{X}}(\boldsymbol{\xi})$, we define

$$\begin{aligned} \mathcal{E}^{\mathcal{P}-1}(T) = \text{span} \{ \boldsymbol{\varphi}^l \}_{l=1}^{n_{\mathcal{E}}}, \quad \boldsymbol{\varphi}^l(\mathbf{x}) &= \hat{\varphi}_{l,1}(\boldsymbol{\xi}) \mathbf{a}^1 + \hat{\varphi}_{l,2}(\boldsymbol{\xi}) \mathbf{a}^2, \quad l = 1, \dots, n_{\mathcal{E}}, \\ \text{with } \text{curl}_{\Gamma} \boldsymbol{\varphi}^l(\mathbf{x}) &= \left(\frac{\partial \hat{\varphi}_{l,2}(\boldsymbol{\xi})}{\partial \xi_1} - \frac{\partial \hat{\varphi}_{l,1}(\boldsymbol{\xi})}{\partial \xi_2} \right) \mathbf{a}^{12}. \end{aligned} \quad (4.15)$$

3. Let $\{\hat{v}_l\}_{l=1}^{n_{\mathcal{Q}}}$ denote a fixed basis of $\mathcal{P}^{\mathcal{P}-2}(\hat{T})$. At $\mathbf{x} = \hat{\mathbf{X}}(\boldsymbol{\xi})$, we define

$$\begin{aligned} \mathcal{Q}^{\mathcal{P}-2}(T) = \text{span} \{ v_l \}_{l=1}^{n_{\mathcal{Q}}}, \quad v_l(\mathbf{x}) &= \hat{v}_l(\boldsymbol{\xi}) \mathbf{a}^{12}, \quad l = 1, \dots, n_{\mathcal{Q}}, \\ \text{with } v_l &= \text{curl}_{\Gamma} \boldsymbol{\varphi}^{i_l}, \quad i_l \in \{1, \dots, n_{\mathcal{E}}\}. \end{aligned} \quad (4.16)$$

The element shape functions and vector fields are smooth and non-polynomial unless the parametrization $\hat{\mathbf{X}}$ is linear. The spaces of element shape functions, however, naturally inherit the most important properties from the polynomial spaces.

Lemma 4.2.1 *The element shape functions spanning $\mathcal{H}^{\mathcal{P}}(T)$ are hierarchical. Also, the element shape vector fields spanning $\mathcal{E}^{\mathcal{P}-1}(T)$ are hierarchical. Moreover, the sequence*

$$\mathcal{H}^{\mathcal{P}}(T) \xrightarrow{\nabla_{\Gamma}} \mathcal{E}^{\mathcal{P}-1}(T) \xrightarrow{\text{curl}_{\Gamma}} \mathcal{Q}^{\mathcal{P}-2}(T) \quad (4.17)$$

is exact.

Proof: The bases for $\mathcal{H}^{\mathcal{P}}(T)$ and $\mathcal{E}^{\mathcal{P}-1}(T)$ are hierarchical because the corresponding polynomial bases $\mathcal{P}^{\mathcal{P}}(\hat{T})$ and $\mathcal{P}^{\mathcal{P}-1}(\hat{T})$ are hierarchical. The sequence (4.17) is exact because the underlying polynomial sequence (4.5) is exact. \square

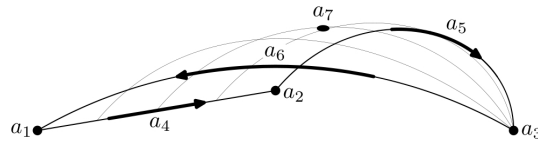


Figure 4.7.: Symbolical vertex nodes, midedge nodes and middle node of T .

As illustrated in Figure 4.7, the geometrical entities of the curvilinear element T are given abstract notations, i.e., we introduce the set of vertex nodes a_i with assigned order one for $i = 1, 2, 3$. Further, we introduce the midedge nodes a_{3+i} with assigned order p_i for $i = 1, 2, 3$ and, also, the middle node a_7 with assigned order p .

Definition 11 The parametric element (T, \mathbf{p}) is a structure with the following attributes.

1. The geometry of the parametric element is given by a smooth bijection $\hat{\mathbf{X}}: \hat{T} \rightarrow T$.
2. A set of bases for the spaces $\mathcal{H}^{\mathcal{P}}(T)$, $\mathcal{E}^{\mathcal{P}-1}(T)$ and $\mathcal{Q}^{\mathcal{P}-2}(T)$. The bases for $\mathcal{H}^{\mathcal{P}}(T)$ and $\mathcal{E}^{\mathcal{P}-1}(T)$ are hierarchical and (4.17) is exact.

Table 4.2.: Notations for the hierarchical element shape functions of second kind for $p \geq 2$

	Set	Notation	Index k	Index i	Index l
$\mathcal{H}^p(T)$	a_i	φ_k^i	$k = 1$	$i = 1, 2, 3$	$l = 0$
	a_{3+i}	φ_k^i	$2 \leq k \leq p_i$	$i = 1, 2, 3$	$l = 0$
	a_7	φ_k^{3+l}	$3 \leq k \leq p$	$i = 0$	$1 \leq l \leq k - 2$
$\mathcal{E}^{p-1}(T)$	a_{3+i}	φ_k^i	$0 \leq k \leq p_i - 1$	$i = 1, 2, 3$	$l = 0$
	a_7	φ_k^{3+l}	$2 \leq k \leq p - 1$	$i = 0$	$1 \leq l \leq 2(k - 1) + 1$
$\mathcal{Q}^{p-2}(T)$	a_7	v_k^l	$0 \leq k \leq p - 2$	$i = 0$	$\begin{cases} l = 1, & k = 0 \\ 1 \leq l \leq k + 1 & k > 0 \end{cases}$

The indexing of the element shape functions spanning the local spaces $\mathcal{H}^p(T)$, $\mathcal{E}^{p-1}(T)$ and $\mathcal{Q}^{p-2}(T)$ is the same as for master element shape functions. Again, there is an isomorphism between the single running index introduced in Definition 10 and the nomenclature presented in Table 4.2. The index notation listed in Table 4.2 is used if the information captured in the indices is explicitly needed.

4.2.3. The Parametric Spaces

In this subsection, the finite-dimensional spaces used later as approximations of the infinite-dimensional trace spaces are defined. Thus, the basis functions which span these so-called parametric spaces are defined on the whole boundary Γ and not on elements $\Gamma_i \subset \Gamma$. However, the spaces of element shape functions defined in Subsection 4.2.2 serve as building blocks to construct the basis functions. The new aspect here is that the elements are connected to each other by vertices and edges and, thus, the order of approximation on edges between neighboring elements should coincide. To precisely formulate this condition, consider Γ as either the boundary of a curvilinear Lipschitz polyhedron or of class C^r with $r \geq 1$ described by a set of parametric elements

$$\{(\Gamma_i, \mathbf{p}_i)\}_{i=1}^N \quad \text{with} \quad \Gamma = \bigcup_{i=1}^N \overline{\Gamma}_i, \quad (4.18)$$

where $\mathbf{p}_i = (p_i, p_{i,1}, p_{i,2}, p_{i,3})^\top$ with $p_{i,j} \leq p_i$ for $j = 1, 2, 3$. Moreover, we consider a decomposition of Γ in sets of vertices \mathbf{v}_i , edges e_i and elements Γ_i . Let

$$S_I = \{\mathbf{v}_i\}_{i=1}^{N_I}, \quad S_{II} = \{e_i\}_{i=1}^{N_{II}}, \quad S_{III} = \{\Gamma_i\}_{i=1}^N, \quad (4.19)$$

then

$$\Gamma = S_I \cup S_{II} \cup S_{III}. \quad (4.20)$$

The hp -meshes which suit our purposes can be defined now.

Definition 12 Let Γ be given by (4.18) with (4.19). The hp -mesh is called regular, if for an arbitrary pair of elements Γ_i and Γ_j with $i \neq j$, it holds that

1. the intersection $\overline{\Gamma}_i \cap \overline{\Gamma}_j$ is either empty,
2. or, there exist $e_l \in S_{II}$ and $\mathbf{v}_{l_1}, \mathbf{v}_{l_2} \in S_I$ such that $\overline{\Gamma}_i \cap \overline{\Gamma}_j = e_l \cup \mathbf{v}_{l_1} \cup \mathbf{v}_{l_2}$,
3. or, there exists $\mathbf{v}_l \in S_I$ such that $\overline{\Gamma}_i \cap \overline{\Gamma}_j = \mathbf{v}_l$.

Table 4.3.: Notations for the basis functions, elements of second kind for $p \geq 2$

	Set	Notation	Index k	Index $l = l(k)$	Index i
$\mathcal{H}_h^p(\Gamma)$	S_I	$\phi_{k,l}^{I,i}$	$k = 1$	$l = 0$	$1 \leq i \leq N_I$
	S_{II}	$\phi_{k,l}^{II,i}$	$2 \leq k \leq p_{e_i}$	$l = 0$	$1 \leq i \leq N_{II}$
	S_{III}	$\phi_{k,l}^{III,i}$	$3 \leq k \leq p_{\Gamma_i}$	$1 \leq l \leq k - 2$	$1 \leq i \leq N$
$\mathcal{E}_h^{p-1}(\Gamma)$	S_I	—	—	—	—
	S_{II}	$\phi_{k,l}^{II,i}$	$0 \leq k \leq p_{e_i} - 1$	$l = 0$	$1 \leq i \leq N_{II}$
	S_{III}	$\phi_{k,l}^{III,i}$	$2 \leq k \leq p_{\Gamma_i} - 1$	$1 \leq l \leq 2(k - 1) + 1$	$1 \leq i \leq N$
$\mathcal{Q}_h^{p-2}(\Gamma)$	S_I	—	—	—	—
	S_{II}	—	—	—	—
	S_{III}	$\nu_{k,l}^{III,i}$	$0 \leq k \leq p_{\Gamma_i} - 2$	$\begin{cases} l = 0, & k = 0 \\ 1 \leq l \leq k + 1 & k > 0 \end{cases}$	$1 \leq i \leq N$

The hp -mesh is called compatible if neighboring elements impose the same order of approximation on the common edge, or, in other words, if each edge $e_i \in S_{II}$ is assigned a unique order p_{e_i} .

Let Γ be described by a regular and compatible hp -mesh (4.18) with the components (4.19), then, the parametric spaces can be defined.

Definition 13 The parametric space $\mathcal{H}_h^p(\Gamma)$ is spanned by three sets of basis functions. The first set contains basis functions connected to the set of vertices S_I . The support of the basis function $\phi_{1,0}^{I,i}$ which belongs to $v_i \in S_I$ comprises all parametric elements which share the vertex v_i . Let us assume that the number of these support elements is $m = m(i) \in \mathbb{N}$. We denote the support elements by Γ_{i_l} , where $l = 1, \dots, m(i)$, and the index i_l refers to the actual number of the element in the set S_{III} . Then, $1 \leq i \leq N_I$

$$\text{supp } \phi_{1,0}^{I,i} = \bigcup_{l=1}^m \overline{\Gamma_{i_l}}, \quad m = m(i) \in \mathbb{N}.$$

The basis function $\phi_{1,0}^{I,i}$ is defined as follows

$$\phi_{1,0}^{I,i} \Big|_{\Gamma_j} = \begin{cases} \varphi_1^{i_{\text{loc}}} \in \mathcal{H}^p(\Gamma_j), & j \in \{i_1, \dots, i_m\}, \\ 0, & j \notin \{i_1, \dots, i_m\}. \end{cases} \quad (4.21)$$

Here, $i_{\text{loc}} \in \{1, 2, 3\}$ refers to the local vertex node number. The first lower index, $k = 1$, corresponds to the order of the basis function and the second lower index, $l = 0$, does not bear any meaning and it is, therefore, zero.

The second set of basis functions is connected to the set of edges S_{II} . The support of the basis function $\phi_{k,0}^{II,i}$ belongs to $e_i \in S_{II}$ and it coincides with the two elements $\Gamma_{i_1}, \Gamma_{i_2}$ which share the edge e_i . Let

$$\text{supp } \phi_{k,0}^{II,i} = \overline{\Gamma_{i_1}} \cup \overline{\Gamma_{i_2}}, \quad 1 \leq i \leq N_{II}.$$

We define

$$\phi_{k,0}^{II,i} \Big|_{\Gamma_j} = \begin{cases} \varphi_k^{i_{\text{loc}}} \in \mathcal{H}^p(\Gamma_j), & j \in \{i_1, i_2\}, \\ 0, & j \notin \{i_1, i_2\}. \end{cases} \quad (4.22)$$

Here, $i_{\text{loc}} \in \{1, 2, 3\}$ refers to the local midedge node number and k refers to the order of the basis function. The range of k is listed in Table 4.3. All basis functions of this second set vanish at the vertices $v_i \in S_I$ and

this is why we call any linear combination

$$v = \sum_{i=1}^{N_{II}} \sum_k \alpha_{k,0}^{II,i} \phi_{k,0}^{II,i}, \quad \alpha_{k,0}^{II,i} \in \mathbb{C},$$

an edge bubble function.

The third set of basis functions is connected to the set of elements S_{III} . The support of the basis function $\phi_{k,l}^{III,i}$ is $\bar{\Gamma}_i$. We define

$$\phi_{k,l}^{III,i} \Big|_{\Gamma_j} = \begin{cases} \varphi_k^{3+l} \in \mathcal{H}^p(\Gamma_i), & j = i, \\ 0, & j \neq i. \end{cases} \quad (4.23)$$

Here, the index k refers to the order of the basis function and the additional index l refers to the l th basis function of order k . The ranges of l and k are listed in Table 4.3. All basis functions of this third set vanish at the vertices $v_i \in S_I$ and on the edges $e_i \in S_{II}$ and this is why we call any linear combination

$$v = \sum_{i=1}^{N_{III}} \sum_{k,l} \alpha_{k,l}^{III,i} \phi_{k,l}^{III,i}, \quad \alpha_{k,l}^{III,i} \in \mathbb{C},$$

a bubble function.

Since Γ is at least a Lipschitz continuous manifold, all basis functions are at least globally continuous by definition and it holds

$$\mathcal{H}_h^p(\Gamma) \subset C(\Gamma) \subset H^{\frac{1}{2}}(\Gamma). \quad (4.24)$$

Definition 14 The parametric space $\mathcal{E}_h^{p-1}(\Gamma)$ is spanned by two sets of basis vector fields. With the notations from the Definitions 12 and 13, the basis vector fields are defined as follows

$$\phi_{k,0}^{II,i} \Big|_{\Gamma_j} = \begin{cases} \varphi_k^{i_{loc}} \in \mathcal{E}^{p-1}(\Gamma_j), & j \in \{i_1, i_2\}, \\ \mathbf{0}, & j \notin \{i_1, i_2\}, \end{cases} \quad 1 \leq i \leq N_{II}, \quad (4.25)$$

$$\phi_{k,l}^{III,i} \Big|_{\Gamma_j} = \begin{cases} \varphi_k^{3+l} \in \mathcal{E}^{p-1}(\Gamma_i), & j = i, \\ \mathbf{0}, & j \neq i, \end{cases} \quad 1 \leq i \leq N. \quad (4.26)$$

Here, the index k refers to the order of the basis function and the additional index l refers to the l th basis function of order k . The range of the indices l and k are listed in Table 4.3. The basis vector fields which belong to the element interiors have a vanishing tangential component on the edges and, therefore, any linear combination

$$\mathbf{v} = \sum_{i=1}^{N_{III}} \sum_{k,l} \alpha_{k,l}^{III,i} \phi_{k,l}^{III,i}, \quad \alpha_{k,l}^{III,i} \in \mathbb{C},$$

is called vector-valued bubble function.

The continuity of the basis vector fields can be assessed by considering a decomposition with respect to the bidual basis vector fields. The support of any basis vector field comprises maximal two elements Γ_i and Γ_j . Without restriction of any kind, we can assume that (2.97)-(2.99) hold since Γ is at least Lipschitz continuous. Thus, for an arbitrary basis vector field ϕ , (2.100) is fulfilled and, therefore,

$$\mathcal{E}_h^{p-1}(\Gamma) \subset \mathbf{H}_R^{\frac{1}{2}}(\Gamma). \quad (4.27)$$

From (4.15), we can even conclude that the scalar-valued projection $\phi_R = \phi \cdot \mathbf{a}_1$ is strongly continuous on $\text{supp}\phi = \Gamma_i \cup \Gamma_j$ as the parallel projections of the polynomial master element functions coincide on the common edge e_{ij} due to the definition of $\mathcal{P}^{p-1}(\hat{T})$.

Definition 15 The parametric space $\mathcal{Q}_h^{p-2}(\Gamma)$ is spanned by functions of the form

$$\nu_{k,l}^{III,i} \Big|_{\Gamma_j} = \begin{cases} v_k^l \in \mathcal{Q}^{p-2}(\Gamma_i), & j = i, \\ 0, & j \neq i. \end{cases} \quad 1 \leq i \leq N. \quad (4.28)$$

The range of the indices l and k are listed in Table 4.3.

The lowest order basis functions of $\mathcal{Q}_h^{p-2}(\Gamma)$ are the piecewise constant functions. All others basis functions are middle node shape functions which vanish on the edges and at the vertices. Thus, it holds

$$\mathcal{Q}_h^{p-2}(\Gamma) \subset L^2(\Gamma) \subset H^{-\frac{1}{2}}(\Gamma). \quad (4.29)$$

Note that by the indices given in the Definitions 13-15, each basis function is uniquely defined by four indices $\{*, i, k, l\}$. The index $*$ stands for I , II or III and it specifies one of the sets S_I , S_{II} or S_{III} . The index i refers to the global node number in the actual ordered set S_* . The index k is the order and the index l is used to distinguish basis functions of the same order when necessary. An ordered list of the basis functions of a parametric space gives rise to an isomorphism

$$\{*, i, k, l\} \mapsto l_{\text{glob}} \quad (4.30)$$

Whenever there is no need to write the four indices $\{*, i, k, l\}$, the simple index l_{glob} is used.

Finally, the restriction of a basis function to a support element corresponds to a specific element shape function. This means that when the support element is determined, Γ_i for instance, there exists a unique relation

$$l_{\text{glob}} \mapsto (i, l_{\text{loc}}) \quad (4.31)$$

between the global basis function with global number l_{glob} and the element shape function with local number l_{loc} in the ordered set of element shape functions with domain Γ_i .

4.2.4. Projection Based Interpolation

The parametric spaces introduced in Subsection 4.2.3 are finite-dimensional subspaces of the infinite-dimensional trace spaces defined in Section 2.5. To estimate their approximation properties, we need to say first how to determine the approximant. This is achieved by applying the projection-based interpolation operators Π^1 , Π^c and Π^0 . The projection-based interpolation operators involve operations as point evaluation or integration on edges and, thus, they are defined on spaces of more regular functions as introduced by (2.112)-(2.114).

The basic assumptions behind the construction of Π^1 , Π^c and Π^0 are locality, optimality and global continuity [26,27]. Locality means that the projection-based interpolation can be performed element-wise. Optimality means that the error between the approximant and the exact function should be minimized with respect to an appropriate norm. This step requires the solution of a linear system of equations because the minimization of an energy functional is equivalent to a variational problem. Finally, the interpolant must preserve global properties depicted in (4.24), (4.27) and (4.29).

The projection-based interpolation operators build the most fundamental block to set-up a high order boundary element implementation. The focus of the following presentation are not theoretical details but the goal is to state the formulae which are finally implemented. For a more comprehensive derivation and, especially, a more detailed explanation of the steps of simplification we refer to [27].

Let $s \geq 1$. The operator

$$\Pi^1: H_{pw}^s(\Gamma) \rightarrow \mathcal{H}_h^p(\Gamma) \quad (4.32)$$

Π^1 is defined on continuous functions. The construction proposed in [27] determines the interpolant

$\Pi^1(u) \in \mathcal{H}_h^p(\Gamma)$ in maximal three steps

$$\Pi^1(u)(\mathbf{x}) = \underbrace{\sum_{i=1}^{N_I} \alpha_{1,0}^{I,i} \phi_{1,0}^{I,i}(\mathbf{x})}_{= u^I(\mathbf{x})} + \underbrace{\sum_{i=1}^{N_{II}} \sum_{k=2}^{p_{e_i}} \alpha_{k,0}^{II,i} \phi_{k,0}^{II,i}(\mathbf{x})}_{= u^{II}(\mathbf{x})} + \underbrace{\sum_{i=1}^N \sum_{k=3}^{p_{\Gamma_i}} \sum_{l=1}^{k-2} \alpha_{k,l}^{III,i} \phi_{k,l}^{III,i}(\mathbf{x})}_{= u^{III}(\mathbf{x})}. \quad (4.33)$$

The first step returns u^I , which is the interpolation of the values at the vertices $\mathbf{v}_i \in S_I$, namely,

$$\alpha_{1,0}^{I,i} = u(\mathbf{v}_i).$$

Thus, u^I is a globally continuous function and it is of order $p = 1$. Moreover, u^I is exact at all vertices and, this means, that all remaining steps should not change this interpolation property. This is certainly assured if u^{II} is an edge bubble function and u^{III} is a bubble function. Thus, the goal of the second step is to find an edge bubble function u^{II} such that the remaining error ($u^I + u^{II} - u$) is minimal with respect to an appropriate edge norm. The norm which is used for practical computations is the first order Sobolev norm weighted with an additional geometrical factor. It is defined locally on each edge $e_i \in S_{II}$ by

$$\|v\|_{e_i}^2 = \int_{e_i} \left| \frac{dv}{dl} \right|^2 \underbrace{\left(\frac{dl}{dt} \right)}_{\text{weight}} dl = \int_0^1 \left| \frac{d\hat{v}}{dt} \right|^2 dt.$$

Here, \hat{v} coincides with $v|_{e_i}$ in parameter coordinates, i.e., on the reference interval $(0,1)$ and e_i is parametrized by $t \in (0,1)$. The minimization problem is formulated in terms of the quadratic functionals

$$J^{II,i}(v) = \frac{1}{2} \int_{e_i} \left| \frac{dv}{dl} \right|^2 \frac{dl}{dt} dl,$$

where v denotes an arbitrary edge bubble function. Thus, find u^{II} such that for all $e_i \in S_{II}$, it holds

$$J^{II,i}(u^I + u^{II} - u) = \min_v J^{II,i}(v),$$

where the minimization takes place over all edge bubble functions v . Each local minimization problem is equivalent to a variational problem on each edge $e_i \in S_{II}$: find u^{II} such that on each $e_i \in S_{II}$ for all $\phi_{k,0}^{II,i}$ it holds [27]

$$2 \leq k \leq p_{e_i} : \int_{e_i} \frac{du^{II}}{dl} \frac{d\phi_{k,0}^{II,i}}{dl} \frac{dl}{dt} dl = \int_{e_i} \frac{d(u - u^I)}{dl} \frac{d\phi_{k,0}^{II,i}}{dl} \frac{dl}{dt} dl. \quad (4.34)$$

To explain the third step, we introduce on each element $\Gamma_i \in S_{III}$ the quadratic functional

$$J^{III,i}(v) = \frac{1}{2} \int_{\Gamma_i} |\nabla_{\Gamma} v|^2 d\sigma,$$

where v denotes an arbitrary bubble function. To obtain the best approximation, a bubble function u^{III} shall be found such that for all $\Gamma_i \in S_{III}$, it holds

$$J^{III,i}(\Pi^1(u) - u) = \min_v J^{III,i}(v)$$

for all bubble functions v . These local minimization problems for u^{III} are equivalent to the following set of linear equations on each $\Gamma_i \in S_{III}$

$$3 \leq k \leq p_{\Gamma_i}, 1 \leq l \leq k-2 : \quad \int_{\Gamma_i} \nabla_{\Gamma} u^{III} \cdot \nabla_{\Gamma} \phi_{k,l}^{III,i} d\sigma = \int_{\Gamma_i} \nabla_{\Gamma} (u - u^I - u^{II}) \cdot \nabla_{\Gamma} \phi_{k,l}^{III,i} d\sigma.$$

Thus, the residuum that remains after the second step is minimized with respect to all $H_0^1(\Gamma_i)$ semi-norms [27].

The projection-based interpolant $\Pi^1(u)$ is at least globally continuous.

When the mesh Γ consists only of plane elements, it is called linear. As shown in [27], the projection-based interpolation operator Π^1 reproduces polynomials on linear meshes, i.e.,

$$\forall q \in \mathcal{P}^p(\Gamma) : \quad \Pi^1(q)(\mathbf{x}) - q(\mathbf{x}) = 0.$$

This is used to prove the following approximation property as it is done in [26, 52], for instance.

Theorem 4.2.2 *Let Γ be given by a regular hp -mesh consisting of isoparametric elements of uniform order $p \geq 2$. Let $u \in H_{pw}^s(\Gamma)$ for $1 \leq s \leq p+1$, then, it holds*

$$\|u - \Pi^1(u)\|_{H^1(\Gamma)} \leq Ch^{\min(s,p+1)} \|u\|_{H_{pw}^s(\Gamma)}. \quad (4.35)$$

The constant C depends on the order of approximation p , on the derivatives of the local parametrizations $\tilde{\mathbf{X}}_i$ up to order p and on the uniformity of the mesh size h .

Let $s \geq 1$, the projection-based interpolation operator

$$\Pi^c : \mathbf{H}^s(\text{curl}_{\Gamma}, \Gamma) \rightarrow \mathcal{E}_h^{p-1}(\Gamma), \quad (4.36)$$

is obtained by a three-step algorithm [27], i.e.,

$$\Pi^c(\mathbf{u})(\mathbf{x}) = \underbrace{\sum_{i=1}^{N_{II}} \alpha_{0,0}^{II,i} \phi_{0,0}^{II,i}(\mathbf{x})}_{=\mathbf{u}^I(\mathbf{x})} + \underbrace{\sum_{i=1}^{N_{II}} \sum_{k=1}^{p_{e_i}-1} \alpha_{k,0}^{II,i} \phi_{k,0}^{II,i}(\mathbf{x})}_{=\mathbf{u}^{II}(\mathbf{x})} + \underbrace{\sum_{i=1}^N \sum_{k=2}^{p_{\Gamma_i}-1} \sum_{l=1}^{2(k-1)+1} \alpha_{k,l}^{III,i} \phi_{k,l}^{III,i}(\mathbf{x})}_{=\mathbf{u}^{III}(\mathbf{x})}. \quad (4.37)$$

As for Π^1 , the first step is an interpolation. The lowest order basis vector fields, $\phi_{0,0}^{II,i}$, are called Nédélec functions. Within the basis of $\mathcal{E}_h^{p-1}(\Gamma)$, they play a peculiar role. The coefficients for the Nédélec functions are

$$\alpha_{0,0}^{II,i} = \int_{e_i} \mathbf{u} \cdot \boldsymbol{\tau}_i dl.$$

The second contribution, u^{II} , is such that the quadratic functional

$$J^{II,i}(\mathbf{v} \cdot \boldsymbol{\tau}_i) = \frac{1}{2} \int_{e_i} |\mathbf{v} \cdot \boldsymbol{\tau}_i|^2 \frac{dl}{dt} dl$$

is minimized over all vector-valued edge bubble functions \mathbf{v} . This leads to the local sets of linear

equations which determine \mathbf{u}^{II}

$$1 \leq k \leq p_{e_i} - 1 : \quad \int_{e_i} (\mathbf{u}^{II} \cdot \boldsymbol{\tau}_i) (\boldsymbol{\phi}_{k,0}^{II,i} \cdot \boldsymbol{\tau}_i) \frac{dl}{dt} dl = \int_{e_i} ((\mathbf{u} - \mathbf{u}^I) \cdot \boldsymbol{\tau}_i) (\boldsymbol{\phi}_{k,0}^{II,i} \cdot \boldsymbol{\tau}_i) \frac{dl}{dt} dl.$$

Thus, by the second step the error of the residuum is minimized locally with respect to the edge vector bubble functions and with respect to the edge norm

$$\|\mathbf{v}\|_{e_i}^2 = \int_{e_i} |\mathbf{v} \cdot \boldsymbol{\tau}_i|^2 \frac{dl}{dt} dl.$$

Once the interpolant over the element boundary is determined, locality and optimality again implies that a projection on the vector-valued bubble functions should be used to determine the optimal \mathbf{u}^{III} . The choice of the local functionals follows from the energy norm of the space $\mathbf{H}(\text{curl}_\Gamma, \Gamma_i)$ and it reads for each $\Gamma_i \in S_{III}$

$$J^{III,i}(\mathbf{v}) = \frac{1}{2} \left(\|\mathbf{v}\|_{\mathbf{L}^2(\Gamma_i)}^2 + \|\text{curl}_\Gamma(\mathbf{v})\|_{\mathbf{L}^2(\Gamma_i)}^2 \right),$$

where \mathbf{v} is an arbitrary vector-valued bubble function. Again, the vector-valued bubble function \mathbf{u}^{III} is computed such that for all $\Gamma_i \in S_{III}$, it holds

$$J^{III,i}(\Pi^c(\mathbf{u}) - \mathbf{u}) = \min_{\mathbf{v}} J^{III,i}(\mathbf{v}).$$

This minimization problem is equivalent to local variational formulations: find \mathbf{u}^{III} such that on all elements $\Gamma_i \in S_{III}$ and for all $\boldsymbol{\phi}_{k,l}^{III,i}$ it holds

$$\begin{aligned} & \int_{\Gamma_i} \left(\text{curl}_\Gamma \mathbf{u}^{III} \text{curl}_\Gamma \boldsymbol{\phi}_{k,l}^{III,i} + \mathbf{u}^{III} \cdot \boldsymbol{\phi}_{k,l}^{III,i} \right) d\sigma \\ &= \int_{\Gamma_i} \left(\text{curl}_\Gamma (\mathbf{u} - \mathbf{u}^I - \mathbf{u}^{II}) \text{curl}_\Gamma \boldsymbol{\phi}_{k,l}^{III,i} + (\mathbf{u} - \mathbf{u}^I - \mathbf{u}^{II}) \cdot \boldsymbol{\phi}_{k,l}^{III,i} \right) d\sigma. \end{aligned} \quad (4.38)$$

The exact sequence property implies that the vector bubbles contain gradients of scalar bubbles. This implies that the following compatibility equation is automatically satisfied

$$\int_{\Gamma_i} (\Pi^c(\mathbf{u}) - \mathbf{u}) \cdot \nabla_\Gamma \boldsymbol{\phi}_{k+1,l}^{III,i} d\sigma = 0.$$

Reimposing the compatibility condition in the original system at the expense of a Lagrange multiplier p , we obtain

$$\begin{aligned} \int_{\Gamma_i} \left(\text{curl}_\Gamma (\Pi^c(\mathbf{u}) - \mathbf{u}) \text{curl}_\Gamma \boldsymbol{\phi}_{k,l}^{III,i} + (\Pi^c(\mathbf{u}) - \mathbf{u}) \cdot \boldsymbol{\phi}_{k,l}^{III,i} \right) d\sigma + \int_{\Gamma_i} \nabla_\Gamma p \cdot \boldsymbol{\phi}_{k,l}^{III,i} d\sigma &= 0, \\ \int_{\Gamma_i} (\Pi^c(\mathbf{u}) - \mathbf{u}) \cdot \nabla_\Gamma \boldsymbol{\phi}_{k+1,l}^{III,i} d\sigma &= 0. \end{aligned}$$

In order to obtain commutativity of the projection-based interpolation on the master element, namely, $\Pi^c(\nabla_\Gamma \hat{\varphi}) = \nabla_\Gamma \Pi^1(\hat{\varphi})$, it is necessary to relax the first variational formulation. Therefore, the contributions are written now separately and the element shape functions in parameter

coordinates are inserted. According to Definition 10, it holds

$$\begin{aligned}
 \int_{\Gamma_i} \operatorname{curl}_{\Gamma} \mathbf{u} \operatorname{curl}_{\Gamma} \phi_{k,l}^{III,i} \, d\sigma &= \int_{\hat{T}} \operatorname{curl}_{\Gamma} \hat{\mathbf{u}} \operatorname{curl}_{\Gamma} \hat{\varphi}_k^{3+l} J_i \, d\xi \\
 &= \int_{\hat{T}} \left(\frac{\partial \hat{u}_2}{\partial \xi_1} - \frac{\partial \hat{u}_1}{\partial \xi_2} \right) \mathbf{a}^{i,12} \left(\frac{\partial \hat{\varphi}_{k,2}^{3+l}}{\partial \xi_1} - \frac{\partial \hat{\varphi}_{k,1}^{3+l}}{\partial \xi_2} \right) \mathbf{a}^{i,12} J_i \, d\xi, \\
 \int_{\Gamma_i} \mathbf{u} \cdot \phi_{k,l}^{III,i} \, d\sigma &= \int_{\hat{T}} (\hat{u}_1 \mathbf{a}^{i,1} + \hat{u}_2 \mathbf{a}^{i,2}) \cdot (\hat{\varphi}_{k,1}^{3+l} \mathbf{a}^{i,1} + \hat{\varphi}_{k,2}^{3+l} \mathbf{a}^{i,2}) J_i \, d\xi, \\
 \int_{\Gamma_i} \nabla_{\Gamma} p \cdot \phi_{k,l}^{III,i} \, d\sigma &= \int_{\hat{T}} \left(\frac{\partial \hat{p}}{\partial \xi_1} \mathbf{a}^{i,1} + \frac{\partial \hat{p}}{\partial \xi_2} \mathbf{a}^{i,2} \right) \cdot (\hat{\varphi}_{k,1}^{3+l} \mathbf{a}^{i,1} + \hat{\varphi}_{k,2}^{3+l} \mathbf{a}^{i,2}) J_i \, d\xi.
 \end{aligned}$$

It is shown in [27] that the skipping of the second term is reasonable by an asymptotic consideration $J_i \rightarrow 0$. This simplification, moreover, enables $\Pi^c(\nabla_{\Gamma} \hat{\varphi}) = \nabla_{\Gamma} \Pi^1(\hat{\varphi})$ on \hat{T} . The variational formulation (4.38) is finally replaced by a two-step projection on every element $\Gamma_i \in S_{III}$, i.e., \mathbf{u}^{III} is such that on every $\Gamma_i \in S_{III}$ it holds

$$2 \leq k \leq p_{\Gamma_i} - 1, \quad 1 \leq l \leq 2(k-2) + 1 :$$

$$\int_{\Gamma_i} \operatorname{curl}_{\Gamma} \mathbf{u}^{III} \operatorname{curl}_{\Gamma} \phi_{k,l}^{III,i} \, d\sigma + \int_{\Gamma_i} \nabla_{\Gamma} p \cdot \phi_{k,l}^{III,i} \, d\sigma = \int_{\Gamma_i} \operatorname{curl}_{\Gamma} (\mathbf{u} - \mathbf{u}^{II} - \mathbf{u}^I) \operatorname{curl}_{\Gamma} \phi_{k,l}^{III,i} \, d\sigma,$$

$$3 \leq k \leq p_{\Gamma_i}, \quad 1 \leq l \leq k-2 :$$

$$\int_{\Gamma_i} \mathbf{u}^{III} \cdot \nabla_{\Gamma} \phi_{k,l}^{III,i} \, d\sigma = \int_{\Gamma_i} (\mathbf{u} - \mathbf{u}^{II} - \mathbf{u}^I) \cdot \nabla_{\Gamma} \phi_{k,l}^{III,i} \, d\sigma.$$

The continuity of the approximant $\Pi^c(\mathbf{u})$ corresponds to the continuity of the basis functions it is built of. Thus, $\Pi^c(\mathbf{u})$ is a tangential vector field with a globally continuous component parallel to each edge $e_i \in S_{II}$.

It is proved in [27] that Π^c reproduces tangential polynomial vector fields on linear meshes, i.e.,

$$\forall \mathbf{q} \in \mathcal{P}^{p-1}(\Gamma) : \quad \Pi^c(\gamma_R \mathbf{q})(\mathbf{x}) - \gamma_R \mathbf{q}(\mathbf{x}) = 0.$$

This is used to proof the approximation properties as stated in Theorem 4.2.3 on linear meshes [55], see also [6, 16].

Theorem 4.2.3 *Let Γ be given by a linear mesh. Consider $\mathcal{E}^{p-1}(\Gamma)$ with uniform order $p-1 \geq 1$. The projection-based interpolation operator Π^c fulfills for $\mathbf{u} \in \mathbf{H}^s(\operatorname{curl}_{\Gamma}, \Gamma)$*

$$\|\mathbf{u} - \Pi^c(\mathbf{u})\|_{H^{-\frac{1}{2}}(\operatorname{curl}_{\Gamma}, \Gamma)} \leq Ch^{\min(p-1, s)} \|\mathbf{u}\|_{\mathbf{H}^{s-\frac{1}{2}}(\operatorname{curl}_{\Gamma}, \Gamma)}. \quad (4.39)$$

Let $s \geq 0$. The third operator

$$\Pi^0 : H_{pw}^s(\Gamma) \rightarrow \mathcal{Q}_h^{p-2}(\Gamma) \quad (4.40)$$

returns in one step the approximant

$$\Pi^0(u)(\mathbf{x}) = \sum_{i=1}^N \sum_{k=0}^{p_{\Gamma_i}-2} \sum_{l=1}^{p_{\Gamma_i}-1} \alpha_{k,l}^{III,i} \nu_{k,l}^{III,i}(\mathbf{x}) = u^{III}(\mathbf{x}). \quad (4.41)$$

For all $\Gamma_i \in S_{III}$, the following set of linear equations

$$0 \leq k \leq p_{\Gamma_i} - 2, 1 \leq l \leq p_{\Gamma_i} - 1 : \quad \int_{\Gamma_i} u^{III} \nu_{k,l}^{III,i} d\sigma = \int_{\Gamma_i} u \nu_{k,l}^{III,i} d\sigma$$

is solved to determine the $L^2(\Gamma)$ projection u^{III} . As the lowest order basis functions are globally discontinuous, the approximant $\Pi^0(u) \in \mathcal{Q}_h^{p-2}(\Gamma)$ is also discontinuous.

The proof of the following theorem can be found in [52], for instance.

Theorem 4.2.4 *Let Γ be given by a regular hp -mesh consisting of isoparametric elements of uniform order $p \geq 2$, this means that the space $\mathcal{Q}^{p-2}(\Gamma)$ is spanned by the piecewise constant functions for $p = 2$. The projection-based interpolation operator Π^0 fulfills for $u \in H_{pw}^s(\Gamma)$*

$$\|u - \Pi^0(u)\|_{L^2(\Gamma)} \leq Ch^{\min(p-1,s)} \|u\|_{H_{pw}^s(\Gamma)}. \quad (4.42)$$

The constant C depends on the order of approximation p , on the derivatives of the local parametrizations $\hat{\mathbf{X}}_i$ up to order p and on the uniformity of the mesh size h .

The following diagram may serve to summarize the contents of this subsection. We have given explicit formulae for the projection-based interpolation operators which connect the infinite-dimensional trace spaces with the finite-dimensional parametric spaces. For $s \geq 1$, we have

$$\begin{array}{ccccc} H_{pw}^s(\Gamma) & \xrightarrow{\nabla_\Gamma} & \mathbf{H}^s(\text{curl}_\Gamma, \Gamma) & \xrightarrow{\text{curl}_\Gamma} & H_{pw}^{s-1}(\Gamma) \\ H_{pw}^s(\Gamma) & & \mathbf{H}^s(\text{curl}_\Gamma, \Gamma) & & H_{pw}^{s-1}(\Gamma) \\ \Pi^1 \downarrow & & \Pi^c \downarrow & & \Pi^0 \downarrow \\ \mathcal{H}_h^p(\Gamma) & \xrightarrow{\nabla_\Gamma} & \mathcal{E}_h^{p-1}(\Gamma) & \xrightarrow{\text{curl}_\Gamma} & \mathcal{Q}_h^{p-2}(\Gamma). \end{array} \quad (4.43)$$

The differential operators on the second row are skipped to emphasize that the diagram does not commute on curved surfaces.

4.2.5. The Bidual Spaces

Given a basis $\{\varphi_{l_{\text{glob}}}^{l_{\text{glob}}}\}_{l_{\text{glob}}=1}^{N_\mathcal{E}}$ of the parametric space $\mathcal{E}_h^{p-1}(\Gamma)$, the so-called bidual space $\mathcal{V}_h^{p-1}(\Gamma)$ is defined as linear hull of basis functions $\varphi_{l_{\text{glob}}}$ given in terms of $\varphi_{l_{\text{glob}}}^{l_{\text{glob}}}$ according to

$$\varphi_{l_{\text{glob}}} = \mathbf{n} \times \varphi_{l_{\text{glob}}}^{l_{\text{glob}}}, \quad l_{\text{glob}} = 1, \dots, N_\mathcal{V} = N_\mathcal{E}. \quad (4.44)$$

Then, the following diagram commutes

$$\begin{array}{ccccc} \mathcal{H}_h^p(\Gamma) & \xrightarrow{\nabla_\Gamma} & \mathcal{E}_h^{p-1}(\Gamma) & \xrightarrow{\text{curl}_\Gamma} & \mathcal{Q}_h^{p-2}(\Gamma) \\ \downarrow 1 & & \downarrow \mathbf{n} \times & & \downarrow 1 \\ \mathcal{H}_h^p(\Gamma) & \xrightarrow{\text{curl}_\Gamma} & \mathcal{V}_h^{p-1}(\Gamma) & \xrightarrow{\text{div}_\Gamma} & \mathcal{Q}_h^{p-2}(\Gamma). \end{array} \quad (4.45)$$

The projection-based interpolation operator Π^d for the parametric space $\mathcal{V}_h^{p-1}(\Gamma)$ is also defined in terms of Π^c , namely,

$$\Pi^d: \mathbf{H}^s(\text{div}_\Gamma, \Gamma) \rightarrow \mathcal{V}_h^{p-1}(\Gamma), \quad \Pi^d(\mathbf{u}) = \mathbf{n} \times \Pi^c(\mathbf{u}) \quad (4.46)$$

and we obtain

$$\begin{array}{ccccc}
 H_{pw}^s(\Gamma) & \xrightarrow{\text{curl}_\Gamma} & \mathbf{H}^s(\text{div}_\Gamma, \Gamma) & \xrightarrow{\text{div}_\Gamma} & H_{pw}^s(\Gamma) \\
 H_{pw}^s(\Gamma) & & \mathbf{H}^s(\text{div}_\Gamma, \Gamma) & & H_{pw}^s(\Gamma) \\
 \Pi^1 \downarrow & & \Pi^d \downarrow & & \Pi^0 \downarrow \\
 \mathcal{H}_h^p(\Gamma) & \xrightarrow{\text{curl}_\Gamma} & \mathbf{V}_h^{p-1}(\Gamma) & \xrightarrow{\text{div}_\Gamma} & \mathcal{Q}_h^{p-2}(\Gamma).
 \end{array} \tag{4.47}$$

Recall the fundamental observations we read off the commuting diagram (2.111) describing the infinite-dimensional trace spaces. Exactly the same conclusions are to draw from (4.45).

1. There is a (horizontal) relation between the parametric spaces established by the locally exact sequences.
2. There is a (diagonal) relation between the trace spaces established by the fact that the rows are in duality to each other. This means especially that $\mathcal{Q}_h^{p-2}(\Gamma)$ is the dual of $\mathcal{H}_h^p(\Gamma)$ and $\mathbf{V}_h^{p-1}(\Gamma)$ is the dual of $\mathcal{E}_h^{p-1}(\Gamma)$ or vice versa.
3. There is a (vertical) relation between the parametric spaces established by isomorphisms, i.e., the identity mapping 1 and the isomorphism $\mathbf{n} \times$.

The key point here is that the (vertical) isomorphisms are in line with the concept of the biduality: starting with a fixed set of bases for the spaces in the upper row, we apply the isomorphisms and obtain basis functions of the spaces in the lower row which are automatically given in terms of the bidual vector fields being appropriate for a (diagonal) pairing with respect to the inner products of the pivot spaces $L^2(\Gamma)$ and $\mathbf{L}_t^2(\Gamma)$, respectively.

Consider, for instance, an arbitrary basis function with support Γ_i such that

$$\begin{aligned}
 \mathcal{H}_h^p(\Gamma) : \quad \phi_{l_{\text{glob}}} |_{\Gamma_i} &= \varphi^{i, l_{\text{loc}}} = \hat{\varphi}_{l_{\text{loc}}}, \\
 \mathcal{E}_h^{p-1}(\Gamma) : \quad \phi_{l_{\text{glob}}}^{l_{\text{loc}}} |_{\Gamma_i} &= \varphi^{i, l_{\text{loc}}} = \hat{\varphi}_{l_{\text{loc},1}} \mathbf{a}^{i,1} + \hat{\varphi}_{l_{\text{loc},2}} \mathbf{a}^{i,2}, \\
 \mathcal{Q}_h^{p-2}(\Gamma) : \quad \nu_{l_{\text{glob}}} |_{\Gamma_i} &= \nu^{i, l_{\text{loc}}} = \hat{\nu}_{l_{\text{loc}}} \mathbf{a}^{i,12}.
 \end{aligned}$$

In the following, we simply write l instead of l_{loc} . The element shape function is given in terms of master element shape functions due to Definition 10. The corresponding element shape functions of the bidual spaces in the lower row of (4.45) are defined by the isomorphism 1 and $\mathbf{n} \times$

$$\begin{array}{ccccc}
 \hat{\varphi}_l & \xrightarrow{\nabla_\Gamma} & \hat{\varphi}_{l,1} \mathbf{a}^{i,1} + \hat{\varphi}_{l,2} \mathbf{a}^{i,2} & \xrightarrow{\text{curl}_\Gamma} & \hat{\nu}_l \mathbf{a}^{i,12} \\
 \downarrow 1 & & \downarrow \mathbf{n} \times & & \downarrow 1 \\
 J_i^{-1} \hat{\varphi}_l \mathbf{a}_{i,12} & \xrightarrow{\text{curl}_\Gamma} & J_i^{-1} (\hat{\varphi}_{l,2} \mathbf{a}_{i,1} - \hat{\varphi}_{l,1} \mathbf{a}_{i,2}) & \xrightarrow{\text{div}_\Gamma} & J_i^{-1} \hat{\nu}_l.
 \end{array} \tag{4.48}$$

Now, the circle is closed as (4.48) corresponds to the commuting diagram (2.34) describing the smooth case. The only non-trivial isomorphism concerns $\mathbf{V}_h^{p-1}(\Gamma)$ and it is reasonable to write the formulae again, i.e.,

$$\mathbf{V}_h^{p-1}(\Gamma) : \quad \phi_{l_{\text{glob}}} |_{\Gamma_i} = \varphi_{i,l} = J_i^{-1} (\hat{\varphi}_{l,2} \mathbf{a}_{i,1} - \hat{\varphi}_{l,1} \mathbf{a}_{i,2}) \in \mathbf{V}^{p-1}(\Gamma_i). \tag{4.49}$$

with

$$\text{div}_\Gamma \varphi_{i,l} = \frac{1}{J_i} \left(\frac{\partial \hat{\varphi}_{l,2}}{\partial \xi_1} - \frac{\partial \hat{\varphi}_{l,1}}{\partial \xi_2} \right) = \text{curl}_\Gamma \varphi^{i,l} = \frac{1}{J_i} \hat{\nu}_l = \nu_{i,l} \in \mathcal{Q}^{p-2}(\Gamma_i). \tag{4.50}$$

4.3. Conclusion

A high order boundary element implementation which can be used to solve elliptic as well as Maxwell problems relies on the appropriate construction of finite-dimensional test and trial spaces. A possible construction has been explained in detail in this chapter. The basic concepts are inspired by the high order finite element methods. Most fundamental for a systematic construction of the so-called parametric spaces are two construction principles: the exact sequence property and the hierarchy of the basis functions.

A boundary element implementation has to account for two-dimensional, closed surfaces embedded in \mathbb{R}^3 . This is a challenge because the manifolds which are considered may be curved and, consequently, a high order, non-linear approximation of the geometry should be employed. The formulae derived in this chapter are of enormous importance because they stay valid for arbitrary non-linear parametrizations of the boundary.

An open question and subject of future research is to prove the asymptotic approximation properties of the parametric space $\mathcal{E}_h^{p-1}(\Gamma)$ when the manifold Γ is given by isoparametric elements of high polynomial order.

Another topic of future research is concerned with the projection-based interpolation operators. The operators as they are defined right now yield a discretization procedure which lacks consistency as the diagrams (4.43) and (4.47), respectively, do not commute in general. An idea to solve this problem is to formulate the projection-based interpolation operators in terms of bidual bases. Commutativity might be restored as due to the biduality of the basis functions, the metric cancels out.

HIGH ORDER BEM FOR PEC

5.1. Introduction

In this chapter, the high order boundary element methods are analyzed. The starting point to apply a boundary element method is a uniquely solvable variational formulation of a boundary integral equation. The relevant functional setting is dictated by the infinite-dimensional trace spaces defined in Section 2.5, i.e.,

$$H^{\frac{1}{2}}(\Gamma), \quad H^{-\frac{1}{2}}(\text{curl}_{\Gamma}, \Gamma), \quad H^{-\frac{1}{2}}(\text{div}_{\Gamma}, \Gamma), \quad H^{-\frac{1}{2}}(\Gamma).$$

We assume that Γ is exactly described by a discrete mesh

$$\Gamma = \bigcup_{k=1}^N \overline{\Gamma_k}.$$

This assumption allows for the definition of the parametric spaces

$$\mathcal{H}_h^p(\Gamma), \quad \mathcal{E}_h^{p-1}(\Gamma), \quad \mathcal{V}_h^{p-1}(\Gamma), \quad \mathcal{Q}_h^{p-2}(\Gamma).$$

They serve as finite-dimensional approximations of the above trace spaces according to the results of Subsection 4.2.3. Besides the parametric spaces, the projection-based interpolation operators

$$\Pi^1, \quad \Pi^c, \quad \Pi^d, \quad \Pi^0$$

from the Subsections 4.2.4 and 4.2.5 are well defined.

Solving a boundary value problem by a boundary element method means a two-step procedure. First, the boundary integral equations must be solved to obtain boundary data and, then, this data is used to evaluate a representation formula for the solution of the boundary value problem.

In Chapter 3, the electromagnetic scattering from a perfectly conducting body Ω has been theoretically analyzed. Due to the results obtained in the Subsections 3.2.2 and 3.3.2, the electromagnetic scattering suits as a model problem to apply the high order boundary element methods. The question that comes now is if the numerical solution converges towards the exact solution. It is answered in Section 5.2 for the classical formulation and Section 5.3 is concerned with the stabilized formulation. The case $\kappa = 0$ is treated separately in Section 5.4. We end this chapter by explicit formulae to compute the matrix entries of the various linear operators appearing by discretization. This is done in Section 5.5. The principal ideas are summarized in Section 5.6.

5.2. The Classical Formulation

The unique solvability of the Galerkin formulations in the infinite-dimensional space $H^{-\frac{1}{2}}(\text{div}_{\Gamma}, \Gamma)$ is a necessary but not sufficient condition to prove that the discretized Galerkin formulations in

$\mathbf{V}_h^{p-1}(\Gamma)$ yield convergent numerical schemes. The numerical analysis is very involved because the unique solvability of the variational formulations is shown by the help of a Hodge decomposition. Discrete Hodge decompositions, however, are not conforming anymore and, to obtain convergence results, a more general theory must be applied. It turns out that three properties are necessary to guarantee optimal convergence of the Galerkin solution [11, 19], namely,

(A) There exists a stable direct splitting $H^{-\frac{1}{2}}(\operatorname{div}_\Gamma, \Gamma) = V(\Gamma) \oplus W(\Gamma)$ such that Theorem 3.2.10 holds.

(B) There exists a finite-dimensional space $\mathbf{V}_h^{p-1}(\Gamma)$ with corresponding decomposition

$$\mathbf{V}_h^p(\Gamma) = V_N(\Gamma) + W_N(\Gamma), \quad W_N \subset W(\Gamma), \quad N = N(p, h). \quad (5.1)$$

The discrete splitting is uniformly stable with respect to the typical mesh size h and the uniform polynomial degree p .

(C) The gap property holds, namely,

$$\sup_{\mathbf{v}_N \in V_N} \inf_{\mathbf{v} \in V} \frac{\|\mathbf{v} - \mathbf{v}_N\|_{H^{-\frac{1}{2}}(\operatorname{div}_\Gamma, \Gamma)}}{\|\mathbf{v}_N\|_{H^{-\frac{1}{2}}(\operatorname{div}_\Gamma, \Gamma)}} \leq C \sqrt{\frac{h}{p+1}}. \quad (5.2)$$

Provided (A)-(C) hold, it is shown in [19] that the boundary element method returns the best approximation of \mathbf{j}^t in $\mathbf{V}_h^{p-1}(\Gamma)$.

In a recent paper by Bespalov, Heuer and Hiptmair [6], it is proved for the case of linear meshes that the Hodge decomposition of $H^{-\frac{1}{2}}(\operatorname{div}_\Gamma, \Gamma)$ from Lemma 2.5.3 and the parametric space $\mathbf{V}_h^{p-1}(\Gamma)$ fulfill the conditions (A)-(C) and the discrete the Hodge decomposition (5.1) is generated by the projection-based interpolation operator Π^d defined in Subsection 4.2.5. Theorem 5.2.1 summarizes the fundamental result about the best approximation properties of the Galerkin solution.

Theorem 5.2.1 *Assume that $\kappa^2 > 0$ is not an interior eigenvalue of the **curl curl** operator and let \mathbf{j}^t denote the solution of (3.62). There exists $h_0 > 0$ and $C_0 > 0$ such that for the right hand side $\mathbf{m} \times \mathbf{n} \in H^{-\frac{1}{2}}(\operatorname{curl}_\Gamma, \Gamma)$ and for uniform order of approximation p satisfying $\sqrt{\frac{h}{p+1}} < C_0$, $h < h_0$, the boundary element discretization of (3.62) admits a unique solution $\mathbf{j}_{hp}^t \in \mathbf{V}_h^{p-1}(\Gamma)$. The Galerkin solution \mathbf{j}_{hp}^t converges quasi-optimally, i.e.,*

$$\|\mathbf{j}^t - \mathbf{j}_{hp}^t\|_{H^{-\frac{1}{2}}(\operatorname{div}_\Gamma, \Gamma)} \leq C \inf_{\mathbf{v} \in \mathbf{V}_h^{p-1}} \|\mathbf{j}^t - \mathbf{v}\|_{H^{-\frac{1}{2}}(\operatorname{div}_\Gamma, \Gamma)}.$$

Both constants C_0 and C may depend on the geometry Γ .

Provided $\mathbf{j}^t \in \mathbf{H}_{pw}^s(\operatorname{div}_\Gamma, \Gamma)$ for $s > 0$, the h -version of the high order boundary element scheme shows asymptotic rates of convergence due to Theorem 4.2.3.

Theorem 5.2.1 holds also for the direct formulation as only the right hand side is different. However, in the remaining part of this work, the indirect formulation

$$\langle \gamma_R \mathbf{S}_\kappa(\mathbf{j}^t), \boldsymbol{\phi} \rangle_{-\frac{1}{2}} - \frac{1}{\kappa^2} \langle \operatorname{div}_\Gamma \boldsymbol{\phi}, \gamma_0 \mathbf{S}_\kappa(\operatorname{div}_\Gamma(\mathbf{j}^t)) \rangle_{\frac{1}{2}} = \langle \mathbf{m} \times \mathbf{n}, \boldsymbol{\phi} \rangle_{-\frac{1}{2}} \quad (5.3)$$

is considered and we start to explain how to discretize (5.3). Let $\{\boldsymbol{\phi}_l\}_{l=1}^{N_V}$ denote the set of vector-valued basis functions spanning the parametric space $\mathbf{V}_h^{p-1}(\Gamma)$. As the Galerkin solution \mathbf{j}_{hp}^t lies

itself in $\mathbf{V}_h^{p-1}(\Gamma)$, there is a unique representation by a linear combination of the basis functions

$$\mathbf{j}_{hp}^t = \sum_{l=1}^{N_\nu} \alpha_l \phi_l, \quad \text{with } \boldsymbol{\alpha}_c = (\alpha_1, \dots, \alpha_{N_\nu})^\top \in \mathbb{C}^{N_\nu}. \quad (5.4)$$

We call (5.4) the ansatz for the Galerkin solution with unknown coefficient vector $\boldsymbol{\alpha}_c$. For an approximation of the Dirichlet data \mathbf{m} by $\mathbf{m}_{hp} \in \mathbf{V}_h^{p-1}(\Gamma)$, the projection-based interpolation operator Π^d is applied

$$\mathbf{m}_{hp} = \Pi^d(\mathbf{m}),$$

where

$$\mathbf{m}_{hp} = \sum_{l=1}^{N_\nu} \beta_l \phi_l, \quad \text{with } \boldsymbol{\beta} = (\beta_1, \dots, \beta_{N_\nu})^\top \in \mathbb{C}^{N_\nu}$$

with known coefficient vector $\boldsymbol{\beta}$.

These representations comprise only regular vector fields and thus, inserting them into (5.3) yields integrals over Γ with weakly singular kernels. Theorem 5.2.1 guarantees that there exists exactly one vector $\boldsymbol{\alpha}_c$ with

$$(\gamma_R \mathbf{S}_\kappa(\mathbf{j}_{hp}^t), \phi_l)_\Gamma - \frac{1}{\kappa^2} (\operatorname{div}_\Gamma \phi_l, \gamma_0 \mathbf{S}_\kappa(\operatorname{div}_\Gamma \mathbf{j}_{hp}^t))_\Gamma = (\mathbf{m}_{hp} \times \mathbf{n}, \phi_l)_\Gamma \quad (5.5)$$

for all $1 \leq l \leq N_\nu$. This set of linear equations is conveniently written in a matrix-vector form. The linear operators which are needed for this formulation are defined now.

Definition 16 Consider a regular hp -mesh for Γ . Let $\{\phi_l\}_{l=1}^{N_\nu}$ denote the vector-valued basis functions spanning the parametric space $\mathbf{V}_h^{p-1}(\Gamma)$.

1. The lk th entry of the matrix $\mathbf{M} \in \mathbb{C}^{N_\nu \times N_\nu}$ is defined by

$$(\mathbf{M})_{lk} = (\phi_k \times \mathbf{n}, \phi_l)_\Gamma = \int_\Gamma \phi_l(\mathbf{x}) \cdot (\phi_k(\mathbf{x}) \times \mathbf{n}(\mathbf{x})) \, d\sigma_x. \quad (5.6)$$

\mathbf{M} is called the mass matrix.

2. The lk th entry of the matrix $\mathbf{A}_\kappa \in \mathbb{C}^{N_\nu \times N_\nu}$ is defined by the following weakly singular double integral

$$(\mathbf{A}_\kappa)_{lk} = (\gamma_R \mathbf{S}_\kappa(\phi_k), \phi_l)_\Gamma = \int_\Gamma \int_\Gamma \phi_l(\mathbf{x}) \cdot (G_\kappa(\mathbf{x} - \mathbf{y}) \phi_k(\mathbf{y})) \, d\sigma_y \, d\sigma_x. \quad (5.7)$$

\mathbf{A}_κ is called the vectorial single layer potential matrix.

3. The lk th entry of the matrix $\tilde{\mathbf{V}}_\kappa \in \mathbb{C}^{N_\nu \times N_\nu}$ is defined by the following weakly singular double integral

$$(\tilde{\mathbf{V}}_\kappa)_{lk} = (\operatorname{div}_\Gamma \phi_l, \gamma_0 \mathbf{S}_\kappa(\operatorname{div}_\Gamma \phi_k))_\Gamma = \int_\Gamma \int_\Gamma \operatorname{div}_\Gamma \phi_l(\mathbf{x}) G_\kappa(\mathbf{x} - \mathbf{y}) \operatorname{div}_\Gamma \phi_k(\mathbf{y}) \, d\sigma_y \, d\sigma_x. \quad (5.8)$$

$\tilde{\mathbf{V}}_\kappa$ is called the scalar single layer potential matrix for the Maxwell system.

With this notation, (5.5) becomes

$$\left(\mathbf{A}_\kappa - \frac{1}{\kappa^2} \tilde{\mathbf{V}}_\kappa \right) \boldsymbol{\alpha}_c = \mathbf{M} \boldsymbol{\beta}. \quad (5.9)$$

The system matrix

$$\mathbf{A}_c = \mathbf{A}_\kappa - \frac{1}{\kappa^2} \tilde{\mathbf{V}}_\kappa \quad (5.10)$$

of the classical boundary element method is regular due to Theorem 5.2.1. However, the scalar single layer potential matrix for the Maxwell system, $\tilde{\mathbf{V}}_\kappa$, is never regular. The reason for this is the non-trivial null-space of the surface divergence. The null-space consists of vector fields of the following form

$$\boldsymbol{\phi} = \mathbf{curl}_\Gamma \phi \quad \text{with } \phi \in \mathcal{H}_h^p(\Gamma). \quad (5.11)$$

This means that the equation $\tilde{\mathbf{V}}_\kappa \tilde{\boldsymbol{\alpha}} = \mathbf{0}$ has always non-trivial solutions $\tilde{\boldsymbol{\alpha}}$ and

$$\text{rank}(\tilde{\mathbf{V}}_\kappa) < N_\mathcal{V}. \quad (5.12)$$

The impact of the singular matrix $\tilde{\mathbf{V}}_\kappa$ on the condition number of the system matrix is significant for small wave numbers. To see this, consider the scaled equation

$$\left(\kappa^2 \mathbf{A}_\kappa - \tilde{\mathbf{V}}_\kappa\right) \boldsymbol{\alpha}_c = \kappa^2 \mathbf{M} \boldsymbol{\beta}. \quad (5.13)$$

5.3. The Stabilized Formulation

As alternative to the classical formulation, the stabilized formulation has been developed in Subsection 3.3.2. It is given by a system of variational equations

$$\begin{cases} \langle \gamma_R \mathbf{S}_\kappa(\mathbf{j}^t), \boldsymbol{\phi} \rangle_{-\frac{1}{2}} + \langle \text{div}_\Gamma \boldsymbol{\phi}, \gamma_0 S_\kappa(\rho_\Gamma^t) \rangle_{\frac{1}{2}} = \langle \mathbf{m} \times \mathbf{n}, \boldsymbol{\phi} \rangle_{-\frac{1}{2}}, \\ \langle \nu, \gamma_0 S_\kappa(\text{div}_\Gamma \mathbf{j}^t) \rangle_{\frac{1}{2}} + \kappa^2 \langle \nu, \gamma_0 S_\kappa(\rho_\Gamma^t) \rangle_{\frac{1}{2}} = 0, \end{cases} \quad (5.14)$$

where, in addition to the Neumann data \mathbf{j}^t , the density ρ_Γ^t appears. To discretize the system (5.14), we need an ansatz for $\mathbf{j}_{hp}^t \in \mathcal{V}_h^{p-1}(\Gamma)$ and an ansatz for $\rho_{hp}^t \in \mathcal{Q}_h^{p-2}(\Gamma)$, namely,

$$\mathbf{j}_{hp}^t = \sum_{l=1}^{N_\mathcal{V}} \alpha_{1,l} \boldsymbol{\phi}_l, \quad \text{with } \boldsymbol{\alpha}_1 = (\alpha_{1,1}, \dots, \alpha_{1,N_\mathcal{V}})^\top \in \mathbb{C}^{N_\mathcal{V}}, \quad (5.15)$$

$$\rho_{hp}^t = \sum_{k=1}^{N_\mathcal{Q}} \alpha_{2,k} \nu_k, \quad \text{with } \boldsymbol{\alpha}_2 = (\alpha_{2,1}, \dots, \alpha_{2,N_\mathcal{Q}})^\top \in \mathbb{C}^{N_\mathcal{Q}}. \quad (5.16)$$

This means that $\boldsymbol{\alpha}_s = (\boldsymbol{\alpha}_1, \boldsymbol{\alpha}_2)^\top$ is searched such that

$$\begin{cases} \left(\gamma_R \mathbf{S}_\kappa(\mathbf{j}_{hp}^t), \boldsymbol{\phi}_l \right)_\Gamma + \left(\text{div}_\Gamma \boldsymbol{\phi}_l, \gamma_0 S_\kappa(\rho_{hp}^t) \right)_\Gamma = \left(\mathbf{m}_{hp} \times \mathbf{n}, \boldsymbol{\phi}_l \right)_\Gamma, \\ \left(\nu_k, \gamma_0 S_\kappa(\text{div}_\Gamma \mathbf{j}_{hp}^t) \right)_\Gamma + \kappa^2 \left(\nu_k, \gamma_0 S_\kappa(\rho_{hp}^t) \right)_\Gamma = 0, \end{cases} \quad (5.17)$$

for all $1 \leq l \leq N_\mathcal{V}$ and for all $1 \leq k \leq N_\mathcal{Q}$. Before we address the question if (5.17) is solvable and if the solution $\boldsymbol{\alpha}_s$ is unique, we introduce two more linear operators.

Definition 17 Consider a regular hp -mesh for Γ . Let $\{\boldsymbol{\phi}_l\}_{l=1}^{N_\mathcal{V}}$ denote the vector-valued basis functions spanning the parametric space $\mathcal{V}_h^{p-1}(\Gamma)$ and let $\{\nu_l\}_{l=1}^{N_\mathcal{Q}}$ denote the basis functions spanning $\mathcal{Q}_h^{p-2}(\Gamma)$.

1. The lk th entry of the scalar single layer potential matrix $\mathbf{V}_\kappa \in \mathbb{C}^{N_\mathcal{Q} \times N_\mathcal{Q}}$ is defined by a weakly singular double integral

$$(\mathbf{V}_\kappa)_{lk} = (\nu_l, \gamma_0 S_\kappa(\nu_k))_\Gamma = \int_\Gamma \int_\Gamma \nu_l(\mathbf{x}) G_\kappa(\mathbf{x} - \mathbf{y}) \nu_k(\mathbf{y}) d\sigma_y d\sigma_x. \quad (5.18)$$

2. The lk th entry of the transition matrix $\mathbf{Q}_\kappa \in \mathbb{C}^{N_\mathcal{V} \times N_\mathcal{Q}}$ is defined by a weakly singular double integral

$$(\mathbf{Q}_\kappa)_{lk} = (\operatorname{div}_\Gamma \phi_l, \gamma_0 S_\kappa(\nu_k))_\Gamma = \int_\Gamma \int_\Gamma \operatorname{div}_\Gamma \phi_l(\mathbf{x}) G_\kappa(\mathbf{x} - \mathbf{y}) \nu_k(\mathbf{y}) d\sigma_y d\sigma_x. \quad (5.19)$$

With these linear operators, we can write (5.17) in matrix-vector notation, namely,

$$\begin{pmatrix} \mathbf{A}_\kappa & \mathbf{Q}_\kappa \\ \mathbf{Q}_\kappa^\top & \kappa^2 \mathbf{V}_\kappa \end{pmatrix} = \begin{pmatrix} \boldsymbol{\alpha}_1 \\ \boldsymbol{\alpha}_2 \end{pmatrix} = \begin{pmatrix} \mathbf{M}\boldsymbol{\beta} \\ \mathbf{0} \end{pmatrix}. \quad (5.20)$$

To show that any solution of (5.20) yields a solution of the classical system (5.9), we will use properties of the single layer potential matrix for the Helmholtz equation, \mathbf{V}_κ . As always, we exclude values for κ^2 that correspond to interior eigenvalues for the Laplace or the **curl curl** operator and consider h small enough to ensure that κ^2 is not an interior eigenvalue of the discretized Laplace operator. Then, due to Theorem 3.2.7, the operator $\gamma_0 S_\kappa$ is coercive and injective and, therefore, the matrix \mathbf{V}_κ is invertible.

Lemma 5.3.1 *Assume that $\kappa^2 > 0$ is not an interior eigenvalue of the Laplace operator or the **curl curl** operator. There exists $h_0 > 0$ and C_0 such that for all $h < h_0$, the linear system (5.20) is uniquely solvable. The first component $\boldsymbol{\alpha}_1$ of the solution vector $\boldsymbol{\alpha}_s = (\boldsymbol{\alpha}_1, \boldsymbol{\alpha}_2)^\top$ is a solution of the classical problem (5.9), namely $\boldsymbol{\alpha}_1 = \boldsymbol{\alpha}_c$.*

Proof:¹ The idea is to consider the linear operators $\tilde{\mathbf{V}}_\kappa$ and \mathbf{Q}_κ and to show that there exists a matrix $\mathbf{D} \in \mathbb{R}^{N_\mathcal{V} \times N_\mathcal{Q}}$ such that

$$\tilde{\mathbf{V}}_\kappa = \mathbf{D}\mathbf{V}_\kappa\mathbf{D}^\top, \quad (5.21)$$

$$\mathbf{Q}_\kappa = \mathbf{D}\mathbf{V}_\kappa. \quad (5.22)$$

Provided (5.21) and (5.22) hold, we can further use that \mathbf{V}_κ is symmetric and invertible and obtain

$$\begin{aligned} \frac{1}{\kappa^2} \tilde{\mathbf{V}}_\kappa &= \frac{1}{\kappa^2} \mathbf{D}\mathbf{V}_\kappa\mathbf{D}^\top = \frac{1}{\kappa^2} \mathbf{D}\mathbf{V}_\kappa(\mathbf{V}_\kappa^{-1}\mathbf{V}_\kappa)\mathbf{D}^\top = (\mathbf{D}\mathbf{V}_\kappa)(\kappa^2\mathbf{V}_\kappa)^{-1}(\mathbf{D}\mathbf{V}_\kappa)^\top \\ &= \mathbf{Q}_\kappa(\kappa^2\mathbf{V}_\kappa)^{-1}\mathbf{Q}_\kappa^\top. \end{aligned} \quad (5.23)$$

Thus, the system matrix of the classical method (5.10) is exactly the Schur complement of the stabilized system matrix, i.e.,

$$\mathbf{A}_\kappa - \frac{1}{\kappa^2} \tilde{\mathbf{V}}_\kappa = \mathbf{A}_\kappa - \mathbf{Q}_\kappa(\kappa^2\mathbf{V}_\kappa)^{-1}\mathbf{Q}_\kappa^\top.$$

Thus, (5.20) is uniquely solvable with $\boldsymbol{\alpha}_c = \boldsymbol{\alpha}_1$.

To prove (5.21) and (5.22), recall that the surface divergence

$$\operatorname{div}_\Gamma: \mathcal{V}_h^{p-1}(\Gamma) \rightarrow \mathcal{Q}_h^{p-2}(\Gamma)$$

is surjective and, by virtue of (4.50), the surface divergence applied on any $\phi_l \in \mathcal{V}_h^{p-1}(\Gamma)$ is a linear operation of the form

$$\operatorname{div}_\Gamma \phi_l = \sum_{i=1}^{N_\mathcal{Q}} d_{li} \nu_i, \quad l = 1, \dots, N_\mathcal{V}. \quad (5.24)$$

¹The proof presented here is due to an idea of Stefan Kurz. In the original version we have shown (5.23) by a direct computation of the matrix entries.

Thus, we obtain (5.21) and (5.22) by inserting (5.24) into (5.8) and (5.19) and extracting the linear operator

$$\mathbf{D} \in \mathbb{R}^{N_{\mathcal{V}} \times N_{\mathcal{Q}}} : \quad (\mathbf{D})_{li} = d_{li}, \quad l = 1, \dots, N_{\mathcal{V}}, i = 1, \dots, N_{\mathcal{Q}}.$$

□

By Lemma 5.3.1 it is shown that the solution of the stabilized system returns exactly the same solution as the classical system and, therefore, we inherit the convergence properties of Theorem 5.2.1.

However, different from the classical formulation, the stabilized formulation allows the limiting case $\kappa = 0$. It is shown in Section 5.4 that the resulting system corresponds to a classical saddle point formulation for the electrostatic case and one has to deal with the one-dimensional null-space which appeared already when we considered the infinite-dimensional situation in Section 3.4.

5.4. The Electrostatic Case

To understand the algebraic properties of the linear system (5.20), it is useful to investigate again the electrostatic case as the stabilized formulation turns for $\kappa = 0$ into the saddle point problem discussed in Section 3.4

$$\begin{cases} \langle \gamma_R \mathbf{S}_0(\mathbf{j}^t), \phi \rangle_{-\frac{1}{2}} + \langle \operatorname{div}_{\Gamma} \mathbf{j}^t, \gamma_0 S_0(\rho_{\Gamma}^t) \rangle_{\frac{1}{2}} = \langle \mathbf{m} \times \mathbf{n}, \phi \rangle_{-\frac{1}{2}}, \\ \langle \nu, \gamma_0 S_0(\operatorname{div}_{\Gamma} \mathbf{j}^t) \rangle_{\frac{1}{2}} = 0. \end{cases} \quad (5.25)$$

The unique solvability of (5.25) has been proved in Theorem 3.4.3 if $\mathbf{j}^t, \phi \in H^{-\frac{1}{2}}(\operatorname{div}_{\Gamma}, \Gamma)$ and $\rho_{\Gamma}^t, \nu \in H_{**}^{-\frac{1}{2}}(\Gamma)$, respectively. When testing in the bigger space $H^{-\frac{1}{2}}(\Gamma)$, the formulation has a one-dimensional kernel, namely, the non-trivial solutions of the variational problem

$$\forall \nu \in H^{-\frac{1}{2}}(\Gamma) : \quad \langle \nu, \gamma_0 S_0 \phi \rangle_{\frac{1}{2}} = \langle \nu, 1 \rangle_{\frac{1}{2}} \quad (5.26)$$

as those lie in the null-space of the operator $\mathbf{curl}_{\Gamma} : H^{\frac{1}{2}}(\Gamma) \rightarrow H^{-\frac{1}{2}}(\operatorname{div}_{\Gamma}, \Gamma)$. Thus, by continuity, it is clear that the discretization of the stabilized formulation (5.20) converges to the following system

$$\begin{pmatrix} \mathbf{A}_0 & \mathbf{Q}_0 \\ \mathbf{Q}_0^{\top} & \mathbf{0} \end{pmatrix} \begin{pmatrix} \alpha_1 \\ \alpha_2 \end{pmatrix} = \begin{pmatrix} \mathbf{M}\beta \\ \mathbf{0} \end{pmatrix}, \quad (5.27)$$

where the system matrix is singular with

$$\operatorname{rank} \begin{pmatrix} \mathbf{A}_0 & \mathbf{Q}_0 \\ \mathbf{Q}_0^{\top} & \mathbf{0} \end{pmatrix} = N_{\mathcal{V}} + N_{\mathcal{Q}} - 1. \quad (5.28)$$

To obtain a linear system which is regular in the limit, one has to eliminate the one-dimensional null-space, as it is done in [8, 54] by a stabilization term.

5.5. The Linear Operators

The formulae given in Definition 16 and Definition 17 have just symbolic character. In order to obtain expressions which allow for a numerical integration, we need to employ the parametrization of Γ leading to integrations over \hat{T} . Switching to master element coordinates allows to employ the master element shape functions.

Since all element shape functions are given in terms of master element shape functions, namely, for $\mathbf{x} = \hat{\mathbf{X}}_i(\boldsymbol{\xi})$, any integration over the support of a basis function decomposes into integrations

over the reference triangle \hat{T} . One way of generating the system matrices is to systematically sum up the element contributions to the global matrix entries given in the Definitions 16 and 17. Explicit formulae for these element contributions for each matrix are given now. In order to indicate that there might be more element contributions to the same global degree of freedom, the notation $+ =$ is used.

First, we consider the mass matrix \mathbf{M} . For two basis function $\phi_{l_{\text{glob}}}, \phi_{k_{\text{glob}}} \in \mathbf{V}_h^{p-1}(\Gamma)$ with common support element Γ_i , the corresponding element shape functions are given by

$$\phi_{l_{\text{glob}}}|_{\Gamma_i} = \varphi_{i,l_{\text{loc}}} \quad \text{and} \quad \phi_{k_{\text{glob}}}|_{\Gamma_i} = \varphi_{i,k_{\text{loc}}}.$$

In the following, we simply write l and k instead of l_{loc} and k_{loc} .

Thus, the element shape functions $\varphi_{i,l}, \varphi_{i,k} \in \mathbf{V}^{p-1}(\Gamma_i)$ contribute to the $(l_{\text{glob}}, k_{\text{glob}})$ th entry of \mathbf{M} . With (4.49), (4.15) and (2.96), the element contribution to the entry in \mathbf{M} reads

$$\begin{aligned} (\mathbf{M})_{l_{\text{glob}}, k_{\text{glob}}} + &= \int_{\Gamma_i} \varphi_{i,l}(\mathbf{x}) \cdot (\varphi_{i,k}(\mathbf{x}) \times \mathbf{n}(\mathbf{x})) \, d\sigma_{\mathbf{x}} = \int_{\Gamma_i} \varphi_{i,l}(\mathbf{x}) \cdot \varphi_{i,k}(\mathbf{x}) \, d\sigma_{\mathbf{x}} \\ &= \int_{\hat{T}} \frac{1}{J_i} (\hat{\varphi}_{l,2}(\boldsymbol{\xi}) \mathbf{a}_{i,1} - \hat{\varphi}_{l,1}(\boldsymbol{\xi}) \mathbf{a}_{i,2}) \cdot (\hat{\varphi}_{k,1}(\boldsymbol{\xi}) \mathbf{a}^{i,1} + \hat{\varphi}_{k,2}(\boldsymbol{\xi}) \mathbf{a}^{i,2}) \, J_i \, d\boldsymbol{\xi} \\ &= \int_{\hat{T}} (\hat{\varphi}_{l,2}(\boldsymbol{\xi}) \hat{\varphi}_{k,1}(\boldsymbol{\xi}) - \hat{\varphi}_{l,1}(\boldsymbol{\xi}) \hat{\varphi}_{k,2}(\boldsymbol{\xi})) \, d\boldsymbol{\xi}. \end{aligned} \quad (5.29)$$

All entries which belong to a pair of basis functions whose supports do not intersect are zero and, thus, the mass matrix \mathbf{M} is sparse.

To obtain an explicit formula for the element contribution to the vectorial single layer potential matrix \mathbf{A}_κ , consider two basis functions $\phi_{l_{\text{glob}}}, \phi_{k_{\text{glob}}} \in \mathbf{V}_h^{p-1}(\Gamma)$ with

$$\phi_{l_{\text{glob}}}|_{\Gamma_i} = \varphi_{i,l} \quad \text{and} \quad \phi_{k_{\text{glob}}}|_{\Gamma_j} = \varphi_{j,k}.$$

Thus, the element shape functions $\varphi_{i,l} \in \mathbf{V}^{p-1}(\Gamma_i)$ and $\varphi_{j,k} \in \mathbf{V}^{p-1}(\Gamma_j)$ contribute to the entry with index $(l_{\text{glob}}, k_{\text{glob}})$. By (4.49), we obtain

$$\begin{aligned} (\mathbf{A}_\kappa)_{l_{\text{glob}}, k_{\text{glob}}} + &= \int_{\Gamma_i} \varphi_{i,l}(\mathbf{x}) \cdot \int_{\Gamma_j} G_\kappa(\mathbf{x} - \mathbf{y}) \varphi_{j,k}(\mathbf{y}) \, d\sigma_{\mathbf{y}} \, d\sigma_{\mathbf{x}} = \\ &= \int_{\hat{T}} \int_{\hat{T}} \frac{1}{J_i} (\hat{\varphi}_{l,2}(\boldsymbol{\xi}) \mathbf{a}_{i,1} - \hat{\varphi}_{l,1}(\boldsymbol{\xi}) \mathbf{a}_{i,2}) \cdot \left(G_\kappa(\mathbf{x}(\boldsymbol{\xi}) - \mathbf{y}(\boldsymbol{\eta})) \frac{1}{J_j} (\hat{\varphi}_{k,2}(\boldsymbol{\eta}) \mathbf{a}_{j,1} - \hat{\varphi}_{k,1}(\boldsymbol{\eta}) \mathbf{a}_{j,2}) \right) \, J_i J_j \, d\boldsymbol{\xi} \, d\boldsymbol{\eta} \\ &= \int_{\hat{T}} \int_{\hat{T}} (\hat{\varphi}_{l,2}(\boldsymbol{\xi}) \mathbf{a}_{i,1} - \hat{\varphi}_{l,1}(\boldsymbol{\xi}) \mathbf{a}_{i,2}) \cdot (G_\kappa(\mathbf{x}(\boldsymbol{\xi}) - \mathbf{y}(\boldsymbol{\eta})) (\hat{\varphi}_{k,2}(\boldsymbol{\eta}) \mathbf{a}_{j,1} - \hat{\varphi}_{k,1}(\boldsymbol{\eta}) \mathbf{a}_{j,2}(\boldsymbol{\eta}))) \, d\boldsymbol{\xi} \, d\boldsymbol{\eta} \\ &= \int_{\hat{T}} \int_{\hat{T}} \begin{pmatrix} \hat{\varphi}_{l,1} \\ \hat{\varphi}_{l,2} \end{pmatrix}^\top \begin{pmatrix} G_\kappa(\mathbf{a}_{i,2} \cdot \mathbf{a}_{j,2}) & -G_\kappa(\mathbf{a}_{i,2} \cdot \mathbf{a}_{j,1}) \\ -G_\kappa(\mathbf{a}_{i,1} \cdot \mathbf{a}_{j,2}) & G_\kappa(\mathbf{a}_{i,1} \cdot \mathbf{a}_{j,1}) \end{pmatrix} \begin{pmatrix} \hat{\varphi}_{k,1} \\ \hat{\varphi}_{k,2} \end{pmatrix} \, d\boldsymbol{\xi} \, d\boldsymbol{\eta}. \end{aligned} \quad (5.30)$$

The same pairing contributes to the scalar single layer potential matrix for the Maxwell system

$\tilde{\mathbf{V}}_\kappa$ and yields with (4.50)

$$\begin{aligned}
 (\tilde{\mathbf{V}}_\kappa)_{l_{\text{glob}}, k_{\text{glob}}} &+ = \int_{\Gamma_i} \operatorname{div}_\Gamma \boldsymbol{\varphi}_{i,l}(\mathbf{x}) \int_{\Gamma_j} G_\kappa(\mathbf{x} - \mathbf{y}) \operatorname{div}_\Gamma \boldsymbol{\varphi}_{j,k}(\mathbf{y}) \, d\sigma_y \, d\sigma_x \\
 &= \int_{\hat{T}} \int_{\hat{T}} \frac{1}{J_i} \left(\frac{\partial \hat{\varphi}_{l,2}}{\partial \xi_1}(\boldsymbol{\xi}) - \frac{\partial \hat{\varphi}_{l,1}}{\partial \xi_2}(\boldsymbol{\xi}) \right) G_\kappa(\mathbf{x}(\boldsymbol{\xi}) - \mathbf{y}(\boldsymbol{\eta})) \frac{1}{J_j} \left(\frac{\partial \hat{\varphi}_{k,2}}{\partial \eta_1}(\boldsymbol{\eta}) - \frac{\partial \hat{\varphi}_{k,1}}{\partial \eta_2}(\boldsymbol{\eta}) \right) J_i J_j \, d\xi \, d\eta \\
 &= \int_{\hat{T}} \int_{\hat{T}} \left(\frac{\partial \hat{\varphi}_{l,2}}{\partial \xi_1}(\boldsymbol{\xi}) - \frac{\partial \hat{\varphi}_{l,1}}{\partial \xi_2}(\boldsymbol{\xi}) \right) G_\kappa(\mathbf{x}(\boldsymbol{\xi}) - \mathbf{y}(\boldsymbol{\eta})) \left(\frac{\partial \hat{\varphi}_{k,2}}{\partial \eta_1}(\boldsymbol{\eta}) - \frac{\partial \hat{\varphi}_{k,1}}{\partial \eta_2}(\boldsymbol{\eta}) \right) \, d\xi \, d\eta. \quad (5.31)
 \end{aligned}$$

The support of an arbitrary basis function $\nu_{l_{\text{glob}}} \in \mathcal{Q}_h^{p-2}(\Gamma)$ is only a single element in the mesh, $\operatorname{supp} \nu_{l_{\text{glob}}} = \Gamma_i$, for instance, and it holds

$$\nu_{l_{\text{glob}}} = \nu_{l_{\text{loc}}}.$$

Again, we simply write l instead of l_{loc} and due to (4.16), the formula for an element contribution to the matrix \mathbf{V}_κ reads

$$\begin{aligned}
 (\mathbf{V}_\kappa)_{l_{\text{glob}}, k_{\text{glob}}} &+ = \int_{\Gamma_i} v_{i,l}(\mathbf{x}) \int_{\Gamma_j} G_\kappa(\mathbf{x} - \mathbf{y}) v_{j,k}(\mathbf{y}) \, d\sigma_y \, d\sigma_x \\
 &= \int_{\hat{T}} \int_{\hat{T}} \frac{1}{J_i} \hat{v}_l(\boldsymbol{\xi}) G_\kappa(\mathbf{x}(\boldsymbol{\xi}) - \mathbf{y}(\boldsymbol{\eta})) \frac{1}{J_j} \hat{v}_k(\boldsymbol{\eta}) J_i J_j \, d\xi \, d\eta \\
 &= \int_{\hat{T}} \int_{\hat{T}} \hat{v}_l(\boldsymbol{\xi}) G_\kappa(\mathbf{x}(\boldsymbol{\xi}) - \mathbf{y}(\boldsymbol{\eta})) \hat{v}_k(\boldsymbol{\eta}) \, d\xi \, d\eta. \quad (5.32)
 \end{aligned}$$

Finally, an element contribution to the rectangular transition matrix \mathbf{Q}_κ is given by

$$\begin{aligned}
 (\mathbf{Q}_\kappa)_{l_{\text{glob}}, k_{\text{glob}}} &+ = \int_{\Gamma_i} \operatorname{div}_\Gamma \boldsymbol{\varphi}_{i,l}(\mathbf{x}) \int_{\Gamma_j} G_\kappa(\mathbf{x} - \mathbf{y}) v_{j,k}(\mathbf{y}) \, d\sigma_y \, d\sigma_x \\
 &= \int_{\hat{T}} \int_{\hat{T}} \frac{1}{J_i} \left(\frac{\partial \hat{\varphi}_{l,2}}{\partial \xi_1}(\boldsymbol{\xi}) - \frac{\partial \hat{\varphi}_{l,1}}{\partial \xi_2}(\boldsymbol{\xi}) \right) G_\kappa(\mathbf{x}(\boldsymbol{\xi}) - \mathbf{y}(\boldsymbol{\eta})) \frac{1}{J_j} \hat{v}_k(\boldsymbol{\eta}) J_i J_j \, d\xi \, d\eta \\
 &= \int_{\hat{T}} \int_{\hat{T}} \left(\frac{\partial \hat{\varphi}_{l,2}}{\partial \xi_1}(\boldsymbol{\xi}) - \frac{\partial \hat{\varphi}_{l,1}}{\partial \xi_2}(\boldsymbol{\xi}) \right) G_\kappa(\mathbf{x}(\boldsymbol{\xi}) - \mathbf{y}(\boldsymbol{\eta})) \hat{v}_k(\boldsymbol{\eta}) \, d\xi \, d\eta. \quad (5.33)
 \end{aligned}$$

To realize the boundary element methods derived from the direct representation formula, (3.60), the so-called double layer potential matrix appears on the right hand side. According to (3.50), the entry with index $(l_{\text{glob}}, k_{\text{glob}})$ reads

$$(\mathbf{D}_\kappa)_{l_{\text{glob}}, k_{\text{glob}}} = (\gamma_R \mathbf{S}_M(\boldsymbol{\phi}_{k_{\text{glob}}}), \boldsymbol{\phi}_{l_{\text{glob}}})_\Gamma = \int_\Gamma \int_\Gamma \boldsymbol{\phi}_{l_{\text{glob}}}(\mathbf{x}) \cdot \left(\nabla_{\mathbf{x}} G_\kappa(\mathbf{x} - \mathbf{y}) \times \boldsymbol{\phi}_{k_{\text{glob}}}(\mathbf{y}) \right) \, d\sigma_y \, d\sigma_x.$$

The same pair of element shape functions contributing to the vectorial single layer potential matrix,

leads the explicit formula

$$\begin{aligned}
(\mathbf{D}_\kappa)_{l_{\text{glob}}, k_{\text{glob}}} &+ = \int_{\Gamma_i} \int_{\Gamma_j} \boldsymbol{\varphi}_{j,l}(\mathbf{x}) \cdot (\nabla_{\mathbf{x}} G_\kappa(\mathbf{x} - \mathbf{y}) \times \boldsymbol{\varphi}_{i,k}(\mathbf{y})) \, d\sigma_y \, d\sigma_x = \\
&= \int_{\hat{T}} \int_{\hat{T}} (\hat{\varphi}_{l,2}(\boldsymbol{\xi}) \mathbf{a}_{i,1} - \hat{\varphi}_{l,1}(\boldsymbol{\xi}) \mathbf{a}_{i,2}(\boldsymbol{\xi})) \cdot ((\nabla_{\mathbf{x}} G_\kappa(\mathbf{x}(\boldsymbol{\xi}) - \mathbf{y}(\boldsymbol{\eta})) \times (\hat{\varphi}_{k,2}(\boldsymbol{\eta}) \mathbf{a}_{j,1} - \hat{\varphi}_{k,1}(\boldsymbol{\eta}) \mathbf{a}_{j,2}))) \, d\xi \, d\eta \\
&= \int_{\hat{T}} \int_{\hat{T}} \begin{pmatrix} \hat{\varphi}_{l,1} \\ \hat{\varphi}_{l,2} \end{pmatrix}^\top \begin{pmatrix} \nabla G_\kappa \cdot (\mathbf{a}_{i,2} \times \mathbf{a}_{j,2}) & -\nabla G_\kappa \cdot (\mathbf{a}_{i,2} \times \mathbf{a}_{j,1}) \\ -\nabla G_\kappa \cdot (\mathbf{a}_{i,1} \times \mathbf{a}_{j,2}) & \nabla G_\kappa \cdot (\mathbf{a}_{i,1} \times \mathbf{a}_{j,1}) \end{pmatrix} \begin{pmatrix} \hat{\varphi}_{k,1} \\ \hat{\varphi}_{k,2} \end{pmatrix} \, d\xi \, d\eta. \quad (5.34)
\end{aligned}$$

The formulae (5.29)-(5.34) are crucial for the high order boundary element methods as they are valid for any high order approximation of the boundary. Appropriate integration schemes to compute the singular integrals can be found in [52], for instance.

5.6. Conclusion

The numerical analysis of the high order boundary element methods is the subject of this chapter. The most fundamental result has been that the classical formulation gives rise to a numerical scheme with quasi-optimal convergence. It has been shown that also on the discrete level, the stabilized formulation is equivalent to the classical formulation and, thus, the stabilized formulation gives rise to a stable numerical boundary element method.

The content of Section 5.5 is of principal importance for the realization of a high order boundary implementation because explicit formulae for the matrix entries are given. The formulae (5.29) to (5.34) are general in the sense that they are valid for any non-linear parametrization of the elements. In this context, it is to emphasize that it has been proved as a byproduct of our approach that the information about the embedding of the boundary Γ into \mathbb{R}^3 is completely contained in the kernels

$$\begin{aligned}
&G_\kappa \quad \text{for} \quad \tilde{\mathbf{V}}_\kappa, \mathbf{V}_\kappa, \mathbf{Q}_\kappa, \\
&\begin{pmatrix} G_\kappa(\mathbf{a}_{i,2} \cdot \mathbf{a}_{j,2}) & -G_\kappa(\mathbf{a}_{i,2} \cdot \mathbf{a}_{j,1}) \\ -G_\kappa(\mathbf{a}_{i,1} \cdot \mathbf{a}_{j,2}) & G_\kappa(\mathbf{a}_{i,1} \cdot \mathbf{a}_{j,1}) \end{pmatrix} \quad \text{for} \quad \mathbf{A}_\kappa, \\
&\begin{pmatrix} \nabla G_\kappa \cdot (\mathbf{a}_{i,2} \times \mathbf{a}_{j,2}) & -\nabla G_\kappa \cdot (\mathbf{a}_{i,2} \times \mathbf{a}_{j,1}) \\ -\nabla G_\kappa \cdot (\mathbf{a}_{i,1} \times \mathbf{a}_{j,2}) & \nabla G_\kappa \cdot (\mathbf{a}_{i,1} \times \mathbf{a}_{j,1}) \end{pmatrix} \quad \text{for} \quad \mathbf{D}_\kappa.
\end{aligned}$$

All other expressions in the integrands and especially the mass matrix \mathbf{M} are independent of the parametrizations $\hat{\mathbf{X}}_i$. This result is fundamental when it comes to realization of a high order boundary element method as the evaluation of the integration points can be precomputed on the master element shape functions and used when needed.

Connected with the linear operators was the question how to compute the system matrices with optimal memory requirements. Similar to the classical boundary element methods, the high order boundary element methods lead to fully populated system matrices. It is well-known that a possible tool to deal with this difficulty is the adaptive cross approximation. The assembling of the matrices of the high order scheme is done order-wise, which means that the matrices possess an additional, hierarchic structure and the adaptive cross approximation [51] must be applied to submatrices. This so-called high-dimensional adaptive cross approximation has already been implemented and the optimal handling of it and further research on the subject will be done in the future.

NUMERICAL RESULTS

6.1. Introduction

In this chapter, the Dirichlet boundary value problem describing the scattered electric field \mathbf{E}

$$\left\{ \begin{array}{ll} \mathbf{curl} \mathbf{curl} \mathbf{E} - \kappa^2 \mathbf{E} = \mathbf{0}, & \text{in } \Omega^c, \\ \gamma_D \mathbf{E} = \mathbf{m}, & \text{on } \Gamma, \\ \left| (\mathbf{curl} \mathbf{E}(\mathbf{x}) \times \frac{\mathbf{x}}{|\mathbf{x}|} - i\omega\varepsilon \mathbf{E}(\mathbf{x})) \right| = \mathcal{O}\left(\frac{1}{|\mathbf{x}|^2}\right), & \text{for } |\mathbf{x}| \rightarrow \infty \end{array} \right. \quad (6.1)$$

is considered. In the context of boundary element methods, we seek the densities \mathbf{j}^t and ρ_Γ^t such that

$$\mathbf{E}(\mathbf{x}) = \int_{\Gamma} G_\kappa(\mathbf{x} - \mathbf{y}) \mathbf{j}^t(\mathbf{y}) d\sigma_y - \nabla \int_{\Gamma} G_\kappa(\mathbf{x} - \mathbf{y}) \rho_\Gamma^t(\mathbf{y}) d\sigma_y \quad (6.2)$$

is a solution of (6.1) and such that the weak form of the continuity equation

$$\int_{\Gamma} G_\kappa(\mathbf{x} - \mathbf{y}) \operatorname{div}_\Gamma \mathbf{j}^t(\mathbf{y}) d\sigma_y = -\kappa^2 \int_{\Gamma} G_\kappa(\mathbf{x} - \mathbf{y}) \rho_\Gamma^t(\mathbf{y}) d\sigma_y \quad (6.3)$$

holds. Besides the representation formula (6.2), it is convenient to use the far-field approximation

$$\mathbf{E}_{\text{far}}(\theta, \phi) = \frac{1}{r} \int_{\Gamma} \frac{e^{i\kappa \mathbf{e}_r \cdot \mathbf{y}}}{4\pi} \mathbf{j}^t(\mathbf{y}) d\sigma_y \quad (6.4)$$

for $\mathbf{x} = r\mathbf{e}_r(\theta, \phi)$. How to derive the far-field approximation is explained in Appendix B.

The theoretical results from Chapter 5 suggest that the high order boundary element methods are suitable numerical schemes to compute an approximation \mathbf{E}_{hp} and this remains to verify. The results presented in this chapter are realizations of the discrete formulations discussed in Chapter 5. In order to understand the high order boundary element methods, it is fundamental to analyze the error of the geometrical input data and its impact on the input \mathbf{m}_{hp} as well as the error of the solution.

So far, we did not consider a geometrical input error because we assumed that the manifold Γ is exactly given by a discrete mesh. This is, however, an idealistic situation and, in general, the discrete mesh is only an approximation of the exact geometry. From now on, we denote by Γ the exact geometry and by Γ_{hp} the computational boundary approximating Γ . In our case, Γ_{hp} consists of isoparametric elements $\{(\Gamma_i, p)\}_{i=1}^N$ of uniform order p and characteristic mesh size h , namely,

$$\Gamma_{hp} = \bigcup_{i=1}^N \overline{\Gamma}_i.$$

The characteristic mesh size h is the minimal length of all edges in Γ_{hp} , for instance. The elements Γ_i in the mesh Γ_{hp} are given by polynomial parametrizations of maximal order p , i.e.,

$$\hat{\mathbf{X}}_i: \hat{T} \rightarrow \Gamma_i, \quad \hat{\mathbf{X}}_i \in \left(\mathcal{P}^p(\hat{T})\right)^3.$$

Once Γ_{hp} is determined, the parametric spaces

$$\mathcal{H}^p(\Gamma_{hp}), \quad \mathcal{E}^{p-1}(\Gamma_{hp}), \quad \mathcal{V}^{p-1}(\Gamma_{hp}), \quad \mathcal{Q}^{p-2}(\Gamma_{hp})$$

from Subsection 4.2.3 are defined because all bases are given in terms of the parametrizations of the elements. Moreover, the projection-based interpolation operators from the Subsections 4.2.4 and 4.2.5 are defined and, thus, we obtain especially the approximated Dirichlet data by

$$\mathbf{m}_{hp} = \Pi^d(\mathbf{m}) = \sum_{l=1}^{N_V} \beta_l \phi_l, \quad \boldsymbol{\beta} = (\beta_1, \dots, \beta_{N_V})^\top \in \mathbb{C}^{N_V}.$$

The necessary input data to start the boundary element scheme is on the one hand the mesh Γ_{hp} and on the other hand the Dirichlet data \mathbf{m}_{hp} . The pair $(\Gamma_{hp}, \mathbf{m}_{hp})$ specifies the discretization of the boundary value problem (6.1). We say that $(\Gamma_{hp}, \mathbf{m}_{hp})$ defines the hp -model and the term setting-up the hp -model describes the two approximation steps which lead to the hp -model.

To control the errors of the numerical input and output data, we will use different error estimators. Approximations of traces on Γ_{hp} such as \mathbf{m}_{hp} and \mathbf{j}_{hp}^t are measured with respect to Err_1 which is

$$\text{Err}_1 = \left(\int_{\Gamma_{hp}} |\mathbf{f}_{hp}(\mathbf{x}) - \mathbf{f}(B(\mathbf{x}))|^2 d\sigma_x \right)^{\frac{1}{2}} / \left(\int_{\Gamma} |\mathbf{f}(\mathbf{x})|^2 d\sigma_x \right)^{\frac{1}{2}}. \quad (6.5)$$

Here, $B: \Gamma_{hp} \rightarrow \Gamma$ denotes a projection on the exact geometry and, thus, the geometrical approximation is explicitly considered. This kind of error estimator is necessary to compare the numerical solution with an analytical solution which is available on the exact geometry Γ . To assess the accuracy of the scattered field \mathbf{E}_{hp} and $\mathbf{E}_{hp, \text{far}}$ in Ω^c , we compute

$$\text{Err}_2 = \frac{1}{M} \sum_{i=1}^M |\mathbf{F}_{hp}(\mathbf{x}_i) - \mathbf{F}(\mathbf{x}_i)|. \quad (6.6)$$

Here, M is the number of the sample points.

In the Sections 6.2 and 6.3, the performance of the high order boundary element methods is analyzed for different hp -models and different Galerkin formulations. The goal of Section 6.2 is to demonstrate convergence of the classical formulations with respect to uniform h -refinement and fixed uniform order $p = 1, \dots, 4$. This means that the number of elements N are quadrupled and the convergence factor (CF) is computed by dividing either Err_1 or Err_2 of the numerical solutions obtained on subsequently refined meshes. The qualitative relation between the convergence factor and the convergence rate (CR) is $\text{CR} \approx \log_2 \text{CF}$.

In Section 6.3, we compare the numerical stability of the classical method with the numerical stability of the stabilized method with respect to the limit $\kappa \rightarrow 0$. Here, it is the condition number of the system matrices which is analyzed.

6.2. The Classical Formulation

In this section, we present numerical solutions for the classical formulation leading to

$$\mathbf{A}_c \boldsymbol{\alpha} = \boldsymbol{\beta}_c \quad \text{with} \quad \mathbf{A}_c = \left(\mathbf{A}_\kappa - \frac{1}{\kappa^2} \tilde{\mathbf{V}}_\kappa \right) \quad \text{and} \quad \boldsymbol{\beta}_c = \mathbf{M} \boldsymbol{\beta}. \quad (6.7)$$

The accuracy of the Galerkin solution

$$\mathbf{j}_{hp}^t = \sum_{l=1}^{N_\gamma} \alpha_l \phi_l \quad (6.8)$$

and the accuracy of the scattered electric field at $\mathbf{x} \in \Omega^c$

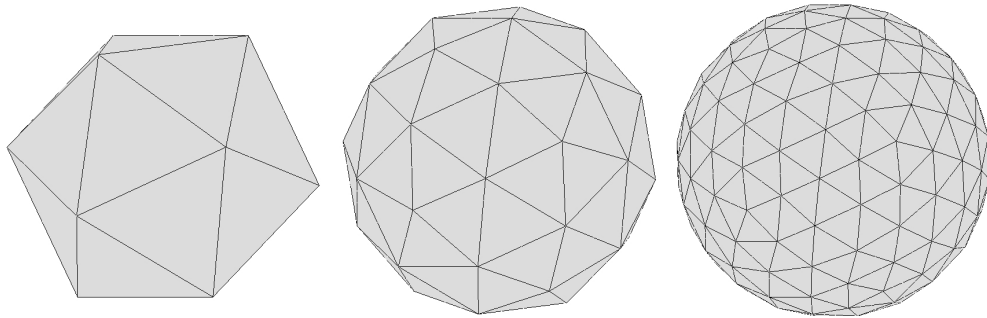
$$\mathbf{E}_{hp}(\mathbf{x}) = \int_{\Gamma_{hp}} G_\kappa(\mathbf{x} - \mathbf{y}) \mathbf{j}_{hp}^t(\mathbf{y}) d\sigma_y + \frac{1}{\kappa^2} \nabla \int_{\Gamma_{hp}} G_\kappa(\mathbf{x} - \mathbf{y}) \operatorname{div}_\Gamma \mathbf{j}_{hp}^t(\mathbf{y}) d\sigma_y, \quad (6.9)$$

$$\mathbf{E}_{hp,\text{far}}(\theta, \phi) = \frac{1}{r} \frac{1}{4\pi} \int_{\Gamma_{hp}} e^{i\kappa \mathbf{e}_r \cdot \mathbf{y}} \mathbf{j}_{hp}^t(\mathbf{y}) d\sigma_y \quad (6.10)$$

depend on the specific hp -model. In the following subsections, we investigate three different hp -models. The first scattering problem we look at is the plane wave scattering from the unit sphere S^2 . In Subsection 6.2.1, S^2 is approximated by linear elements. The same scattering problem for an isoparametric approximation of S^2 is discussed in Subsection 6.2.2. In Subsection 6.2.3, we study a plane wave scattering at a more realistic geometry, the boundary of a ship, which is exactly given by a linear mesh.

6.2.1. Icosaeder

Figure 6.1.: Approximation of the sphere by uniform refinement of the icosaeeder.



In this subsection high order trial and test functions are employed on a linear mesh. The geometry we start with to obtain a linear approximation of the unit sphere S^2 is the icosaeeder shown in Figure 6.1 on the left. After two steps of uniform refinement of the icosaeeder, the mesh on the right with $N = 320$ triangles is obtained.

It is well known that the boundary value problem describing the scattering of a plane wave from the unit sphere can be solved analytically. Explicit formulae for the Mie series describing the exact surface current \mathbf{j}^t , the Mie series for the scattered electrical field \mathbf{E} in Ω^c and the far-field approximation are given in Appendix B.

We assume that Ω^c is dielectric with

$$\varepsilon = \varepsilon_0 = 8.854 \cdot 10^{-12} \frac{\text{As}}{\text{Vm}} \quad \text{and} \quad \mu = \mu_0 = 4\pi \cdot 10^{-7} \frac{\text{Vs}}{\text{Am}}.$$

The wave vector $\boldsymbol{\kappa}$ and its absolute value, the wave number, $\kappa = |\boldsymbol{\kappa}|$, are related to the material data by the dispersion relation

$$\kappa = |\boldsymbol{\kappa}| = \omega \sqrt{\varepsilon_0 \mu_0}.$$

The scattering is initiated by an incoming signal of the form

$$\mathbf{E}^i(\mathbf{x}, t) = \tilde{\mathbf{E}}^i(\mathbf{x}) e^{-i\omega t} = e^{i(\boldsymbol{\kappa} \cdot \mathbf{x} - \omega t)} \mathbf{e}.$$

Here, we choose the angular frequency ω and the plane of propagation $\{\boldsymbol{\kappa}, \mathbf{e}\}$ to be

$$\omega = 1.5 \cdot 10^9 \frac{1}{\text{s}}, \quad \boldsymbol{\kappa} = \kappa(0, 0, -1)^\top, \quad \mathbf{e} = \mathbf{e}_1.$$

Thus, the complex valued amplitude of the plane wave reads

$$\tilde{\mathbf{E}}^i(\mathbf{x}) = e^{-i\kappa x_3} \mathbf{e}_1.$$

The wave number κ does not coincide with interior eigenvalues, neither of the Laplace operator nor the **curl curl** operator [30, 60]. The tilde is skipped in the following. All lengths are normalized to 1 m, and, thus, the electric field can be regarded dimensionless due to the linearity of the problem.

A uniform h -refinement yields quadratic convergence of the approximation S_h^2 to the exact geometry S^2 in L^2 -norm.

The convergence of the high order boundary element method (6.7) with respect to uniform h -refinement is reported in Table 6.1. Each block row of Table 6.1 contains the convergence analysis for fixed uniform order of approximation p , where Nédélec elements of first kind are used and p varies from $p = 1$ to $p = 4$. The number of elements N and the corresponding number of global degrees of freedom $N_{\mathcal{V}}$ for $\mathcal{V}^{p-1}(S_h^2)$ are listed in the second column. The columns three to six contain the numerical convergence analysis for input and output data of the high order boundary element method. The convergence for uniform h -refinement for the input data $\mathbf{m}_{hp} = \Pi^d(\mathbf{m})$ is reported in the third column. The fourth column shows the accuracy of the numerical solution \mathbf{j}_{hp}^t . The difference between the numerical data and the exact data is measured by Err_1 with $B: S_h^2 \rightarrow S^2$, $B(\mathbf{x}) = \mathbf{x}/|\mathbf{x}|$. The scattered field \mathbf{E} in the exterior domain Ω^c is analyzed in the fifth column. Here, the representation formula (6.9) is evaluated in $M = 360$ sample points distributed on a sphere $S_r^2(\mathbf{0})$ with radius $r = 2$. The difference between the numerical solution and the exact solution is measured by Err_2 defined by (6.6). Err_2 is also used to assess the accuracy of the far-field approximation $\mathbf{E}_{hp, \text{far}}$ and the corresponding results are shown in the sixth column.

The high order Galerkin ansatz does not lead to an increase of the convergence rates because the geometrical error decreases only by a convergence rate $\text{CR} \approx \log_2 \text{CF}$, see Appendix A. This does not contradict Theorem 5.2.1 because quasi-optimality was proved under the essential assumption that the linear mesh is exact, i.e., $\Gamma = \Gamma_{hp}$. This is, however, an ideal situation and one has to consider the impact of the geometrical approximation error. The stability estimates given by the lemma of Strang show explicitly that the geometrical error deteriorates the convergence rate of the Galerkin solution whenever the geometrical convergence rate is lower than the asymptotic convergence of the Galerkin solution [52]. Thus, whenever the surface Γ is not exactly given by plane triangles and the uniform h -refinement of a linear mesh is used to approximate the geometry, the convergence is bounded to a quadratic rate.

Table 6.1.: Convergence analysis for high order BEM with icosaeader as test geometry, Nédélec's first sequence.

Order	N	$N_{\mathcal{V}}$	$\ \mathbf{m}_{hp} - \mathbf{m}\ $		$\ \mathbf{j}_{hp}^t - \mathbf{j}^t\ $		$\ \mathbf{E}_{hp} - \mathbf{E}\ $		$\ \mathbf{E}_{hp, \text{far}} - \mathbf{E}_{\text{far}}\ $	
			Err ₁	CF	Err ₁	CF	Err ₂	CF	Err ₂	CF
$p = 1$	20	30	9.33e-1	/	0.15e-1	/	4.85e-1	/	0.45e+1	/
	80	120	5.20e-1	1.8	6.99e-1	2.2	1.75e-1	2.8	0.16e+1	2.8
	320	480	2.65e-1	2.0	4.01e-1	1.7	4.35e-2	4.0	3.91e-1	4.0
	1280	1920	1.33e-1	2.0	1.87e-1	2.1	1.07e-2	4.1	9.63e-2	4.1
$p = 2$	20	100	6.56e-1	/	7.59e-1	/	2.85e-1	/	0.28e+1	/
	80	400	2.53e-1	2.6	2.69e-1	2.8	8.67e-2	3.3	8.16e-1	3.4
	320	1600	1.01e-1	2.5	9.04e-2	3.0	2.24e-2	3.9	2.09e-1	3.9
	1280	6400	4.60e-2	2.2	3.59e-2	2.5	5.67e-3	4.0	5.29e-2	4.0
$p = 3$	20	210	5.94e-1	/	6.31e-1	/	2.63e-1	/	0.26e-1	/
	80	840	2.28e-1	2.7	2.27e-1	2.8	8.36e-2	3.1	7.93e-1	3.2
	320	3360	9.63e-2	2.4	8.95e-2	2.5	2.21e-2	3.8	2.06e-1	3.8
	1280	13440	4.54e-2	2.1	4.18e-2	2.1	5.64e-3	3.9	5.26e-2	3.9
$p = 4$	20	360	5.87e-1	/	6.12e-1	/	2.61e-1	/	0.56e+1	/
	80	1440	2.27e-1	2.6	2.28e-1	2.7	8.34e-2	3.1	7.91e-1	3.2
	320	5760	9.63e-2	2.4	9.04e-2	2.5	2.21e-2	3.8	2.06e-1	3.8
	1280	23040	4.54e-2	2.1	4.22e-2	2.1	5.64e-3	3.9	5.26e-2	3.9

6.2.2. Isoparametric Sphere

When the boundary is given analytically, the projection-based interpolation operator Π^1 can be employed to obtain a high order polynomial approximation of the geometry. The usage of isoparametric elements of order p means that this geometrical approximation is of the same order p as the approximation of the physical unknowns. Different from the previous section, the local parametrizations of the elements are polynomials and, thus, the elements are curved triangles. The numerical tests presented in this subsection use isoparametric elements of uniform order p . The exact geometry is again the unit sphere $S^2 \subset \mathbb{R}^3$ and the computational domain is denoted S_{hp}^2 . Details on the geometrical approximation of the sphere are given in Appendix A. It is shown in Table A.1 that a uniform order of approximation p yields a convergence factor $\text{CF} = 2^{(p+1)}$, thus a convergence rate $\text{CR} = p + 1$. Figure 6.2 shows the triangulation of the isoparametric sphere with $N = 128$ elements

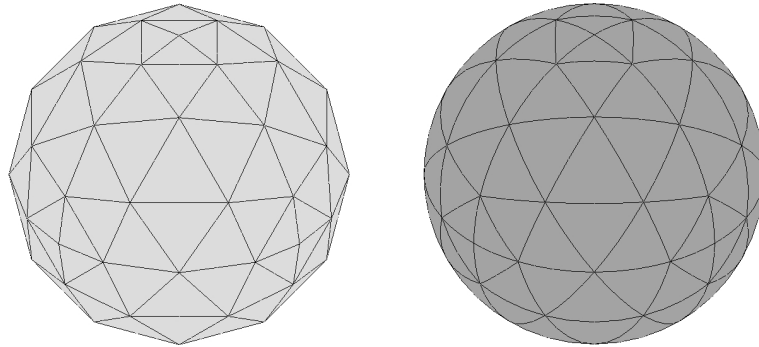
Figure 6.2.: Isoparametric approximation S_{hp}^2 of S^2 with $p = 1$ and $p = 4$ for $N = 128$.

Table 6.2.: Convergence analysis for high order BEM with isoparametric sphere as test geometry, Nédélec's first sequence.

Order	N	$N_{\mathcal{V}}$	$\ \mathbf{m}_{hp} - \mathbf{m}\ $		$\ \mathbf{j}_{hp}^t - \mathbf{j}^t\ $		$\ \mathbf{E}_{hp} - \mathbf{E}\ $		$\ \mathbf{E}_{hp,\text{far}} - \mathbf{E}_{\text{far}}\ $	
			Err ₁	CF	Err ₁	CF	Err ₂	CF	Err ₂	CF
$p = 1$	128	192	4.41e-1	/	5.60e-1	/	1.15e-1	/	0.11e+1	/
	512	768	2.24e-1	2.0	4.72e-1	1.2	3.01e-2	3.8	2.78e-1	3.8
	2048	3072	1.13e-1	2.0	1.51e-1	3.1	7.44e-3	4.0	6.68e-2	4.2
	8192	12288	5.63e-2	2.0	6.38e-2	2.4	1.85e-3	4.0	1.66e-2	4.0
$p = 2$	32	160	3.20e-1	/	1.06e-1	/	7.72e-2	/	6.70e-1	/
	128	640	1.01e-1	3.2	1.88e-1	0.6	9.07e-3	8.5	7.75e-2	8.6
	512	2560	2.74e-2	3.7	4.11e-2	4.6	6.25e-4	15	5.40e-3	14
	2048	10240	6.99e-3	3.9	1.09e-2	3.8	4.77e-5	13	4.16e-4	13
$p = 3$	32	336	1.50e-1	/	0.12e+1	/	2.32e-2	/	1.88e-2	/
	128	1344	2.60e-2	5.8	4.12e-2	29	1.07e-3	22	9.04e-3	21
	512	5376	3.54e-3	7.3	5.24e-3	7.9	4.07e-5	26	3.71e-4	24
	2048	21504	4.53e-4	7.8	6.37e-4	8.2	2.23e-6	18	2.04e-5	18
$p = 4$	8	144	3.73e-1	/	9.20e-1	/	1.29e-1	/	0.12e+1	/
	32	576	6.36e-2	5.9	1.08e-1	8.5	4.50e-3	29	4.27e-2	27
	128	2304	5.72e-3	11	9.21e-3	12	7.75e-5	58	6.60e-4	65
	512	9216	4.05e-4	14	6.60e-4	14	8.68e-7	89	7.98e-6	83

for $p = 1$ on the left and $p = 4$ on the right. Thus, the geometrical error decreases faster as the optimal convergence rate of the Galerkin solution.

The convergence of the high order boundary element method (6.7) with respect to uniform h -refinement is reported in Table 6.2. For isoparametric elements of uniform order p , the input data \mathbf{m}_{hp} converges towards the exact trace \mathbf{m} with a convergence factor $\text{CF} = 2^p$, i.e., with a convergence rate of $\text{CR} = p$. This is the optimal convergence due to the projection-based interpolation operator Π^d . The solution of the boundary element method \mathbf{j}_{hp}^t converges towards the exact trace \mathbf{j}^t by convergence rate $\text{CR} = p$ as well. This is the quasi-optimal convergence of the numerical method. The point evaluations shown in the last two columns converge approximately by $\text{CR} = p + 1$. To get a visual impression, Figure 6.3 shows the absolute values of the Cartesian components of the numerical solution, $|\mathbf{j}_{hp,k}^t|$ for $k = 1, 2, 3$ on the left and the point-wise difference $|\mathbf{j}_{hp,k}^t - \mathbf{j}_k^t|$ for $k = 1, 2, 3$ on the right. The plots belong to the hp -model with $N = 128$ and $p = 4$. Note that the point-wise error in the upper right figure is localized where the plane of propagation of the incoming signal intersects with S_{hp}^2 . The hot spot might result from the difficult mesh topology at the intersection point, see Figure 6.2.

To check the efficiency of this high order boundary element method, the number of degrees of freedom are fixed to $N_{\mathcal{V}} \approx 1000$. In order to obtain a hp -model with approximately this number of degrees of freedom for $p = 1$ to $p = 4$, the element number N varies as well as the kind of Nédélec elements. As presented in Table 6.3, the computations with high order elements are more accurate for the same numerical costs. The polar plots in the Figure 6.4 and 6.5 show the far-field approximation of \mathbf{E}_{far} given by the Mie series together with the numerical results $\mathbf{E}_{hp,\text{far}}$ for $p = 1$ and $p = 4$.

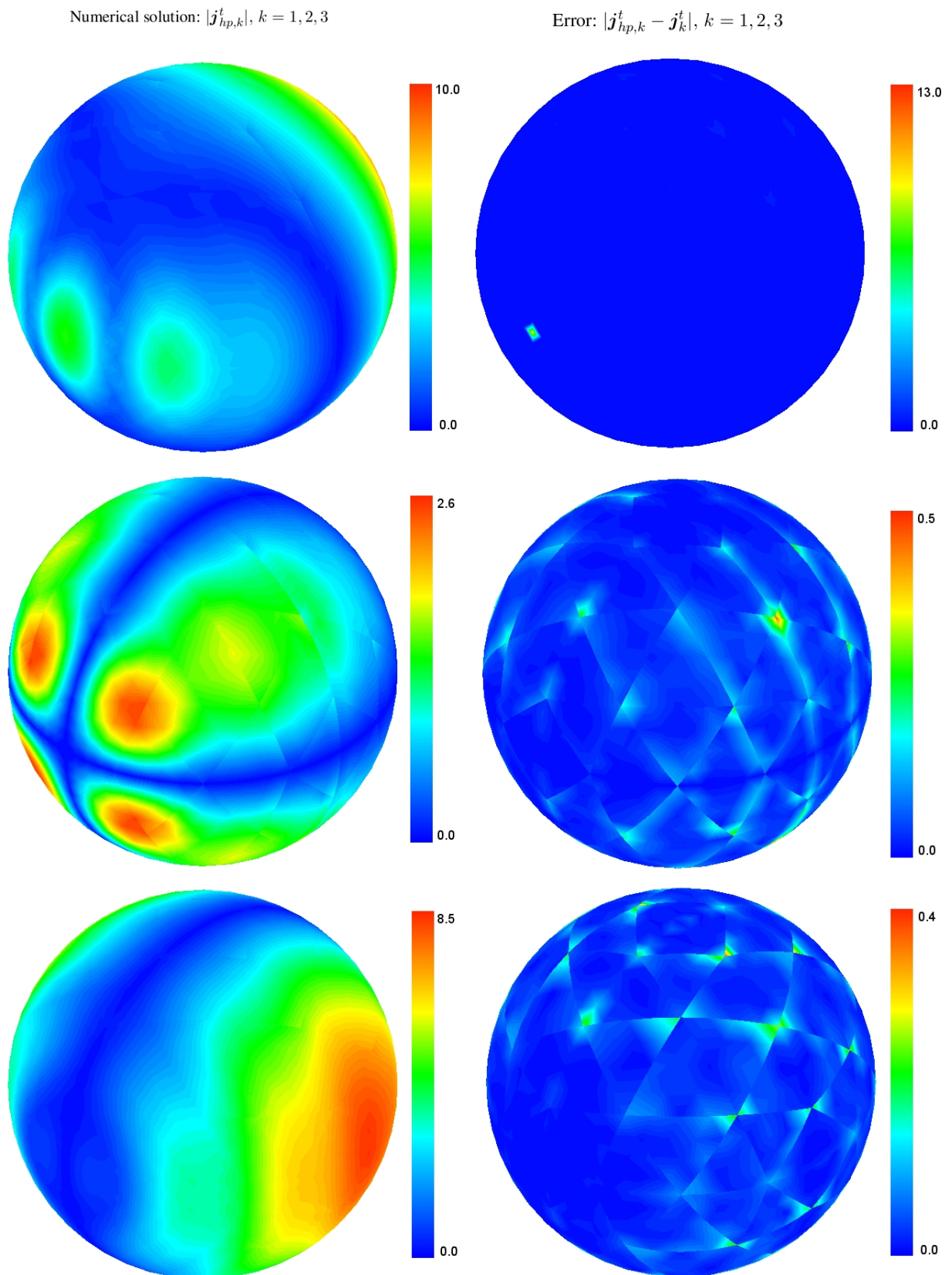
Figure 6.3.: Numerical solution on the left and point-wise error on the right for $p = 4$ and $N = 128$.

Figure 6.4.: Far-field pattern of the electric field in yz -plane visualizing test runs $p = 1, 4$ from Table 6.3.

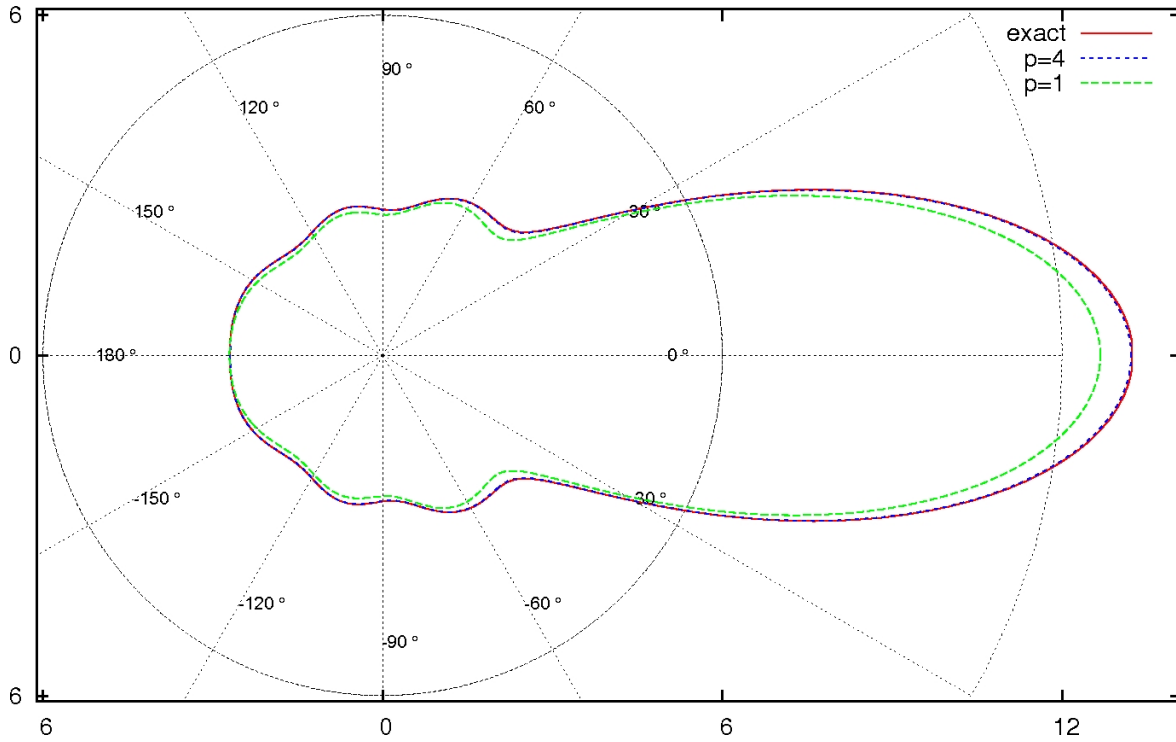


Figure 6.5.: Far-field pattern of the electric field in xz -plane visualizing test runs $p = 1, 4$ from Table 6.3.

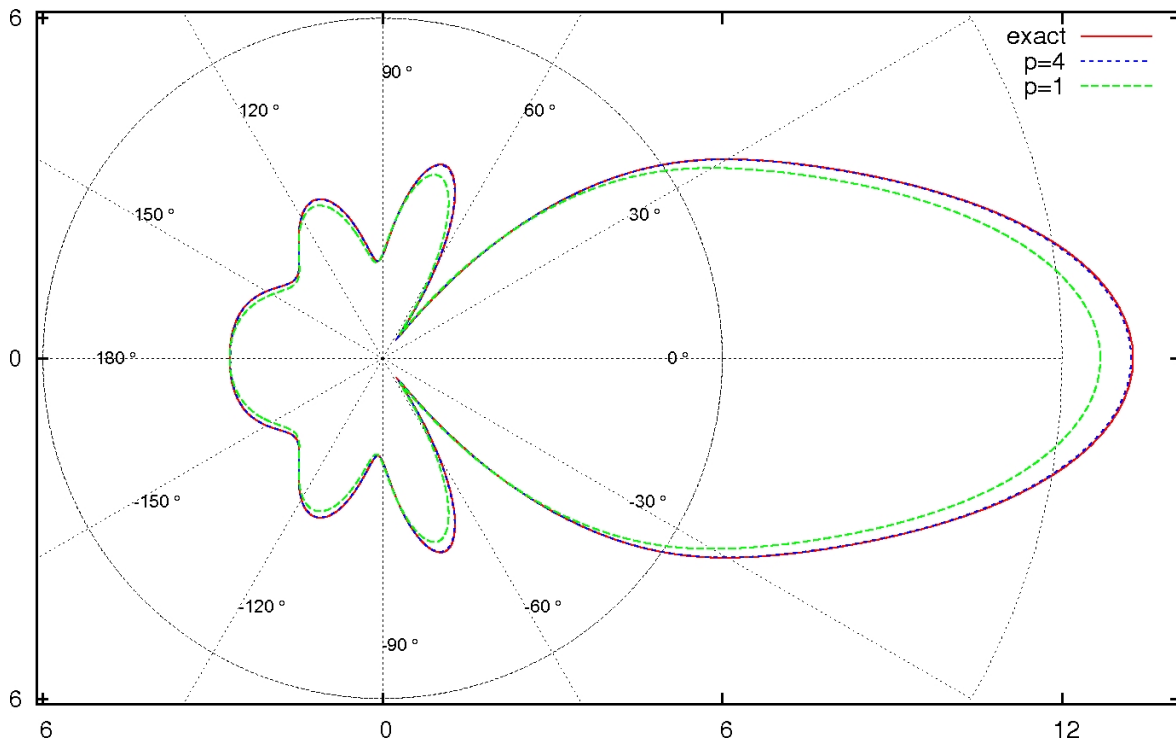
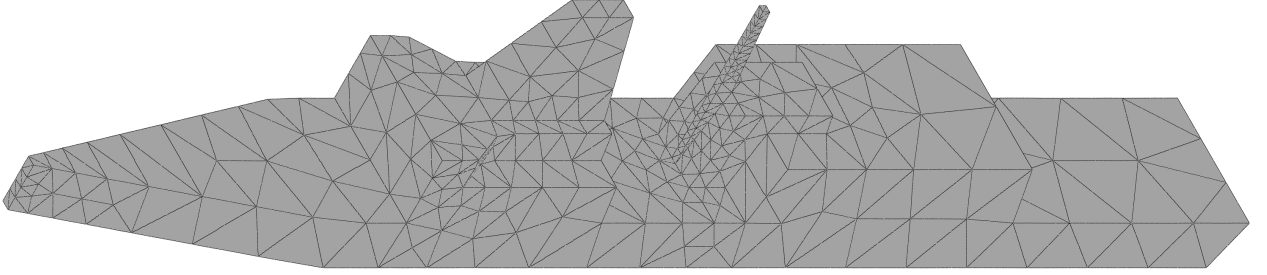


Table 6.3.: Comparable degrees of freedom solving plane wave scattering at the sphere.

Order	Nédélec	N	$N_{\mathcal{V}}$	$\ \mathbf{m}_{hp} - \mathbf{m}\ $	$\ \mathbf{j}_{hp}^t - \mathbf{j}^t\ $	$\ \mathbf{E}_{hp} - \mathbf{E}\ $	$\ \mathbf{E}_{hp, \text{far}} - \mathbf{E}_{\text{far}}\ $
				Err ₁	Err ₁	Err ₂	Err ₂
$p = 1$	1	648	972	1.87e-1	7.79e-1	2.38e-2	2.14e-1
$p = 2$	1	200	1000	6.68e-2	1.02e-1	3.90e-3	3.33e-2
$p = 3$	2	128	940	4.08e-2	1.08e-1	4.37e-3	4.25e-2
$p = 4$	2	72	1008	2.29e-2	6.52e-2	1.47e-3	1.34e-2

Figure 6.6.: Ship with $N = 926$ elements.

6.2.3. Ship

The boundary Γ of the ship shown in Figure 6.6 is given analytically by a triangular mesh. The mesh contains triangles with varying sizes, the minimal mesh size is $h_{\min} = 0.38$ m, the maximal mesh size is $h_{\max} = 7.67$ m. The exterior domain Ω^c is dielectric with ε_0 and μ_0 . The plane wave scattering is initiated by an incoming signal of the form

$$\mathbf{E}^i(\mathbf{x}, t) = \tilde{\mathbf{E}}^i(\mathbf{x})e^{-i\omega t} = e^{i(\boldsymbol{\kappa} \cdot \mathbf{x} - \omega t)} \mathbf{e},$$

where

$$\omega = 3.14 \cdot 10^8 \frac{1}{s}, \quad \boldsymbol{\kappa} = \left(-0.785 \frac{1}{m}, -0.453 \frac{1}{m}, -0.524 \frac{1}{m} \right)^\top, \quad \mathbf{e} = (-0.66, 0.436, 0.112)^\top.$$

Thus, the wave number and the wave length can be computed and we get

$$\begin{aligned} \kappa &= |\boldsymbol{\kappa}| = 1.047 \frac{1}{m}, \\ \lambda &= 6.0 \text{ m}. \end{aligned}$$

As usual, we omit the tilde and denote the complex valued amplitude of the plane wave by \mathbf{E}^i . Figure 6.7 shows as an example the first vector component, i.e., $(\mathbf{m}_{hp})_1 = \text{Re}(\mathbf{m}_{hp})_1 + i \text{Im}(\mathbf{m}_{hp})_1$ of the Dirichlet trace \mathbf{m}_{hp} which is obtained for $p = 4$. The length of the ship is 100 m such that about sixteen periods of the wave take place on Γ . Thus, this scattering problem is a high frequency problem.

As there is no analytical solution for the ship, a numerical solution computed by the commercial software package FEKO is used as a reference [32]. The reference solution is obtained on a triangular mesh with $N = 40072$ elements. The reference solution is computed by Nédélec elements of first kind with uniform order $p = 1$ which yields $N_{\mathcal{V}} = 60108$ unknowns. The high order boundary

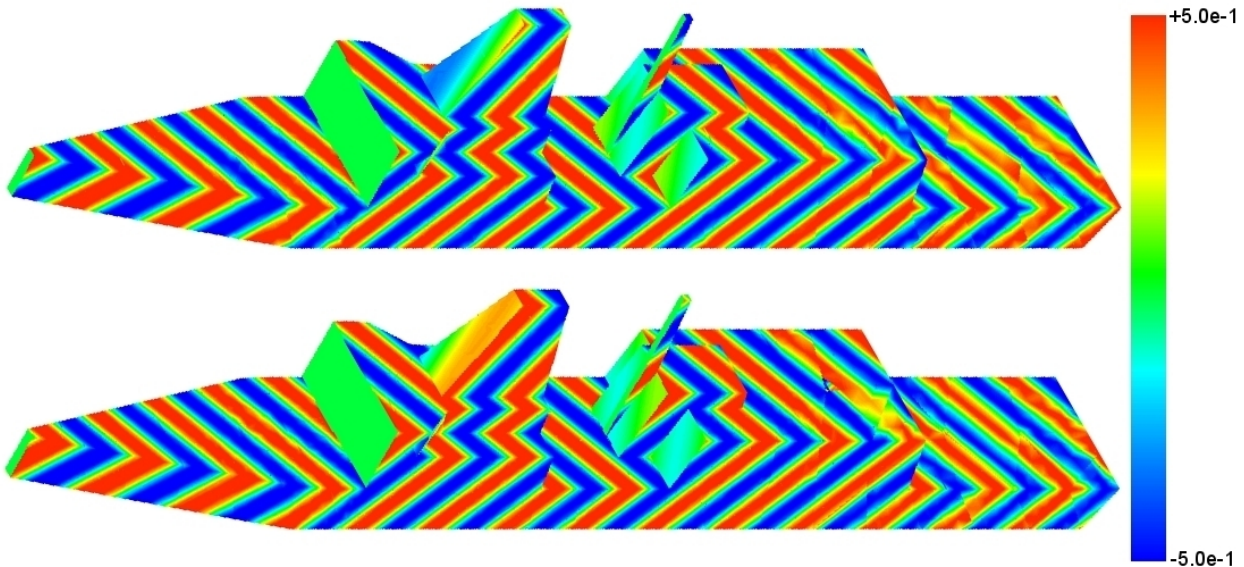
Figure 6.7.: Dirichlet data: Real part $\text{Re}(\mathbf{m}_{hp})_1$ on top, $\text{Im}(\mathbf{m}_{hp})_1$ below for $p = 4$.


Table 6.4.: Electromagnetic scattering at the ship geometry, Nédélec's first sequence.

	Order	Nédélec	N	N_V	$\ \mathbf{m}_{hp} - \mathbf{m}\ _{L^2(\Gamma)}$	$\text{Err}_2 \mathbf{E}_{\text{far}}$
reference solution	$p = 1$	1	40072	60108	—	—
	$p = 2$	1	3704	18520	1.21e-1	2.61e-1
	$p = 3$	1	926	9723	1.65e-1	2.88e-1
	$p = 4$	1	926	16668	5.02e-2	2.56e-1

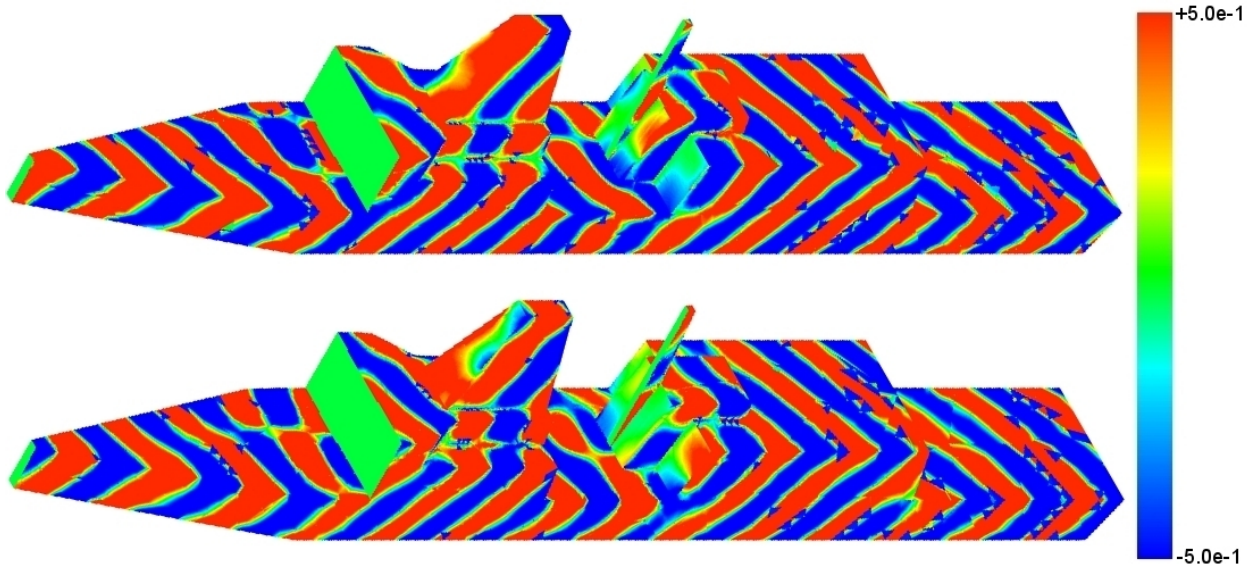
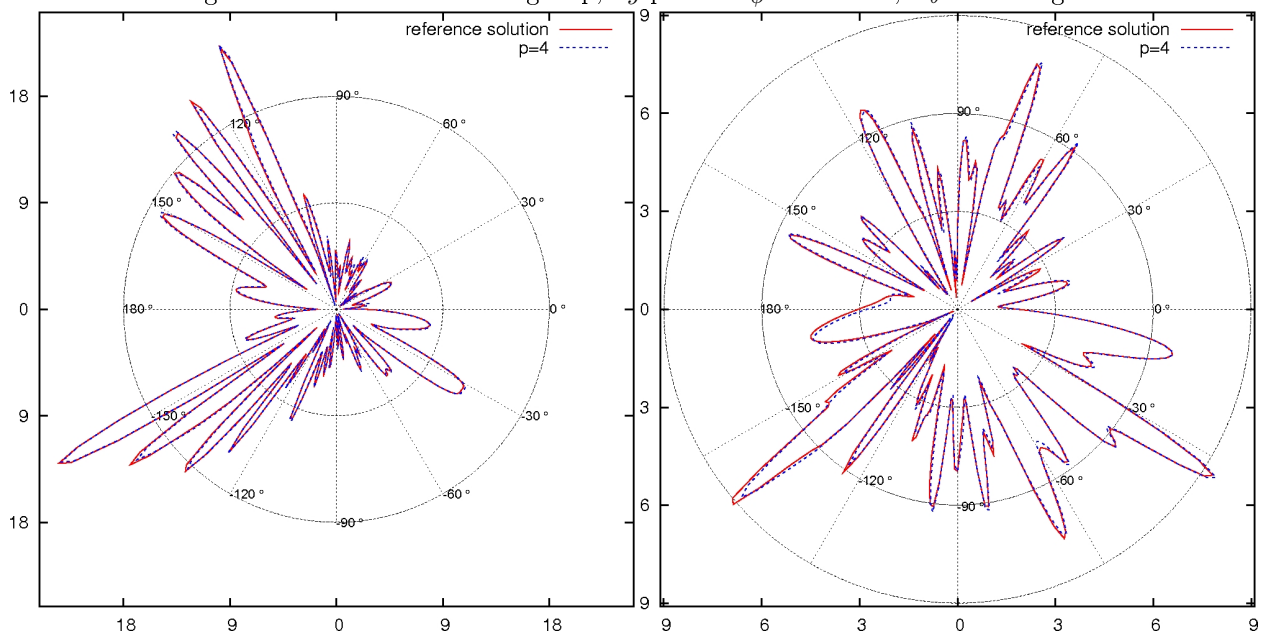
element method given by (6.7) is applied with varying orders of approximation, namely, from $p = 2$ to $p = 4$. The relative point-wise error of the far-field approximation $\mathbf{E}_{hp,\text{far}}$ is reported in the sixth column in Table 6.4. Note, that the reference solution itself is a numerical approximation of the exact solution, thus, the error listed in the Table 6.4 does not report on convergence towards the exact solution but it shows that all numerical solutions are close to each other. This is also seen by Figure 6.9 where the far-field approximation of the angular components E_θ and E_ϕ obtained by a scan in the xy -plane are plotted.

6.3. The Stabilized Formulation

In Section 5.3, theoretical considerations concerning the loss of the continuity equation

$$\kappa^2 \langle \gamma_n \mathbf{E}, \varphi \rangle = \langle \gamma_N \mathbf{E}, \nabla \varphi \rangle$$

for the limiting case $\kappa = 0$ lead to an alternative boundary element method as solution scheme for the scattering problem (6.1). The alternative method has been derived from the Picard system. It has been proved in Section 5.3, that the Picard system yields a uniquely solvable Galerkin method. Those are called the stabilized formulations. As far as theory is concerned, the classical and the

Figure 6.8.: Neumann data: $\text{Re}(\mathbf{j}_{hp}^t)_1$ on top, $\text{Im}(\mathbf{j}_{hp}^t)_1$ below for $p = 4$.Figure 6.9.: Far-field scattering ship, xy -plane: E_ϕ on the left, E_θ on the right

stabilized formulations are formally equivalent for all $\kappa > 0$. Thus, the necessity to derive a stabilized formulation comes from praxis. It is due to the fact that iterative solvers applied to (6.7) do not converge for small κ . The goal of this section is to demonstrate that this low frequency problem does not occur for the stabilized formulation. The focus of this section is therefore not the convergence analysis of the high order boundary element methods but the numerical robustness of the classical formulation versus the numerical robustness of the stabilized formulation with respect to $\kappa \rightarrow 0$.

Recall that the discretization of the stabilized formulation leads to

$$\mathbf{A}_s \boldsymbol{\alpha}_s = \boldsymbol{\beta}_s, \quad (6.11)$$

with

$$\mathbf{A}_s = \begin{pmatrix} \mathbf{A}_\kappa & \mathbf{Q}_\kappa \\ \mathbf{Q}_\kappa^\top & \kappa^2 \mathbf{V}_\kappa \end{pmatrix}, \quad \boldsymbol{\alpha}_s = \begin{pmatrix} \boldsymbol{\alpha}_1 \\ \boldsymbol{\alpha}_2 \end{pmatrix}, \quad \boldsymbol{\beta}_s = \begin{pmatrix} \mathbf{M}\boldsymbol{\beta} \\ \mathbf{0} \end{pmatrix}.$$

An appropriate norm to characterize the numerical solution $(\mathbf{j}_{hp}^t, \rho_{hp}^t)$ reads

$$\|(\mathbf{j}_{hp}^t, \rho_{hp}^t)\| = \left(\|\mathbf{j}_{hp}^t\|_{\mathbf{L}_t^2(\Gamma_{hp})}^2 + \|\operatorname{div}_\Gamma \mathbf{j}_{hp}^t\|_{L^2(\Gamma_{hp})}^2 + \|\rho_{hp}^t\|_{L^2(\Gamma_{hp})}^2 \right)^{\frac{1}{2}}. \quad (6.12)$$

As proved in Section 5.4 the system matrix \mathbf{A}_s is singular for $\kappa = 0$ and this means \mathbf{A}_s becomes ill conditioned for $\kappa \rightarrow 0$. The null-space has dimension one and this means that the set of singular values of \mathbf{A}_s

$$\operatorname{sing}(\mathbf{A}_s) = \{\sigma_1, \dots, \sigma_{N_V + N_Q}\}, \quad \text{with } \sigma_i \leq \sigma_{i+1} \text{ for } i = 1, \dots, N_V + N_Q - 1,$$

contains an isolated singular value σ_1 which converges to zero for $\kappa \rightarrow 0$ while all other singular values are uniformly bounded away from zero. Isolated singularities do not destroy the matrix properties in the sense that iterative solvers still converge. This is why one usually neglects the isolated singular values when computing the condition number. As \mathbf{A}_s must have an isolated singular value σ_1 , we define the essential condition number for \mathbf{A}_s by

$$\operatorname{cond}(\mathbf{A}_s) = \frac{\max_i \sigma_i}{\min_{i, i \neq 1} \sigma_i} = \frac{\sigma_{N_V + N_Q}}{\sigma_2}. \quad (6.13)$$

We call $\operatorname{cond}(\mathbf{A}_s)$ the essential condition number to indicate that the isolated singular value is left out.

As mentioned above, we aim to compare the properties of \mathbf{A}_s with the properties of \mathbf{A}_c from (6.7)

$$\mathbf{A}_c \boldsymbol{\alpha}_c = \boldsymbol{\beta}_c.$$

The set of singular values of \mathbf{A}_c

$$\operatorname{sing}(\mathbf{A}_c) = \{\sigma_1, \dots, \sigma_{N_V}\}, \quad \text{with } \sigma_i \leq \sigma_{i+1} \text{ for } i = 1, \dots, N_V - 1,$$

has no isolated singular values and thus, the condition number is defined by

$$\operatorname{cond}(\mathbf{A}_c) = \frac{\max_i \sigma_i}{\min_i \sigma_i} = \frac{\sigma_{N_V}}{\sigma_1}. \quad (6.14)$$

The numerical solution consists only of \mathbf{j}_{hp}^t and an appropriate energy norm reads

$$\|\mathbf{j}_{hp}^t\| = \left(\|\mathbf{j}_{hp}^t\|_{\mathbf{L}_t^2(\Gamma_{hp})}^2 + \|\operatorname{div}_\Gamma \mathbf{j}_{hp}^t\|_{L^2(\Gamma_{hp})}^2 \right)^{\frac{1}{2}}. \quad (6.15)$$

The scattering problem which is considered for the stability test is again the plane wave scattering from the unit sphere S^2 . The incoming harmonic signal is given by

$$\mathbf{E}^i(\mathbf{x}) = e^{-i\kappa x_3} \mathbf{e}_1.$$

and the material parameters of the exterior domain Ω^c are

$$\varepsilon = \varepsilon_0 = 8.854 \cdot 10^{-12} \frac{\text{As}}{\text{Vm}} \quad \text{and} \quad \mu = \mu_0 = 4\pi \cdot 10^{-7} \frac{\text{Vs}}{\text{Am}}.$$

Two test series are presented, the first for uniform order of approximation $p = 1$ and the second for uniform order of approximation $p = 4$. In both cases, we consider the isoparametric spheres S_{hp}^2 with $N = 128$ elements shown in Figure 6.2. Nédélec elements of first kind lead to the numbers of degrees of freedom $N_{\mathcal{V}}$ and $N_{\mathcal{Q}}$ specified in Table 6.5. The stability of the system matrices is analyzed for an exponential decrease of κ , as seen in the first row of Table 6.6. We start with $\kappa = 5.0 \frac{1}{\text{m}}$ and go down to $\kappa = 5.0 \cdot 10^{-4} \frac{1}{\text{m}}$. Moreover, all linear systems are solved with a direct solver from the linear algebra package LAPACK.

Table 6.5.: Number of degrees of freedom for the model problem.

N	p	$N_{\mathcal{V}}$	$N_{\mathcal{Q}}$
128	1	192	128
128	4	1792	768

The evaluation of the first test is reported in Table 6.6. The first column shows the decrease of the wave number κ . The second column contains the information on the relative errors of the Dirichlet trace \mathbf{m}_{hp} and the Neumann trace \mathbf{j}_{hp}^t . The input and output coincides for the classical and the stabilized method because a direct solver is used. In the third column of Table 6.6 the behavior of the classical method is shown. The energy norm (6.15) given on the left decreases by the same rate as the wave number κ . The condition number $\text{cond}(\mathbf{A}_c)$ of the system matrix shows an exponential increase depending on κ . This is the low frequency problem for the classical method. The set of singular values of \mathbf{A}_c is shown in Figure 6.10 for $\kappa = 5.0 \cdot 10^{-4} \frac{1}{\text{m}}$. Obviously, the singular values cluster in two pairs leading to the break-down of iterative solvers. The asymptotic increase of the condition number $\text{cond}(\mathbf{A}_c)$ for the complete test run is seen in Figure 6.11.

The corresponding results for the stabilized method are presented in the fourth column of Table 6.6. The energy norm (6.12) for the solution $(\mathbf{j}_{hp}^t, \rho_{hp}^t)$ is shown on the left and the comparison with the norm of the classical solution shows that the surface charge density ρ_{hp}^t contributes mostly. The block column entitled 'Matrix' shows the essential condition number of \mathbf{A}_s and the isolated singular value σ_1 . Most important is that the essential condition number stays constant with respect to $\kappa \rightarrow 0$. All singular values of the system matrix \mathbf{A}_c for $\kappa = 5.0 \cdot 10^{-4} \frac{1}{\text{m}}$ are plotted in Figure 6.10. The singular value σ_1 is isolated from the rest of the singular values as expected. The essential condition numbers $\text{cond}(\mathbf{A}_s)$ for the complete test run are shown in Figure 6.11. The essential condition numbers stays constant, in difference to the condition number of the classical system matrix.

An overview on the numerical tests for $p = 4$ is presented in Table 6.7. The same qualitative results show that the stabilized method is robust with respect to $\kappa \rightarrow 0$. The spectra of the system matrices for $\kappa = 5.0 \cdot 10^{-4} \frac{1}{\text{m}}$ are seen in Figure 6.12 and the condition numbers of the system matrices for all tests are plotted in Figure 6.13.

Figure 6.10.: All singular values of \mathbf{A}_c and \mathbf{A}_s for $p = 1$ and $\kappa = 5.0 \cdot 10^{-4} \frac{1}{m}$.

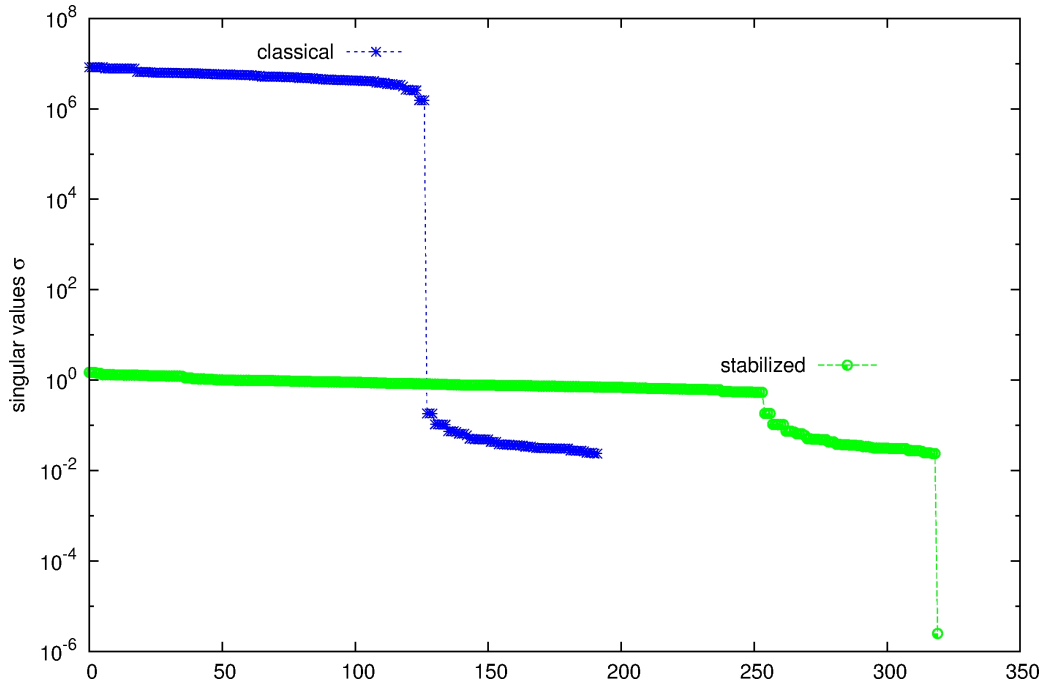


Figure 6.11.: Stability of system matrices \mathbf{A}_c vs. \mathbf{A}_s for $p = 1$.

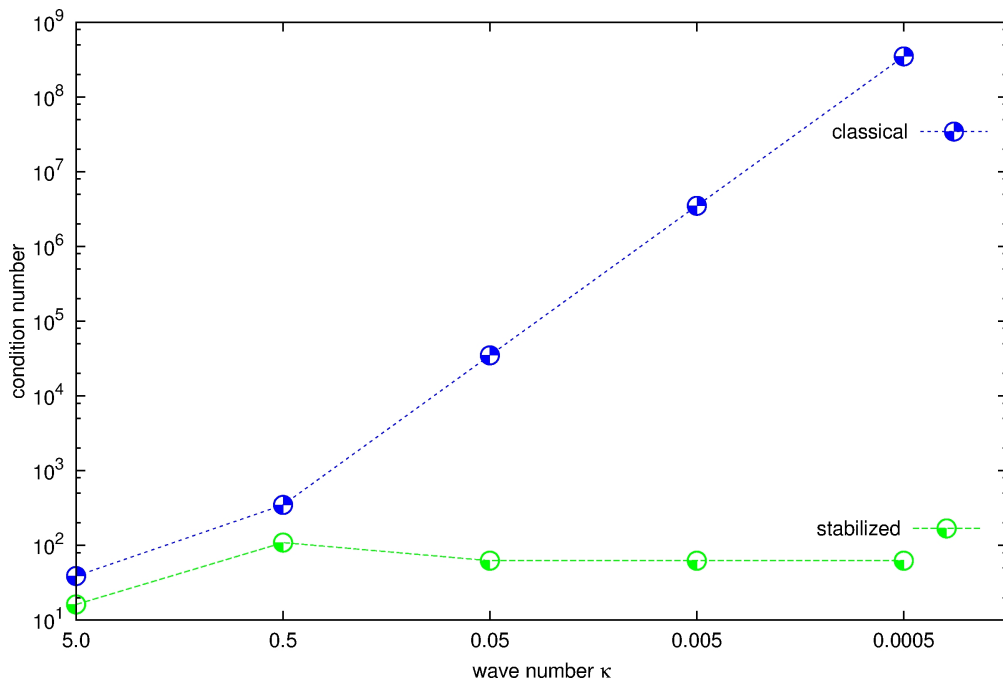


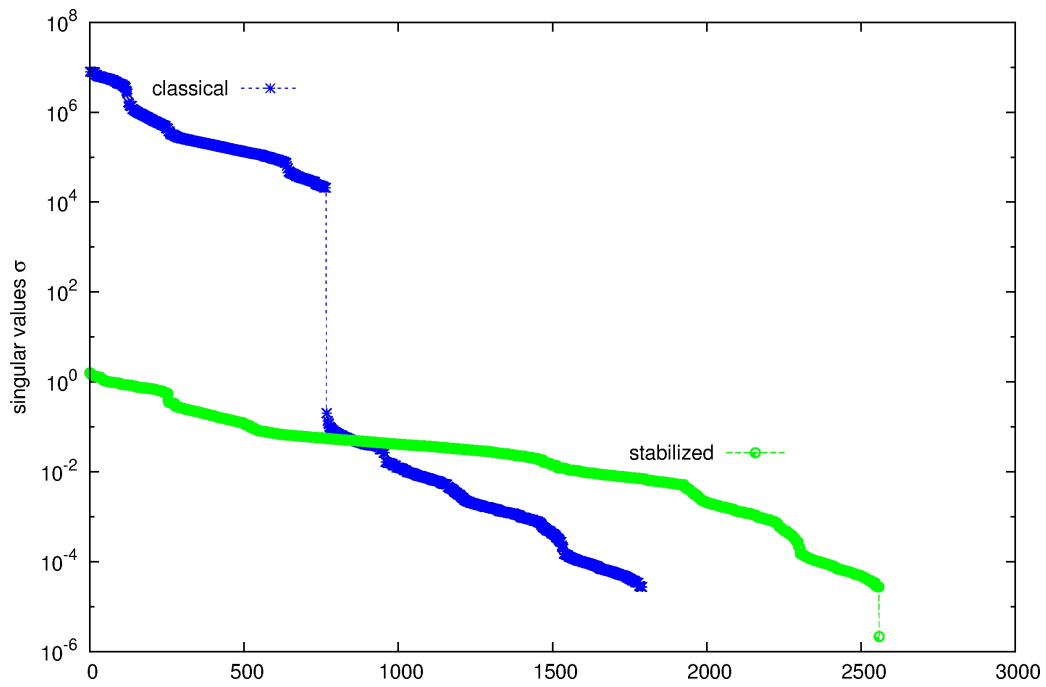
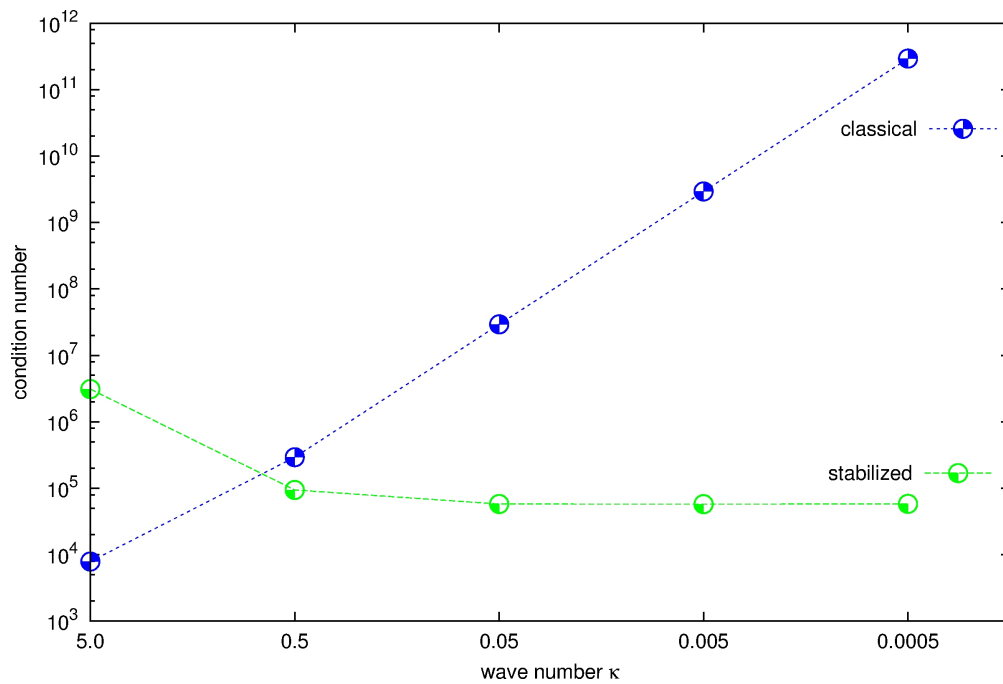
Figure 6.12.: All singular values of \mathbf{A}_c and \mathbf{A}_s for $p = 4$ and $\kappa = 5.0 \cdot 10^{-4} \frac{1}{m}$.Figure 6.13.: Stability of system matrices \mathbf{A}_c vs. \mathbf{A}_s for $p = 4$.

Table 6.6.: Stabilization for low frequencies on S_{hp}^2 with $N = 128$ and $p = 1$

$p = 1$	Err ₁	Err ₁	Classical (6.7)		Stabilized (6.11)		
			Energy Norm	Matrix	Energy Norm	Matrix	
$\kappa \left[\frac{1}{m} \right]$	\mathbf{m}_{hp}	\mathbf{j}_{hp}^t	\mathbf{j}_{hp}^t	cond(\mathbf{A}_c)	$(\mathbf{j}_{hp}^t, \rho_{hp}^t)$	cond(\mathbf{A}_s)	σ_1
5.0e-0	4.41e-1	5.10e-1	5.62e+1	3.9e+1	13.7	1.6e+1	3.5e-1
5.0e-1	1.54e-1	1.42e-1	0.16e+1	3.5e+2	4.82	1.1e+2	2.3e-2
5.0e-2	1.48e-1	1.60e-1	7.33e-2	3.5e+4	4.09	6.2e+1	2.4e-2
5.0e-3	1.48e-1	1.60e-1	7.34e-3	3.5e+6	4.09	6.2e+1	2.5e-4
5.0e-4	1.48e-1	1.60e-1	7.29e-4	3.5e+8	4.09	6.2e+1	2.5e-6

 Table 6.7.: Stabilization for low frequencies on S_{hp}^2 with $N = 128$ and $p = 4$

$p = 4$	Err ₁	Err ₁	Classical (6.7)		Stabilized (6.11)		
			Energy Norm	Matrix	Energy Norm	Matrix	
$\kappa \left[\frac{1}{m} \right]$	\mathbf{m}_{hp}	\mathbf{j}_{hp}^t	\mathbf{j}_{hp}^t	cond(\mathbf{A}_c)	$(\mathbf{j}_{hp}^t, \rho_{hp}^t)$	cond(\mathbf{A}_s)	σ_1
5.0e-0	8.19e-3	2.46e-2	4.83e+1	7.9e+3	18.0	3.1e+6	2.7e-3
5.0e-1	4.97e-4	5.33e-3	0.15e+1	2.9e+5	4.82	9.4e+4	2.7e-3
5.0e-2	4.51e-4	7.35e-3	7.16e-2	2.9e+7	4.00	5.8e+4	2.7e-3
5.0e-3	4.50e-4	1.40e-2	7.07e-3	2.9e+9	4.00	5.8e+4	2.7e-3
5.0e-4	4.50e-4	1.19e-1	7.07e-4	2.9e+11	4.00	5.8e+4	2.1e-4

6.4. Conclusion

The numerical tests presented here show that the theoretical results developed in Chapter 5 are of practical importance. The model problem to assess the stability and robustness of the boundary element implementation is the scattering of a plane wave at a perfectly conducting body. The key result is that our implementation offers stable numerical methods for all frequencies, except for interior resonances of the **curlcurl** operator or the Laplace operator. The high order elements are appropriate to solve high frequency problems whereas the stabilized formulation is robust in the low frequency regime.

To verify the asymptotic convergence of the Galerkin solution, the plane wave scattering at the unit sphere has been considered. The h -version of the classical high order boundary element method shows convergence of the Galerkin solution of order p when isoparametric elements of uniform order p are used. To obtain this result, it is essential that the geometrical error decreases faster than order p . This is either achieved by the use of the exact geometry or by a high order approximation of the geometry.

The efficiency of the high order boundary element methods are demonstrated by solving a high frequency problem proposed by our industrial partner EM Software & Systems GmbH, Böblingen, Germany. To obtain comparable far-field approximations of the scattered electric field, the high order boundary element methods needed less than a third of the unknowns than needed by the software package FEKO using linear edge elements.

In what concerns the numerical stability of the boundary element methods for low frequencies,

the condition numbers of the system matrices for the classical and the stabilized method have been compared. The condition number of the classical method blows up for low frequencies whereas the essential condition number characterizing the system matrix of the stabilized method stays constant. In accordance to the theoretical considerations concerning the stabilized method, there is only one isolated singular value which converges to zero and all other singular values are uniformly bounded away from zero. These algebraic properties are independent of the order of approximation and stay valid for uniform order $p = 1$ to $p = 4$.

The solver used for all numerical experiments shown in this chapter are standard direct solvers from the library LAPACK. Future research in this field is about the developing of appropriate preconditioner for the linear system and the use of iterative solvers.

SUMMARY

This thesis is a major contribution to the state of research in the field of boundary element methods in general and to the electromagnetic engineering sciences in particular. The first contribution is the development and implementation of high order boundary element methods. It is explained how to set up a high order boundary element implementation which provides solvers for elliptic, Maxwell and mixed problems. The second contribution is a complete mathematical theory for a stabilized boundary variational formulation describing scattering problems. The stabilized formulation presented in this thesis is equivalent to the classical formulations, however, it does not suffer from the low-frequency break-down. The high order methods have been applied to the classical and stabilized formulations describing electromagnetic scattering and the theoretical results on asymptotic convergence and stability have been verified by the numerical computations. A short review on how the discussion about these topics has been realized in the thesis is now given, followed by an outlook on future work.

The solutions of second order boundary value problems can be described by certain surface and volume potentials when a fundamental solution of the underlying partial differential equation is known. The mathematical background which is needed to analyze the mapping properties of these surface potentials is given in Chapter 2.

The scattering problems derived from the Maxwell equations belong to the class of problems which are solvable by the boundary element methods. The theory concerned with the classical formulation is presented in Chapter 3. Besides this, the stabilized formulation is developed. The lower the frequency of the incoming wave, the more important becomes the Gauß law because it recovers the quasi-electrostatic character of the electric scattered field. In terms of the boundary data this means, however, that one has to solve also for the normal trace of the electric field. This is achieved by the use of the stabilized formulation. A mathematical theory of the stabilized formulation is presented and the unique solvability of the boundary integral variational formulation is proved. Further, it is explained that the stabilized formulation turns into a saddle point problem describing an electrostatic potential in the limiting, electrostatic case.

Different from the classical boundary element formulation, the stabilized formulation belongs to the class of mixed problems. This means that different trace spaces are needed to formulate the variational formulation. By learning from the high order finite element methods, it is clear that the approximations of the different function spaces are not independent from each other. It is of fundamental importance to understand that the trace spaces are connected by surface differential operators. The simultaneous, high order approximation of the trace spaces relies on the construction of locally exact sequences. It is explained in Chapter 4 how to define finite-dimensional counterparts for the relevant trace spaces that may appear in boundary element formulations. A feature which is important for practical reasons is that our access allows for curvilinear element shapes.

In Chapter 5, the most important results on the numerical analysis of the high order boundary element methods describing the scattering problems are given. Besides the well-known results concerning the classical formulation, the stabilized formulation is analyzed and algebraic properties of the system matrices are discussed with the help of the electrostatic case.

Various numerical tests presented in Chapter 6 prove that the h -version of the high order boundary element methods converge quasi optimally. For the scattering problems, this means that convergence of order p is obtained provided isoparametric elements of uniform order p are used. To analyze the numerical robustness of the stabilized formulation, an exponential decrease of the wave number is considered and it is shown that the essential condition number of the system matrix stays constant.

The implementation provides all necessary tools to use the high order boundary element method with locally varying order of approximation and this feature will be tested and examined next.

Besides that, future work will focus on the automatic hp -adaptivity. To enable automatic hp -adaptivity, the projection-based interpolation operators are already equipped with more flexibility, i.e., the constrained approximation necessary for hanging nodes. Also, appropriate numerical integration schemes for the system matrices have been written and tested. In order to run the code in hp -adaptive mode, an appropriate automatic refinement strategy with optimal local error estimators must be developed furthermore.

Another question concerns the optimal compression algorithm for the system matrices. First tests show that the adaptive cross approximation is suitable for the high order boundary element methods. However, the built-in of more sophisticated solvers still needs to be done.

In what concerns theoretical topics, there will be ongoing research on the concept of biduality. The biduality has been a recurring theme throughout the thesis expressing a fundamental relation between the metric-free differential geometrical apparatus and the most basic duality pairings needed to apply the Hilbert space theory. The benefits of the consistent use of the biduality concept has become most obvious when writing down the explicit formulae for the system matrices of the boundary element method. It is most likely that a rewriting of all projection-based interpolation operators using the biduality concept brings insights that might clarify what needs to be done to render the de Rham diagrams commutative and to prove approximation theorems on curved surfaces.

CODE VERIFICATION

This chapter contains supplementary numerical results concerning the projection-based interpolation operators Π^1, Π^d and Π^0 from Subsection 4.2.4 and 4.2.5. Recall that the projection-based interpolation operators are essential to set up the hp -model, namely, to project the given boundary data into the parametric spaces and, also, to provide a high order mesh approximation. We focus on the high order mesh generation first.

The numerical results for plane wave scattering presented in Subsection 6.2.2 built up on the use of isoparametric elements. The starting point for the high order approximation of the unit sphere S^2 is an exact parametrization by spherical coordinates, for instance,

$$S^2 = \{\mathbf{x} = \mathbf{r}(\varphi, \theta), 0 \leq \varphi < 2\pi, 0 \leq \theta \leq \pi\}, \quad \mathbf{r}(\varphi, \theta) = \begin{pmatrix} \cos \varphi \sin \theta \\ \sin \varphi \sin \theta \\ \cos \theta \end{pmatrix}. \quad (\text{A.1})$$

Let S^2 be covered by a finite number of curvilinear triangles

$$S^2 = \bigcup_{i=1}^N \overline{S}_i, \quad S_i \cap S_j = \emptyset \text{ for } i \neq j,$$

with characteristic element size h . When p is specified, the projection-based interpolant $\Pi^1(\mathbf{u})$ with respect to this cover is computed. By this, an approximation S_{hp}^2 of S^2 is obtained such that each triangle S_i of the exact mesh is approximated by a parametric element (Γ_i, p) . The collection of the parametric elements covers S_{hp}^2 , i.e.,

$$S_{hp}^2 = \bigcup_{i=1}^N \overline{\Gamma}_i, \quad \Gamma_i \cap \Gamma_j = \emptyset \text{ for } i \neq j.$$

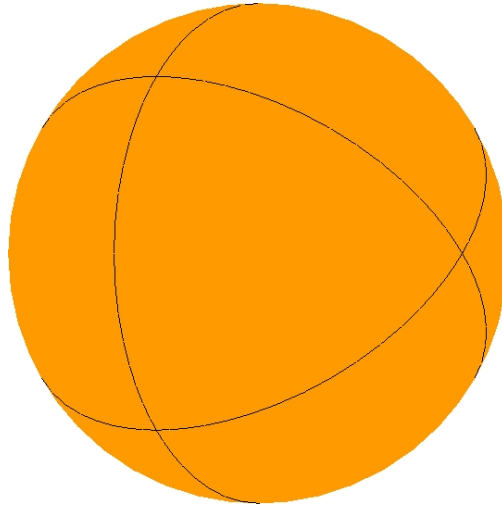
Clearly, the local parametrizations are polynomials of order p with domain \hat{T} , i.e.,

$$\hat{\mathbf{X}}_i: \hat{T} \rightarrow \Gamma_i, \quad i = 1, \dots, N.$$

The construction starts with a decomposition of the unit sphere in spherical octants shown in Figure A.1. The vertices, the edges and the interior of each octant is analytically given and, thus, the projection-based interpolation operator Π^1 of order p is applied to determine the polynomial approximation of each octant. For a uniform refinement of the sphere, each spherical octant gets divided into four smaller triangles, see Figure A.2. Again, the geometry of the subtriangles is analytically given and Π^1 is applied. The triangulations shown in Figure A.2 illustrate the approximations for the original geometry with $N = 8$ elements and two refinement steps for $p = 1$ and $p = 4$. The meshes on the right have $N = 128$ elements.

The convergence of the high order approximation of the sphere can be analyzed with respect to

Figure A.1.: Sphere divided in spherical octants.



the error

$$\text{Err}_3 = \left(\int_{S_{hp}^2} (|\Pi^1(\mathbf{r})(\mathbf{x})| - 1)^2 d\sigma_x \right)^{\frac{1}{2}} / \sqrt{4\pi}. \quad (\text{A.2})$$

The results reported in the third column of Table A.1 show that $\text{CF} = 2^{(p+1)}$ for uniform order of approximation p . The so-called convergence factor (CF) is computed by dividing the error Err_3 of the approximations obtained on subsequently refined meshes. The relation between the convergence factor and the convergence rate is $\text{CR} \approx \log_2 \text{CF}$. Thus, the geometrical error decreases by $\text{CR} = p + 1$ and this means, especially, that the convergence of a linear mesh with plane triangles towards the unit sphere is only quadratic, $\text{CR} = 2$.

Further, the operators Π^1, Π^d and Π^0 are tested on polynomials of arbitrary polynomial degree q on the isoparametric sphere S_{hp}^2 . As the parametrizations are non-linear mappings, it is clear that polynomials cannot be reproduced exactly. Let

$$\text{Err}_4 = \left(\int_{S_{hp}^2} |\Pi(f)(\mathbf{x}) - f(B(\mathbf{x}))|^2 d\sigma_x \right)^{\frac{1}{2}} / \left(\int_{S^2} |f(\mathbf{x})|^2 d\sigma_x \right)^{\frac{1}{2}}. \quad (\text{A.3})$$

where Π, f stands for one of the following pairs

$$\begin{aligned} \Pi &= \Pi^1 \text{ or } \Pi = \Pi^0, & f(\mathbf{x}) = u(\mathbf{x}) &= (x_1^2 + x_2^2)(x_1 - x_1^2)(x_2 - x_2^2) \in \mathcal{P}^6(\mathbb{R}^3), \\ \Pi &= \Pi^d, & f(\mathbf{x}) = \mathbf{u}(\mathbf{x}) &= (x_1^6, -x_2^6, 0)^\top \in \mathcal{P}^6(\mathbb{R}^3). \end{aligned}$$

The fourth to the sixth column of Table A.1 show the convergence rates for projection-based interpolation obtained by Π^1, Π^d and Π^0 with respect to uniform h -refinement. This means that the number of elements N are quadrupled and the convergence factor (CF) is computed by dividing the error Err_4 of the approximations obtained on subsequently refined meshes.

It is verified that Π^1 yields a convergence of order $p + 1$, whereas the convergence rate of Π^d and Π^0 is p . For these tests, Nédélec elements of first kind are used. Note, that the projection-based interpolation operators Π^d and Π^c are equivalent and there is no need to show the results explicitly for Π^c .

Figure A.2.: Uniform refinements of the sphere with $p = 1$ above and $p = 4$ below.

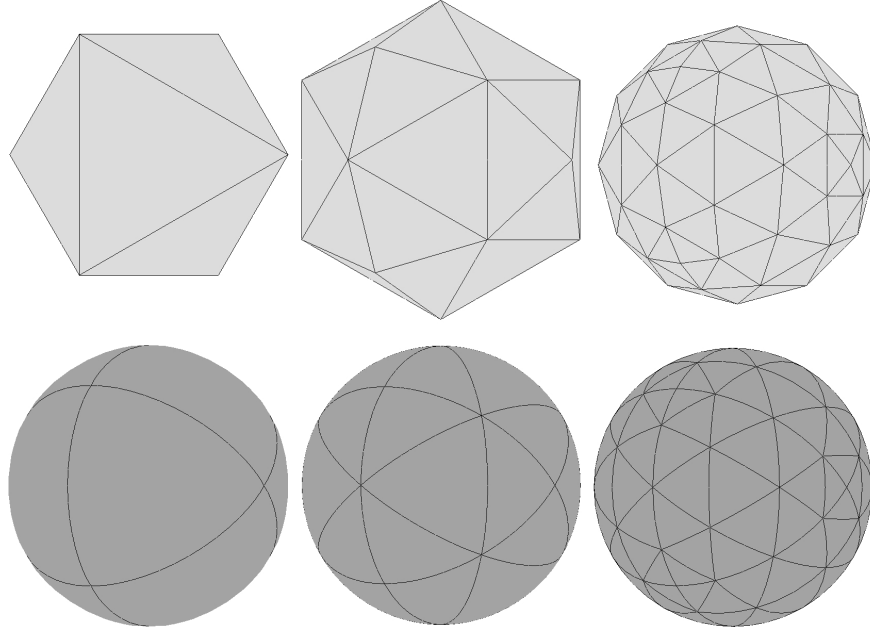


Table A.1.: Projection based interpolation by Π^1 , Π^d and Π^0

Order	N	S_{hp}^2		$\Pi^1(u) \in \mathcal{H}_h^p(S_{hp}^2)$		$\Pi^d(u) \in \mathcal{V}_h^{p-1}(S_{hp}^2)$		$\Pi^0(u) \in \mathcal{Q}_h^{p-2}(S_{hp}^2)$	
		Err ₃	CF	Err ₄	CF	Err ₄	CF	Err ₄	CF
$p = 1$	32	1.15e-1	–	4.98e-1	–	6.56e-1	–	5.37e-1	–
	128	3.20e-2	3.6	1.04e-1	4.8	4.33e-1	1.5	2.01e-1	2.7
	512	8.36e-3	3.8	2.61e-2	4.0	2.35e-1	1.8	1.12e-1	1.8
	2048	2.12e-3	3.9	6.54e-3	4.0	1.19e-1	2.0	5.62e-2	2.0
	8192	5.30e-4	4.0	1.64e-3	4.0	5.89e-2	2.0	2.82e-2	2.0
$p = 2$	32	1.14e-2	–	8.67e-2	–	4.03e-1	–	1.07e-1	–
	128	1.40e-3	8.1	1.31e-2	6.6	1.17e-1	3.4	4.74e-2	2.3
	512	1.68e-4	8.3	1.86e-3	7.0	3.10e-2	3.8	1.21e-2	3.9
	2048	2.06e-5	8.2	2.38e-4	7.8	7.90e-3	3.9	3.08e-3	3.9
	8192	2.56e-6	8.0	2.99e-4	8.0	1.98e-3	4.0	7.73e-4	4.0
$p = 3$	32	3.26e-3	–	2.92e-2	–	1.10e-1	–	5.68e-2	–
	128	2.05e-4	16	2.54e-3	12	2.53e-2	4.4	6.72e-3	8.5
	512	1.29e-5	16	1.65e-4	15	3.42e-3	7.4	9.75e-4	6.9
	2048	8.17e-7	16	1.06e-5	16	4.33e-4	7.9	1.24e-4	7.9
	8192	5.12e-8	16	6.65e-7	16	5.45e-5	7.9	1.56e-5	7.9
$p = 4$	32	4.66e-4	–	9.80e-3	–	5.90e-2	–	1.34e-2	–
	128	1.83e-5	26	3.52e-4	28	5.13e-3	12	1.34e-3	10
	512	6.74e-7	27	1.33e-5	27	3.56e-4	14	8.51e-4	16
	2048	2.13e-8	32	4.31e-7	31	2.35e-5	15	5.44e-6	16
	8192	6.69e-10	32	1.36e-8	32	1.47e-6	16	3.42e-7	16

MIE SERIES

The verification of numerical results builds up on reference solutions. A reference solution might be given by a commercial software as in case of the ship geometry from Subsection 6.2.3, or by an analytical solution. If no analytical solution is given, it is helpful to analyze some other characteristics of the solution and, then, to check if the numerical solution fulfills them. The scattered electromagnetic field for instance exhibits the characteristic behavior of a spherical wave far away from the scatterer. We derive the so-called far-field approximation for the scattered electric field. In the second part of this chapter, the analytical formulae for the Mie series are presented.

Let $\mathbf{E} : \Omega^c \rightarrow \mathbb{C}^3$ denote a solution of the following boundary value problem

$$\left\{ \begin{array}{ll} \mathbf{curl} \mathbf{curl} \mathbf{E} - \kappa^2 \mathbf{E} = \mathbf{0}, & \text{in } \Omega^c, \\ \gamma_D \mathbf{E} = \mathbf{m}, & \text{on } \Gamma, \\ \left| \mathbf{curl} \mathbf{E}(\mathbf{x}) \times \frac{\mathbf{x}}{|\mathbf{x}|} - i\omega\varepsilon \mathbf{E}(\mathbf{x}) \right| = \mathcal{O}\left(\frac{1}{|\mathbf{x}|^2}\right), & \text{for } |\mathbf{x}| \rightarrow \infty. \end{array} \right. \quad (\text{B.1})$$

Here, the wave number $\kappa > 0$ and the Dirichlet trace $\mathbf{m} = -\gamma_D \mathbf{E}^i$ is given by an incoming electrical signal \mathbf{E}^i . It has been shown in Subsection 3.2.1, (3.46) and (3.56), that \mathbf{E} at $\mathbf{x} \in \Omega^c$ can be represented by

$$\mathbf{E}(\mathbf{x}) = \int_{\Gamma} G_{\kappa}(\mathbf{x} - \mathbf{y}) \mathbf{j}^t(\mathbf{y}) d\sigma_y + \frac{1}{\kappa^2} \int_{\Gamma} \nabla_{\mathbf{x}} G_{\kappa}(\mathbf{x} - \mathbf{y}) \operatorname{div}_{\Gamma} \mathbf{j}^t(\mathbf{y}) d\sigma_y,$$

where the surface current density \mathbf{j}^t is the Neumann trace of the total field $\mathbf{E}^t = \mathbf{E} + \mathbf{E}^i$, i.e.,

$$\mathbf{j}^t = \gamma_N \mathbf{E}^t = \gamma_N (\mathbf{E} + \mathbf{E}^i).$$

Recall that for $\mathbf{x} \neq \mathbf{y}$

$$G_{\kappa}(\mathbf{x} - \mathbf{y}) = \frac{1}{4\pi} \frac{e^{-i\kappa|\mathbf{x}-\mathbf{y}|}}{|\mathbf{x} - \mathbf{y}|} \quad \text{and} \quad \nabla_{\mathbf{x}} G_{\kappa}(\mathbf{x} - \mathbf{y}) = G_{\kappa}(\mathbf{x} - \mathbf{y}) \left(-i\kappa - \frac{1}{|\mathbf{x} - \mathbf{y}|} \right) \frac{\mathbf{x} - \mathbf{y}}{|\mathbf{x} - \mathbf{y}|}.$$

Thus, it holds

$$\mathbf{E}(\mathbf{x}) = \int_{\Gamma} G_{\kappa}(\mathbf{x} - \mathbf{y}) \mathbf{j}^t(\mathbf{y}) d\sigma_y + \frac{1}{\kappa^2} \int_{\Gamma} G_{\kappa}(\mathbf{x} - \mathbf{y}) \left(-i\kappa - \frac{1}{|\mathbf{x} - \mathbf{y}|} \right) \frac{\mathbf{x} - \mathbf{y}}{|\mathbf{x} - \mathbf{y}|} \operatorname{div}_{\Gamma} \mathbf{j}^t(\mathbf{y}) d\sigma_y. \quad (\text{B.2})$$

We introduce the following notations for the spherical unit vectors

$$\mathbf{e}_r = \begin{pmatrix} \cos \varphi \sin \theta \\ \sin \varphi \sin \theta \\ \cos \theta \end{pmatrix}, \quad \mathbf{e}_{\varphi} = \begin{pmatrix} -\sin \varphi \\ \cos \varphi \\ 0 \end{pmatrix}, \quad \mathbf{e}_{\theta} = \begin{pmatrix} \cos \varphi \cos \theta \\ \sin \varphi \cos \theta \\ -\sin \theta \end{pmatrix}.$$

With $r = |\mathbf{x}|$ for $\mathbf{x} \in \Omega^c$ and $r' = |\mathbf{y}|$ for $\mathbf{y} \in \Gamma$, we rewrite $|\mathbf{x} - \mathbf{y}|$ for $r \rightarrow \infty$

$$\begin{aligned} |\mathbf{x} - \mathbf{y}| &= (r^2 + r'^2 - 2\mathbf{x} \cdot \mathbf{y})^{1/2} = r \left(1 + \frac{r'^2}{r^2} - \frac{2}{r} \mathbf{e}_r \cdot \mathbf{y} \right)^{1/2} \\ &= r \left(1 - \frac{2}{r} \mathbf{e}_r \cdot \mathbf{y} + \mathcal{O}\left(\frac{1}{r^2}\right) \right)^{1/2}, \end{aligned}$$

and for the reciprocal expression, one obtains

$$\frac{1}{|\mathbf{x} - \mathbf{y}|} = \frac{1}{r} \left(1 - \frac{2}{r} \mathbf{e}_r \cdot \mathbf{y} + \mathcal{O}\left(\frac{1}{r^2}\right) \right)^{-1/2}.$$

For $r \rightarrow \infty$, it holds further $\mathbf{e}_r \cdot \mathbf{y}/r \rightarrow 0$ for any $\mathbf{y} \in \Gamma$, and, therefore,

$$\left(1 - \frac{2}{r} \mathbf{e}_r \cdot \mathbf{y} + \mathcal{O}\left(\frac{1}{r^2}\right) \right)^{-1/2} = 1 + \frac{1}{r} \mathbf{e}_r \cdot \mathbf{y} + \mathcal{O}\left(\frac{1}{r^2}\right).$$

With respect to the limit $r \rightarrow \infty$, we can neglect all terms of higher order $\mathcal{O}(1/r^2)$ and obtain

$$\begin{aligned} |\mathbf{x} - \mathbf{y}| &\approx r \left(1 - \frac{1}{r} \mathbf{e}_r \cdot \mathbf{y} \right), \\ \frac{1}{|\mathbf{x} - \mathbf{y}|} &\approx \frac{1}{r} \left(1 + \frac{1}{r} \mathbf{e}_r \cdot \mathbf{y} \right) \approx \frac{1}{r}, \\ \frac{\mathbf{x} - \mathbf{y}}{|\mathbf{x} - \mathbf{y}|} &\approx \mathbf{e}_r - \frac{\mathbf{y}}{r}. \end{aligned}$$

Consequently, the asymptotic behavior of the oscillatory kernel for $r \rightarrow \infty$ is

$$\frac{e^{-i\kappa|\mathbf{x}-\mathbf{y}|}}{|\mathbf{x} - \mathbf{y}|} \approx \frac{1}{r} e^{-i\kappa r (1 - \frac{1}{r} \mathbf{e}_r \cdot \mathbf{y})} = \frac{e^{-i\kappa r}}{r} e^{i\kappa \mathbf{e}_r \cdot \mathbf{y}}.$$

The indirect representation formula (B.2) yields for $r \rightarrow \infty$ a spherical wave

$$\mathbf{E}(\mathbf{x}(r, \varphi, \theta)) \approx \frac{e^{-i\kappa r}}{\kappa r} \left(\frac{\kappa}{4\pi} \int_{\Gamma} e^{i\kappa \mathbf{e}_r \cdot \mathbf{y}} \mathbf{j}^t(\mathbf{y}) d\sigma_y - \frac{i}{4\pi} \mathbf{e}_r \int_{\Gamma} e^{i\kappa \mathbf{e}_r \cdot \mathbf{y}} \operatorname{div}_{\Gamma} \mathbf{j}^t(\mathbf{y}) d\sigma_y \right). \quad (\text{B.3})$$

The term in the brackets is the amplitude of the spherical wave. Obviously, the amplitude does not depend on r anymore but only on θ and φ . Note further, that the radial component of the scattered far-field vanishes for $r \rightarrow \infty$, as an integration by parts of the second integral in (B.3) yields

$$\begin{aligned} i \int_{\Gamma} e^{i\kappa \mathbf{e}_r \cdot \mathbf{y}} \operatorname{div}_{\Gamma} \mathbf{j}^t(\mathbf{y}) d\sigma_y &= -i \int_{\Gamma} \nabla_{\Gamma} (e^{i\kappa \mathbf{e}_r \cdot \mathbf{y}}) \cdot \mathbf{j}^t(\mathbf{y}) d\sigma_y \\ &= \kappa \int_{\Gamma} e^{i\kappa \mathbf{e}_r \cdot \mathbf{y}} \mathbf{e}_r \cdot \mathbf{j}^t(\mathbf{y}) d\sigma_y. \end{aligned} \quad (\text{B.4})$$

The far-field approximation \mathbf{E}_{far} is defined as follows

$$\mathbf{E}_{\text{far}}(\varphi, \theta) = \frac{1}{r} \frac{1}{4\pi} \int_{\Gamma} e^{i\kappa \mathbf{e}_r \cdot \mathbf{y}} \mathbf{j}^t(\mathbf{y}) d\sigma_y = E_{\text{far},\theta} \mathbf{e}_{\theta} + E_{\text{far},\varphi} \mathbf{e}_{\varphi},$$

with the angular components

$$E_{\text{far},\theta} = \frac{1}{r} \frac{1}{4\pi} \left(\int_{\Gamma} e^{i\kappa \mathbf{e}_r \cdot \mathbf{y}} \mathbf{j}^t(\mathbf{y}) d\sigma_{\mathbf{y}} \right) \cdot \mathbf{e}_{\theta} \quad \text{and} \quad E_{\text{far},\varphi} = \frac{1}{r} \frac{1}{4\pi} \left(\int_{\Gamma} e^{i\kappa \mathbf{e}_r \cdot \mathbf{y}} \mathbf{j}^t(\mathbf{y}) d\sigma_{\mathbf{y}} \right) \cdot \mathbf{e}_{\varphi}. \quad (\text{B.5})$$

One of the few problems in electromagnetic scattering which possess an analytical solution is the plane wave scattering at a perfectly conducting sphere. A detailed derivation of the Mie series is found in many textbooks. The formulae we outline here are proved in [4] and [34]. Let us assume that the electric field of a uniform plane wave is polarized in \mathbf{e}_1 direction and it is traveling along the \mathbf{e}_3 axis. The electric field of the incident wave reads

$$\mathbf{E}^i(\mathbf{x}) = e^{-i\kappa x_3} \mathbf{e}_1 = e^{-i\kappa r \cos \theta} \mathbf{e}_1.$$

In the following, we use

$$\hat{H}_n^{(2)}(\kappa r) = (\kappa r) h_n^{(2)}(\kappa r) \quad \text{and} \quad \hat{J}_n(\kappa r) = (\kappa r) j_n(\kappa r),$$

where $h_n^{(2)}$ denotes the n th spherical Hankel function of second kind, j_n the n th spherical Bessel function. Moreover, P_n^1 denotes the n th associated Legendre function. The radius a of the unit sphere S^2 is $a = 1$ and we define the coefficients for the Mie series

$$\begin{aligned} a_n &= i^{-n} \frac{(2n+1)}{n(n+1)}, \\ b_n &= -a_n \frac{\hat{J}'_n(a\kappa)}{\hat{H}_n^{(2)'}(a\kappa)} = -a_n \frac{\hat{J}'_n(\kappa)}{\hat{H}_n^{(2)'}(\kappa)}, \\ c_n &= -a_n \frac{\hat{J}_n(a\kappa)}{\hat{H}_n^{(2)}(a\kappa)} = -a_n \frac{\hat{J}_n(\kappa)}{\hat{H}_n^{(2)}(\kappa)}. \end{aligned}$$

The surface current $\mathbf{j}^t = \gamma_N \mathbf{E}^t$ of the total electric field $\mathbf{E}^t = \mathbf{E} + \mathbf{E}^i$ is given by infinite sums

$$\begin{aligned} \mathbf{j}^t \cdot \mathbf{e}_{\theta} = j_{\theta}^t &= \cos \varphi \sum_{n=1}^{\infty} a_n \left(\frac{\sin \theta \frac{\partial}{\partial(\cos \theta)} P_n^1(\cos \theta)}{\frac{\partial}{\partial \kappa} \hat{H}_n^{(2)}(\kappa)} + \frac{i P_n^1(\cos \theta)}{\sin \theta \hat{H}_n^{(2)}(\kappa)} \right), \\ \mathbf{j}^t \cdot \mathbf{e}_{\varphi} = j_{\varphi}^t &= \sin \varphi \sum_{n=1}^{\infty} a_n \left(\frac{P_n^1(\cos \theta)}{\sin \theta \frac{\partial}{\partial \kappa} \hat{H}_n^{(2)}(\kappa)} - \frac{\sin \theta \frac{\partial}{\partial(\cos \theta)} P_n^1(\cos \theta)}{i \hat{H}_n^{(2)}(\kappa)} \right). \end{aligned}$$

The analytical formulae for the evaluation of the scattered electric field at $\mathbf{x} = \mathbf{x}(r, \theta, \varphi) \in \Omega^c$ is given by

$$\mathbf{E} = E_r \mathbf{e}_r + E_{\theta} \mathbf{e}_{\theta} + E_{\varphi} \mathbf{e}_{\varphi}$$

with

$$\begin{aligned} E_r(r, \varphi, \theta) &= -i \cos \varphi \sum_{n=1}^{\infty} b_n \left(\frac{\partial^2}{\partial(\kappa r)^2} \hat{H}_n^{(2)}(\kappa r) + \hat{H}_n^{(2)}(\kappa r) \right) P_n^1(\cos \theta), \\ E_{\theta}(r, \varphi, \theta) &= \frac{1}{\kappa r} \cos \varphi \sum_{n=1}^{\infty} \left(i b_n \frac{\partial}{\partial(\kappa r)} \hat{H}_n^{(2)}(\kappa r) \sin \theta \frac{\partial}{\partial(\cos \theta)} P_n^1(\cos \theta) - c_n \hat{H}_n^{(2)}(\kappa r) \frac{P_n^1(\cos \theta)}{\sin \theta} \right), \\ E_{\varphi}(r, \varphi, \theta) &= \frac{1}{\kappa r} \sin \varphi \sum_{n=1}^{\infty} \left(i b_n \frac{\partial}{\partial(\kappa r)} \hat{H}_n^{(2)}(\kappa r) \frac{P_n^1(\cos \theta)}{\sin \theta} - c_n \hat{H}_n^{(2)}(\kappa r) \sin \theta \frac{\partial}{\partial(\cos \theta)} P_n^1(\cos \theta) \right). \end{aligned}$$

The angular components $E_{\text{far},\theta}$ and $E_{\text{far},\varphi}$ of the far-field approximation \mathbf{E}_{far} read

$$\begin{aligned} E_{\text{far},\theta}(\varphi, \theta) &= \frac{i \cos \varphi}{\kappa r} \sum_{n=1}^{\infty} i^n \left(b_n \sin \theta \frac{\partial}{\partial(\cos \theta)} P_n^1(\cos \theta) - c_n \frac{P_n^1(\cos \theta)}{\sin \theta} \right), \\ E_{\text{far},\varphi}(\varphi, \theta) &= \frac{i \sin \varphi}{\kappa r} \sum_{n=1}^{\infty} i^n \left(b_n \frac{P_n^1(\cos \theta)}{\sin \theta} - c_n \sin \theta \frac{\partial}{\partial(\cos \theta)} P_n^1(\cos \theta) \right). \end{aligned}$$

ELLIPTIC PROBLEMS

We aim to present in this chapter numerical results for the high order boundary element methods applied to an elliptic problem. In the context of the boundary element methods, elliptic operators allow for a systematic and general theory and the fundamentals of this theory are given in [44,52], for instance. Of major importance here is the fact that the theoretical results are valid for the high order schemes. Besides the well documented theory, one finds publications concerned with numerics of boundary element methods for elliptic problems. Of particular importance for our presentation is [51] because we are going to apply the high order methods on the model problem presented in Subsection 4.2.4 of [51].

The simplest example for a second order partial differential equation is the Laplace equation for a scalar function $u: \mathbb{R}^3 \rightarrow \mathbb{R}$ satisfying for $\mathbf{x} \in \Omega \subset \mathbb{R}^3$

$$-\Delta u(\mathbf{x}) = -\sum_{i=1}^3 \frac{\partial^2}{\partial x_i^2} u(\mathbf{x}) = 0. \quad (\text{C.1})$$

It is shown in [39] that the Laplace equation occurs, for instance, when modelling electrostatic potentials. We consider (C.1) together with Dirichlet boundary conditions, this means that the interior Dirichlet trace of the function u is given for $\mathbf{x} \in \Gamma = \partial\Omega$

$$m(\mathbf{x}) = \gamma_0 u(\mathbf{x}). \quad (\text{C.2})$$

Note, that the symbol γ_0 denotes the trace taken from inside of Ω on the boundary Γ .

Theorem C.0.1 *Let Ω be a Lipschitz domain. The boundary value problem (C.1)-(C.2) is for $m \in H^{\frac{1}{2}}(\Gamma)$ uniquely solvable with $u \in H^1(\Omega)$.*

The solution of the Dirichlet boundary value problem (C.1)-(C.2) can formally be represented at almost every $\mathbf{x} \in \Omega$ by

$$u(\mathbf{x}) = \int_{\Gamma} G_0(\mathbf{x} - \mathbf{y}) \gamma_1 u(\mathbf{y}) \, d\sigma_{\mathbf{y}} - \int_{\Gamma} \mathbf{n}(\mathbf{y}) \cdot \nabla_{\mathbf{y}} G_0(\mathbf{x} - \mathbf{y}) \gamma_0 u(\mathbf{y}) \, d\sigma_{\mathbf{y}}.$$

Thus, u is represented by two boundary integral operators. The first is called the single layer potential, it holds

$$S_0: H^{-\frac{1}{2}}(\Gamma) \rightarrow H^1(\Omega) \quad \text{with} \quad S_0(j) = \int_{\Gamma} G_0(\mathbf{x} - \mathbf{y}) j(\mathbf{y}) \, d\sigma_{\mathbf{y}},$$

where $G_0: \mathbb{R}^3 \setminus \{\mathbf{0}\} \rightarrow \mathbb{R}$ denotes the fundamental solution of the Laplace equation, namely,

$$G_0(\mathbf{x}) = \frac{1}{4\pi|\mathbf{x}|}.$$

The second integral operator is called the double layer potential

$$W_0: H^{\frac{1}{2}}(\Gamma) \rightarrow H^1(\Omega) \quad \text{with} \quad W_0(m) = \int_{\Gamma} \mathbf{n}(\mathbf{y}) \cdot \nabla_{\mathbf{y}} G_0(\mathbf{x} - \mathbf{y}) m(\mathbf{y}) \, d\sigma_{\mathbf{y}}.$$

Now and in the following, the interior Neumann trace is denoted $j = \gamma_1 u$. With these notations, we obtain for $\mathbf{x} \in \Omega$ the following direct representation formula

$$u(\mathbf{x}) = S_0(j)(\mathbf{x}) - W_0(m)(\mathbf{x}). \quad (\text{C.3})$$

A boundary integral equation for unknown Neumann trace j is formally obtained when the Dirichlet trace γ_0 is applied to (C.3), i.e.,

$$\gamma_0 u = \gamma_0 S_0(j) - \gamma_0 W_0(m). \quad (\text{C.4})$$

This boundary integral equation is, for instance, studied in [24, 52, 54].

Theorem C.0.2 *Due to the $H^{-\frac{1}{2}}(\Gamma)$ -ellipticity of the operator $\gamma_0 S_0: H^{-\frac{1}{2}}(\Gamma) \rightarrow H^{\frac{1}{2}}(\Gamma)$, (C.4) admits a unique solution $j \in H^{-\frac{1}{2}}(\Gamma)$ with*

$$\|j\|_{H^{-\frac{1}{2}}(\Gamma)} \leq c \|m\|_{H^{\frac{1}{2}}(\Gamma)}. \quad (\text{C.5})$$

The Neumann trace solves for all $\nu \in H^{-\frac{1}{2}}(\Gamma)$

$$\langle \nu, \gamma_0 S_0(j) \rangle_{\frac{1}{2}} = \langle \nu, m + \gamma_0 W_0(m) \rangle_{\frac{1}{2}}. \quad (\text{C.6})$$

To set up the hp -model, we consider a high order approximation Γ_{hp} of the exact boundary Γ and a high order approximation m_{hp} of the analytically given Dirichlet data m . Let $\{\phi_i\}_{i=1}^{N_{\mathcal{H}}}$ denote a basis of $\mathcal{H}_h^{\mathcal{P}}(\Gamma_{hp})$, then we obtain the latter by applying the projection-based interpolation operator Π^1 , i.e.,

$$m_{hp} = \Pi^1(m) = \sum_{i=1}^{N_{\mathcal{H}}} \beta_i \phi_i. \quad (\text{C.7})$$

Let $\{\nu_i\}_{i=1}^{N_{\mathcal{Q}}}$ denote the basis of $\mathcal{Q}_h^{p-2}(\Gamma_{hp})$, then the Galerkin ansatz for the discrete Neumann trace reads

$$j_{hp} = \sum_{i=1}^{N_{\mathcal{Q}}} \alpha_i \nu_i. \quad (\text{C.8})$$

Thus, the discretization of (C.6)

$$(\nu_i, \gamma_0 S_0(j_{hp}))_{\Gamma_{hp}} = (\nu_i, m_{hp} + \gamma_0 W_0(m_{hp}))_{\Gamma_{hp}} \quad \text{for all } i = 1, \dots, N_{\mathcal{Q}}, \quad (\text{C.9})$$

leads to a linear system of equations

$$\mathbf{S}\boldsymbol{\alpha} = (\mathbf{I} + \mathbf{W})\boldsymbol{\beta}, \quad \boldsymbol{\alpha} = (\alpha_1, \dots, \alpha_{N_{\mathcal{Q}}})^{\top}, \quad \boldsymbol{\beta} = (\beta_1, \dots, \beta_{N_{\mathcal{H}}})^{\top}, \quad (\text{C.10})$$

for the unknown coefficient vector $\boldsymbol{\alpha}$ from (C.8). The following result is proved in [52].

Theorem C.0.3 *Provided the exact solution j of the boundary integral equation (C.4) is more regular, namely, $j \in H^s(\Gamma)$ for $s \geq 0$. Then, the numerical solution $j_{hp} \in \mathcal{H}_h^{\mathcal{P}}(\Gamma_{hp})$ for a regular*

hp-mesh Γ_{hp} with isoparametric elements of uniform order p converges quasi-optimally with

$$\|j - j_{hp}\|_{H^{-\frac{1}{2}}(\Gamma)} \leq Ch^{\frac{1}{2} + \min(p+1, s)} \|j\|_{H^s(\Gamma)}, \quad (\text{C.11})$$

where C depends on the order of approximation p and the uniformity of the mesh.

We present now numerical results for the reference solution

$$u(\mathbf{x}) = (1 + x_1) \exp(2\pi x_2) \cos(2\pi x_3). \quad (\text{C.12})$$

Thus, the function u is an analytical solution for the Dirichlet boundary value problem

$$\begin{cases} -\Delta u(\mathbf{x}) = 0 & \text{in } \Omega, \\ m(\mathbf{x}) = \gamma_0 u(\mathbf{x}) & \text{on } \Gamma. \end{cases}$$

Note that the reference solution u is an exact solution for all geometrical approximations Γ_{hp} of Γ . Different from the Mie series analyzed in Chapter 5, there is no need to explicitly account for the approximation of the boundary Γ . A suitable error estimator to analyze the accuracy of input and output data reads

$$\text{Err}_5 = \frac{\|f_{hp} - f\|_{L^2(\Gamma_{hp})}}{\|f\|_{L^2(\Gamma_{hp})}}, \quad \text{where } f = m \text{ or } f = j. \quad (\text{C.13})$$

To check the accuracy of the numerical solution inside the unit ball Ω we use

$$\text{Err}_6 = \frac{1}{M} \sum_{i=1}^M |u_{hp}(\mathbf{x}_i) - u(\mathbf{x}_i)|, \quad (\text{C.14})$$

where $M = 360$ and the sample points \mathbf{x}_i are uniformly distributed on the slope

$$\mathbf{x}(t) = \begin{pmatrix} -0.3 \\ -0.5 \\ -0.7 \end{pmatrix} + t \begin{pmatrix} 0.6 \\ 1.0 \\ 1.4 \end{pmatrix}, \quad 0 \leq t \leq 1. \quad (\text{C.15})$$

The first test geometry is the unit sphere $\Gamma = S^2$ approximated by isoparametric elements of uniform order $p = 1$ up to $p = 4$. The result of the computations is shown in Table C.1. Each block row contains the convergence analysis with respect to uniform h -refinement. The number of boundary elements N , and the dimension $N_{\mathcal{H}}$ of the parametric space $\mathcal{H}_h^p(\Gamma_{hp})$ and the dimension $N_{\mathcal{Q}}$ of the parametric space $\mathcal{Q}^{p-2}(\Gamma_{hp})$ are listed in the first column. The convergence factor (CF) is computed by dividing the error of the numerical solutions on subsequently refined meshes. The results given in the columns three and four show that the Nédélec elements of first kind of order p yield a convergence factor $\text{CF} = 2^{(p+1)}$ for Dirichlet data m and $\text{CF} = 2^p$ for Neumann data j . This corresponds to the convergence rate $\text{CR} = p + 1$ for m and $\text{CR} = p$ for j , respectively.

In order to analyze the efficiency of the high order methods, we choose the isoparametric sphere with $p = 1$ with $N = 1152$ elements and compare the numerical solution with a computation performed on the isoparametric sphere with $p = 4$ and $N = 128$ elements. These *hp*-meshes yield comparable numbers of unknowns in $\mathcal{Q}_h^{p-2}(\Gamma_{hp})$ as seen in the third column of Table C.2. As reported by the fifth and the sixth column of Table C.2, the high order method performs better while the numerical costs are approximately the same. For a visual comparison, Figure C.1 contains plots of the exact solution u and the approximations for $p = 1$ and $p = 4$ on the slope (C.15).

Our second test geometry is the uniformly refined icoesaeder as approximation of the unit sphere S^2 . The result of the computations are shown in Table C.3. Each block row contains the con-

Table C.1.: Convergence analysis for interior Laplace problem, solution u from (C.12)

Isoparametric Sphere with Nédélec elements of first kind									
Order	N	$N_{\mathcal{H}}$	$N_{\mathcal{Q}}$	$\ m_{hp} - m\ $		$\ j_{hp} - j\ $		$\ u_{hp} - u\ $	
				Err ₅	CF	Err ₅	CF	Err ₆	CF
$p = 1$	32	18	32	5.13e-1	/	1.03e-1	/	2.17e+1	/
	128	66	128	2.65e-1	3.2	7.46e-1	1.4	0.26e+1	8.2
	512	258	512	7.58e-1	2.0	3.68e-1	2.0	5.04e-1	5.2
	2048	1026	2048	1.94e-2	3.8	1.75e-1	2.1	1.26e-1	4.0
$p = 2$	32	66	96	9.95e-1	/	6.87e-1	/	0.11e+1	/
	128	258	384	1.32e-1	7.5	2.22e-1	3.1	5.29e-1	2.0
	512	1026	1536	1.63e-2	8.0	9.62e-2	2.3	2.21e-2	24
	2048	4098	6144	2.05e-3	7.9	2.79e-2	3.4	1.42e-3	16
$p = 3$	32	146	192	3.15e-1	/	4.20e-1	/	0.24e+1	/
	128	578	768	2.32e-2	14	1.00e-2	4.2	1.55e-1	16
	512	2306	3072	1.98e-3	12	1.55e-2	6.5	1.87e-3	83
	2048	9218	12288	1.42e-4	14	1.92e-3	8.1	9.66e-5	19
$p = 4$	8	66	80	6.47e-1	/	6.66e-1	/	0.67e+1	/
	32	258	320	8.04e-1	8.0	2.46e-1	2.7	7.72e-2	87
	128	1026	1280	6.40e-3	13	2.57e-2	9.6	1.22e-2	6.3
	512	4098	5120	2.73e-4	23	2.40e-3	11	5.90e-5	207

Figure C.1.: Numerical results from Table C.2 for $p = 1, 4$ on slope (C.15).

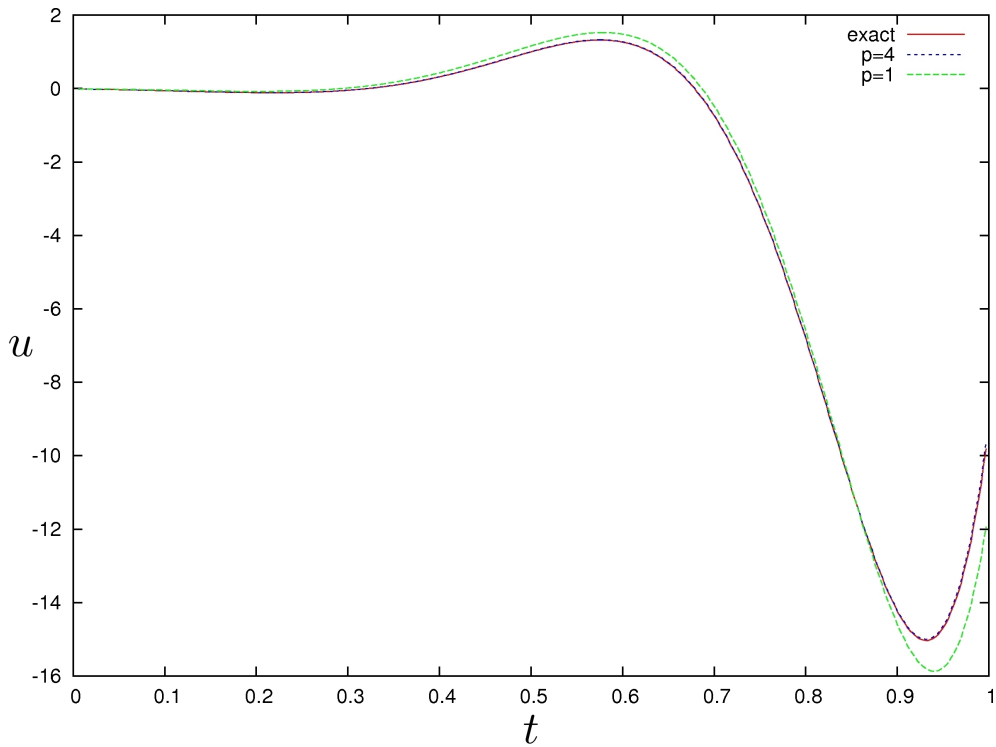


Table C.2.: Comparable degrees of freedom for the Laplace problem, direct formulation

Order	Nédélec	N	$N_{\mathcal{Q}}$	$\ m_{hp} - m\ $	$\ j_{hp} - j\ $	$\ u_{hp} - u\ $
				Err ₅	Err ₅	Err ₆
$p = 1$	1	1152	1152	5.78e-2	2.10e-1	2.25e-1
$p = 4$	1	128	1280	6.40e-3	2.56e-2	1.22e-2

Table C.3.: Direct single layer formulation for interior Laplace, solution u from (C.12)

Icosaeder with Nédélec elements of first kind									
Order	N	$N_{\mathcal{H}}$	$N_{\mathcal{Q}}$	$\ m_{hp} - m\ $		$\ j_{hp} - j\ $		$\ u_{hp} - u\ $	
				Err ₅	CF	Err ₅	CF	Err ₆	CF
$p = 1$	42	80	42	4.97e-1	/	9.86e-1	/	0.45e+1	/
	162	320	162	2.19e-1	2.3	4.95e-1	2.0	4.21e-1	11
	642	1280	642	6.08e-2	3.6	2.20e-1	2.3	1.02e-1	4.1
	2652	5120	2652	1.54e-2	3.9	1.04e-1	2.1	2.52e-2	4.0
$p = 2$	12	42	60	5.40e-1	/	9.91e-1	/	0.39e+1	/
	42	162	240	1.73e-1	3.1	3.44e-1	2.9	2.54e-1	15
	162	642	960	2.89e-2	6.0	1.17e-1	2.9	1.43e-2	18
	642	2652	3840	3.50e-3	8.3	3.63e-2	3.2	8.96e-4	16
$p = 3$	12	92	120	3.10e-1	/	5.11e-1	/	0.15e+1	/
	42	362	480	3.69e-2	4.5	1.23e-1	4.2	1.03e-1	14
	162	1442	1920	2.23e-3	17	1.81e-2	6.8	2.18e-3	47
	642	5726	7680	1.88e-4	12	2.33e-3	7.8	3.15e-5	69
$p = 4$	12	162	200	7.72e-2	/	2.50e-1	/	6.80e-1	/
	42	642	800	4.43e-3	17	2.63e-2	9.5	3.25e-3	209
	162	2562	3200	2.90e-4	15	1.93e-3	14	2.14e-4	15
	642	10242	12800	7.96e-6	36	1.46e-4	13	1.06e-6	202

vergence analysis for uniform h -refinement. The number of boundary elements, and the assigned dimensions of the parametric spaces $\mathcal{H}_h^{\mathcal{P}}(\Gamma_{hp})$ and $\mathcal{Q}^{p-2}(\Gamma_{hp})$ for Nédélec elements of first kind are listed in the first column. Again, Err₅ is used to estimate the relative error of the projection-based interpolation $m_{hp} = \Pi^1(m)$ and the numerical solution j_{hp} . Further, the point-wise absolute error Err₆ is considered to analyze the evaluation on the slope (C.15). The convergence factors reported by Table C.3 show the same qualitative behavior as for the isoparametric sphere. This was exhibited already because the function u is an analytical solution for all geometries and the low order approximation of the unit sphere does not pollute the error.

POLYNOMIAL EXACT SEQUENCES

For a multi index $\mathbf{p} = (p, p_1, p_2, p_3) \in \mathbb{N}^4$ we define

$$\begin{aligned} \mathcal{P}^{\mathbf{p}}(\hat{T}) &= \left\{ u \in \mathcal{P}^{\mathbf{p}}(\hat{T}) : u|_{\hat{e}_i} \in \mathcal{P}^{p_i}(\hat{e}_i), i = 1, 2, 3 \right\}, \\ \mathcal{P}^{\mathbf{p}}(\hat{T}) &= \left\{ \mathbf{u} \in \mathcal{P}^{\mathbf{p}}(\hat{T}), \mathbf{u} \cdot \hat{\boldsymbol{\tau}}_i \in \mathcal{P}^{p_i}(\hat{e}_i), i = 1, 2, 3 \right\}. \end{aligned}$$

The gradient and the scalar curl operator connect these polynomial spaces by the following exact sequence

$$\mathcal{P}^{\mathbf{p}}(\hat{T}) \xrightarrow{\nabla_{\Gamma}} \mathcal{P}^{\mathbf{p}-1}(\hat{T}) \xrightarrow{\text{curl}_{\Gamma}} \mathcal{P}^{\mathbf{p}-2}(\hat{T}). \quad (\text{D.1})$$

The construction of a particular basis for $\mathcal{P}^{\mathbf{p}}(\hat{T})$ presented in the following is due to Zaglmayr and Schöberl [53] and the pioneering work on this subject is due to Nédélec [46, 47]. It builds up on Legendre polynomials $\ell_p : [-1, 1] \rightarrow [-1, 1]$ of arbitrary order $p \geq 0$. The latter are defined by the following recurrence relation

$$\begin{aligned} \ell_0(t) &= 1, \\ \ell_1(t) &= t, \\ (k+1)\ell_{k+1}(t) &= (2k+1)t\ell_k(t) - k\ell_{k-1}(t), \quad 1 \leq k \leq p-1. \end{aligned}$$

The Legendre polynomials span the polynomial space $\mathcal{P}^p([-1, 1])$ and they are orthogonal with respect to the inner product of $L^2([-1, 1])$, this means

$$\forall l, k \in \mathbb{N}_0 : \int_{-1}^1 \ell_k(t)\ell_l(t) dt = \frac{2}{2k+1} \delta_{kl}.$$

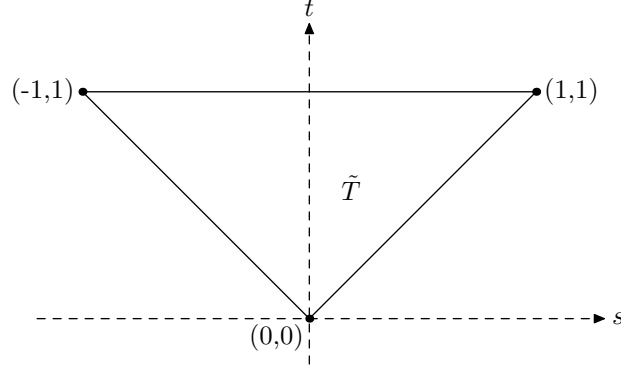
Furthermore, we need the triangular domain \tilde{T} plotted in Figure D.1

$$\tilde{T} = \{(s, t) \in \mathbb{R}^2, t > |s|, s \in (-1, 1), t \in (0, 1)\},$$

$$\partial\tilde{T} = e_1 \cup e_2 \cup e_3 = \{(s, 1) \in \mathbb{R}^2, s \in [-1, 1]\} \cup \{(1-s, 1-s), s \in (0, 1)\} \cup \{(-s, s), s \in (0, 1)\}.$$

The so-called scaled and integrated Legendre polynomials $L_k^S : \tilde{T} \rightarrow [-1, 1]$ of polynomial order $k \geq 2$ are given by the recurrence relation

$$\begin{aligned} L_2^S(s, t) &= \frac{1}{2}(s^2 - t^2), \\ L_3^S(s, t) &= \frac{1}{3}s(s^2 - t^2), \\ (k+1)L_{k+1}^S(s, t) &= (2k-1)sL_k^S(s, t) - (k-2)t^2L_{k-1}^S(s, t), \quad k \geq 3. \end{aligned}$$


 Figure D.1.: The triangular domain \tilde{T} .

The restriction of L_k^S to the horizontal edge e_1 , is denoted $L_k^S(\cdot, 1)$. It holds that $L_k^S(\cdot, 1) \in P_0^k([-1, 1])$ where the lower index means that the polynomials vanish at the vertices, i.e.,

$$L_k^S(-1, 1) = L_k^S(1, 1) = 0.$$

However, the restriction on the other two edges of \tilde{T} vanishes identically

$$\forall t \in (0, 1]: \quad L_k^S(-t, t) = L_k^S(1-t, 1-t) = 0.$$

Thus, the polynomials L_k^S vanish on all vertices of \tilde{T} and, thus, they are suited for the construction of high order shape functions on the reference triangle. By the use of the barycentric coordinates of the reference triangle $\lambda_i: \hat{T} \rightarrow (0, 1)$

$$\begin{aligned} \lambda_1(\boldsymbol{\xi}) &= 1 - (\xi_1 + \xi_2), \\ \lambda_2(\boldsymbol{\xi}) &= \xi_1, \\ \lambda_3(\boldsymbol{\xi}) &= \xi_2, \end{aligned}$$

we introduce three parametrizations of the domain \tilde{T}

$$(s(\boldsymbol{\xi}), t(\boldsymbol{\xi}))^{[n_1, n_2]} = (\lambda_{n_1}(\boldsymbol{\xi}) - \lambda_{n_2}(\boldsymbol{\xi}), \lambda_{n_1}(\boldsymbol{\xi}) + \lambda_{n_2}(\boldsymbol{\xi}))^\top,$$

where the double index refers to one of the midedge nodes of the reference triangle, i.e.,

$$\hat{a}_4 : n_1 = 1, n_2 = 2, \quad \hat{a}_5 : n_1 = 2, n_2 = 3, \quad \hat{a}_6 : n_1 = 3, n_2 = 1.$$

And we define

$$u_k^{[n_1, n_2]}(\boldsymbol{\xi}) = L_k^S((s, t)^{[n_1, n_2]}(\boldsymbol{\xi})), \quad k \geq 2.$$

The functions $u_k^{[n_1, n_2]}$ are polynomials of order $k \geq 2$ defined on \hat{T} . They are zero at all vertex nodes of the reference triangle \hat{T} . Moreover, the midedge node specified by the double index $[n_1, n_2]$ belongs to $u_k^{[n_1, n_2]}$ in the sense that $u_k^{[n_1, n_2]}$ also vanishes on the other two edges. Furthermore, we use the parametrization of the interval $[-1, 1]$ in terms of the barycentric coordinates

$$t: \hat{T} \rightarrow [-1, 1], \quad t(\boldsymbol{\xi}) = \lambda_3(\boldsymbol{\xi}) - \lambda_1(\boldsymbol{\xi}) - \lambda_2(\boldsymbol{\xi})$$

to define the polynomials

$$v_{k+1}^{[3]}(\boldsymbol{\xi}) : \hat{T} \rightarrow [-1, 1], \quad v_{k+1}^{[3]}(\boldsymbol{\xi}) = \lambda_3(\boldsymbol{\xi}) \ell_k(t(\boldsymbol{\xi})), \quad k \geq 0.$$

The functions $v_{k+1}^{[3]}$ are at least linear polynomials and vanish all on the edge with double index $[1, 2]$. The polynomials $u_k^{[n_1, n_2]}$ and $v_{k+1}^{[3]}$ are the so-called building blocks for the construction of the polynomial exact sequence (D.1). Let $\boldsymbol{p} = (p, p_1, p_2, p_3)$ be fixed with

$$p \geq 2 \quad \text{and} \quad 2 \leq p_i \leq p.$$

In the following it is described in detail how to construct hierarchical bases for the polynomial spaces $\mathcal{P}^{\boldsymbol{p}}(\hat{T})$, $\mathcal{P}^{p-1}(\hat{T})$ and $\mathcal{P}^{p-2}(\hat{T})$ of variable order $\boldsymbol{p} = (p, p_1, p_2, p_3)$. In each basis, the basis functions are ordered according to increasing polynomial degree. Each basis function is uniquely defined by two indices. The lower index k at the basis function coincides with its polynomial degree and the upper index i is a symbolic running index to distinguish functions of the same polynomial degree k . This notational convention is made explicit for some examples at the end of this chapter, see Table D.2.

The first shape functions to build up a basis for $\mathcal{P}^{\boldsymbol{p}}(\hat{T})$ are the linear polynomials

$$\begin{aligned} \hat{a}_1 : \quad \hat{\varphi}_1^1(\boldsymbol{\xi}) &= \lambda_1(\boldsymbol{\xi}) \\ \hat{a}_2 : \quad \hat{\varphi}_1^2(\boldsymbol{\xi}) &= \lambda_2(\boldsymbol{\xi}) \\ \hat{a}_3 : \quad \hat{\varphi}_1^3(\boldsymbol{\xi}) &= \lambda_3(\boldsymbol{\xi}). \end{aligned}$$

The functions $\hat{\varphi}_1^i$ are denoted vertex node shape functions because

$$\hat{\varphi}_1^i(\hat{\boldsymbol{v}}_j) = \delta_{ij}, \quad i, j = 1, 2, 3. \quad (\text{D.2})$$

If the polynomial degree of the edge nodes exceeds one, $1 < p_i \leq p$, we add polynomials of higher order. Hierarchical basis means that the choice of a of these polynomials is such that they vanish on all vertex nodes. The polynomials $u_k^{[n_1, n_2]}$ satisfy this requirement. We obtain the following construction rule for the midedge node shape functions

$$\begin{aligned} \hat{a}_4 : \quad \text{for } 2 \leq k \leq p_1 \quad \hat{\varphi}_k^1(\boldsymbol{\xi}) &= u_k^{[1, 2]}(\boldsymbol{\xi}), \\ \hat{a}_5 : \quad \text{for } 2 \leq k \leq p_2 \quad \hat{\varphi}_k^2(\boldsymbol{\xi}) &= u_k^{[2, 3]}(\boldsymbol{\xi}), \\ \hat{a}_6 : \quad \text{for } 2 \leq k \leq p_3 \quad \hat{\varphi}_k^3(\boldsymbol{\xi}) &= u_k^{[3, 1]}(\boldsymbol{\xi}). \end{aligned}$$

Whenever $p_i \geq 3$, the vertex node and midedge node shape functions alone do not span $\mathcal{P}^{\boldsymbol{p}}(\hat{T})$. Following the hierarchical construction principle, polynomials of degree $3 \leq k \leq p$ which vanish on all edges are added. Recall that the functions $v_{j+1}^{[3]}$ vanish on the horizontal edge e_1 . Thus, the middle node shape functions

$$\hat{a}_7 : \quad \text{for } 3 \leq k = l + j + 1 \leq p \quad \hat{\varphi}_k^i(\boldsymbol{\xi}) = u_l^{[1, 2]}(\boldsymbol{\xi}) v_{j+1}^{[3]}(\boldsymbol{\xi}), \quad j \geq 0, l \geq 2,$$

have the desired property. The set vertex, midedge and middle node functions is a basis of $\mathcal{P}^{\boldsymbol{p}}(\hat{T})$ and we call the basis functions the master element shape functions. Note, that the lower index k of an arbitrary master element shape functions refers to its polynomial degree. The running index $i = i(l, j)$ is necessary to distinguish master element shape functions of the same polynomial degree.

If $\boldsymbol{p} = (p, p, p, p)$ we say that the master element has uniform order p . This means, that the polynomial space $\mathcal{P}^{\boldsymbol{p}}(\hat{T})$ for uniform order $p = 3$ is spanned by the ten functions: the vertex node

shape functions

$$\begin{aligned}\hat{a}_1 : \quad \hat{\varphi}_1^1(\boldsymbol{\xi}) &= 1 - (\xi_1 + \xi_2), \\ \hat{a}_2 : \quad \hat{\varphi}_1^2(\boldsymbol{\xi}) &= \xi_1, \\ \hat{a}_3 : \quad \hat{\varphi}_1^3(\boldsymbol{\xi}) &= \xi_2,\end{aligned}$$

two midedge node shape function per edge

$$\begin{aligned}\hat{a}_4 : \quad \hat{\varphi}_2^1(\boldsymbol{\xi}) &= \frac{1}{2} \left((1 - 2\xi_1 - \xi_2)^2 - (1 - \xi_2)^2 \right), \\ \hat{\varphi}_3^1(\boldsymbol{\xi}) &= \frac{1}{2} (1 - 2\xi_1 - \xi_2) \left((1 - 2\xi_1 - \xi_2)^2 - (1 - \xi_2)^2 \right), \\ \hat{a}_5 : \quad \hat{\varphi}_2^2(\boldsymbol{\xi}) &= -2\xi_1\xi_2, \\ \hat{\varphi}_3^2(\boldsymbol{\xi}) &= -2\xi_1\xi_2(\xi_1 - \xi_2), \\ \hat{a}_6 : \quad \hat{\varphi}_2^3(\boldsymbol{\xi}) &= \frac{1}{2} \left((1 - 2\xi_2 - \xi_1)^2 - (1 - \xi_1)^2 \right), \\ \hat{\varphi}_3^3(\boldsymbol{\xi}) &= \frac{1}{2} (1 - 2\xi_2 - \xi_1) \left((1 - 2\xi_2 - \xi_1)^2 - (1 - \xi_1)^2 \right),\end{aligned}$$

and one middle node function

$$\hat{a}_7 \quad \hat{\varphi}_3^4(\boldsymbol{\xi}) = \frac{1}{2} \left((1 - 2\xi_1 - \xi_2)^2 - (1 - \xi_2)^2 \right) \xi_2.$$

Due to (D.1), high order elements for $\mathcal{P}^{p-1}(\hat{T})$ are given by differentiation for $p \geq 2$. The differentiation of the linear functions $\hat{\varphi}_1^k$ returns three linear dependent vector fields. However, one obtains a set of linear independent vector fields by

$$\begin{aligned}\hat{a}_4 : \quad \hat{\varphi}_0^1(\boldsymbol{\xi}) &= \nabla_{\Gamma} \lambda_1(\boldsymbol{\xi}) \lambda_2(\boldsymbol{\xi}) - \nabla_{\Gamma} \lambda_2(\boldsymbol{\xi}) \lambda_1(\boldsymbol{\xi}), \\ \hat{a}_5 : \quad \hat{\varphi}_0^2(\boldsymbol{\xi}) &= \nabla_{\Gamma} \lambda_2(\boldsymbol{\xi}) \lambda_3(\boldsymbol{\xi}) - \nabla_{\Gamma} \lambda_3(\boldsymbol{\xi}) \lambda_2(\boldsymbol{\xi}), \\ \hat{a}_6 : \quad \hat{\varphi}_0^3(\boldsymbol{\xi}) &= \nabla_{\Gamma} \lambda_3(\boldsymbol{\xi}) \lambda_1(\boldsymbol{\xi}) - \nabla_{\Gamma} \lambda_1(\boldsymbol{\xi}) \lambda_3(\boldsymbol{\xi}).\end{aligned}$$

These vector fields are called first order Nédélec elements. Different from our notational convention, the lower index is zero although the vector fields $\hat{\varphi}_0^k$ are linear vector fields. This is the only exception from our notational convention and it is used to emphasize that the construction of the first order Nédélec elements differs from the general construction principle. For $p_i \geq 2$, we obtain all midedge node shape vector fields by differentiation

$$\begin{aligned}\hat{a}_4 : \quad \text{for } 1 \leq k < p_1 \quad \hat{\varphi}_k^1(\boldsymbol{\xi}) &= \nabla_{\Gamma} \hat{\varphi}_{k+1}^1, \\ \hat{a}_5 : \quad \text{for } 1 \leq k < p_2 \quad \hat{\varphi}_k^2(\boldsymbol{\xi}) &= \nabla_{\Gamma} \hat{\varphi}_{k+1}^2, \\ \hat{a}_6 : \quad \text{for } 1 \leq k < p_3 \quad \hat{\varphi}_k^3(\boldsymbol{\xi}) &= \nabla_{\Gamma} \hat{\varphi}_{k+1}^3.\end{aligned}$$

Correspondingly, $p \geq 3$ yields middle node shape vector fields. However, as the gradient is not surjective on $\mathcal{P}^{p-1}(\hat{T})$, we have to add linear independent polynomial vector fields. Our construction is as follows

$$\begin{aligned}\hat{a}_7 : \quad \text{for } 2 \leq k = 2 + j < p \quad \hat{\varphi}_k^{i_1}(\boldsymbol{\xi}) &= \hat{\varphi}_0^1(\boldsymbol{\xi}) v_{j+1}^{[3]}(\boldsymbol{\xi}), \\ \text{for } 2 \leq k = l + j < p \quad \hat{\varphi}_k^{i_2}(\boldsymbol{\xi}) &= \nabla_{\Gamma} u_l^{[1,2]}(\boldsymbol{\xi}) v_{j+1}^{[3]}(\boldsymbol{\xi}) - u_l^{[1,2]}(\boldsymbol{\xi}) \nabla_{\Gamma} v_{j+1}^{[3]}(\boldsymbol{\xi}), \\ \text{for } 2 \leq k = l + j < p \quad \hat{\varphi}_k^{i_3}(\boldsymbol{\xi}) &= \nabla_{\Gamma} u_l^{[1,2]}(\boldsymbol{\xi}) v_{j+1}^{[3]}(\boldsymbol{\xi}) + u_l^{[1,2]}(\boldsymbol{\xi}) \nabla_{\Gamma} v_{j+1}^{[3]}(\boldsymbol{\xi}).\end{aligned}$$

The lower index k refers again to the polynomial degree of the vector fields and the upper indices i_1, i_2, i_3 are all running indices to distinguish the vector fields of the same polynomial order. In Table D.2, we use the shorter notations

$$\hat{\varphi}_k^{i_2}(\boldsymbol{\xi}) = \nabla_{\Gamma} \varphi_{k+1,-}^{i_2}(\boldsymbol{\xi}) \quad \text{and} \quad \hat{\varphi}_k^{i_3}(\boldsymbol{\xi}) = \nabla_{\Gamma} \varphi_{k+1}^{i_2}(\boldsymbol{\xi}).$$

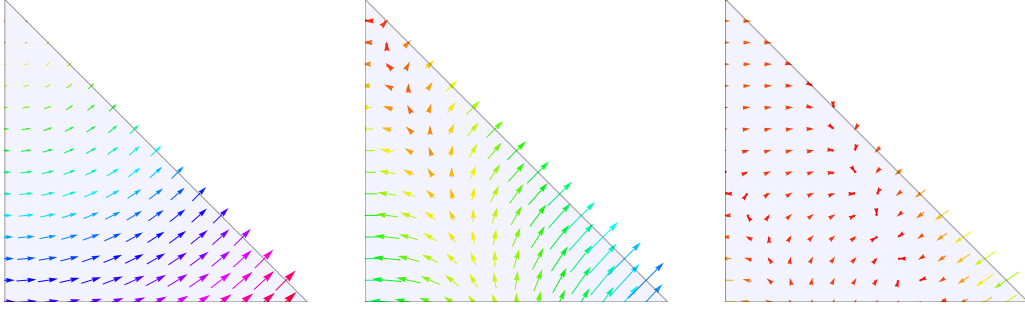


Figure D.2.: Vector fields $\hat{\varphi}_0^1, \hat{\varphi}_1^1, \hat{\varphi}_2^1$ for midedge node \hat{a}_4 .

The explicit formulae for shape vector fields for uniform order $p = 3$ comprise three vector fields per edge node

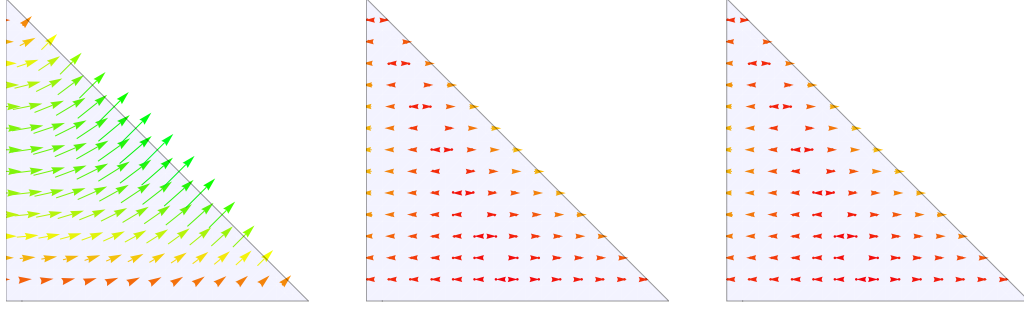
$$\begin{aligned} \hat{a}_4 : \hat{\varphi}_0^1(\boldsymbol{\xi}) &= (\xi_2 - 1, -\xi_1)^\top, \\ \hat{\varphi}_1^1(\boldsymbol{\xi}) &= (4\xi_1 + 2\xi_2 - 2, 2\xi_1)^\top, \\ \hat{\varphi}_2^1(\boldsymbol{\xi}) &= ((1 - \xi_2)^2 - 3(1 - 2\xi_1 - \xi_2)^2, -\frac{3}{2}(1 - 2\xi_1 - \xi_2)^2 + \frac{1}{2}(1 - \xi_2)(3 - 4\xi_1 - 3\xi_2))^\top, \\ \hat{a}_5 : \hat{\varphi}_0^2(\boldsymbol{\xi}) &= (\xi_2, -\xi_1)^\top, \\ \hat{\varphi}_1^2(\boldsymbol{\xi}) &= (-2\xi_2, -2\xi_1)^\top, \\ \hat{\varphi}_2^2(\boldsymbol{\xi}) &= (2\xi_2^2 - 4\xi_2\xi_1, -2\xi_1^2 + 4\xi_1\xi_2)^\top, \\ \hat{a}_6 : \hat{\varphi}_0^3(\boldsymbol{\xi}) &= (\xi_2, 1 - \xi_1)^\top, \\ \hat{\varphi}_1^3(\boldsymbol{\xi}) &= (4\xi_2 + 2\xi_1 - 2, 2\xi_2)^\top, \\ \hat{\varphi}_2^3(\boldsymbol{\xi}) &= ((1 - \xi_1)^2 - 3(1 - 2\xi_2 - \xi_1)^2, -\frac{3}{2}(1 - 2\xi_2 - \xi_1)^2 + \frac{1}{2}(1 - \xi_1)(3 - 4\xi_2 - 3\xi_1))^\top, \end{aligned}$$

and three vector fields attributed to the middle node

$$\begin{aligned} \hat{a}_7 : \hat{\varphi}_2^4(\boldsymbol{\xi}) &= \xi_2(\xi_2 - 1, -\xi_1)^\top, \\ \hat{\varphi}_2^5(\boldsymbol{\xi}) &= 2\xi_2(2\xi_1 + \xi_2 - 1, \xi_1)^\top - \frac{1}{2}((1 - 2\xi_1 - \xi_2)^2 - (1 - \xi_2)^2)(0, 1)^\top, \\ \hat{\varphi}_2^6(\boldsymbol{\xi}) &= 2\xi_2(2\xi_1 + \xi_2 - 1, \xi_1)^\top + \frac{1}{2}((1 - 2\xi_1 - \xi_2)^2 - (1 - \xi_2)^2)(0, 1)^\top. \end{aligned}$$

Note, that the first summand of the vector fields $\hat{\varphi}_2^5$ and $\hat{\varphi}_2^6$ coincides and that the contribution which is different is much smaller. This is the reason why the fields are not distinguishable in Figure D.3.

Due to the surjectivity of curl_{Γ} from $\mathcal{P}^{p-1}(\hat{T})$ on $\mathcal{P}^{p-2}(\hat{T})$, the construction principle for $\mathcal{P}^{p-2}(\hat{T})$


 Figure D.3.: Vector fields $\hat{\varphi}_2^4, \hat{\varphi}_2^5, \hat{\varphi}_2^6$ for middle node \hat{a}_7 .

is clear, i.e.,

$$\begin{aligned} \hat{a}_7 : \quad & p = 2 \quad \hat{v}_0(\boldsymbol{\xi}) = 1, \\ & 1 \leq k < p - 1 \quad \hat{v}_k^{i_1}(\boldsymbol{\xi}) = \text{curl}_\Gamma \hat{\varphi}_{k+1}^{i_1}(\boldsymbol{\xi}), \\ & 1 \leq k < p - 1 \quad \hat{v}_k^{i_2}(\boldsymbol{\xi}) = \text{curl}_\Gamma \hat{\varphi}_{k+1}^{i_2}(\boldsymbol{\xi}). \end{aligned}$$

Note, that $\hat{v}_0 = \text{curl}_\Gamma \hat{\varphi}_0^i = 1$ for all $i = 1, 2, 3$. For uniform $p = 3$ we obtain three master element shape functions

$$\begin{aligned} \hat{a}_7 : \quad & \hat{v}_0(\boldsymbol{\xi}) = 1, \\ & \hat{v}_1^1(\boldsymbol{\xi}) = 1 - 3\xi_2, \\ & \hat{v}_1^2(\boldsymbol{\xi}) = 4(1 - 2\xi_1 - \xi_2). \end{aligned}$$

All other vector basis fields are gradients and therefore they do not contribute to a basis for $\mathcal{P}^{p-2}(\hat{T})$.

Nédélec elements of first kind are another choice for the definition of the master element due to the following exact sequence for $\mathbf{p} = (p, p_1, p_2, p_3)$

$$\mathcal{P}^{\mathbf{p}}(\hat{T}) \xrightarrow{\nabla_\Gamma} \mathcal{P}^{\mathbf{p}-1}(\hat{T}) \oplus \tilde{\mathcal{P}}^{\tilde{\mathbf{p}}}(\hat{T}) \xrightarrow{\text{curl}_\Gamma} \mathcal{P}^{\mathbf{p}-1}(\hat{T}),$$

where

$$\begin{aligned} \mathbf{p} - \mathbf{1} &= (p - 1, p_1 - 1, p_2 - 1, p_3 - 1), \\ \tilde{\mathbf{p}} &= (p, p_1 - 1, p_2 - 1, p_3 - 1). \end{aligned}$$

This is an extension to the original sequence. The idea is to change the polynomial order of the vector shape functions by adding the midedge shape vector fields of order $p + 1$ which are not gradient fields. One has to leave the gradient fields out to keep the exact sequence property. For details on this, we refer to [27] and Table D.2.

Table D.1 lists the numbers of degrees of freedom which belong to variable order $\mathbf{p} = (p, p_1, p_2, p_3)$ for $p \geq 2$ in case of elements of first kind and $p \geq 1$ in case of elements of second kind. The variable order elements are crucial for automatic hp -refinement. The presented computations, however, are done with uniform order of approximation only.

Table D.2 contains an overview on the systematic built-up of high order shape functions, up to uniform order $p = 4$. Note that for elements of second type we listed in the first column of the table all lowest order elements, namely, the barycentric coordinates spanning $\mathcal{P}^1(\hat{T})$, the linear Nédélec elements spanning a subspace of $\mathcal{P}^1(\hat{T})$ and the constant function spanning $\mathcal{P}^0(\hat{T})$. This reflects the feature of the implementation to employ for uniform order $p = 1$ always the lowest order sequence

Table D.1.: Variable order of approximation and corresponding number of degrees of freedom.

Nédélec elements of second kind for $\mathbf{p} = (p, p_1, p_2, p_3)$, $p \geq 2$			
Number of element degrees of freedom			
Node	$\mathcal{P}^{\mathbf{p}}(\hat{T})$	$\mathcal{P}^{\mathbf{p}-1}(\hat{T})$	$\mathcal{P}^{\mathbf{p}-2}(\hat{T})$
\hat{a}_1	1	—	—
\hat{a}_2	1	—	—
\hat{a}_3	1	—	—
\hat{a}_4	$p_1 - 1$	p_1	—
\hat{a}_5	$p_2 - 1$	p_2	—
\hat{a}_6	$p_3 - 1$	p_3	—
\hat{a}_7	$(p-2)(p-1)/2$	$p(p-2)$	$(p-1)p/2$
# d.o.f.	$3 + \sum_{i=1}^3 (p_i - 1) + (p-2)(p-1)/2$	$\sum_{i=1}^3 p_i + p(p-2)$	$(p-1)p/2$

Nédélec elements of first kind for $\mathbf{p} = (p, p_1, p_2, p_3)$, $p \geq 1$			
Number of element degrees of freedom			
Node	$\mathcal{P}^{\mathbf{p}}(\hat{T})$	$\mathcal{P}^{\mathbf{p}-1}(\hat{T}) \oplus \tilde{\mathcal{P}}^{\mathbf{p}}(\hat{T})$	$\mathcal{P}^{\mathbf{p}-1}(\hat{T})$
\hat{a}_1	1	—	—
\hat{a}_2	1	—	—
\hat{a}_3	1	—	—
\hat{a}_4	$p_1 - 1$	p_1	—
\hat{a}_5	$p_2 - 1$	p_2	—
\hat{a}_6	$p_3 - 1$	p_3	—
\hat{a}_7	$(p-2)(p-1)/2$	$p(p-1)$	$(p+1)p/2$
# d.o.f.	$3 + \sum_{i=1}^3 (p_i - 1) + (p-2)(p-1)/2$	$\sum_{i=1}^3 p_i + p(p-1)$	$(p+1)p/2$

for both element types.

We close this chapter with some concluding remarks. The sets of polynomial functions comprise obviously linear independent functions and by counting the number of linear independent functions it is also clear that we obtain a complete sets of basis functions [46]. The polynomial spaces presented here possess a hierarchical structure and this hierarchical structure is used in Subsection 4.2.4 to construct projection-based interpolation operators, i.e., the dual basis, to solve approximation problems on the master element or, as it is shown in Chapter 5 on the parametric element.

Table D.2.: Elements of second type above, and elements of first type below.

		$p = 1$	$p = 2$	$p = 3$	$p = 4$
\mathcal{P}^p	Vertices	$\hat{\varphi}_1^1 = \lambda_1$ $\hat{\varphi}_1^2 = \lambda_2$ $\hat{\varphi}_1^3 = \lambda_3$			
	Midedge		$\hat{\varphi}_2^1 = u_2^{[1,2]}$ $\hat{\varphi}_2^2 = u_2^{[2,3]}$ $\hat{\varphi}_2^3 = u_2^{[3,1]}$	$\hat{\varphi}_3^1 = u_3^{[1,2]}$ $\hat{\varphi}_3^2 = u_3^{[2,3]}$ $\hat{\varphi}_3^3 = u_3^{[3,1]}$	$\hat{\varphi}_4^1 = u_2^{[1,2]}$ $\hat{\varphi}_4^2 = u_2^{[2,3]}$ $\hat{\varphi}_4^3 = u_2^{[3,1]}$
	Middle			$\hat{\varphi}_3^4 = u_2^{[1,2]}v_1^{[3]}$	$\hat{\varphi}_4^4 = u_3^{[1,2]}v_1^{[3]}$ $\hat{\varphi}_4^5 = u_2^{[1,2]}v_2^{[3]}$
\mathcal{P}^{p-1}	Midedge	$\hat{\varphi}_0^1$ $\hat{\varphi}_0^2$ $\hat{\varphi}_0^3$	$\hat{\varphi}_1^1 = \nabla_\Gamma \hat{\varphi}_2^1$ $\hat{\varphi}_1^2 = \nabla_\Gamma \hat{\varphi}_2^2$ $\hat{\varphi}_1^3 = \nabla_\Gamma \hat{\varphi}_2^3$	$\hat{\varphi}_2^1 = \nabla_\Gamma \hat{\varphi}_3^1$ $\hat{\varphi}_2^2 = \nabla_\Gamma \hat{\varphi}_3^2$ $\hat{\varphi}_2^3 = \nabla_\Gamma \hat{\varphi}_3^3$	$\hat{\varphi}_3^1 = \nabla_\Gamma \hat{\varphi}_4^1$ $\hat{\varphi}_3^2 = \nabla_\Gamma \hat{\varphi}_4^2$ $\hat{\varphi}_3^3 = \nabla_\Gamma \hat{\varphi}_4^3$
	Middle			$\hat{\varphi}_2^4 = \hat{\varphi}_0^1 v_1^{[3]}$ $\hat{\varphi}_2^5 = \nabla_\Gamma \hat{\varphi}_3^4$ $\hat{\varphi}_2^6 = \nabla_\Gamma \hat{\varphi}_3^4$	$\hat{\varphi}_3^4 = \hat{\varphi}_0^1 v_2^{[3]}$ $\hat{\varphi}_3^5 = \nabla_\Gamma \hat{\varphi}_4^4$ $\hat{\varphi}_3^6 = \nabla_\Gamma \hat{\varphi}_4^5$ $\hat{\varphi}_3^7 = \nabla_\Gamma \hat{\varphi}_4^4$ $\hat{\varphi}_3^8 = \nabla_\Gamma \hat{\varphi}_4^5$
\mathcal{P}^{p-2}	Middle	$\hat{v}_0 = 1$		$\hat{v}_1^1 = \text{curl}_\Gamma \hat{\varphi}_2^4$ $\hat{v}_1^2 = \text{curl}_\Gamma \hat{\varphi}_2^5$	$\hat{v}_2^1 = \text{curl}_\Gamma \hat{\varphi}_3^4$ $\hat{v}_2^2 = \text{curl}_\Gamma \hat{\varphi}_3^5$ $\hat{v}_2^3 = \text{curl}_\Gamma \hat{\varphi}_3^7$
\mathcal{P}^p	Vertices	$\hat{\varphi}_1^1 = \lambda_1$ $\hat{\varphi}_1^2 = \lambda_2$ $\hat{\varphi}_1^3 = \lambda_3$			
	Midedge		$\hat{\varphi}_2^1 = u_2^{[1,2]}$ $\hat{\varphi}_2^2 = u_2^{[2,3]}$ $\hat{\varphi}_2^3 = u_2^{[3,1]}$	$\hat{\varphi}_3^1 = u_3^{[1,2]}$ $\hat{\varphi}_3^2 = u_3^{[2,3]}$ $\hat{\varphi}_3^3 = u_3^{[3,1]}$	$\hat{\varphi}_4^1 = u_2^{[1,2]}$ $\hat{\varphi}_4^2 = u_2^{[2,3]}$ $\hat{\varphi}_4^3 = u_2^{[3,1]}$
	Middle			$\hat{\varphi}_3^4 = u_2^{[1,2]}v_1^{[3]}$	$\hat{\varphi}_4^4 = u_3^{[1,2]}v_1^{[3]}$ $\hat{\varphi}_4^5 = u_2^{[1,2]}v_2^{[3]}$
$\mathcal{P}^{p-1} \oplus \mathcal{P}^{\tilde{p}}$	Midedge	$\hat{\varphi}_0^1$ $\hat{\varphi}_0^2$ $\hat{\varphi}_0^3$	$\hat{\varphi}_1^1 = \nabla_\Gamma \hat{\varphi}_2^1$ $\hat{\varphi}_1^2 = \nabla_\Gamma \hat{\varphi}_2^2$ $\hat{\varphi}_1^3 = \nabla_\Gamma \hat{\varphi}_2^3$	$\hat{\varphi}_2^3 = \nabla_\Gamma \hat{\varphi}_3^1$ $\hat{\varphi}_2^4 = \nabla_\Gamma \hat{\varphi}_3^2$ $\hat{\varphi}_2^5 = \nabla_\Gamma \hat{\varphi}_3^3$	$\hat{\varphi}_3^4 = \nabla_\Gamma \hat{\varphi}_4^1$ $\hat{\varphi}_3^5 = \nabla_\Gamma \hat{\varphi}_4^2$ $\hat{\varphi}_3^6 = \nabla_\Gamma \hat{\varphi}_4^3$
	Middle		$\hat{\varphi}_2^1 = \hat{\varphi}_0^1 v_1^{[3]}$ $\hat{\varphi}_2^2 = \nabla_\Gamma \hat{\varphi}_3^4$	$\hat{\varphi}_3^6 = \nabla_\Gamma \hat{\varphi}_3^4$ $\hat{\varphi}_3^1 = \hat{\varphi}_0^1 v_2^{[3]}$ $\hat{\varphi}_3^2 = \nabla_\Gamma \hat{\varphi}_4^4$ $\hat{\varphi}_3^3 = \nabla_\Gamma \hat{\varphi}_4^5$ $\hat{\varphi}_3^4 = \nabla_\Gamma \hat{\varphi}_4^6$	$\hat{\varphi}_4^7 = \nabla_\Gamma \hat{\varphi}_4^4$ $\hat{\varphi}_4^8 = \nabla_\Gamma \hat{\varphi}_4^5$ $\hat{\varphi}_4^1 = \hat{\varphi}_0^1 v_3^{[3]}$ $\hat{\varphi}_4^2 = \nabla_\Gamma \hat{\varphi}_5^4$ $\hat{\varphi}_4^3 = \nabla_\Gamma \hat{\varphi}_5^5$ $\hat{\varphi}_4^4 = \nabla_\Gamma \hat{\varphi}_5^6$
\mathcal{P}^{p-1}	Middle	$\hat{v}_0 = 1$	$\hat{v}_1^1 = \text{curl}_\Gamma \hat{\varphi}_2^1$ $\hat{v}_1^2 = \text{curl}_\Gamma \hat{\varphi}_2^2$	$\hat{v}_2^1 = \text{curl}_\Gamma \hat{\varphi}_3^1$ $\hat{v}_2^2 = \text{curl}_\Gamma \hat{\varphi}_3^2$ $\hat{v}_2^3 = \text{curl}_\Gamma \hat{\varphi}_3^3$	$\hat{v}_3^1 = \text{curl}_\Gamma \hat{\varphi}_4^1$ $\hat{v}_3^2 = \text{curl}_\Gamma \hat{\varphi}_4^2$ $\hat{v}_3^3 = \text{curl}_\Gamma \hat{\varphi}_4^3$ $\hat{v}_3^4 = \text{curl}_\Gamma \hat{\varphi}_4^4$

Bibliography

- [1] H. Ammari and J.-C. Nédélec. Full low-frequency asymptotics for the reduced wave equation. *Appl. Math. Lett.*, 12(1):127–131, 1999.
- [2] D. N. Arnold, R. S. Falk, and R. Winther. Finite element exterior calculus, homological techniques, and applications. *Acta Numer.*, 15:1–155, 2006.
- [3] D. N. Arnold, R. S. Falk, and R. Winther. Finite element exterior calculus: from Hodge theory to numerical stability. *Bull. Amer. Math. Soc. (N.S.)*, 47(2):281–354, 2010.
- [4] C. Balanis. *Advanced Engineering Electromagnetics, Engineering*. Wiley, New York, 1989.
- [5] A. Besselov and N. Heuer. The *hp*-BEM with quasi-uniform meshes for the electric field integral equation on polyhedral surfaces: a priori error analysis. *Appl. Numer. Math.*, 60(7):705–718, 2010.
- [6] A. Besselov, N. Heuer, and R. Hiptmair. Convergence of the Natural *hp*-BEM for the Electric Field Integral Equation on Polyhedral Surfaces. *J. Numer. Anal.*, 48(4), 2010.
- [7] M. J. Bluck, A. Hatzipetros, and S. P. Walker. Applications of differential forms to boundary integral equations. *IEEE Trans. Antennas and Propagation*, 54(6):1781–1796, 2006.
- [8] J. Breuer. Schnelle Randelementmethoden zur Simulation von elektrischen Wirbelstromfeldern sowie ihrer Wärmeproduktion und Kühlung. *Dissertation, Universität Stuttgart*, 2005.
- [9] F. Brezzi and M. Fortin. *Mixed and Hybrid Finite Element Methods*. Springer, New York, 1991.
- [10] A. Buffa. Some numerical and theoretical problems in computational electromagnetism. *Doctoral thesis, University of Pavia*, 2000.
- [11] A. Buffa and S.H. Christiansen. The electric field integral equation on Lipschitz screens: definitions and numerical approximation. *Numer. Math.*, 94:229–267, 2003.
- [12] A. Buffa and P. Ciarlet, Jr. On traces for functional spaces related to Maxwell’s equations. I. An integration by parts formula in Lipschitz polyhedra. *Math. Methods Appl. Sci.*, 24(1):9–30, 2001.
- [13] A. Buffa and P. Ciarlet, Jr. On traces for functional spaces related to Maxwell’s equations. II. Hodge decompositions on the boundary of Lipschitz polyhedra and applications. *Math. Methods Appl. Sci.*, 24(1):31–48, 2001.
- [14] A. Buffa, M. Costabel, and C. Schwab. Boundary element methods for Maxwell’s equations on non-smooth domains. *Numer. Math.*, 92(4):679–710, 2002.
- [15] A. Buffa, M. Costabel, and D. Sheen. On traces for $\mathbf{H}(\mathbf{curl}, \Omega)$ in Lipschitz domains. *J. Math. Anal. Appl.*, 276(2):845–867, 2002.
- [16] A. Buffa and L. Demkowicz. H^1 , $\mathbf{H}(\mathbf{curl})$ and $\mathbf{H}(\mathbf{div})$ -Conforming Projection-Based Interpolation in Three Dimensions. *ICES Report*, (04-24), 2004.

- [17] A. Buffa and R. Hiptmair. Galerkin boundary element methods for electromagnetic scattering. In *Topics in computational wave propagation*, volume 31 of *Lect. Notes Comput. Sci. Eng.*, pages 83–124. Springer, Berlin, 2003.
- [18] A. Buffa and R. Hiptmair. A coercive combined field integral equation for electromagnetic scattering. *SIAM J. Numer. Anal.*, 42(2):621–640 (electronic), 2004.
- [19] A. Buffa, R. Hiptmair, T. von Petersdorff, and C. Schwab. Boundary element methods for Maxwell transmission problems in Lipschitz domains. *Numer. Math.*, 95(3):459–485, 2003.
- [20] A.H.-D. Cheng and D.T. Cheng. Heritage and early history of the boundary element method. *Eng. Anal.*, 29:268–302, 2005.
- [21] D. L. Colton and R. Kress. *Integral equation methods in scattering theory*. Pure and Applied Mathematics (New York). John Wiley & Sons Inc., New York, 1983. A Wiley-Interscience Publication.
- [22] D. L. Colton and R. Kress. *Inverse acoustic and electromagnetic scattering theory*, volume 93 of *Applied Mathematical Sciences*. Springer-Verlag, Berlin, second edition, 1998.
- [23] M. Costabel. Boundary integral operators on Lipschitz domains: elementary results. *SIAM J. Math. Anal.*, 19(3):613–626, 1988.
- [24] M. Costabel and W. L. Wendland. Strong ellipticity of boundary integral operators. *J. Reine Angew. Math.*, 372:34–63, 1986.
- [25] R. Dautray and J.-L. Lions. *Analyse mathématique et calcul numérique pour les sciences et les techniques. Tome 3*. Collection du Commissariat à l’Énergie Atomique: Série Scientifique. Masson, Paris, 1985.
- [26] L. Demkowicz. Projection-Based Interpolation. *ICES Report*, (03-04), 2004.
- [27] L. Demkowicz. *Computing with hp-adaptive finite elements. Vol. 1*. Applied Mathematics and Nonlinear Science Series. Chapman & Hall/CRC, Boca Raton, FL, 2007.
- [28] L. Demkowicz, J. Kurtz, D. Pardo, M. Paszyński, W. Rachowicz, and A. Zdunek. *Computing with hp-adaptive finite elements. Vol. 2*. Applied Mathematics and Nonlinear Science Series. Chapman & Hall/CRC, Boca Raton, FL, 2008.
- [29] L. Demkowicz and L. Vardapetyan. Modeling of electromagnetic absorption/scattering problems using hp-adaptive finite elements. *Comput. Methods Appl. Mech. Engrg.*, 152(1-2):103–124, 1998. Symposium on Advances in Computational Mechanics, Vol. 5 (Austin, TX, 1997).
- [30] S. Engleder. Stabilisierte Randintegralgleichung für äussere Randwertprobleme der Helmholtz-Gleichung. *Diplomarbeit, Technische Universität Graz*, 2006.
- [31] S. Engleder. Boundary Element Methods for Eddy Current Transmission Problems. *Dissertation, Technische Universität Graz*, 2011.
- [32] EM Software&Systems-S.A. FEKO. Comprehensive Electromagnetic Solutions.
- [33] W. Gui and I. Babuska. The h , p and h - p versions of the finite element method in 1 dimension. III. The adaptive h - p version. *Numer. Math.*, 49(6):659–683, 1986.
- [34] R. Harrington. *Time-Harmonic Electromagnetic Fields*. Wiley-IEEE Press, New York, 2001.

-
- [35] R. Hiptmair. Finite elements in computational electromagnetism. *Acta Numer.*, 11:237–339, 2002.
- [36] R. Hiptmair. Symmetric coupling for eddy current problems. *SIAM J. Numer. Anal.*, 40(1):41–65 (electronic), 2002.
- [37] R. Hiptmair, F. Krämer, and J. Ostrowski. A Robust Maxwell Formulation For All Frequencies. *Research Report, ETH Zürich*, 2008-05, 2008.
- [38] G. C. Hsiao and W. L. Wendland. *Boundary integral equations*, volume 164 of *Applied Mathematical Sciences*. Springer-Verlag, Berlin, 2008.
- [39] J. D. Jackson. *Classical electrodynamics*. John Wiley & Sons Inc., New York, second edition, 1975.
- [40] W. Kühnel. *Differentialgeometrie*. Vieweg+Teubner, 2005.
- [41] L.D. Landau and E.M. Lifshitz. *Course of Theoretical Physics, Vol. 8: Electrodynamics of Continuous Media*. Pergamon, Oxford, 1984.
- [42] R. C. MacCamy and E. Stephan. Solution procedures for three-dimensional eddy current problems. *J. Math. Anal. Appl.*, 101(2):348–379, 1984.
- [43] M. Maischak and E. P. Stephan. Adaptive *hp*-versions of boundary element methods for elastic contact problems. *Comput. Mech.*, 39(5):597–607, 2007.
- [44] W. McLean. *Strongly elliptic systems and boundary integral equations*. Cambridge University Press, Cambridge, 2000.
- [45] P. Monk. *Finite element methods for Maxwell’s equations*. Numerical mathematics and scientific computation. Clarendon Press, 2003.
- [46] J.-C. Nédélec. Mixed finite elements in \mathbf{R}^3 . *Numer. Math.*, 35(3):315–341, 1980.
- [47] J.-C. Nédélec. A new family of mixed finite elements in \mathbf{R}^3 . *Numer. Math.*, 50(1):57–81, 1986.
- [48] J.-C. Nédélec. *Acoustic and electromagnetic equations*, volume 144 of *Applied Mathematical Sciences*. Springer-Verlag, New York, 2001. Integral representations for harmonic problems.
- [49] C.R. Paul and S.A. Nasar. *Introduction to Electromagnetic Fields*. McGraw-Hill, Inc., 1987.
- [50] R. Picard. On the low frequency asymptotics in electromagnetic theory. *J. Reine Angew. Math.*, 354:50–73, 1984.
- [51] S. Rjasanow and O. Steinbach. *The fast solution of boundary integral equations*. Mathematical and Analytical Techniques with Applications to Engineering. Springer, New York, 2007.
- [52] Ch. Sauter, S. und Schwab. *Boundary element methods*, volume 39 of *Springer Series in Computational Mathematics*. Springer-Verlag, Berlin, 2011. Translated and expanded from the 2004 German original.
- [53] J. Schöberl and S. Zaglmayr. High order Nédélec elements with local complete sequence properties. *COMPEL*, 24(2):374–384, 2005.
- [54] O. Steinbach. *Numerical approximation methods for elliptic boundary value problems*. Springer, New York, 2008. Translated from the 2003 German original.
-

- [55] E. P. Stephan, M. Maischak, and F. Leydecker. An *hp*-adaptive finite element/boundary element coupling method for electromagnetic problems. *Comput. Mech.*, 39(5):673–680, 2007.
- [56] M. Taskinen and S. Vanska. Current and Charge Integral Equation Formulations and Picard's Extended Maxwell System. *IEEE Transactions on Antennas and Propagation*, 55(12):3495–3503, Dec 2007.
- [57] F. Trèves. Théorie des distributions et analyse fonctionnelle. *Gaz. Math.*, (98, suppl.):113–118, 2003. Laurent Schwartz (1915–2002).
- [58] W Walter. *Einführung in die Distributionentheorie*. B.I-Hochschultaschenbücher-Verlag, 1970.
- [59] D. Werner. *Funktionalanalysis*. Springer-Verlag, Berlin, extended edition, 2000.
- [60] M. Windisch. Modifizierte Randintegralgleichungen für elektromagnetische Streuprobleme. *Diplomarbeit, Technische Universität Graz*, 2007.